A MINIMUM ENERGY SOLUTION FOR MUSCLE FORCE CONTROL DURING WALKING

by

David Edgar Hardt

B.S.M.E., Lafayette College
(1972)

M.S., Massachusetts Institute of Technology
(1974)

SUBMITTED IN PARTIAL FULFILLMENT

OF THE REQUIREMENTS FOR THE

DEGREE OF DOCTOR OF PHILOSOPHY

at the

MASSACHUSETTS INSTITUTE OF TECHNOLOGY

September, 1978

Signature of Auchor .....
Department of Mechanical Engineering, 1978

Certified by .....
Thesis Supervisor

Accepted by .....
Chairman, Departmental Committee on Graduate Students

A Minimum Energy Solution for Muscle Force Control during Walking

by

David Edgar Hardt

Submitted to the Department of Mechanical Engineering
September, 1978 in partial fulfillment of the requirements for
the Degree of Doctor of Philosophy

ABSTRACT

The problem of determining muscle forces in the leg during walking is addressed using mathematical optimization. This approach is necessitated by the redundant arrangement of the muscles about the joints; but it also serves as a useful analog of the human adaptive motor control system. Minimum muscle energy, defined as the input chemical energy, is forwarded as the criterion of optimality, and a thermodynamic model of muscle is developed to allow implementation of this criterion.

This muscle energy model results from considering the chemico-mechanical dynamics of the energy transfers in muscle. Using bond graph models of these systems along with an existing model of actin and myosin dynamics, a simple static relationship between input chemical power and output mechanical power is established. (This relationship, however, applies only to muscle used in frequency ranges that are characteristic of walking). This chemical power is found to be a linear function of force and a non-linear, monotonic function of muscle contraction velocity.

Experiments are presented that measure lower limb kinematics and myoelectric signals from the surface muscles of the leg. The former are used to calculate the moments required at the joints for a specific subject's movements and these moments define the constraints on the force optimization.

Results of the minimum energy optimization, formulated as a linear program, indicate that the criterion selection affects only the relative load sharing between the active muscles whereas the basic temporal pattern of muscle activation is determined by the input joint moments. The agreement with MES's, which serve only as a temporal comparison, is acceptable, but several muscles that have distinct MES's are never used by the optimization. This problem is partially alleviated by introducing upper bounds on the muscle forces, which distributes the load among more of the muscles.

The validity of the minimum energy criterion is examined in a series of experiments with the subject walking at various speeds. The average total muscle power is calculated using both a minimum energy and a minimum force optimal criterion and these results are compared to classical oxygen consumption - walking speed findings. Although the proper trend in average power with increasing speed is predicted with both criteria (a quadratic relationship) the slope of the predictions is too high. The minimum energy case does, however, have a lower slope than does the minimum force case.

Knowledge of individual muscle forces is essential to a basic understanding of the mechanics of movement, and it would also find immediate application in clinical areas reconstructive orthopedic surgery.

Thesis Supervisor: Robert W. Mann
Title: Whitaker Professor Biomedical Engineering

Doctoral Committee Members

Professor Robert W. Mann
Department of Mechanical Engineering
Massachusetts Institute of Technology

Thesis Committee:

Professor Henry M. Paynter
Department of Mechanical Engineering
Massachusetts Institute of Technology

Professor J. Karl Hedrick
Department of Mechanical Engineering
Massachusetts Institute of Technology

Professor Thomas McMahon
Division of Engineering and Applied Physics
Harvard University

Acknowledgements

It would take many pages to recognize those who have given help, guidance, support and encouragement to me in the past six years. It has come from all groups: faculty, students and staff; and collectively they have made these not only the most educational years of my life, but certainly also the most enjoyable.

The unflagging support of Professor Mann is responsible for much of this; and by "giving me my head," he has afforded me a unique opportunity to define as well as execute a research program. His ability to place the small bits of the puzzle into their proper context will always serve as an example to me. Professor Paynter, with his boundless energy and enthusiasm, made certain parts of this work possible and in particular gave me the confidence to tackle the muscle energetics problem by illustrating the bond graph and resulting system dynamics analog for chemical reactions. Professor Hedrick, both in and out of the classroom, was instrumental in my decision to study and apply system dynamics and controls and his lucid instruction paved the way for the application of optimization techniques here. Professor McMahon, with a talent for seeking simplicity in the understanding of physiological systems, helped to shape my attitude toward this work and to keep its ever growing boundaries in check. His tough criticism and knowledge of related fields were invaluable and much appreciated. I also want to thank Dr. Sheldon Simon of Childrens Hospital for exposing me to the problems of cerebral palsey in children to which this work might eventually be applied.

Maintaining insight and sanity simultaneously is often a chore for

graduate students and here it is peer support that makes the difference. They are the many who would listen attentively to my "dilemma of the day" and offer suggestions, despite their own similar preoccupations. John Dent gets the credit for solving most of these problems and also an award for patience in listening to new ideas far afield from his present concerns. Steve Shladover was also burdened often with the many small problems and he always provided attentive counsel. All members of the Mobility Lab: Don Grimes, Don Darling, Erik Antonsson, Frank Conati and Paul Rushfeldt contributed to the specifics of this work and (more importantly) provided the comradery to help dispel increasingly frequent anxiety attacks. Paul must also be recognized for providing an example of someone who gets the job done, and done with a high standard at all times. His tenacity helped facilitate the execution of much of this work.

Other contributors include Neville Hogan and James Miller both of whom would eagerly enter into long discussion of the fundamentals underlying the planned research and in the process gave of their insight. Max Donath, a fellow gait research "travailler" was also a source of new information and perspective, and as confidant, helped to ease the burden of local disturbances along this road.

Those who guided by embryonic days as a graduate student, Derek Rowell, Peter Lawrence, George Dalrymple and Norm Berube, all contributed to this effort. Ralph Burgess gave frequent and thorough electronics design consultations and to Mark Stern goes well deserved credit for the excellent construction of the MES multiplexer. I must also express my highest gratitude to Lucille Blake for her consistent good

humor throughout all of this.

My father and mother provided the essential encouragement in getting me started and sustained in my engineering studies and the only sadness now is that only my father can witness the culmination of their joint efforts. But most of all, it is because of Susie, who makes each new day fresh and vibrantly alive, that all of this has been accomplished, and this has always been the indispensible ingredient.

David Hardt

This research was supported in part by the Whitaker Health Sciences Fund and by the Whitaker Professorship in Biomedical Engineering.

Table of Contents

Chapter 1 Introduction

Execution of a good design requires that the engineer know something about the environment into which the new device will be placed. If electrical, the input voltages and currents may be necessary; if thermal, the temperature and pressure of the surroundings are probably the most important data. With mechanical systems the primary variables, by definition, are the forces and displacements. From an engineering perspective, the human musculoskeletal system is often approximated by a system of rigid articulated links and the associated actuators; and if designs for new "parts" of this system, such as a limb or joint prosthesis, or repairs such as neurectomies or osteotomies are to be done properly, the mechanical function of the normal system must be understood. For example: in the design of a hip prosthesis the force vector acting on the femoral head should be known so that an accurate stress analysis of a replacement can be performed. Similarly, if the end of the femur is to be relocated by osteotomy (see Harris (1969)), the post-operative forces that the new arrangement will see must be predicted.

Another repair or redesign of the musculoskeletal system is the modification of the normal actuator function in order to change the output. This can include selective tendon cutting (tenotomy) or nerve severing (neurectomy) often performed to assist children with cerebral palsey to walk autonomously (see for example Banks (1960)). This effective muscle paralysis, or even the intentional rearrangement of tendons to circumvent local paralysis (Close (1959)) causes profound mechanical changes most of which are not presently quantified. In this case the ability to characterize the mechanical state before and after surgery has clear advantages over the more conventional empirical approach.

However, the human system is not as accessible as inanimate ones and even rudimentary mechanical data is not available to design engineers or surgeons, which leaves both open to the tragedy of empirical failure. On a less applied level, the understanding of the mechanical functioning of the human locomotion system remains incomplete. Also, neurophysiology suffers from a lack of information about the output of the system being studied, that is the muscle force. The dilemma is that after measuring the externally accessible quantities: limb motion and foot - floor forces, the list of non-invasive measurements ends. Attempts at implanting instrumentation such as the instrumented femoral neck used by Rydell (1966) are often plagued by the abnormal situation into which the subject is placed, leaving the outcome in doubt.

At present it is possible, with external kinematic measurements and dynamic models of the limbs, to calculate the gravitational and inertial component of the joint forces and the complete joint moments required to keep the skeletal system in dynamic equilibrium. Methods for this are varied and several will be discussed in chapter 2, beginning with the pioneering work of Bresler and Frankel (1950) still used today as a standard of comparison. However, the clinical and engineering utility of joint moment data alone is marginal since it represents the integrated effect of the many "linear" actuators (muscles) that act across the joints. The most relevant data are the individual muscle forces themselves which not only act to cause moments about the joints, their primary function, but also, as a consequence of their activity, exert large forces on the bones and thus on the joints. This information, if available, would permit a more complete mechanical characterization of the links (bones), articulations and their bearing material (art-

icular cartilage), and actuators (muscles) of the system and would provide essential predictive capabilities for the engineers, and through them, the surgeons.

To illustrate the importance of muscle forces in the overall mechanical picture, consider the simplified schematic of the lower limb in figure 1-1. The equilibrium of this system, whether in motion or not, is established by exerting the correct moments at the joints, this being accomplished with the muscles some of which are shown as straight lines in the figure 1-1. The forces acting on each skeletal member, as shown in figure 1-2, will consist of forces exerted at the muscle attachments and the reaction force at the joint. The latter will be a vector sum of the muscular forces plus the combined effect of gravitational and inertial forces. The relative magnitude of these components can be illustrated by the static equilibrium of the hip while standing on one leg. Viewed from the front,this situation (shown in figure 1-3) requires a large muscular force to generate the moment necessary to counteract the large gravitational moment of the trunk. In this example the muscular forces, owing to the rather short moment arms of the muscles, are nearly three times as great as the body weight, and the resulting force on the femoral head is clearly dominated by the muscular rather than the gravitional component.

Unfortunately, direct calculation of muscle forces is precluded by their redundant arrangement about each of the joints. There are well over fifty muscles in each leg but only seven or eight major degrees of freedom. Figure 1-4 illustrates this problem for a very simple case using the example of redundant, antagonistically arranged muscles. The result is that the distribution of forces among the muscles is indeterminate, since more than

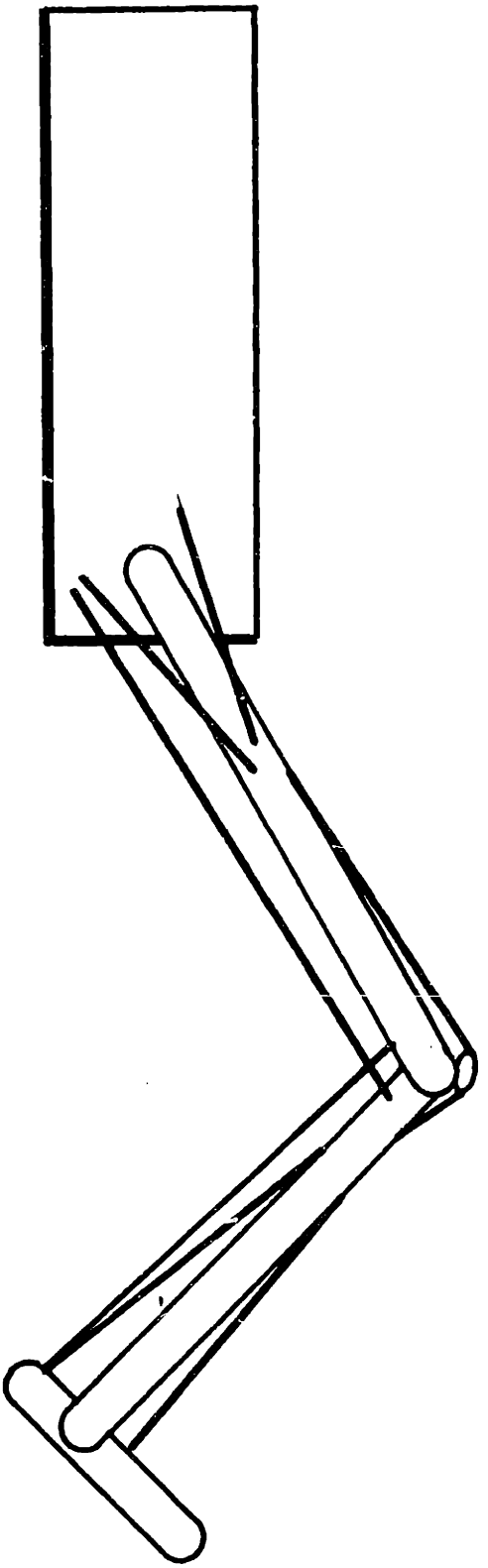

Fig. 1-1 Lower Limb Schematic
The lines represent the location of typical muscles. Notice the single joint and double joint muscles, the

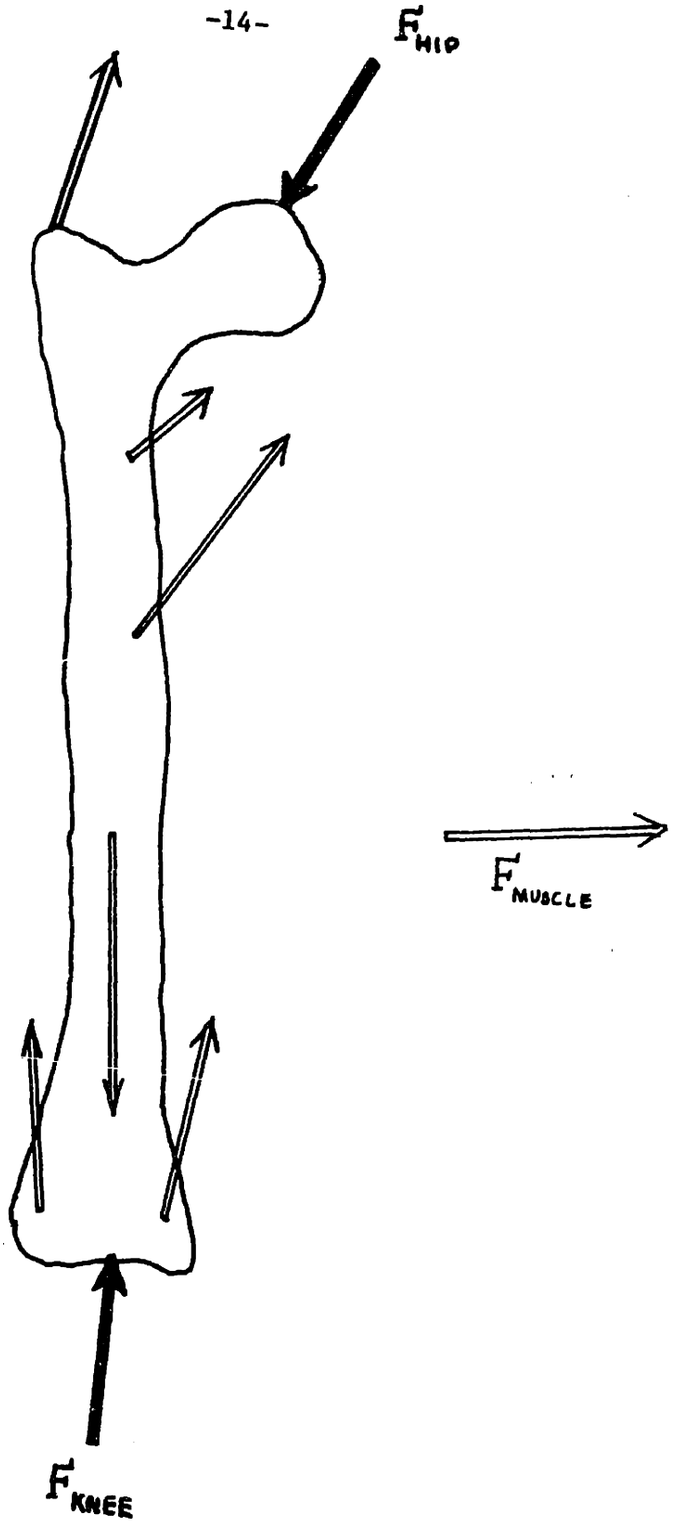

Fig. 1-2 Typical Loads on the Human Femur
Both muscle and joint forces are indicated.

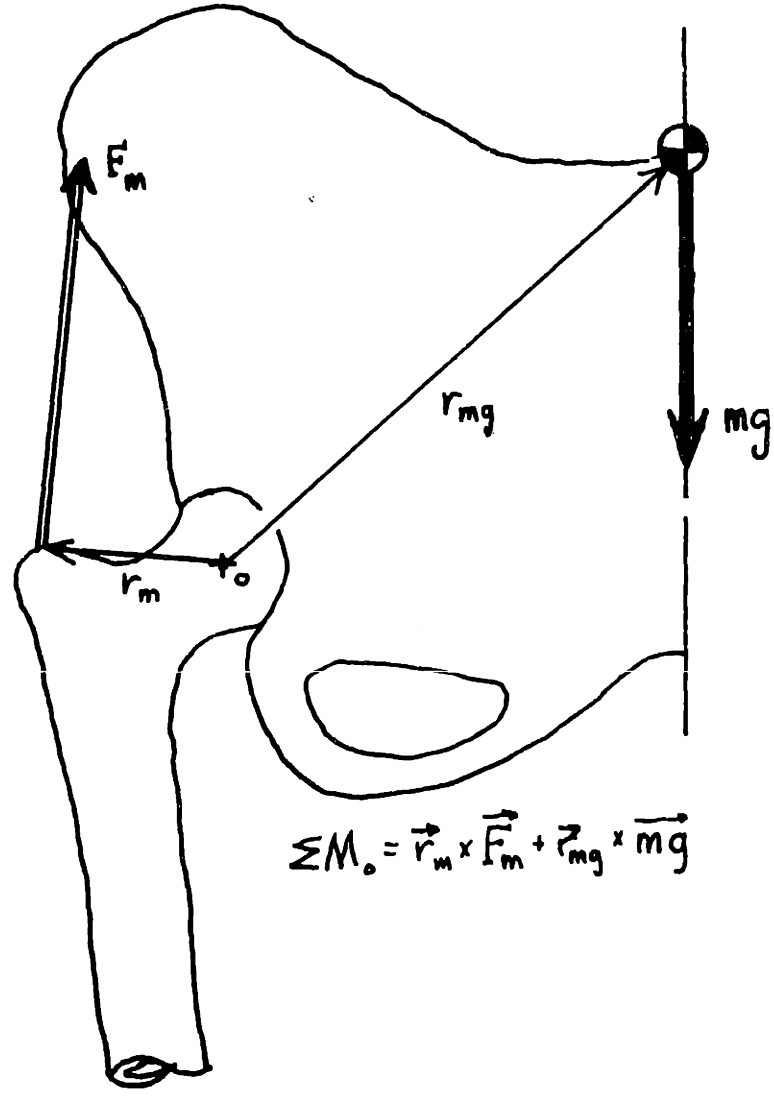

Fig. 1-3 Equilibrium in the Saggital Plane of the Hip
The required muscle force, F_m, is greater than mg since r_m is considerably shorter than r_{mg}.

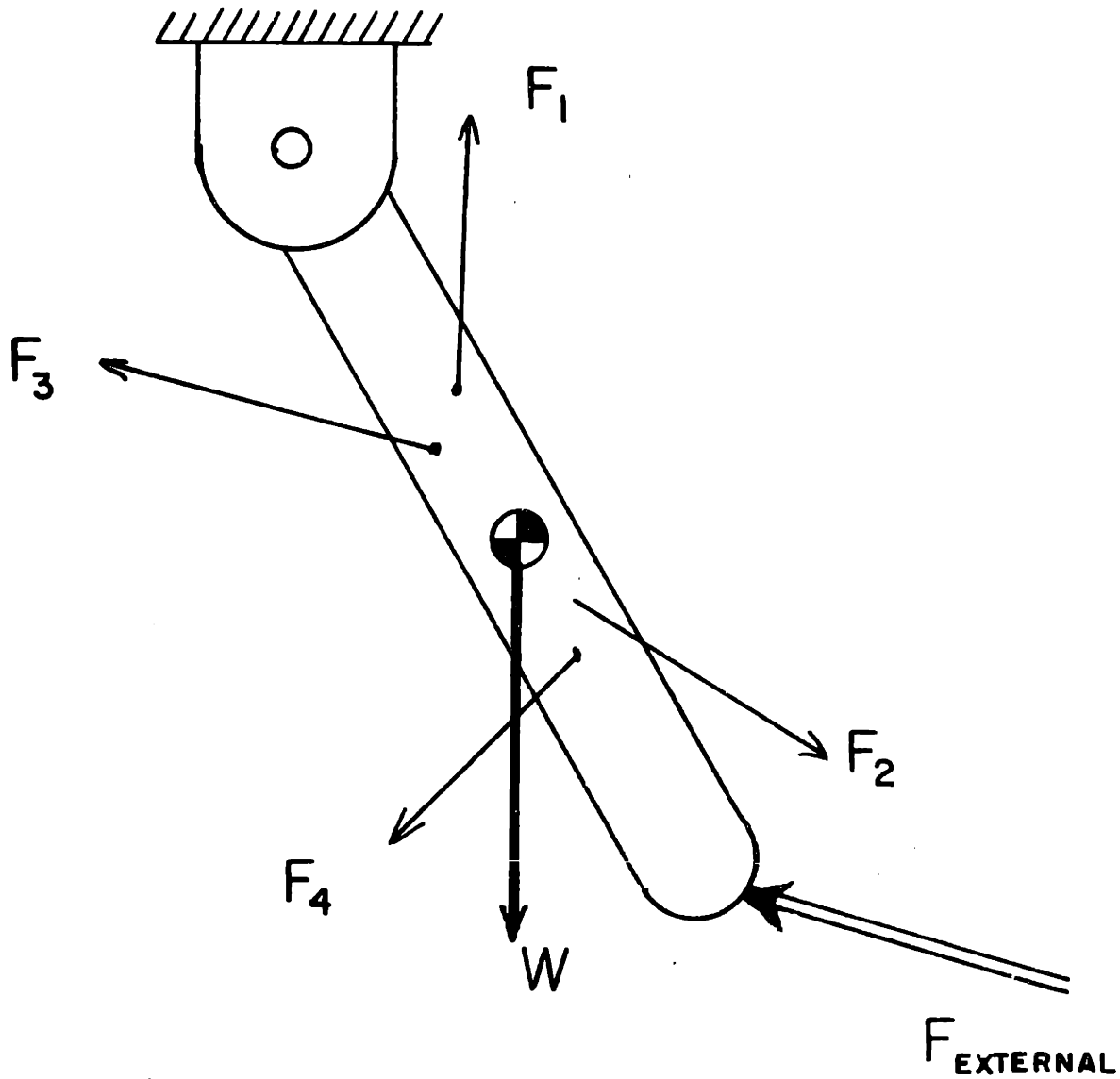

Fig 1-4 Redundant and Antagonistic Muscle Forces
Moment equilibrium of this segment can be acheived with an infinite variety of muscle force combinations. For example, F_1 and F_3, which are antagonists, can be modulated against each other at any overall level provided the net force or bias provides equilibrium. The addition of F_2 and F_4 simply increases the number of possible forces.

one possibility exists for satisfying the joint moment equation. As mentioned above, muscle force is not measurable non-invasively, and since this study is restricted to humans the only means of investigating muscle activity is with myoelectric signals which can only be roughly correlated to muscle force levels.

The problem addressed here is to develop a method of calculating muscle forces based on what information is available, both mechanically and physiologically, that can be used confidently despite the absence of a direct measure of the actual output. Stated more exactly: given the moments acting at all the joints of the legs, $\underline{m}(t)$, predict the muscle force magnitudes of all significant, anatomically distinct muscles, $\underline{f}(t)$, during normal level walking. Assigning a three-dimensional moment arm to each muscle about each joint it spans, and collecting these into a matrix R, which will be limb position dependent thus time dependent, the problem can be stated

$$R(t)\ \underline{f}(t) = \underline{m}(t) \qquad 1\text{-}1$$

The system considered here, shown in figure 1-5, includes the pelvis, femur, tibia fibula, and foot. It is modeled with 31 muscles and 7 rotational degrees of freedom, (3 at the hip, 1 at the knee and 3 at the ankle) so R is a 31 x 7 matrix, $\underline{f}$ a 31 element vector and $\underline{m}$ a 7 element vector. Since the non-square matrix R cannot be inverted, a less direct method of solving equation 1-1 must be pursued.

The minimum energy hypothesis

Given the basic problem of solving matrix equation 1-1, an indeterminate set of linear, time-varying equations, there are at least two approaches that

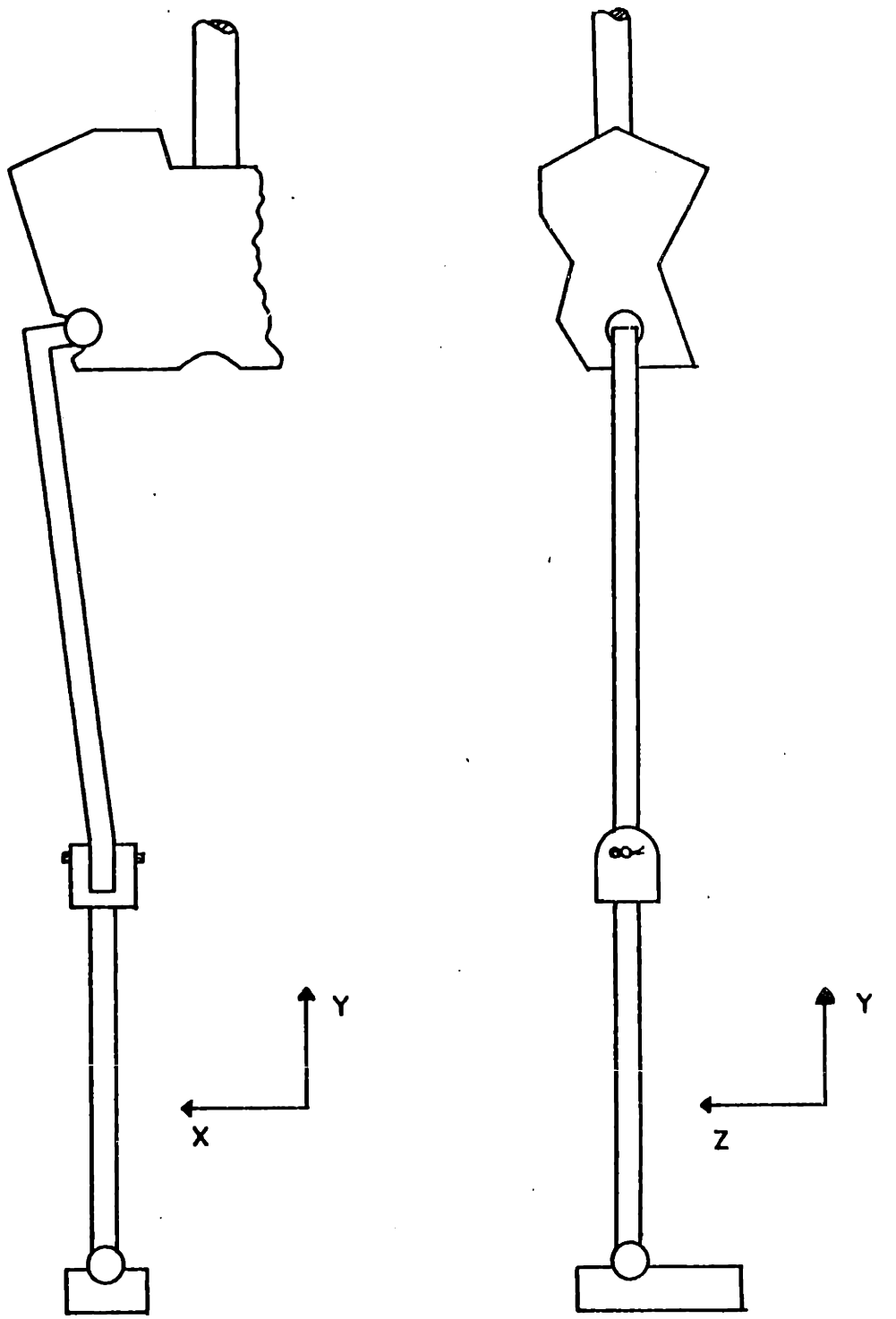

Fig. 1-5 Skeletal Model for the Lower Limb
The hip is assumed to be a ball joint as is the ankle, and the knee is a simple pin joint.

can be taken. The easiest and most obvious is to reduce the number of variables (the separate muscle forces) until the R matrix is square and thus solvable. This approach was taken by Paul (1965), Morrison (1967), and Hatze (1975), all of whom grouped functionally similar muscles into large groups until the required reduction was accomplished. Expanding the R matrix in the other direction would also solve the problem, but this implies that certain physical equality relations involving the muscle forces can be written in sufficient quantity to make R a 31x31 square matrix. It does not appear that such additional relations exist.

The alternative to eliminating variables is to retain all of them, which yields an infinity of possible solutions to equation 1-1, and to pick one of these solutions as being the best based on some criterion of optimality. This approach, pioneered in biological applications by Penrod (1974) and Seireg & Arvikar (1975) must have in addition to the muscle moment equation (1-1) an expression (often called a penalty function) that reflects the selected optimal criterion as a function of the system variables. Many such functions have been proposed, based either on mathematical simplicity or physiological relevance. To emphasize the difficulty of choosing the optimal criterion, Chao and An (1977) included a "shopping list" of their suggestions in a paper addressing the solution of forces in the finger.

There are, therefore, two important questions which need to be addressed: what should the optimal criterion be, and how sensitive is the solution to this choice? This thesis approaches the first question by forwarding a simple hypothesis: the muscles in the legs are activated in such a way as to minimize the input (chemical) energy requirements of the muscles during the walking cycle. This minimum energy hypothesis is based on certain

qualitative and quantitative findings as well as on an underlying assumption about the nature of the motor learning prodess whose final product, the muscle force patterns, is what must be determined.

The pattern of muscular activity that causes coordinated movements such as walking can be thought of as responses to local disturbances superimposed on a program of commands to the system based upon the intention of the individual. This basic pattern is the result of a learning process not unlike that of an adaptive control system. In the latter, shown in figure 1-6 as it would apply here, a plant (the skeletal system) is controlled by actuators (the muscles), which receive commands from the controller (the central and peripheral nervous system). To be considered adaptive, the system must have a means of identifying the system being controlled, and also must be able to modify the control strategy based on this identification along with some performance index or optimal criterion.

The identification process must have full feedback of the output, provided in this case by muscle length (spindles), muscle force (tendon organs), and joint angle sensors; plus feedback of the control signal itself. The latter has been identified anatomically in the CNS, and presently theories of motor neurophysiology are being developed based on this concept of control signal monitoring (Evarts (1972)). With this information it is possible to define a suitable transfer function for the muscle-limb system. The optimal criterion then guides the controller adaptation until the best performance is achieved.

The theoretical possibility of the physiological presence of the optimization process having been forwarded, it has been hypothesized here that this process will be governed by a minimum muscle energy criterion. This follows

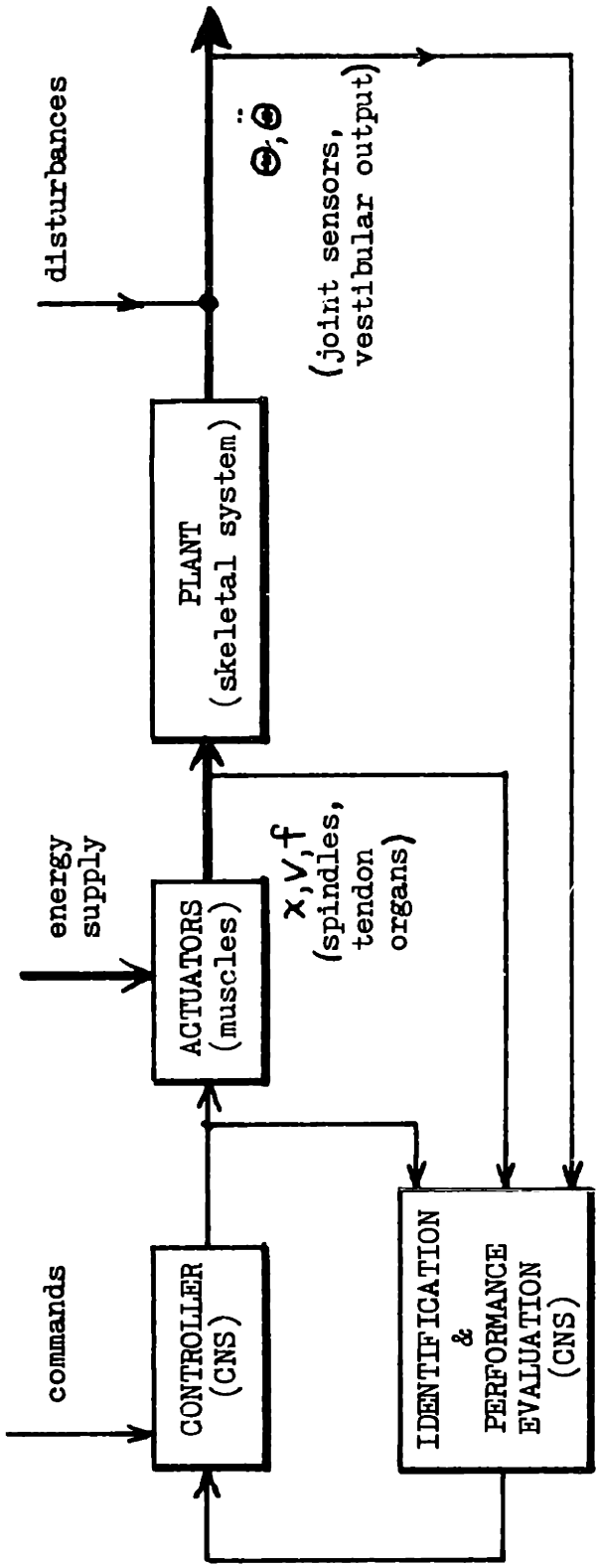

Fig. 1-6 An Adaptive Control Analog for the Human Motor Control System

The essential elements here are the identification and performance evaluation (optimization) process and the feedback of the controller output as well as the actuator and plant outputs.

from several observations of the locomotion process. Saunders et al. (1953) have shown that the general motion of the body during walking is such that the excursions of the center of gravity of the body are minimized, given the kinematic constraints imposed by the linkage representing the legs. Moving to the next level of detail, Chow & Jacobsen (1971) examined the criteria for leg movement, as manifest in the joint angles, given only the motion of the center of gravity and the leg linkage structure. Using a minimum joint power criterion their optimization procedure produced joint angle trajectories that compare favorably with actual measurements. This suggests, but does not confirm, the existence of an energy minimization procedure in the motor learning process.

Since the muscles are the actuators responsible for all significant power production and absorption at the joints, it is a small logical step to postulate a minimum energy criterion for their activation during walking. In fact, strong arguments can be made for the application of this criterion to other activities, at least as an overall goal, with different constraint structures relating the unique properties of the desired motion.

Pedotti (1978), based on his observations when studying the correlation of muscle activity measured with MES's with joint moments and muscle length changes, suggested that the overall criterion for muscle use must be minimum energy. This objective is, of course, applied after all functional requirements have been satisfied. Nubar and Contini (1961) proposed a minimum "effort" criterion for joint moment selection, however, this is not relevant as a criterion here since the effort, although intended to be analogous to energy, was in fact defined by the product of the joint moments squared

and the time interval of application, which is not a power or energy measure. Also, this criterion can only be applied to situations where both legs are in contact with the ground since moment selection freedom must exist.

A further motivation for the minimum energy hypothesis, first forwarded by Hardt (1978), is the philosophy that the optimization must be thought of as an analog of a natural process, thus maximum incorporation of quantifiable physiological properties of the system should be attempted. Characterization of the energetics of the muscles, which is necessary in order to carry out the energy minimization, will include many of these properties. Returning to the control system analogy, the optimization process cannot be expected to operate in the absence of detailed information about the system actuators, thus the energetics plus other properties such as maximum force capabilities or maximum rate of change of force can be included as bounds on the variables of optimization.

Finally, it has been shown by Margaria (1976) that normal walking speed is usually chosen to require the least energy expenditure (as measured by oxygen consumption/distance traveled). Evolutionary needs for minimizing locomotion energy are also obvious.

Problem formulation

The muscle force problem, stated in a somewhat standard optimization format, can be written:

$$\min_{\underline{f}} \; J \tag{1-2}$$

subject to the constraints

$$R(t)\,\underline{f}(t) = \underline{m}(t) \tag{1-3}$$

where J is the optimal criterion and will be a function of the variable $\underline{f}$. Notice now that the moment equation has apparently slipped to a secondary role of acting only as a constraint on the optimal criterion or penalty function. This situation is discussed in chapter 4 in the context of the specific optimization method used here.

The main task in this work is, therefore, the definition of J, and evaluation of that choice based on experiments that measure leg movements during walking to provide the necessary information for the constraints of equation 1-3.

Thesis summary

To investigate the minimum muscle energy hypothesis, several steps, both analytical and experimental, must be followed. Before the minimum energy optimization can be implemented a model of the energetics of muscle, which will relate energy consumption of the muscles to their mechanical output, is necessary. The procedure by which this model was developed is presented in chapter 3. The resulting model is a simple, non-linear algebraic expression relating input and output powers, and is applicable to dynamic muscle use up to a frequency of about 10 Hz.

The actual optimization procedure, which incorporates both the energy model of chapter 3 and the moment constraints of equation 1-1, is formulated in chapter 4. This formulation if highly dependent on the form of the optimal criterion, (equation 1-2) and the static nature of the muscle power relationship from chapter 3 permits the use of a linear programming format. Linear programming also easily handles inequality constraints which are useful in placing bounds on the system variables. The unique properties of a linear programming solution, as they pertain to the muscle force problem, are

also discussed.

The constraint equations of the linear program, which are of course the muscle moment equations (1-1), are based on the structure and movement of the individual subjects under study. In chapter 5, procedures for estimating muscle attachment points, the experimental procedure for measuring limb motion, and the methods used to calculate joint moments are described. Also measured, using methods described in chapter 5, are the myoelectric signals (MES) from the surface muscles of the leg. These signals, when suitably processed, provide a qualitative standard against which the predicted muscle forces can be compared.

The results of experiments on two subjects are presented in chapter 6. The forces predicted by the minimum energy optimization agree well with the MES's except that several muscles show no predicted force although their MES's show considerable activity. The minimum energy criterion is investigated to examine the sensitivity of the force solution to changes in the muscle velocity term, (which is the non-linear element in the muscle energy model). Sensitivity to changes in the criterion itself are also checked, as is the change following introduction of maximum muscle stress constraints. Lastly, the average power consumption predicted by the minimum energy optimization for various walking speeds is compared to that predicted for a minimum force optimization criterion. The comparison of both of these with classical oxygen consumption measurements is then made.

Chapter 2 Review of Literature

The nature of the muscle force problem requires that many separate lines of research be drawn upon for guidance. The general area of gait analysis constitutes a long and rich body of literature and the work here continues from the general results of these studies while also incorporating many of the gait analysis techniques that have been developed. The need to quantify muscle forces has long been recognized and many attempts have been made, for various purposes, to at least partially determine these forces. Because of its relevance here, optimization approaches will be treated separately since they address the general biomechanical problem as well as specific optimization techniques.

The specific literature of muscle energetics is contained separately in chapter 3 and will not be repeated here.

Classical gait analysis

This term is taken to define any attempt to quantify the mechanics of human locomotion. Such work has a long history dating to the 17th century and Steinder (1953) provides an excellent historical review of relevant material up to the 1950's. Since then the majority of work has been aimed at improved instrumentation and data reduction methods, however, the objective remains the same: measure the external mechanical quantities and predict the internal, non-measurable mechanical quantities during human walking.

Gait kinematics

Recording limb motions, for both scientific and artistic reasons, was advanced by the pioneering sequential photography techniques used by Muybridge (c. 1880). Photographic recording, either with multiple exposure of

a single frame or by cinematography, has been the dominant means of kinematic analysis ever since, applied with various techniques depending upon the sophistication required.

The large research effort undertaken in the late 1940's and 1950's at UCAL Berkeley employed the movie film technique. To obtain three dimensional joint positions and the projected angles of the limbs, two cameras were used, one facing the subject and one perpendicular to the plane of progression (see Eberhart et al. (1954)). This arrangement was used to measure axial rotation of the limbs using targets that clamped directly to the subjects bones (Levens et al. (1948)), to study the swing phase motion at the knee for prosthetic design (Bartholomew (1952)), for joint moment determinations (Bresler & Frankel (1950)), and for studies of the general characteristics of human gait (Saunders et al. (1953)). The data was also correlated to myoelectric recordings from the leg muscles to elucidate muscle function during walking (Eberhart et al. (1954)).

The two movie camera method, along with similar procedures using single frame multiple exposures, as was done by Murray (1967) in a classification study of gait characteristics, involves tracking the motion of joint center markers (or other landmarks) in space and computing the resulting limb motions, usually presented as projected limb or joint angles. Typical results are shown in figure 2-1. These methods suffer from the necessarily crude approximation of the joint center location and its representation by a surface marker. A more modern and sophisticated computer - television system, such as those developed by Winter et al. (1972) and McGhee et al. (1974) replaces the movie system with a video system. This automation is

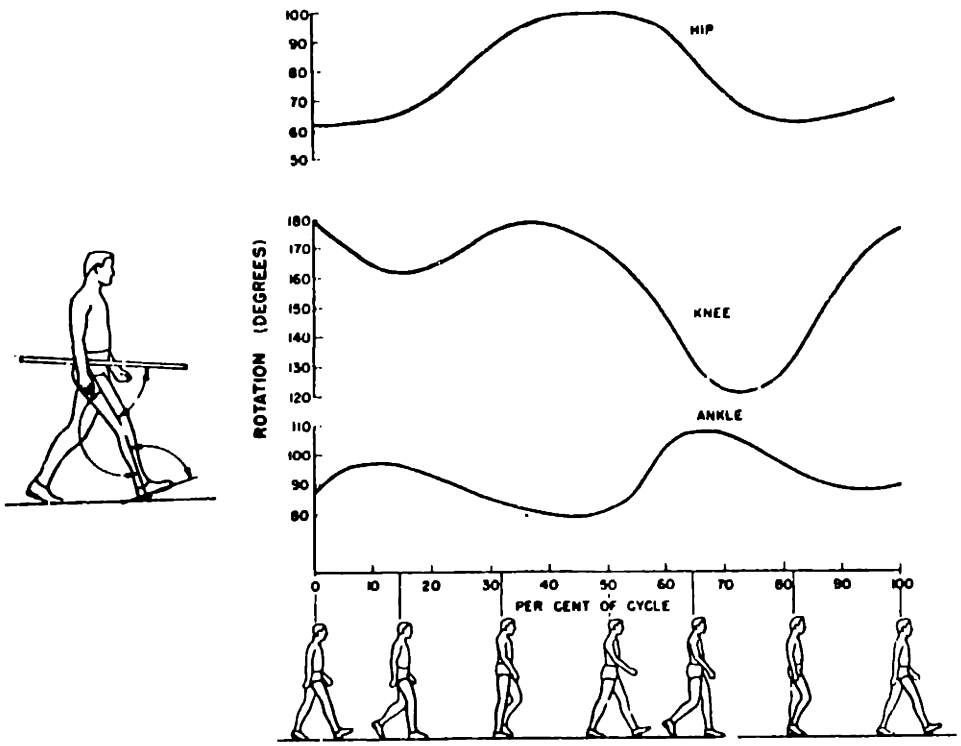

Fig. 2-1 Rotation of the Leg Joint as viewed from the Side (from Eberhart et al.(1954))

done at the expense of increased complexity and accuracy is not significantly increased, especially since the surface marker technique is still employed. However, the rapid turnaround of data and the absence of the time consuming marker point location procedure used in the photographic studies does facilitate a greater throughput of subjects, and the direct input to a computer allows statistical analyses to be performed with greater ease (see for example Winter et al. (1974)).

A superior method of kinematic analysis is one that treats each body segment as a separate, rigid body moving in three dimensional space. No assumption is made about the linkage of which it may be a part. This approach was taken by Conati (1977), who used the SELSPOT system to track the time locus of light emitting diodes (LEDS) attached to each segment. If three non-colinear LEDs are placed on each rigid body, its position and rotational orientation in space can be calculated. Using an algorithm that accepts redundant measurements, and by placing more than three LEDs on each body, Conati was able to increase the accuracy of this determination despite rather noisy point location measurements. This rigid body technique also permits schemes for calculating rather than estimating joint rotation axes and preliminary techniques for this were developed by Antonnson (1978).

Crowninshield (1978a) employed a similar kinematic calculation method, but used flashing LEDs and a pair of oblique, single photographic exposures for individual point location. This system has the virtue of decreased complexity compared to the SELSPOT system but still requires the arduous task of visual location of each point on the photograph.

The SELSPOT system (manufactured by SELCOM AB, Sweden) is a unique point location device which can track thirty separate points in space in real time.

Each point is represented by an infrared LED and the thirty LEDs are time multiplexed for an effective sample rate of up to 300 Hz per point. The location is sensed by a pair of cameras which generate currents proportional to the coordinates of the infrared light spot focused on the receiving plates, and the data is sent in digital form to a computer. Using the kinematic calculation scheme assembled by Conati, full three dimensional position and orientation information for a walking cycle can be produced in a matter of minutes for sample rates well within the bandwidth of limb motion.

Probably the most direct method for measuring joint angles only is the use of goniometers, devices that attach directly to the subject and measure the relative rotations of the limbs. This is the most reliable and simplest method and since it requires very little computation, usually kinematic correction procedures often done in analog form, it can produce the joint angle information in real time. However, the devices suffer from inaccuracies introduced by being off-axis from the actual skeletal members and are cumbersome enough to affect the gait patterns of the wearer.

Data from goniometric studies of the knee(performed at the Mayo Clinic under the direction of C.Y. Chao) were used by Donath (1978) who combined this information from a large population with certain anthropometric measures (such as height, weight, age and sex) to determine the quality of an individuals gait. Using pattern recognition techniques it was possible to correctly delineate normal subjects from post operative knee arthroplasty patients (total knee replacements). His results can be expanded to include several subgroups of abnormality and in addition, the technique provides a quantitative measure of the extent of the abnormality. Thus the effect of

therapy or improved prosthesis design can be more precisely defined.

Inertial properties of the limbs

If the dynamics of the limbs are to be examined, the inertial properties of the segments must be determined. Studies of this type date back to the work of Braune & Fischer (1889) who measured the relative mass, center of gravity location, and moments of inertia on several cadavors. Their work, still in widespread use today, reduced these measurements to a series of coefficients that when applied to the segment type, length, diameter and joint coordinates will estimate the mass, locate the center of gravity, and estimate the moments of inertia referred to the c.g. for individual subjects. The accuracy of these coefficeints is demonstrated by the comparisons included in Contini's review (1972) of various authors methods of mass determination. Another method of locating the c.g. used by Drillis et al. (1964) is to use living subjects and have them move the appropriate limb while the supporting forces are monitored. Inertial properties of limbs with living subjects can be determined with dynamic tests on the limb(s) in question and estimates of natural frequency as well as joint damping can be made (Hatze (1976)).

A detailed treatment of the exact location of segment centers of gravity is that of Dempster (1955) who investigated these properties as part of a human operator study. Much of this data is presented as functions of joint or boney prominence coordinates and is, in general, three dimensional.

Huston et al. (1971) have adopted a geometric model of the body proposed by Hanavan in their studies of body dynamics after impulsive force inputs, such as after an automobile crash. This model approximates each segment as a truncated cone, and with the surface thus described, all

inertial properties can be calculated if a uniform density assumption is made.

Limb dynamics

If the motion and inertial properties of all body segments are known it is possible to calculate the net moments acting on each articulation which are responsible for the observed motions. This "inverse dynamics" problem, so-called because conventional dynamic analysis usually predicts motion from forces, has been approached in several ways, usually dependent upon the form of the input data. The only real difference in computational method depends upon whether the foot - floor force, the only external force on the system, is measured.

If this force (and moment) is measured, the joint moment analysis is greatly simplified since the progression from distal to proximal joints on each segment involves knowing the gravitational and inertial forces on only that segment. The technology of foot - floor force measurement is still advancing and many different designs for force plates have evolved. Basically, the objective is to obtain the force and moment vectors acting on the foot as well as the location of these vectors on the foot. Force plates that accomplish this are described by Eberhart (1954), Cunningham (1958) and Morrison (1967). Problems of frequency response and noise are the most prevalant, but a commercially available plate using quartz piezioelectric crystals as the force sensing device, manufactured by Kistler,has found widespread use because of its accuracy and stability.

The next generation of force plates will remove present restrictions of measurement of only one foot force at a time (which is a limitation during double leg stance and particularly restrictive for leg prosthesis studies)

and of requiring foot fall to occur on one small area of the floor. Estey (1978) has proposed and begun preliminary development of a plate system consisting of many smaller triangular plates which would "pave" the motion study area and thus be sufficiently responsive, delineate and quantify separate foot forces, and not concern the subject with foot placement. Estey has also included an excellent review of force plate designs and developments as part of this work.

With all of the above measurements, the inverse dynamics problem can be solved provided the limb accelerations are available so that inertial forces can be evaluated. These accelerations can be directly measured (Morris (1973)), but the complexity of this instrumentation, which must be used in addition to some inertial reference position measurement device, usually favors instead the double differentiation of the displacement data.

All methods used to differentiate gait displacement data have the common characteristic of careful low-pass filtering of the data before any differentiation is attempted. The well known hazard of differentiation, involving the magnification of higher frequency noise which is present in all gait measurements, necessitated this signal pre-processing. Bresler and Frankel (1950) used graphical differentiation that involves "eyeball" filtering (and considerable man-hours!) The attractive Fourier Series method, wherein displacement data is fit by a Fourier Series that is in turn differentiated analytically, has also been used (see Cappozzo et al. (1975), McGhee (1976) and Hatze (1977)). It is by far the best filtering method since the cutoff characteristics are ideal (the frequency determined by the number of harmonics included), but the input data must be periodic and its period must be well defined, thus forward displacement of the segments is quite difficult

to describe with this technique.

The most straightforward method is direct low-pass filtering followed by direct differentiation, both usually done numerically (see for example Winter et al. (1974)). This general method was used in the experiments described in chapter 5 and is detailed in appendix C.

A different approach, which avoids the differentiation entirely, was investigated by Chao and Rim (1973). They solved the inverse dynamics problem by treating it as a regular dynamics problem with a set of arbitrary moment trajectories at the joints. The calculated displacements of the limbs resulting from these moments are then compared to the measured displacements and an error expression formed. Using a first order gradient optimization method, the assumed initial moment trajectories were modified until the error was reduced to an acceptable level. Although they deemed the method too slow in comparison with conventional methods, it does have the distinct advantage of making the solution somewhat closed loop and can take advantage of the self-filtering properties of the dynamic model. Although the differentiation was eliminated, the filtering cannot be. Using unfiltered data, if the error criterion is set too tight the unwanted high frequency motion components will be included; and if the criterion is too loose the desired lower frequency components may not be correctly matched, thus better control over the harmonic content of the data can be exerted by pre-filtering. This method does deserve more investigation since it provides an independent check on the moments calculated by the conventional means.

If a force plate is not available a more complete model of the body must be used since the motion of all significant segments must be known. McGhee et al. (1976) present some methods for this situation and these are

described in detail in chapter 5 since similar methods were used in the experiments performed here.

Typical joint moment data from lower limb dynamics studies are shown in figure 2-2. The joint forces that are calculated here do not include the muscular component, for reasons stated in chapter 1, and there is an implicit assumption in all of the methods described above that the moments at the joints are provided by pure moment generators. These moments are actually the result of muscle forces acting through moment arms and will add significantly to the loading on the entire skeletal system.

Muscle force analyses

Specific application of muscle force data in clinical as well as research areas has fostered many endeavors aimed at quantifying these forces. Probably the most successful are the studies of Paul (1965) and Morrison (1968). Their main intent was to determine joint forces for use in detailed studies of joint mechanics. The technique was first to determine joint moments using methods described above and then to solve for the muscle forces producing these moments. The problem was rendered solvable by grouping functionally similar muscles together to eliminate the redundancy. Even so, Paul (1967) performed a crude optimization by considering two separate sets of muscle and using their respective solutions to bound the expected correct solution for the joint force. These results have been used to examine muscle function during various actions of the legs (Morrison (1970)) and to provide data for more complete understanding of skeletal mechanics (Paul (1971)). Typical predicted knee force magnitudes (the sum of gravitational, inertial and muscular influences) are shown in figure 2-3.

Similar quantitative studies have been carried out using MES's to deter-

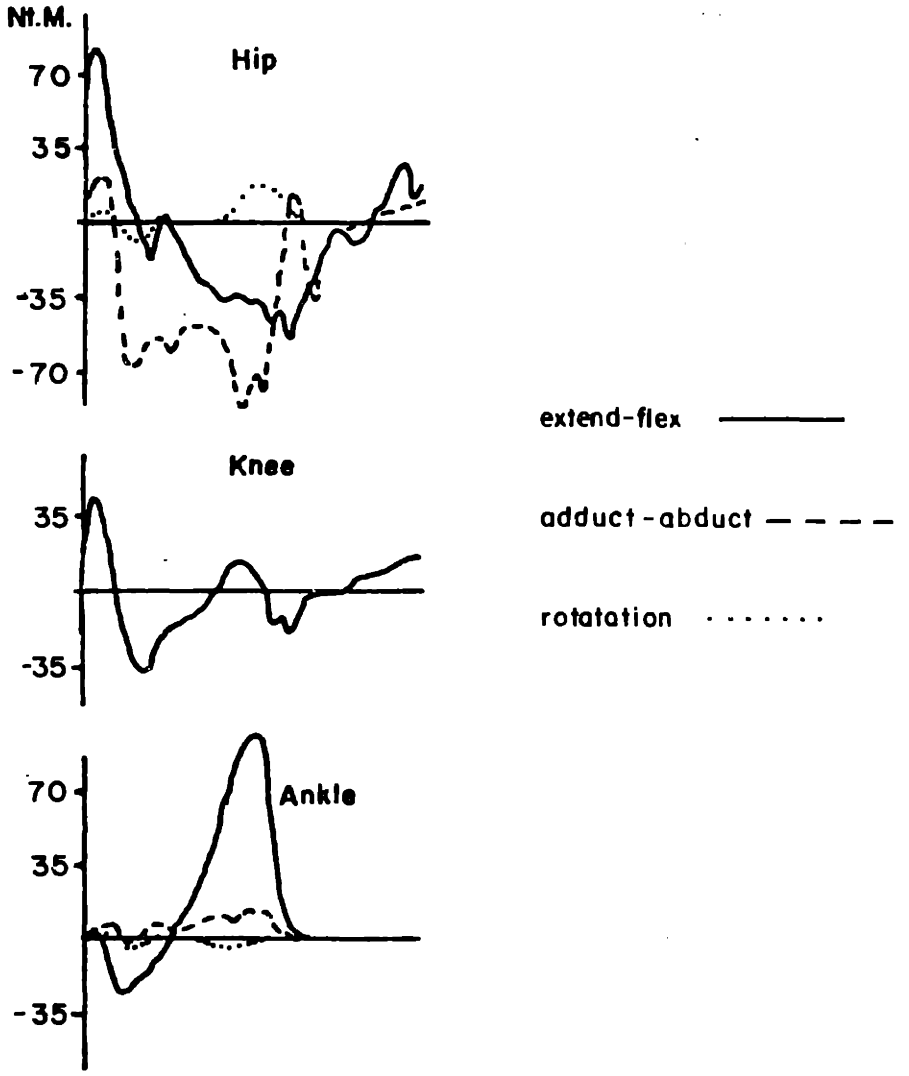

Fig. 2-2 Joint Moment Data (from Bresler & Frankel(1950))

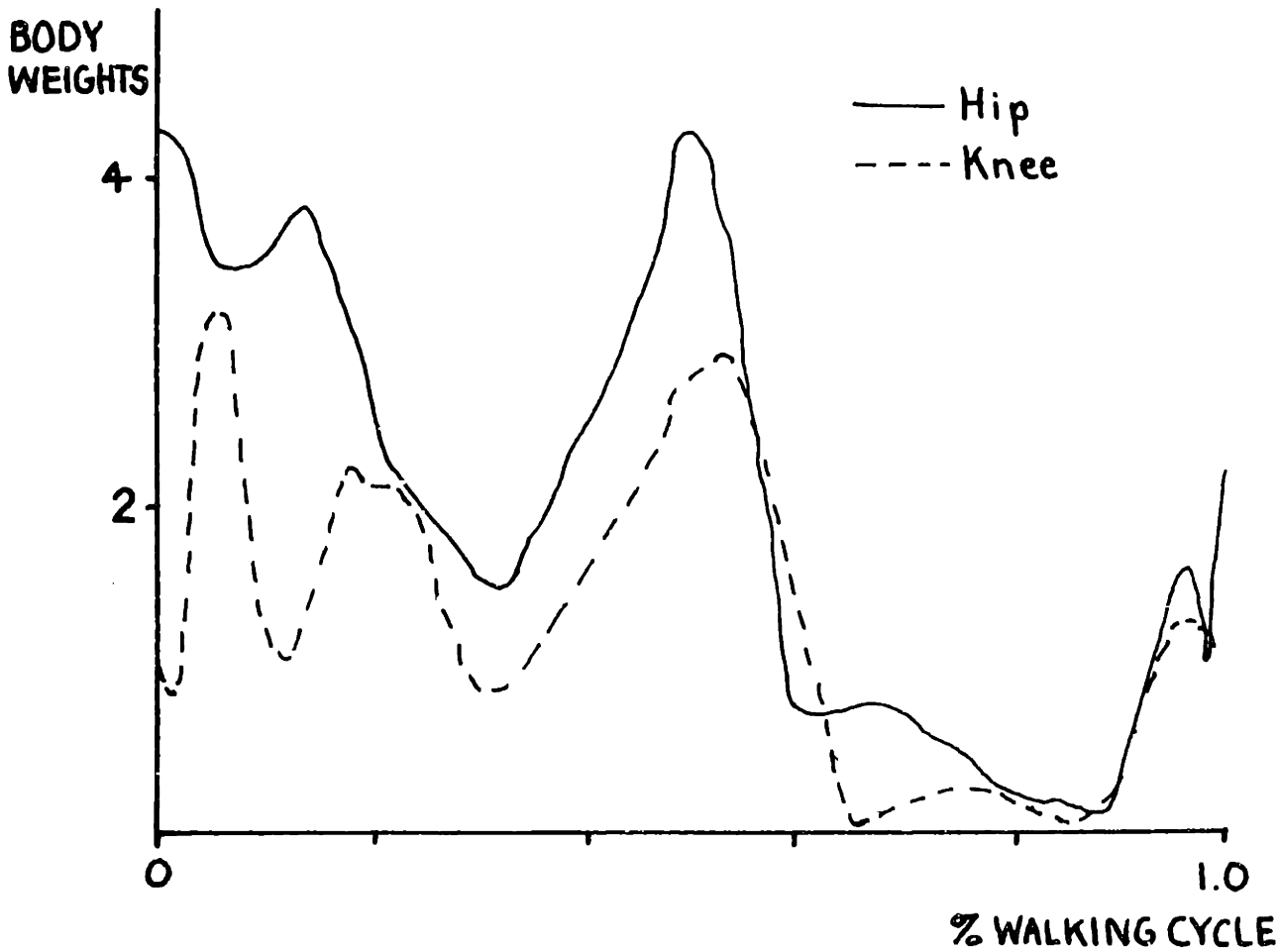

Fig. 2-3 Estimated Joint Forces (Hip data from Paul(1965), and knee data from Morrison (1968))

mine the distribution of forces among redundantly arranged muscles. DeLuca and Forrest (1973), after a detailed analysis of muscle attachment and joint center locations in the shoulder, were able to separate the total isometric abductive load at the shoulder into four separate muscular components by using suitably calibrated MES's from each muscle. The major determinant of this calibration was the maximum or physiological cross-sectional area of each, which was measured with the aid of x-rays. The use of MES data in this way for other than isometric contractions, however, was not investigated.

In a similar fashion, Cnockaert et al. (1975) performed a muscle force analysis for the elbow. Using certain observations about the anatomically evident function of each muscle, they predicted the moment component of each of three elbow flexors. Actual force data was not produced since the muscle moment arms were not considered. This work was also confined to isometric muscle use.

Research into the muscular aspect of locomotion, usually in the form of qualitative or functional studies, has been substantial, and only representative examples will be presented here. Elftman (1938) examined the role of muscle in the potential and kinetic energy changes that are a part of walking and in particular was concerned with the function of multiple joint muscles. Searching for an efficiency benefit from such an arrangement, it was speculated that two or three joint muscles were advantageous because they could combine the functions of several single joint muscles during walking, thus reducing the total amount of tissue that is active at any time. It was acknowledged, however, that there is a compromise involved since two joint muscles can also have unwanted effects at one joint while maintaining equili-

brium at another, which means additional single joint muscles must be used to counteract them. A later work by Elftman (1966) primarily concerned with the mechanics of muscle during gait, attempted to demonstrate the adaptation of muscle properties and their subsequent control to externally observed walking motions.

Cappozzo et al. (1976) performed a study similar to Elftman's (1938) but with much greater quantitative detail. Here the mechanical work done at each joint and the functional muscle group responsible for that work was calculated. This was in turn compared to energy variations of the body as a whole (and its subsystems). While the model developed was not applicable to the heel strike portion of the gait cycle, it did provide a possible means for comparison of pathological gait with normal gait on the basis of joint energy levels.

Pedotti (1978) studied the correlation between muscle activity as measured by MES's with muscle length changes and joint moments during walking. The results suggest the importance of controlling each muscle individually rather than as a functional group, and the hypothesis is forwarded that muscle use during locomotion is governed by a minimum energy criterion (see chapter 1).

Optimization studies of muscle function

Some of the first to attach the redundant muscle force problem "head-on" were Seireg & Arvikar (1973). Using a model of the musculature of the leg that included all significant muscles, the problem was posed as a linear program and solutions were found for static postures. Validity of the solution was examined with MES recordings from the accessible muscles. This

technique was then extended to a model of the essential musculature of the entire body in Arvikar's Ph.D. Thesis (1974) again examining various static postures, and has also been applied to quasi-static walking (Seireg & Arvikar (1975)). In all of the above cases an empirically defined optimal criterion that linearly combined muscle forces and joint moments was used with the relative weighting of the two determined iteratively on the basis of MES agreement. (However, inclusion of joint moments is possible only with double leg support postures, otherwise these moments are uniquely defined for a given posture and/or motion and cannot be varied).

At about the same time, Penrod et al. (1974) applied the linear programming formalism to the problem of muscle forces at the wrist and attempted to associate the basic solution properties of linear programming (explained in chapter 3) with the neurophysiological concept of reciprocal inhibition. (MES results presented in chapter 5 for the leg indicate that antagonist inhibition is not always present despite what the linear program predicts).

Application of linear programming to fully dynamic walking was done by Hardt (1978) and the suggestion was made that choice of the optimal criterion should be based on physiological considerations since empirical or iteratively established definitions were difficult to justify in light of the non-quantitative measure of muscle activity represented by MES's. Also suggested was a crude minimum muscle energy criterion that was shown to produce different, although not necessarily more correct, muscle force predictions.

Other applications of optimization techniques to the redundant muscle problem include that of Chao and An (1977) who investigated the effect of maximum force constraints on a linear programming solution, and Chao et al. (1976) where the solution to the force distributions in the finger was

sought. Pedotti et al. (1978) presented an in-depth investigation of the effect of both linear and non-linear cost functions on a muscle force optimization during walking, when constrained by maximum muscle forces. Their results indicate that the use of an optimal criterion that minimizes the square of the muscle stresses gives the best agreement with MES measurements and neural control models. Unfortunately, the effect of the velocity dependent maximum muscle stress constraints was not separated from the influence of the optimal criterion selection. They also strongly suggest that all data used in muscle force optimizations should come from a single individual. (Pedotti (1977) illustrated the importance of this since his results showed significant inter-subject deviations).

The effect of muscle stress constraints was investigated by Crowninshield (1978a) in a series of experiments on the flexor muscles of the elbow. The best agreement of the predicted forces with the MES's from the flexors was obtained by using maximum stress constraints that were set at levels approximately 20% greater than those that preclude any solution. Although a somewhat arbitrary figure, it reflects the concept of uniform, submaximal muscle stress as a criterion of use, but does so mostly through the use of constraints. The cost or penalty function used in these optimizations, in line with this philosophy, was a linear combination of muscle stresses.

This same technique was applied to leg musculature, primarily to examine the muscle and joint forces at the hip during walking (Crowninshield (1978b). Results were quite similar to those presented by others (Hardt (1978), Pedotti et al. (1978)) in that good MES agreement was found for some muscles

and poor agreement, usually characterized by lack of predicted activity, was shown in others. However, the resulting predicted joint forces may be sufficiently accurate despite this discrepancy since they are less sensitive to the individual muscles used than they are to the moment requirements at the joint.

Optimization has been used in applications other than muscle force determination during walking, quite often when the criterion of optimality is well defined beforehand. Considering the saccadic motion of the eyes, Clark and Stark (1975) proposed a time optimal (bang-bang) control strategy for the ocular muscles. Similarly, Hatze (1975) performed a time optimal study of muscle use in the leg during kicking motions. Experiments in the latter that examined the theoretical results showed excellent correlation in both muscle control (MES) and leg motion patterns provided the subject was trained to perform the task in the predicted amount of time. Hatze also produced predictions of muscle control parameters expressed as frequency of firing and number of active motor units.

Studies that were concerned only with optimal motion of the limb were performed by Chow and Jacobsen (1971) and Ayoub et al.(1974). The former produced accurate predictions of leg motion during walking based on a minimum joint power criterion, given only the kinematic constraints on the ends of the system and the leg structure. Ayoub et al. were concerned with upper extremity trajectories. They concluded that the total power involved in a movement is also the best mechanical criterion for limb movement.

Chapter 3 Development of a Thermodynamic Model of Muscle

Introduction

According to the minimum energy hypothesis formulation in chapter 1, the development of a means of quantifying muscle input power requirements based on variables that can be measured is necessary. In this chapter a model of muscle energetics is presented which permits such a calculation. Since the anticipated penalty function for the muscle force optimization will be in the form of a finite time integral, the integrand, that which is described here, should be the time derivative of energy, that is, power. The requirement is thus defined: given the output mechanical power of the muscle, predict the corresponding chemical power input. The output power will be defined by the product of the velocity of the muscles, fixed by the limb motions, and the force, which is the variable in the optimization process. With the proper model the optimization, as it iterates, chooses forces and thus specifies instantaneous output powers, can calculate the instantaneous chemical input power for use in the penalty function.

Consequently, the need here is to take instantaneous muscle output mechanical powers and predict the instantaneous chemical power for each active muscle. This defines a chemico-mechanical efficiency written here in terms of the mechanical power and the chemical power, the latter defined as the rate of change of the free energy of the reactions associated with muscle contractic

The model is restricted to muscle involved in steady state walking, both energetically and kinematically, and since the ultimate use is in a penalty function a relative inter-muscular rather than absolute measure of energy consumption is all that is required. The energy required to repair the tissue need not be included since it will not depend on the output. The

energy requirements of the activation process are also neglected since they are assumed to be a constant fraction of the energy used to produce mechanical work.

Modeling technique

Both the conversion of energy from one domain to another and energy transfer within one domain always involve dissipation or degradation of some of this energy to a non-useful form. Muscle contraction, which involves the conversion of chemical energy to mechanical energy is always accompanied by some heat production.

If the amount of energy dissipation were in constant proportion to the mechanical output, implying a constant mechanochemical conversion efficiency, the relative inter-muscular chemical energy input would be the same as the mechanical energy output. Accordingly, the only processes of concern here are those which cause the efficiency of conversion to vary with the mechanical state. The approach taken here is first to identify various stages of energy transfer and transduction within the muscle and then to examine the dynamics of these processes relative to the output of the muscle. In this way those processes which have finite but constant efficiencies are not included and only those whose dynamics are in frequency ranges compatible with the output and whose power magnitudes are significant need be considered. As with all models the description should be of minimal complexity for the accuracy required, especially considering the size of the anticipated optimization space.

Previous work

The following is not a rigorous review of muscle efficiency literature,

but rather is intended to indicate the present state of knowledge of muscle efficiency dependence on the mechanical output. The thermal and mechanochemical efficiency of muscle has been evaluated with heat and work measurements (e.g. Hill (1964)), and with chemical work-mechanical work measurements, (e.g. Kushmerick & Davies (1969)). Both of the above studies indicate that the efficiency is not constant but varies greatly with the output power and during contraction goes through a clear maximum (see figure 3-1). Equally significant is the well known difference between energy consumption when contraction occurs (the power producing mode) and the smaller but still positive energy consumption during active lengthening (the power absorbing mode) (Hill (1960)).

The experiments performed by these and other authors use standard loading of the muscle, either isometric or isotonic, and the efficiency dependence on the output (either force or velocity for maximal stimuli) is by definition static and process dynamics cannot be determined from the results. This is also due to the efficiency being defined either from the statically determined relationship between force and velocity as in the Hill data, or from the expression of efficiency as work rather than power ratios thereby filtering out any possible rapid dynamics. As static efficiency data sources however, these papers are outstanding and can serve as a data base for all models of muscle energetics.

When they are derived solely from these findings, however, quantitative models suffer from the problems common to all phenomenonological results, that of generalizability of the resulting empirical functions. In this case it is not known if the efficiency remains statically related to instantaneous force and/or velocity during normal movements or, alternatively,

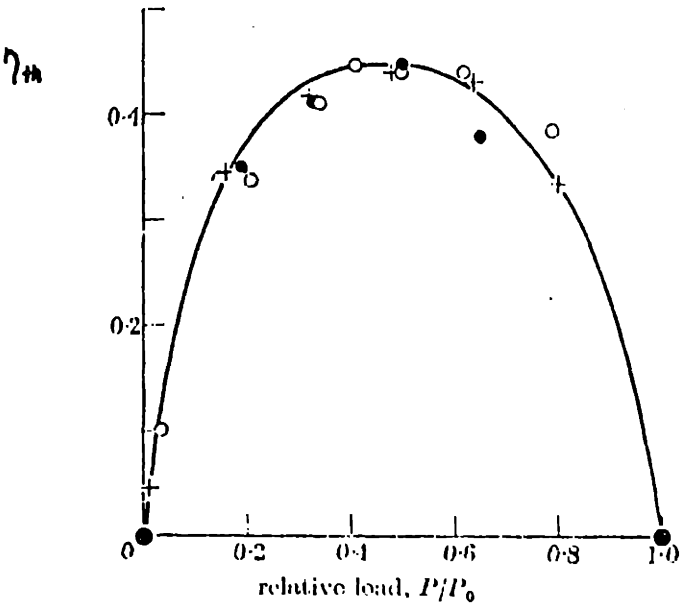

Fig. 3-1 Thermal Efficiency of Muscle as a Function of Force

The efficiency is defined as the ratio of the output mechanical work over the sum of this work and the heat released by the muscle. (From Hill(1964))

whether it is state dependent, i.e. dependent upon the previous history of the output.

Equally critical is the extrapolation of data taken, for example, from frog satorii to other muscle tissues from other species. The proper use of phenomenological data lies in the verification of physically based model results as well as to serve as an initial indication of the ultimate model form. Quite often the entire function of a model is to permit the generalization of specific empirical results without resorting to data extrapolation; this will prove to be the case here.

Summary of proposed model

The model to be described in this chapter is based on two significant findings: 1) All biochemical processes preceding that of the actual chemico-mechanical transduction are either slow enough to have no direct correlation with rapid variations in the output of the muscle and therefore have constant losses, or they have losses that are small compared to those of the contractile process, and 2) the dynamics of the chemico-mechanical transduction process are such that when operating under physiological conditions corresponding to walking the efficiency is in fact statically related only to the velocity of the endpoints of the muscle regardless of the loading profile, and this static function is well described by the empirical results described above. A recently developed model of actin-myosin dynamics is used to verify the later point and is also used to give chemical power output as a function of mechanical power both for active shortening and lengthening.

State dependence for the entire model arises in the transmission of mechanical power through the tendons which have compliance, hence energy stor-

age properties; however, the significance of this compliance to the present problem will be shown to be negligible.

Physical and energetic structure of muscle

Whole muscle can be divided into anatomically distinct structures, each of which has important links to the overall mechanical properties of the tissue. Likewise the chemical energy pathways have their own structure as does the critical chemico-mechanical transduction mechanism where the chemical and mechanical structures become indistinguishable. Starting with the anatomy, the entire muscle can be subdivided as illustrated in figure 3-2 with the smallest unit of contractile tissue defined as the sarcomere. It is in the sarcomeres that the muscle work originates, and the details of this process will follow.

Superimposed on the structure shown in figure 3-2 are the control or neural connections. The finest unit of control is the motor unit which comprises one motor nerve supplying a common signal to several muscle fibers. The "fan out" of this signal depends on the muscle's function and is correlated with the accuracy of control required versus the processing overhead. Actual transmission of the control signal from the myoneural junction to the sarcomere takes place along a system of tubular passages (T system) which provide continuity between the junction and the sarcoplasmic reticulum. In the latter structure, the transmitted electrical signal causes a change in the permeability of its walls and a subsequent diffusion of calcium ions into the sarcoplasm, (the fluid within the sarcomere). The calcium then triggers the chemical events necessary for contraction (Ebhashi et al. (1968)).

The flow of energy from the basic fuel of muscle (assumed hereafter to

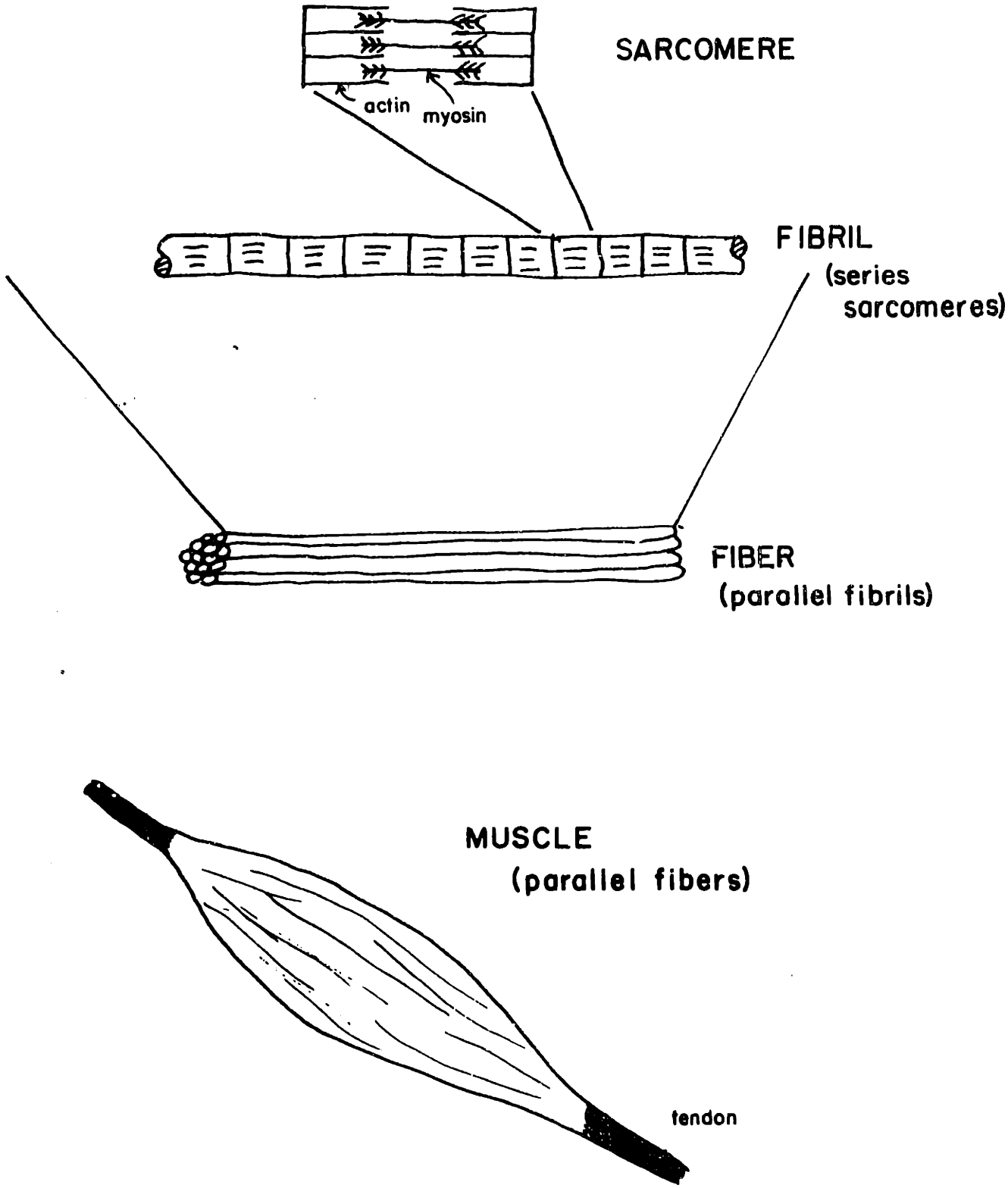

Fig. 3-2 Muscle Components and Configuration

be a glycogen monomer) to the mechanical energy output follows a series of well defined and frequently localizable pathways. For the purpose of this model these can be broken down into four serial groups separated both physically, and as will be established later, by their frequency range of operation. The four groups or components of this system are the:

1) aerobic and anaerobic rephosphorylation processes
2) Lohmann reaction system and ATP hydrolysis
3) chemico-mechanical transduction process (contractile proteins)
4) mechanical transmission elements

Since this model purports to be truly thermodynamic in nature, i.e. concerned with the dynamics of the energetic processes in muscle, the next four sections will deal in depth with each of these components by detailing their function and by assessing their contribution to the empirically demonstrated variable efficiency of muscle. Again the approach of the modelling technique is to first identify the possible sources of dissipation in each system and then to evaluate the dynamics of these sources relative to the observable outputs of muscle, for example the force, length and velocity as seen at the boney attachments.

Aerobic and anaerobic phosphorylation of ATP

The basic function of this process is to recharge or regenerate the basic fuel necessary for contraction: adenosine triphosphate (ATP) from the products of ATP hydrolysis, adenosine diphosphate (ADP) and inorganic phosphate (P_i). Operating against an unfavorable entropy gradient for the resynthesis of ATP from ADP, the free energy of glycogen is used in a long series of enzymatically catalyzed reactions which eventually produce ATP.

This basic process of glycolysis can be described by the net reaction:

$$\frac{1}{n}\ (C_6H_{10}O_5)_n + 3ADP + 3P_i \rightarrow 3ATP + 2Pyruvic\ Acid + 2H_2O \qquad 3\text{-}1$$

(Glycogen) (hydrogen carriers have been omitted)

In the absence of oxygen the pyruvic acid becomes lactic acid which is very slowly removed from the local tissue. In the presence of oxygen the pyruvic acid can enter the tricarboxylic acid cycle (TCA) and the cytochrome chain within the mitochondrial bodies, undergoing the net reaction:

$$Pyruvic\ Acid + 18\ ADP + 18\ P_i + 3\ O_2 \rightarrow 18\ ATP + 3\ H_2O + 3\ CO_2 \qquad 3\text{-}2$$

These two processes produce either 3 ATP per molecule of glycogen under anaerobic conditions or 39 ATP per glycogen with aerobic metabolism, as can be seen from the above stoichiometry. Both these reactions are localized in the sarcoplasm and the TCA cycle requires both a good local blood supply for sufficient oxygen plus the mitochondrial bodies, which are distributed throughout the muscle cells in varying concentrations depending upon the dominant use of the muscle.

Margaria (1976) has shown that despite the difference between these two reactions (3-1 and 3-2) the overall thermal efficiency of both are nearly identical, suggesting that the natural choice of these mechanisms is not based on energy consumption but rather on power or energy rates. Because of these transport property differences muscles used for fast, infrequent activity generally use the anaerobic processes and are limited in contraction duration by the rate of diffusion of lactic acid out to the circulation. Conversely, low power, endurance muscles are marked by high vascularization

and large numbers of mitochondria.

The thermodynamics of these systems, as it relates to the problem at hand, can be dealt with on the basis of the following findings. The first is that the enzymatically catalyzed reactions comprising the rephosphorylation process, (see Carlson & Wilkie (1974), pp 96 and 99 for details), each operate at near equilibrium conditions. Application of the first law of thermodynamics to each of these reactions yields:

$$\Delta G = \Delta H + T\Delta S_{reversible} \qquad 3\text{-}3$$

ΔH = heat of reaction (enthalpy)
ΔG = Gibbs free energy change
ΔS = Entropy change
T = Temperature

Therefore, ΔG is the available energy under reversible or equilibrium conditions. Using elementary non-equilibrium thermodynamic principles, (see Katchalsky & Curran (1965)), the dissipation of this free energy as the reaction proceeds at a finite rate, if no useful work is done i.e. the reaction is autonomous, is described by the entropy production:

$$\frac{dS}{dt} = \frac{\alpha J}{T} \qquad 3\text{-}4$$

α = reaction affinity or driving potential
J = reaction rate or molar flow rate
where α indicates how far the system is from equilibrium.

The reactions in the phosphorylation chain, however, operate near equilibrium and thus, by the definition of equilibrium $(\alpha_{equil.} = 0)$ at low affinity. Therefore, very little entropy production or dissipation occurs. Apparently the need for higher rates of ATP is fulfilled by a greater

density of mitrochondrias, i.e. with parallel reactions, rather than by varying the rates of the cycles over large ranges. (There is some evidence, that part of the phosphorylation chain operates far from equilibrium, but the following finding will prove more significant).

The second finding is that the overall speed of the reaction chain is slow. This of course can be inferred from the low reaction affinities and the overall size of the reaction chains. Evidence for the low rates comes from the studies of D.K. Hill (1940), and Dydynska and Wilkie (1966) both of which showed that the aerobic recovery from sustained contraction in frog muscle exhibits characteristic time constants on the order of twenty minutes @ 0C. or about four to five minutes @ 30 C., (see figure 3-3). It would appear, therefore, that during cyclic muscle activity, the rate of the rephophorylation processes will not follow the muscle output, but will instead operate at the average power requirements of the muscle cycle.

Since they are both time averaging and near equilibrium, the phosphorylation processes, although they have finite but constant losses, need not be considered further under the restrictions of the present model. They do contribute to the overall efficiency of fuel conversion in muscle, but their low pass filter behavior leaves them out of an instantaneous efficiency expression when the assumed cyclic use of muscle is considered.

The Lohmann reaction - local ATP storage and ATP hydrolysis

The principal reaction associated with muscle contraction is the enzymatically catalyzed hydrolysis of ATP to ADP:

$$ATP + H_2O \xrightarrow{ATPase} ADP + P_i \qquad 3\text{-}5$$

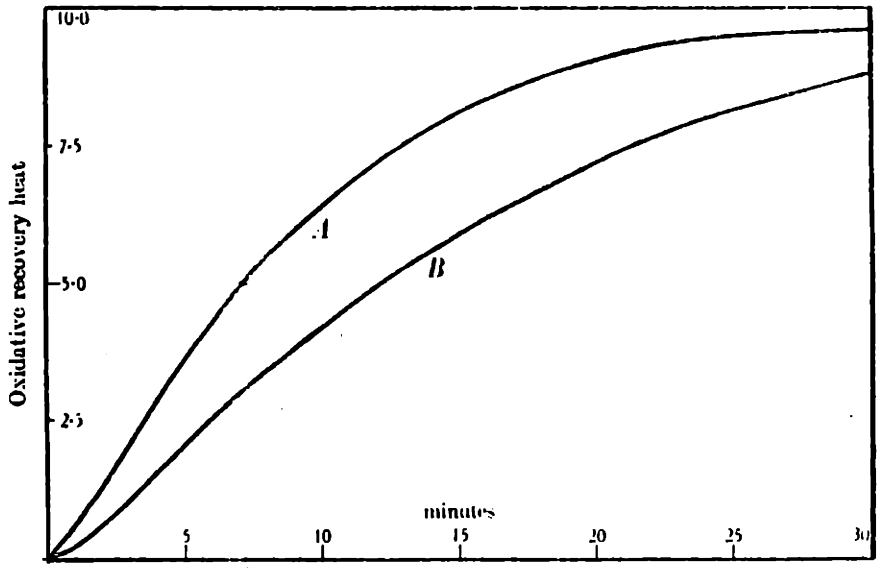

Oxidative recovery heat following a 12 sec. tetanus at 0° C. A, *p*H 7·2; B, *p*H 6·2.

(from Hill(1940))

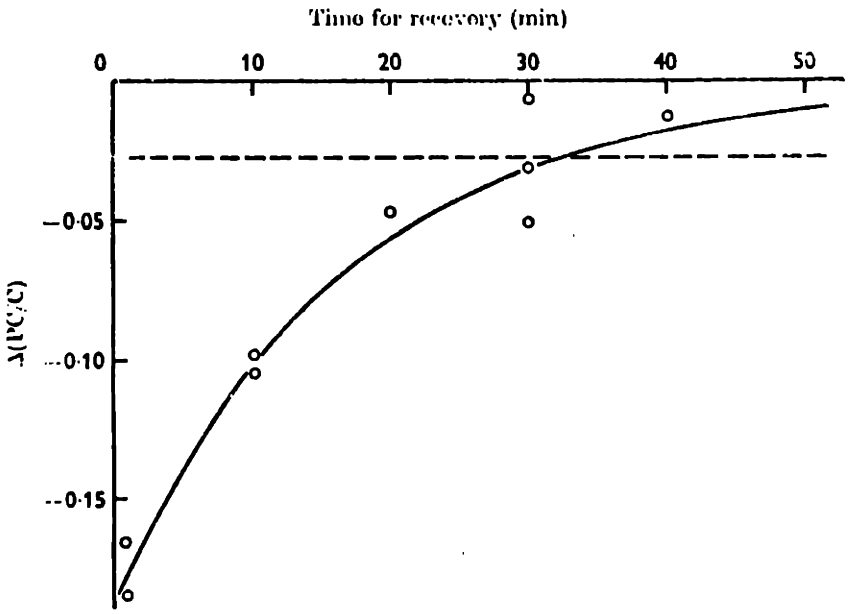

Recovery of phosphocreatine level in oxygenated Ringer fluid at 0° C, following a 30 sec tetanus. Ordinates: difference in (PC C), experimental minus control. Abscissae: time in min. The curve is an exponential with half-time 11·5 min. The horizontal interrupted line shows the standard deviation of Δ(PC, C) when both muscles are at rest.

(from Dydynska & Wilkie (1966))

Fig. 3-3 Aerobic Recovery Rates

Associated with this reaction is a large free energy change (-43 KJ/mole in vivo; Kushmerick, et al. (1969)). It is this free energy which is ultimately converted to useful work and heat. (The details of this conversion process will be the concern of the next section).

Coupled to this hydrolysis reaction is a similar breakdown of creatine phosphate (PCr) to free creatine (Cr) and inorganic phosphate (P_i):

$$PCr + H_2O \rightarrow Cr + P_i$$

also associated with a high free energy change.

When the two above reactions are coupled they form the overall reaction:

$$PCr + ADP \rightleftarrows ATP + Cr \qquad 3\text{-}6$$

the so-called Lohmann reaction. This system serves as a local means of limited but rapid phosphorylation of ADP to ATP. The construct of bond graphs helps to elucidate the coupling of systems (5) and (6) by detailing the various energy interactions in both the chemical and mechanical energy domains. As drawn in figure 3-4, the phosphorylation processes described in the previous section are represented as a source of ATP and a sink for ADP and P_i. The rate of these sources would actually be the average requirements of the system, hence they are not true reservoirs. The graph is characterized by capacitance or chemical potential storage of ATP, ADP, P_i, PCr, and Cr. The multiport reaction R's in the system represent the reaction ports of the ATP hydrolysis and the Lohmann system as well as the energy transduction of reaction free energy to heat and useful work. From this structure, the function of the Lohmann reaction can easily be seen. This function is illustrated by the following scenario.

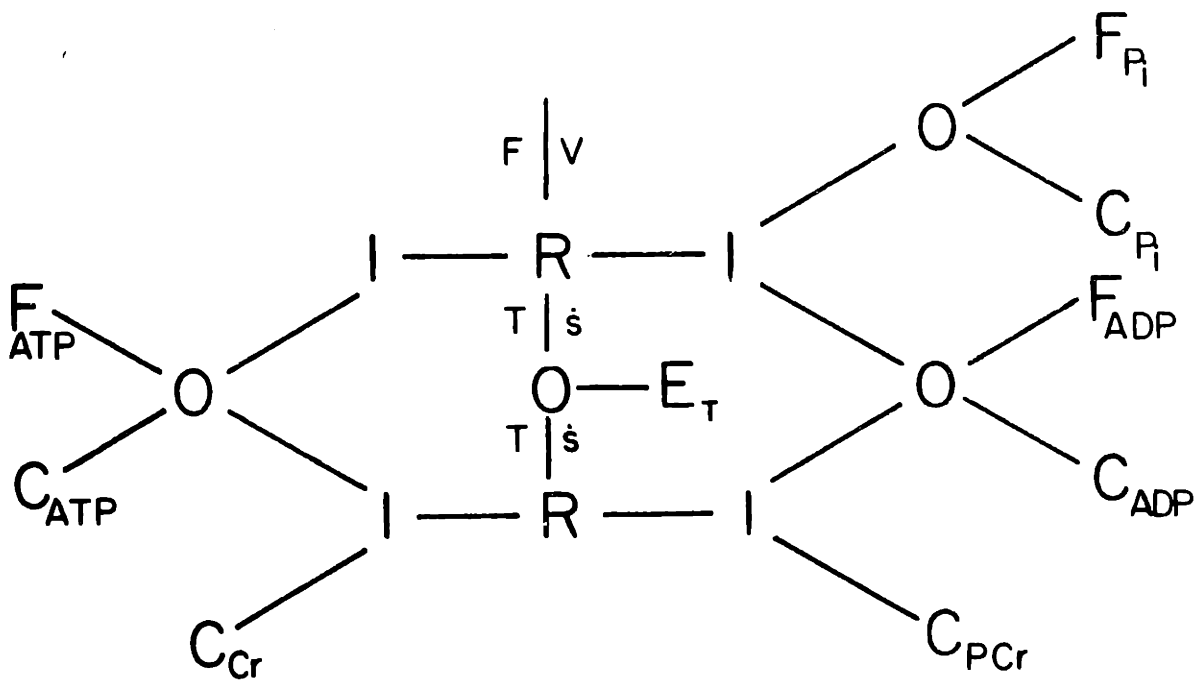

Fig. 3.4 Bond Graph of the Lohmann and ATP Hydrolysis Reactions

Each reaction is centered about a multiport R which serves as a "power divider",and in the case of the ATP hydrolysis reaction this division is among chemical, thermal and mechanical power. (For a complete treatment of bond graphs, including their application to chemical systems, see Paynter(1961))

The C's are species concentrations, the F's are flow sources (used here as an approximation to the slow phophorylation process) and the thermal power is represented by the power pair temperature(T) and entropy flow (ṡ).

If the muscle is contracting cyclically the rate of the ATP hydrolysis will be closely coupled to this activity. (This will be demonstrated in the next section). If no means of phosphorylation existed the ATP would be rapidly depleted and contraction would cease as the hydrolysis reaction affinity or driving potential reached zero. However, the slow constant steady-state flow of ATP resulting from glycogen metabolism would prevent this depletion, but the concentration and therefore the chemical potential of ATP would fluctuate in harmony with the muscle output cycle. Now introduce the Lohmann reaction. This reaction, which operates rapidly and near equilibrium (Carlson & Seiger (1959)), will proceed driven either by a decreasing ATP concentration or an increasing ADP concentration, owing to the following considerations:

$$r_{Lohmann} = \phi(\alpha_{Lohmann})$$

$$\alpha_{Lohmann} = \mu_{ADP} + \mu_{PCr} - (\mu_{ATP} + \mu_{Cr})$$

$$\mu_i = RT \ln(c_i/\hat{c}_i) \qquad 3\text{-}7$$

r = reaction rate

ϕ = general monotonic function

c_i = concentration of i

$\hat{c}_i$ = equilibrium c_i

Therefore the events of contraction will increase the Lohmann reaction affinity and cause it to produce ATP. If the rate of this process is fast enough, the concentration of ATP will not vary over the cycle, thereby maintaining the high ATP reaction affinity apparently necessary for contraction. Empir-

ical confirmation of the constancy of ATP concentration during and after contraction comes from Carlson & Wilkie (1974) p 92.

Upon completion of activity, the flow of ATP from the glycolytic processes increases the concentration of ATP locally. Since the ATP reaction is effectively shut off, i.e. no muscle activity is occurring, this concentration increase will immediately reverse the Lohmann reaction and the "new" chemical potential will be stored by concentrating PCr, and the rapidity of the Lohmann reaction, even in the reverse direction, will prevent any large variation in the concentration of ATP. The overall functioning of this system with a cyclic (or transient) muscle output is shown graphically in figure 3-5. One consequence of this system's dynamics is that PCr can be, indeed must be used as a measure of energy use in <u>in vitro</u> muscle experiments when biochemical assays are taken (e.g. Curtin et al. (1974)). When the phosphorylation and Lohmann reactions are inhibited, the ATP concentration begins to vary directly with muscle use as would be expected from the above discussion (e.g. Kushmerick et al. (1969)).

The specific dynamics of this system alluded to above can be quantified directly from the bond graph, where the constitutive relation between the power pairs: chemical potential (μ) and molar flow (J) for a chemical capacitor is described by:

$$\mu_i = RT \ln(c_i/\hat{c}_i)$$

$$J = \frac{d}{dt}(c_i) \qquad 3\text{-}8$$

where c_i = concentration of i

$\hat{c}_i$ = equilibrium c_i obtained from $K_{eq} = \frac{c_{products}}{c_{reactants}}$

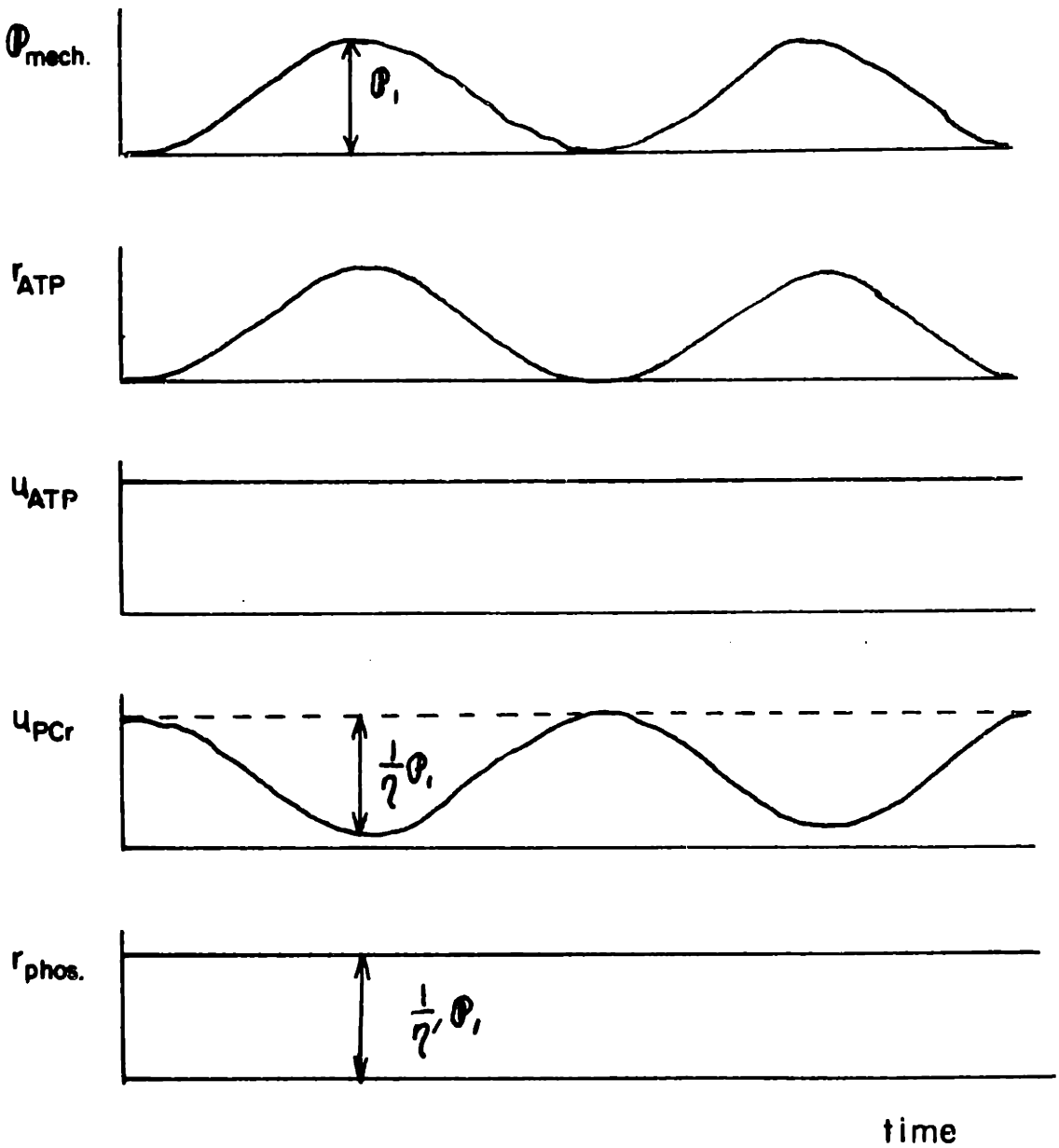

Fig. 3-5 Operation of Muscle Reaction systems for Cyclic, Steady-State Power Output

$\mathcal{P}$ is power, r_{ATP} is the rate of the ATP hydrolysis reaction u's are chemical potentials and r_{phos} is the rate of the phophorylation process. Notice that the Lohmann reaction acts as a filter for the ATP reaction whose chemical potential remains constant despite the varying output.

The reaction affinity is essentially the potential cross the reaction and is defined as the difference between the sum of the reactant potential and the sum of the product potentials:

$$\alpha \equiv \mu_{reactants} - \mu_{products} \qquad 3\text{-}9$$

The rate of the reaction is the constitutive relation for the multiport reaction R. A typical example of such a relation is an uncatalyzed reaction with Arrhenium kinetics described by:

$$(J = k(\exp(\alpha_F/RT) - \exp(\alpha_R/RT)) \qquad 3\text{-}10$$

where α_F = sum of reactant potentials

α_R = sum of product potentials

k = empirically determined constant

However, both the reactions involved here are characterized by enzymatic catalysis and have much more complex kinetics than the above example. To avoid this unnecessary complication of the model development, the concept of frequency separation or relative speed of response is again useful.

<u>In vitro</u> measurements of the initial rate of ATP hydrolysis have shown that it proceeds with characteristic times of order 2 milliseconds, (Gergly (1977)). Based on this consideration it is apparent that ATP hydrolysis does not rate limit the contraction process, whose mechanical outputs proceed (as will be shown later) with characteristic times of order 100 milliseconds. The ATP reaction kinetics are therefore best defined here by the kinetics of the contractile mechanism which can be expressed by the static power bal-

ance

$$\alpha J_{ATP} = P_{mech} \frac{1}{\eta_{cm}} \qquad 3\text{-}11$$

where P_{mech} is the intantaneous mechanical power output

η_{cm} is the chemical-mechanical conversion efficiency,

and αJ_{ATP} is the input chemical power

The kinetics of the Lohmann reaction are characterized by initial rates up to 10 times that of ATP (Schmerlick (1973), Kuby et al. (1954)). Following the same argument applied above, the rate of the Lohmann reaction will be determined by the ATP hydrolysis rate which is in turn governed by the required output of the muscle. Therefore the dynamics of these two fast reactions need not be included since they will follow exactly the requirements of the contractile mechanism. Having successfully obviated modelling enzyme kinetics in detail, the original question of relative dissipation must now be addressed. As developed in the previous section, the entropy production or dissipation of free energy depends both on the reaction rate and the driving potential or affinity of the reaction. From the above it follows that both the ATP hydrolysis and Lohmann reactions will have near-identical rates during contraction, hence, their relative dissipation depends only upon their relative affinities.

From equation 3-8, it is clear that the chemical potential is not a function of a species absolute concentration but rather that concentration relative to the equilibrium concentration. If we consider the metabolic phosphorylative processes to be turned off, the Lohmann reaction - ATP hydro-

lysis system is closed to outside mass flow. At rest, the Lohmann reaction is at equilibrium with the concentrations:

$$\hat{c}_{ATP} = 3\mu m/gr$$

$$\hat{c}_{ADP} = 0.0375\ \mu m/gr$$

$$\hat{c}_{PCr} = 20\ \mu m/gr$$

$$\hat{c}_{cr} = 5\ \mu m/gr$$

These assume an equilibrium constant Keq, of 20 . (Data from Carlson and Wilkie (1974)).

The hydrolysis reaction, since it can be "switched off" and inorganic phosphate removed (Kushmerick (1969)) is not necessarily at equilibrium. Assuming an in vivo free energy change of 43.9 KJ/mole

$$\text{we get } K_{eq} = e^{-\Delta G/RT} = 2.5 \times 10^{7}$$

$$\text{Now given that } \hat{c}_{ATP} = 3\ \mu M/gr$$

$$\text{and } \hat{c}_{ADP} = 0.0375\ \mu M/gr$$

$$\text{we get } \hat{c}_{P_i} = 2.0 \times 10^{9}/\mu M/g^{2}$$

However, Kushmerick reports resting values of $c_{Pi} \simeq 2.27\ \mu M/gr$. This means that the ATP hydrolysis reaction is far from equilibrium as reflected in the reaction affinity

$$\alpha_{ATP} = \mu_{ATP} - \mu_{ADP} - \mu_{pi} = 0 - 0 - RT\ \ell n \frac{2.27}{2.0 \times 10^{9}}$$

$$\text{or} \quad \alpha_{ATP} = 54.0 \frac{mJ}{\mu mole}$$

Also since $\hat{c}_{pi}$ is so large, α_{ATP}, which arises mostly from μ_{Pi} will hardly change under physiological condition.

Conversely, since maximum power outputs/gm muscle tissue are in the range of

$$10 - 34 \frac{mJ}{sec - gm(muscle)} \qquad \text{derived from Hill (1964)}$$

and since the mechanical power - ATP power relationship can be expressed as in equation 3-11:

$$\alpha_{ATP} J_{ATP} = \frac{1}{\eta_{mc}} P_{mech},$$

we see that typical J_{ATP} values will be

$$J_{ATP} = \frac{\frac{1}{\eta_{cm}} P_{mech}}{\alpha_{ATP}} \simeq \frac{\frac{1}{0.5} \times 20 \frac{mJ}{sec \cdot gm}}{54 \frac{mJ}{\mu mole}} = 0.74 \frac{\mu mole}{sec \cdot gm}$$

The Lohmann reaction affinity

$$\alpha_2 = \mu_{PCr} + \mu_{ADP} - \mu_{Cr} - \mu_{ATP}$$

given these flows over a one second period, will never accumulate enough material to match the ATP affinity even to within several orders of magnitude.

The consequence of this is that the entropy production (see equation 3-4) of the Lohmann reaction will be much less than that of the ATP hydrolysis process and the latter will, therefore, be the main determinant of the overall system efficiency.

In closing this section it should be noted that the reaction systems illustrated here are greatly simplified from their true and complete in vivo forms. As illustrated by Woledge (1972) the contraction of muscle and the concomitant biochemical reactions can involve seven or more separate reactions including buffering reactions and less significant reactions involving the phosphorylated compounds (such as the "emergency" myokinase reaction: $2ADP \rightarrow ATP + AMP$ and the accompanying reaction which allows this otherwise slow reaction to proceed). However, the major reactions detailed here appear to be the most significant ones energetically (Woledge (1971)), hence the most important to the present analysis.

As to the extent of knowledge of the biochemical processes in muscle, one present dilemma involves the discrepancy between the observed total output of muscle (heat + work) and the in vivo free energy release of the PCr, (or ATP) hydrolysis reaction, which can be taken as an indication of the total energy consumption. Repeated experiments and analyses (see Woledge (1972), Curtin et al. (1974) and Homsher (1975)) have concluded that this free energy release is insufficient to account for the observed muscle output. (All other rephosphorylation reactions were inhibited in these experiments). At present this discrepancy can apparently be accounted for by a constant "conversion" factor (Kushmerick (1977)), therefore the impact on this analysis is negligible.

It has now been established that the processes up to but not including the ATP hydrolysis do not contribute significantly to the variable efficiency observed in muscle. However, while the high affinity of the ATP reaction provides large amounts of free energy for conversion to mechanical, it also creates the opportunity for degradation of large amounts of this

energy. It would appear that the major source of the variable dissipation which is responsible for the variable efficiency is the mechanochemical transduction process itself. This system will be addressed in the next section.

Mechanochemical energy transduction - the actin myosin system

The central role of muscle, that of producing mechanical work from chemical energy, was represented in the bond graph of the previous section (figure 3-4) by an element with four power ports. This element divides the input chemical energy between the chemical products, the mechanical work output and the heat produced. The process by which this division takes place has long been debated and only recently have models been developed which are based on the microstructure of the system.

Since the previous section established its importance to the variable muscle efficiency, the concern of this section is with the analysis of the energetics of the transduction process using current state of knowledge of sarcomere models based on the sliding filament concept of Huxley (see Mommaerts (1960)).

The microstructure of the sarcomere, the smallest subunit of muscle, is illustrated in figure 3-2. Long filamentous protein molecules, actin and myosin, interdigitate to form the characteristic striations of skeletal muscle. The thick filaments (myosin) appear to "float" between the thin actin filaments which are attached back to back at the Z line. The present theory is that myosin molecules attach to actin, and in the presence of ATP (or actually its bound products of hydrolysis) changes its conformation so as to cause strain in the myosin and eventually cause relative sliding of the fil-

ments. More precisely, the myosin has been shown to have three distinct regions: an aglomeration region (LMM), a free and possibly elastic region (HMM S1), and a pair of globular heads (HMM S2), see figure 3-6. As shown in figure 3-6, a single myosin molecule, or rather its globular head, can attach to a parallel actin fiber and then rotate causing strain in the S1. Morales (1972) notes that the S1-S2 junction remains a free pivot during contraction, therefore the apparent torsional work is done at the actin-myosin interface. (The actual mechanism of the movement is unknown. Some theories include McClare's (1972) molecular coupled oscillaters, used to explain the high efficiencies of transduction, and Harrington's (1971) concept of phase charges from crystalline to amorphous states.)

Corresponding with these mechanical events are a series of biochemical events which as described by Morales follow the sequence:

$$\underset{1}{M\cdot ATP} \quad \underset{2}{M\cdot ADP+P_i} \quad \underset{3}{Act\cdot M^{*}\cdot ADP+P_i} \quad \underset{4}{Act\cdot \overset{*}{M}\cdot ADP+P_i} \quad \underset{5}{Act\cdot M^{*}} \qquad 3\text{-}13$$

where: M= myosin

M^{*}- $\overset{*}{M}$ indicates a conformational change causing the work.

Act = actin

(Notice that the hydrolysis of ATP from step 1 to step 2 is somewhat removed from the actual process of work production. Also the transition from step 5 to 1 indicates that the binding (but not hydrolysis) of ATP is necessary for dissociation of actin and myosin and in its absence they will in fact spontaneously combine (Lehninger (1975)).

Combination of these biochemical facts with mechanical structure of the system permits the dynamics of this process to be analyzed. The discussion

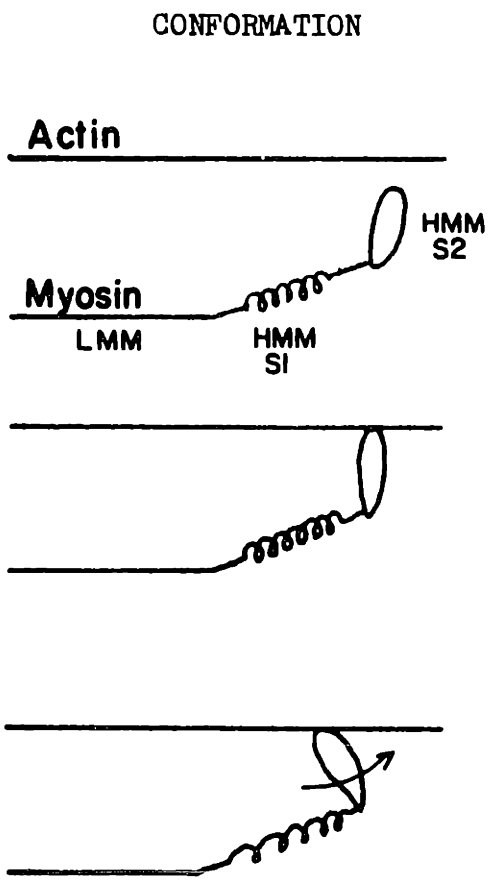

Fig 3-6 A Minimum Actin-Myosin Cycle

The elastic element is assumed to be in HMM S1 but may also reside in LMM. (LMM, HMM S1 & HMM S2 are substructures within the myosin molecule.)

that follows is based on the work of Wood (1976) and Julian et al. (1974). Since it is more intuitive, the physically based model of Julian will be used although the describing equations used in later simulations are from Wood. The major difference between the two is that Wood extended the Julian model to the active lengthening region using the general statistical mechanical theory of muscle contraction developed by T. L. Hill (1974).

The basic concept of the Julian model is description of cross bridge populations as they cycle following the pattern discussed above. A biochemical sequence, such as the five steps of Morales, (equation 3-13), is first simplified to a three state biochemical model shown in figure 3-7. The five steps are lumped into one detached state (steps 1 and 2), and two attached states, one with no strain (steps 3), and one strained state (steps 4 & 5). By considering the entire population of cross bridges in a half sarcomere (~11,000), a statistical approach can be taken, where the transition from one state to another is governed by probability distributions within each state and by the rate constants governing the transition speed (see figure 3-7). For consistency and for anticipated future model refinements, this reaction system is also diagrammed using bond graphs. The lumped chemical capacitors and the multiport R's now have feedback from the strain producing reaction and are position as well as time dependent. This graph will dovetail with the graph of figure 3-4 to form a complete graph of muscle energy interactions. The bond graph also explicitly shows the role of ATP in providing the driving potential for the cycle, and can be used to isolate entropy production sites if desired. Because of their complexity and availability in the original references, the resulting system equations and the details of their derivation are contained in Appendix A. Also included is the numeri-

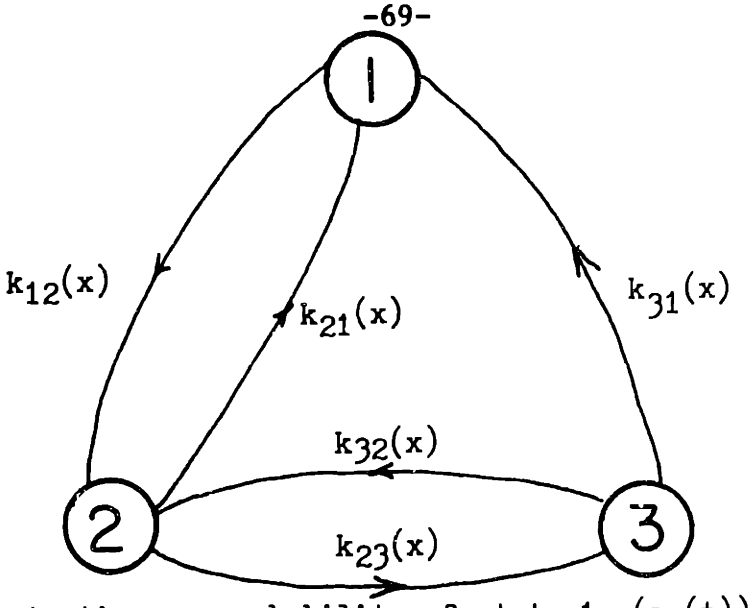

States

1-Detached

2-Attached, no strain

3-Attached, strained

1 - concentration or probability of state 1 $(p_1(t))$
2 concentration or probability of state 2 $(p_2(x,t)$
3 concentration or probability of state 3 $(p_3(x,t)$

k_{ij} - rate constant in direction i-j

x - relative displacement of AM when attached

Biochemical State Diagram for Actin & Myosin (from Wood(1975))

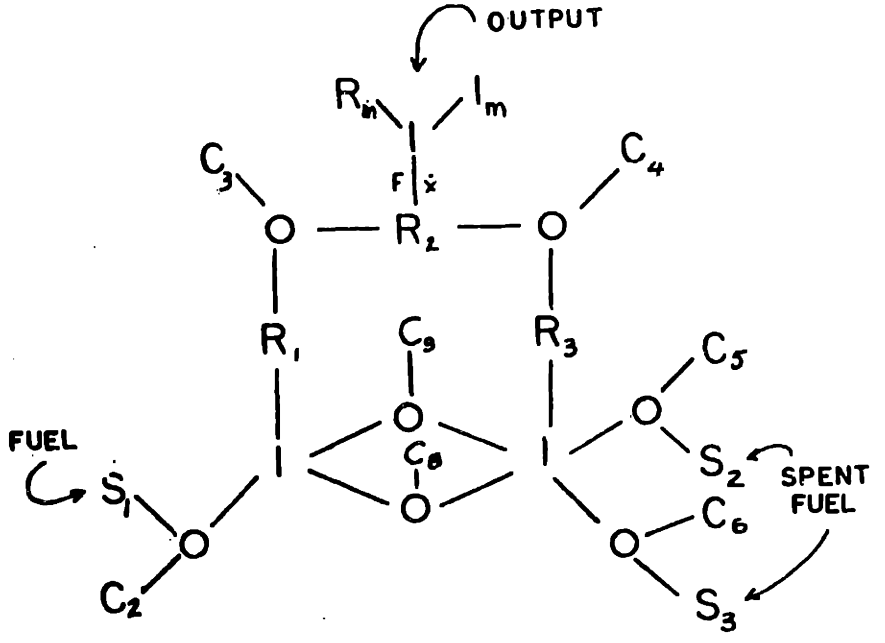

FLOW SOURCES

S_1: ATP

S_2: P_i

S_3: ADP

CHEMICAL CAPACITORS

C_1: Cr

C_2: ATP

C_3: AM*+ATP

C_4: AM*+ADP·P_i

C_5: P_i

C_6: ADP

C_7: PCr

C_8: A

C_9: M

Equivalent Bond Graph including ATP Driving Reaction

Fig.3-7 Actin - Myosin Dynamic Models

cal solution technique used for the simulations here.

The chemical energetics of the model are derived from the rate of ATP splitting represented by the transition from state 3 to state 1. This corresponds to the transition from Morales steps 4 and 5, where ATP's products are released, to step 1 where ATP is bound to myosin and hydrolyzed. By assigning a free energy change to this reaction (e.g. 43.9 KJ/mole from Kushmerick) the rate of energy consumption can be found from:

$$\dot{G} = \frac{dG}{dt} = \mu_{ATP} \; k_{31} \; p_3(x,t) \; dx \qquad 3\text{-}14$$

where μ_{ATP} = free energy of hydrolysis of ATP

p_3 = distribution of state 3 concentration in space and time

k_{31} = rate constant

It is now possible to calculate the dynamic or instantaneous mechanochemical efficiency from the definition:

$$\eta_{mc}(t) = \eta_{mc} \cdot (t) = \frac{F(t)v(t)}{\dot{G}(t)} \qquad 3\text{-}15$$

For the isovelocity case, the case investigated by Hill (1964) and Kushmerick et al. (1969), Wood showed that the above three state actin myosin model (hereafter referred to as AM model), produced a steady state efficiency versus force curve of similar shape to that of Hill, but it was nearly an order of magnitude low in its peak efficiency value, (0.1 vs. 0.6 for Hill and 1.0 for Kushmerick). Wood (1977) has attributed this discrepancy to the insufficiency of the three state approximations as well as the restriction of the attachment transitions to cases where the strain in the elastic element is zero, when in fact it can attach at finite strains due to Brownian motion in the unattached myosin. Unfortunately, to accomplish these modifications

requires a two or threefold increase in complexity and therefore must be ruled out under the guidelines of the present analysis. However, if the present AM model provides the proper static efficiency changes with mechanical output, i.e. produces a properly shaped curve, it could be used with some confidence to generalize the static empirical data to the dynamic case anticipated in the use of muscles during walking.

The following simulations using the AM model curve were performed to evaluate both the static efficiency curve and the dynamics of the instantaneous efficiency under various conditions of loading. The system describing equations were solved numerically using the approximation described in Appendix A. In the simulations that follow conditions were chosen which roughly approximate muscle activation in vivo by introducing a step stimulus and a constant shortening velocity. The stimulus may not be a step in vivo, but it was chosen here as a standard test input for dynamic systems. The conditions of the simulation were, therefore

1) zero initial conditions, i.e. no stimulus:

$$p_2(x,0) = p_3(x,0) = 0$$
$$p_1(0) = 1 \qquad 3\text{-}16$$

2) step stimulus to maximum at $t = 0+$

3) Constant shortening velocity for the duration of simulation.

Static efficiency curves were generated by running the simulations at various velocities and recording the steady state efficiency values. The actual curves generated will be presented later, but the static or steady state efficiency curve is plotted in figure 3-8a. Notice that the abscissa

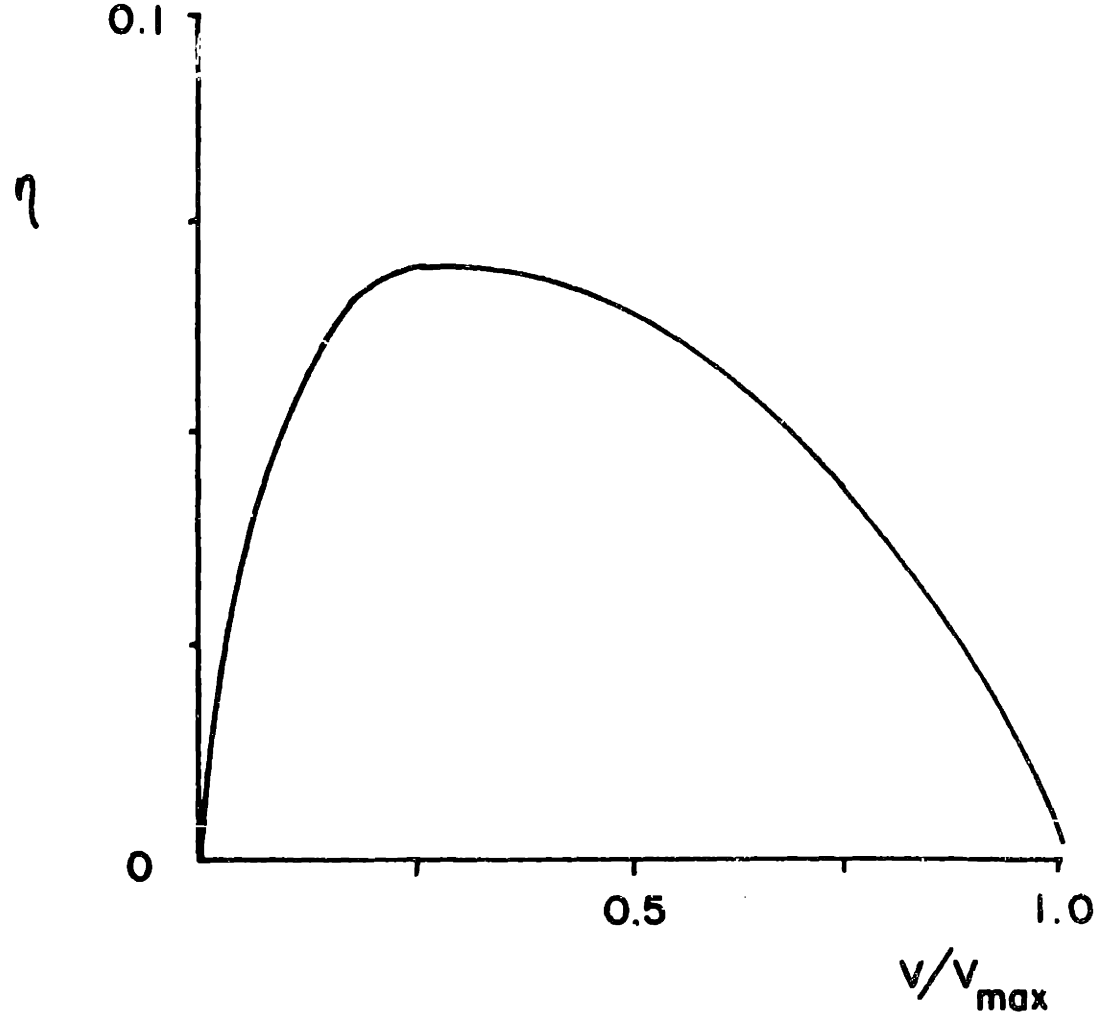

Fig. 3-8a Steady State Efficiency for the AM Model

variable is now v/v_{max} rather than F/F_{max} as used by Hill (1964). The unique relationship between these two quantities affords this interchangeability and it will be shown later than v/v_{max} is the only relevant quantity when viewing the mechanical state of the muscle attachment points.

As a check of the shape of the efficiency curve of figure 3-8a it has been cross plotted in figure 3-8b against the curve of Hill (1964), and the data points of Kushmerick et al. (1969). Each set of data has been normalized vertically with respect to its maximum efficiency.

The AM model curve and the curve of Hill show excellent agreement and the data points of Kushmerick, given their statistical nature, also appear to follow the predicted trends. Based on this result, the AM model is assumed to act as a general predictor of instantaneous muscle efficiency. It will be used not only to extend the static empirical data to dynamic situations, but will also be used to predict the energy consumption involved during actively lengthening, an area not covered by the presently available efficiency data.

To evaluate the dynamics of the instantaneous efficiency, it is necessary to specify stimulus and loading conditions on the model's half sarcomere that are similar or bear a relationship to the anticipated output state of the muscle during normal walking.

From EMG data (Paul (1971)), the period of muscle use can be characterized by 20-50% of the total walking period. Average walking periods are about 1 second long, therefore muscle is active for times of the order of 200-500 milliseconds. The nature of the stimulus seen by the muscle is not well known, but at the sarcomere level it is clearly quantal in form, characterized by action potential spikes whose frequency and spatial distribution to other motor units (and therefore other sarcomeres) can be varied.

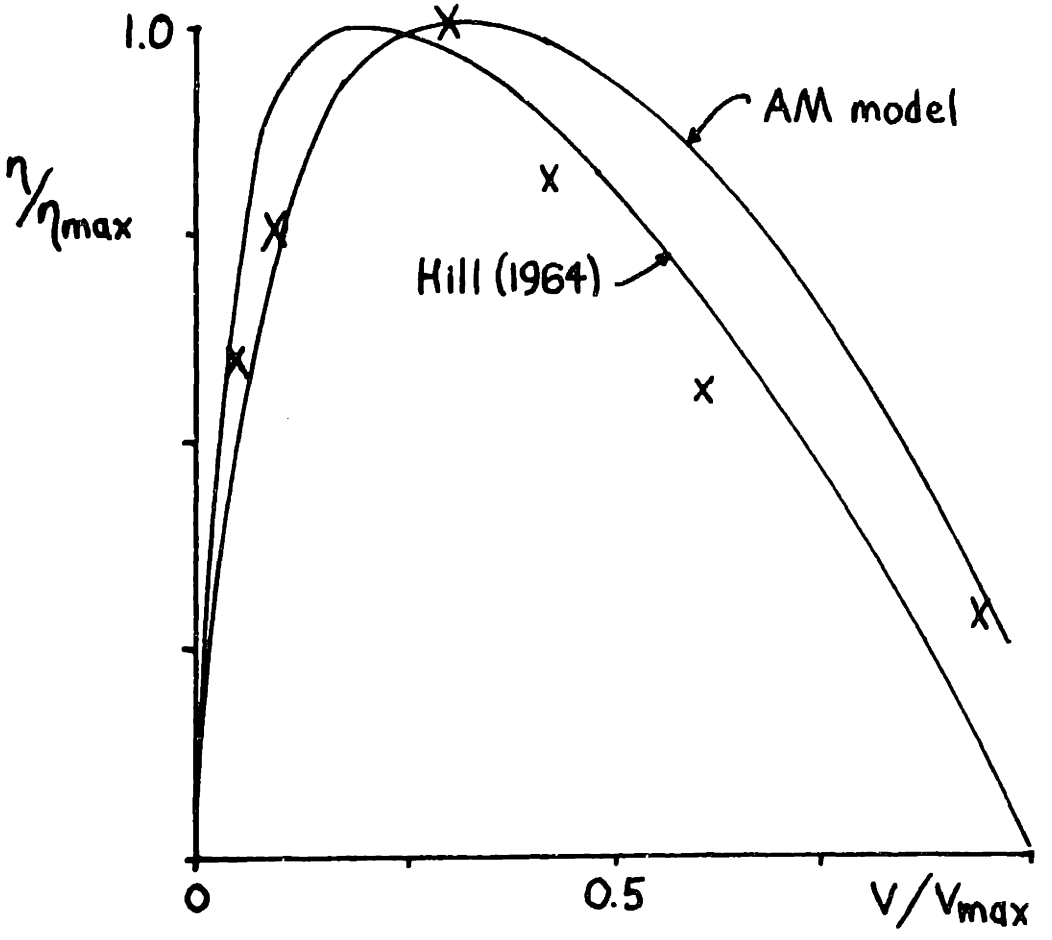

Fig. 3-8b Normalized Efficiency Data
The x's represent data points from Kushmerick (1969)

However, for simplicity in the following simulations the step stimulus will be retained. Variable sarcomere length or incomplete fiber overlap is represented in the model by reducing the total population of possible cross bridges. Since fewer cross bridges form, the force output drops, but so does the ATP flux, causing the net efficiency to remain constant given the same velocity. In fact, Hill (1964) makes the observation that changes from rest length had no effect on the muscle efficiency. Therefore the magnitude of the stimulus used is not important and is chosen as maximal for convenience.

Regarding the shortening velocity, it has been demonstrated (Pedotti (1977)) that most muscle active in gait operates in narrow ranges of relative or length normalized velocity. Accordingly, it is assumed for purposes of simulation that in vivo conditions can be approximated by constant velocities over period of time that are short when compared to the total contraction time. Hence, if the dynamics of the energetic processes are of higher frequency than the overall muscle length changes, that is the efficiency tends to settle to steady state before significant velocity changes occur, the iso-velocity approximation is a good one.

With these specifications the following simulations were performed. As before,the sarcomere begins at rest and receives a step stimulus. It is then allowed to shorten at a constant velocity which varies from trial to trial. Simulations were performed at shortening velocities of .05, .15, .25, .5, .75, and 1.0 v/v_{max} and lengthening velocities of 0.05, 0.15, and 0.25 v/v_{max}, where v_{max} is defined as the velocity of shortening at which force output is zero. For each trial the time history of the force, chemical power, and mechanochemical efficiency were recorded. The former two quantities were normalized to their isometric steady state values. Plots of the

various velocity trials for each of these variables are shown in figures 3-9, 10 and 11. The salient feature of each of these curves is the time to reach steady state values for each quantity. Although an inverse relationship between velocity and settling time emerges, the dynamics of all the quantities and especially the efficiency have response times on the order of 20-50 msec. Furthermore it must be added that the parameter values used for the AM model were taken from experiments performed at 0°C. This cooling is intended to slow the events of contraction and actual response times can be expected to be 4 to 5 times faster.

The essential conclusion from these simulations is that the efficiency response times are at least an order of magnitude faster than the 200-500 msec. characteristic time course of the measureable muscle output. It might be argued that the high efficiency transient after the step times (see figure 3-11) could be used to advantage if the sarcomere was activated for short periods of time with impulse-like calcium concentration profile, however, Wood (1975) has shown that the calcium concentration changes more slowly than the membrane potential. Also the total response, which includes the step-off response, shows a sharp efficiency drop at the end, effectively cancelling the effect of the initial efficiency spike.

At this point the reflection of sarcomere activity at the gross level as well as the choice of force or velocity as the independent variable in the efficiency function needs to be discussed. Countless experiments have verified the Hill equation which states that maximally stimulated muscle shortening at constant loads, shortens at a unique steady state velocity which is an inverse monotonic function of that load (see figure 3-12a). Taking the maximally synchronously stimulated whole muscle as an analog of a quantally

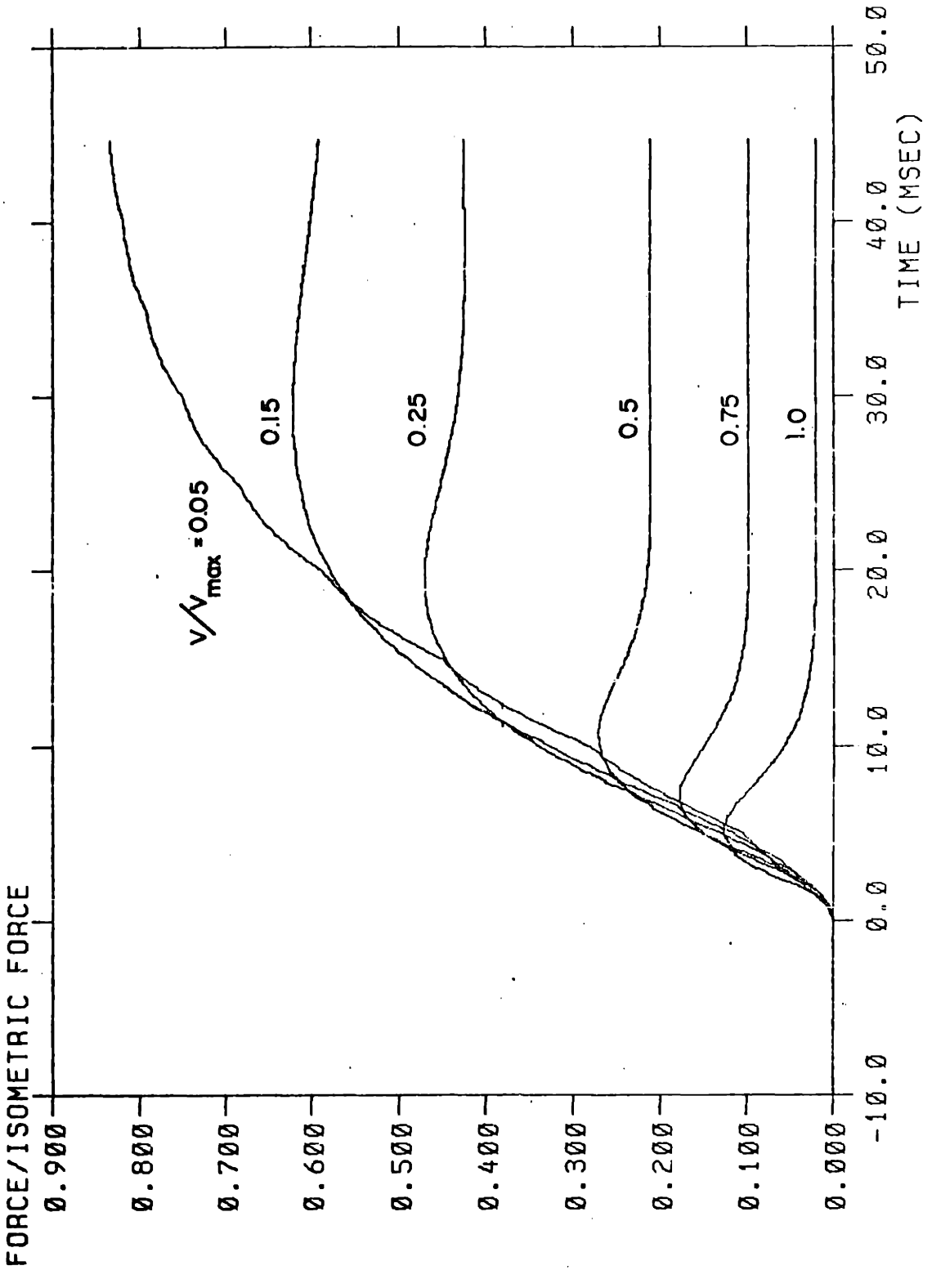

Fig. 3-9 Force Response of the AM Model under Isovelocity Conditions

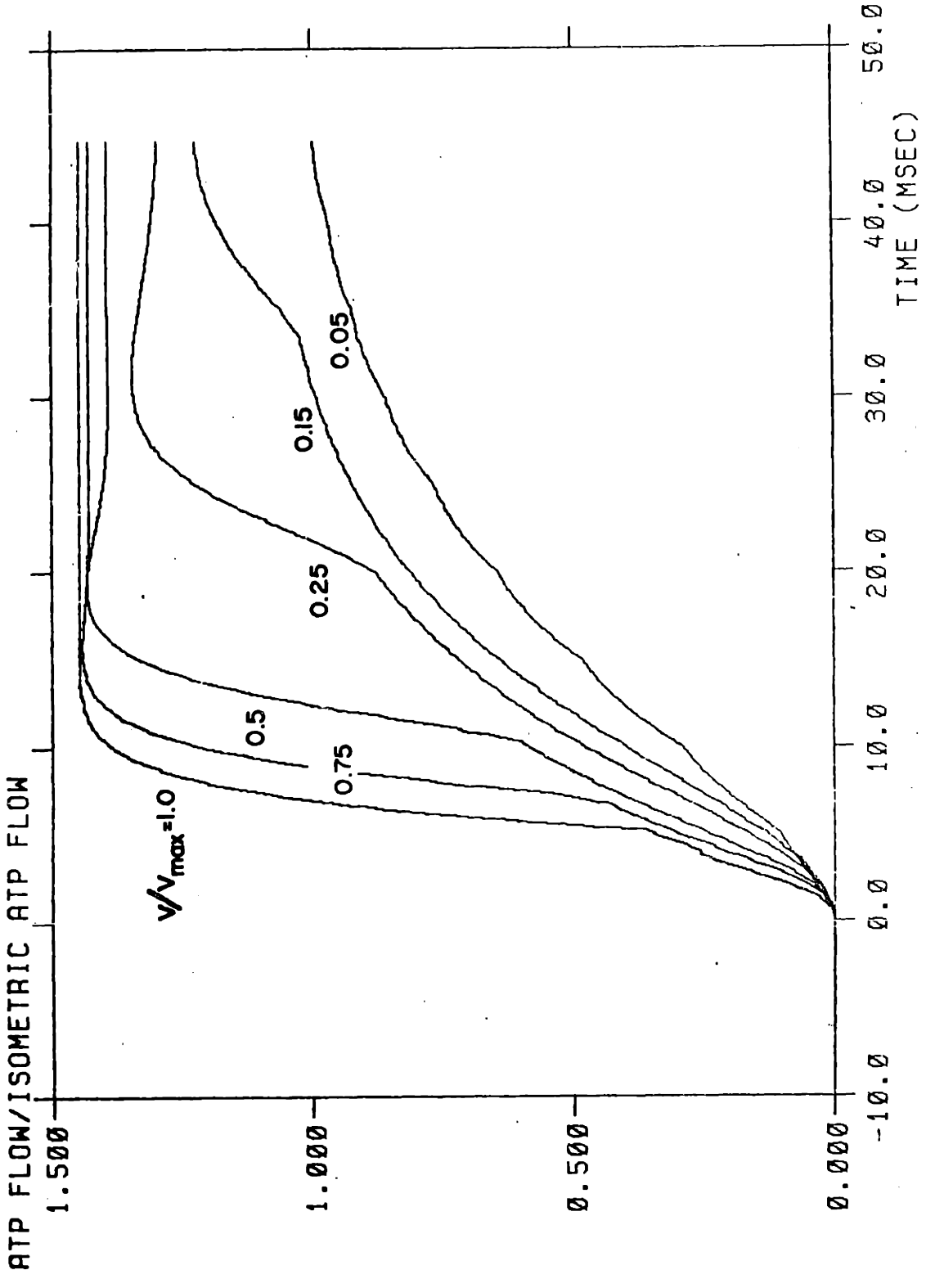

Fig. 3-10 ATP Flow Response for AM Model under Isovelocity Conditions

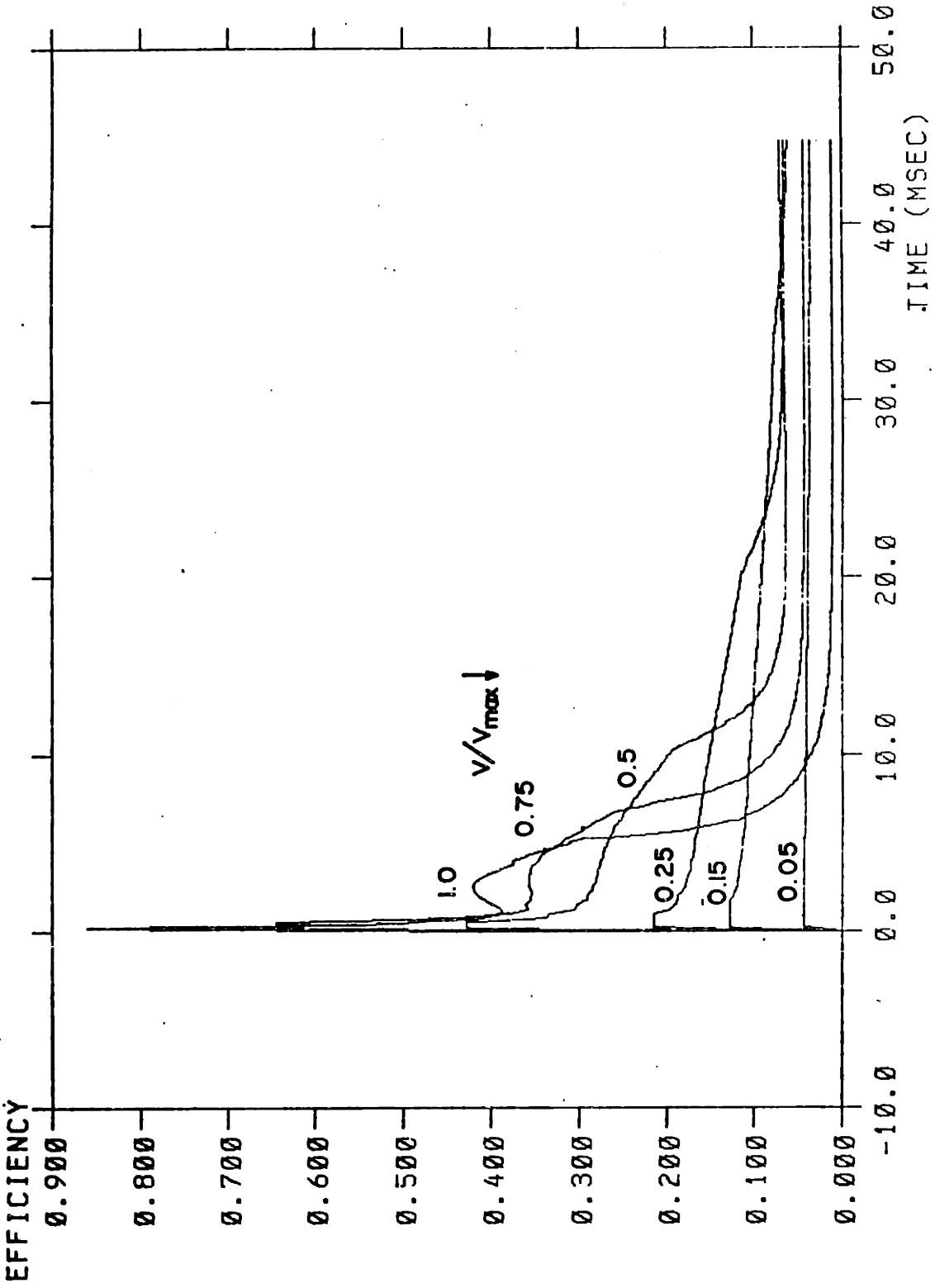

Fig. 3-11 Chemico-mechanical Efficiency Response for AM Model

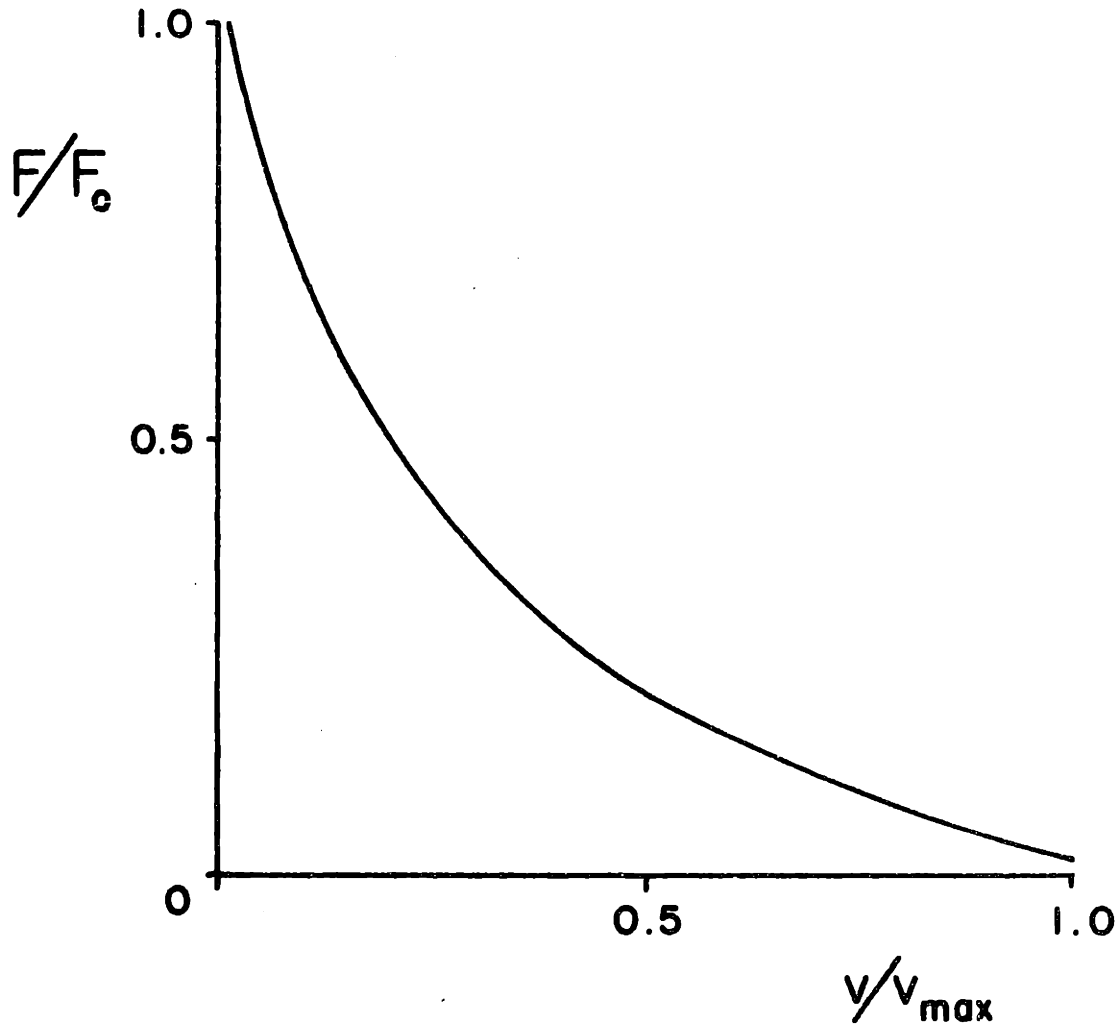

Fig 3-12a Force-Velocity Relationship for Whole, Isolated Muscle from Hill(1953)

stimulated sarcomere, the same relationship is found to exist (see figure 12b), therefore, at the sarcomere level force and velocity are non-independent and either one can be used to characterize the mechanical state of the sarcomere. It is the mechanical arrangement and activation scheme of muscle in vivo that establishes the necessary independence between the power pairs force and velocity.

Sarcomeres are arranged in series to form fibrils and must have common forces. Each sarcomere has the unique relationship between force and velocity:

$$f/f_0 = \phi(v/v_{max}) \qquad 3\text{-}17$$

where $f_o \equiv$ isometric force

$v_{max} \equiv$ zero force velocity

$\phi \equiv$ monotonic function

Identically stimulated sarcomeres in series (as in the fibril) will have a common force but the velocity is now n·v where n is the number of sarcomeres in the series. V_{max} for the fibril is similarly scaled so that v/v_{max}/fibril = v/v_{max}/sarcomere, therefore the force velocity relationship of the fibril is identical to that of the sarcomere (This assumes similar fiber overlap in all sarcomeres). As mentioned earlier, the fibril makes up the motor unit, the smallest unit of control and the many fibrils in a motor unit (20-200) receive a single control signal, therefore identical excitation (except for finite delays due to low nerve conduction velocities). However, when the fibrils are arranged in parallel bundles into muscle fibers having many separate control signals, all that remains common to the sarcomeres is their normalized velocity. Total muscle force can now be modulated independently

stimulated sarcomere, the same relationship is found to exist (see figure 12b), therefore, at the sarcomere level force and velocity are non-independent and either one can be used to characterize the mechanical state of the sarcomere. It is the mechanical arrangement and activation scheme of muscle in vivo that establishes the necessary independence between the power pairs force and velocity.

Sarcomeres are arranged in series to form fibrils and must have common forces. Each sarcomere has the unique relationship between force and velocity:

$$f/f_0 = \phi(v/v_{max}) \qquad 3\text{-}17$$

where $f_o \equiv$ isometric force

$v_{max} \equiv$ zero force velocity

$\phi \equiv$ monotonic function

Identically stimulated sarcomeres in series (as in the fibril) will have a common force but the velocity is now n·v where n is the number of sarcomeres in the series. V_{max} for the fibril is similarly scaled so that v/v_{max}/fibril = v/v_{max}/sarcomere, therefore the force velocity relationship of the fibril is identical to that of the sarcomere. (This assumes similar fiber overlap in all sarcomeres). As mentioned earlier, the fibril makes up the motor unit, the smallest unit of control and the many fibrils in a motor unit (20-200) receive a single control signal, therefore identical excitation (except for finite delays due to low nerve conduction velocities). However, when the fibrils are arranged in parallel bundles into muscle fibers having many separate control signals, all that remains common to the sarcomeres is their normalized velocity.

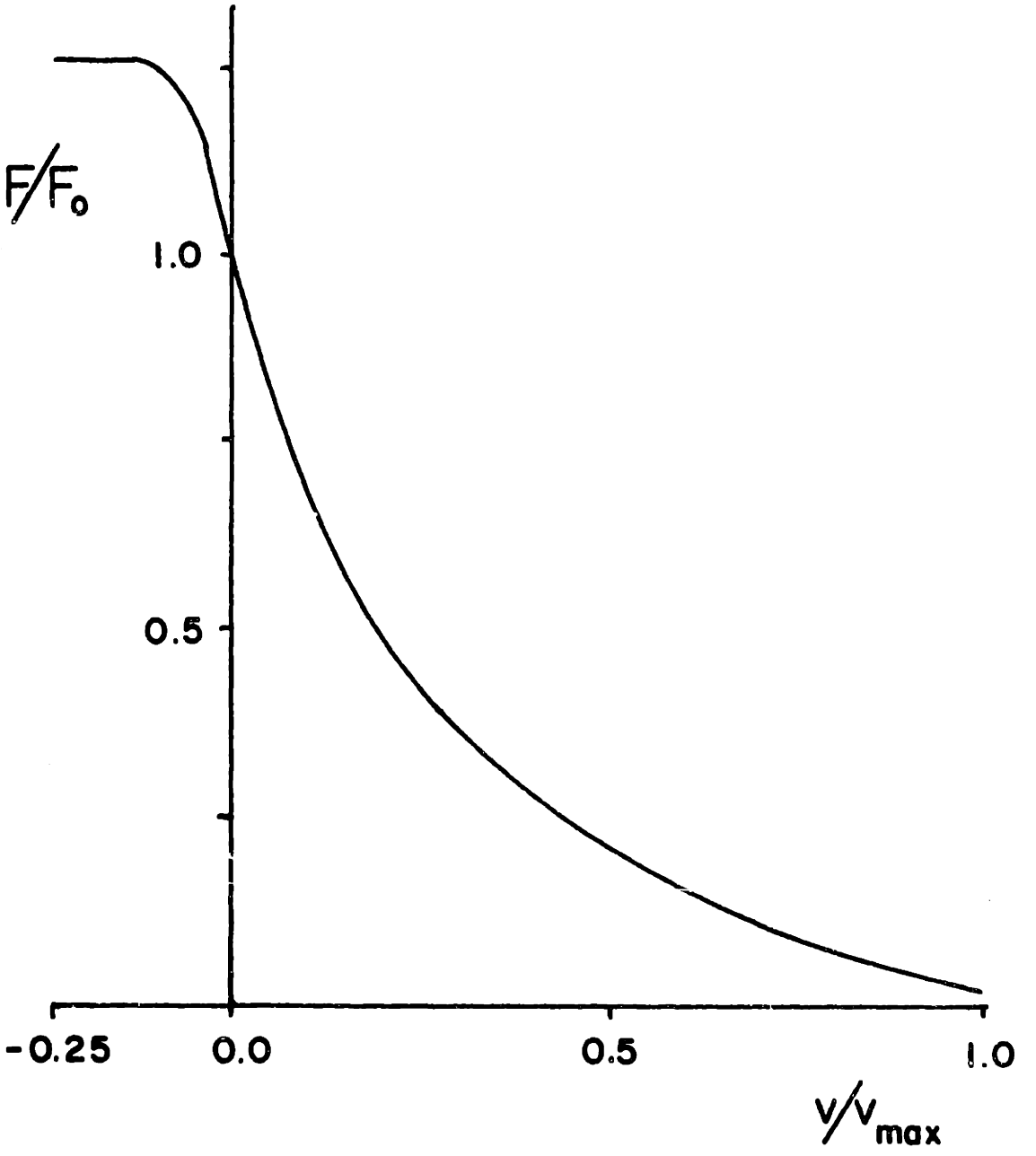

Fig. 3-12b. Force - Velocity Relationship for AM Model

total muscle force can now be modulated independently of the velocity by orchestrating various fibrils, each operating at a force level determined by their velocity, (and secondarily by the stimulus frequency).

This being the case, the only possible choice for the dependent variable in the sarcomere and therefore the whole muscle efficiency function is the normalized shortening velocity which can be measured at the end points of the muscle body and normalized to the predicted no load or maximal shortening velocity.

It is now possible to use the normalized muscle efficiency predicted from isovelocity simulations with the AM model. To apply this to the modeling task at hand, which requires chemical power as a function of mechanical power, the following formula derived from equation 3-15 can be used:

$$\dot{G} = Fv \frac{1}{\eta(v/v_{max})} \qquad 3\text{-}18$$

F = muscle force

v = muscle velocity

$\dot{G}$ = chemical power input

Now, however, the difficulty with the efficiency definition is apparent. Under isometric conditions equation 3-18 predicts zero input when power output ceases. This fallacy can be overcome by taking further advantage of the descriptive AM model.

The desired output of the muscle energy function is the chemical power, and this data, at the sarcomere level, is available from the AM model simulations. Figure 3-10 illustrates the ATP flow rates for the sarcomere. Recalling that the driving potential across this system is kept constant by the Lohmann reaction, this plot also indicates the chemical power flows if

the curve is multiplied by this potential or reaction affinity. Collecting the steady state values as a function of normalized velocity, this static relationship, denoted $\dot{g}(v/v_{max})$, can be plotted as shown in figure 3-13 where $\dot{g}$ is normalized by the isometric value g_o .

Returning to equation 3-18, substituting the sarcomere variables for the efficiency term, the overall muscle chemical power is

$$\dot{G} = [Fv]_{muscle} \left[\frac{\dot{g}(v/v_{max})}{fv}\right]_{sarcomere} \qquad 3\text{-}19$$

$$\left(\eta \equiv \frac{fv}{\dot{g}(v/v_{max})}\Big|_{sarcomere}\right)$$

The normalized sarcomere force, f/f_o, is uniquely related to normalized velocity as was shown in figure 3-12b. Using this fact, 3-19 can be rewritten, with all normalizing constants included, as

$$\dot{G} = [Fv]_{muscle} \left[\frac{\dot{g}/g_o(v/v_{max})}{f/f_o(v/v_{max})} \frac{g_o}{f_o} \frac{1}{v}\right]_{sarcomere} \qquad 3\text{-}20$$

Normalizing both the muscle velocity and the sarcomere velocity by their maximum values yields

$$\dot{G} = \left(\frac{v_{max_{muscle}}}{v_{max_{sarco.}}}\right) [Fv]_{muscle} \left[\frac{\dot{g}/g_o}{f/f_o}(v/v_{max}) \frac{1}{v/v_{max}} g_o/f_o\right]_{sarcomere} \qquad 3\text{-}21$$

By arguments presented earlier, the muscle can be considered a series arrangement of sarcomeres, which leads to

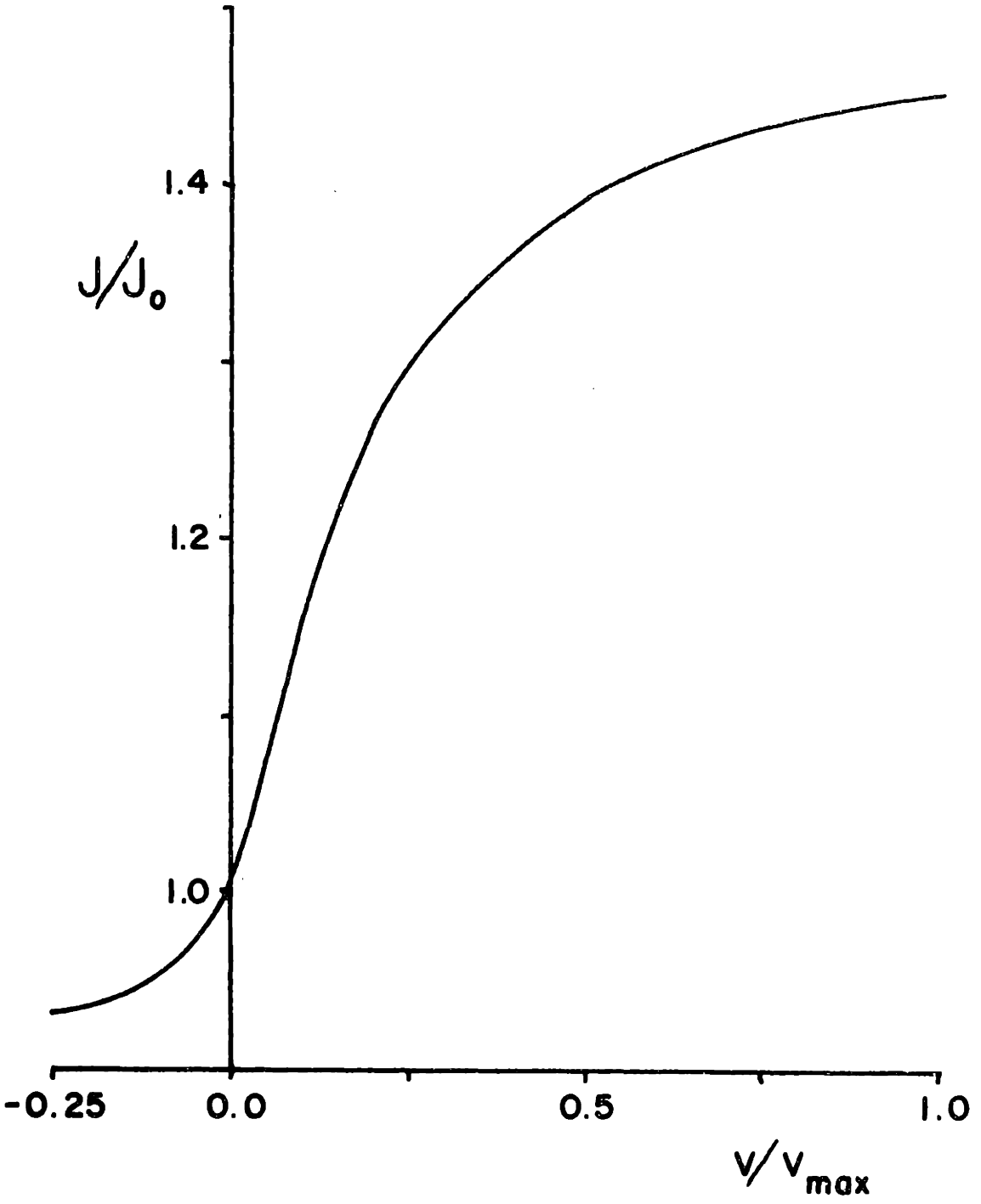

Fig. 3-13 Steady State ATP Flow for AM Model

As mentioned in the text, this curve, when scaled by the ATP reaction affinity, also represents the steady state chemical power.

$$\frac{v_{max_{muscle}}}{v_{max_{sarco.}}} = \frac{\bar{\ell}_{muscle}}{\bar{\ell}_{sarco.}} \qquad 3\text{-}22$$

where $\bar{\ell}$ represents a nominal length. The crucial ratio

$$\frac{\dot{g}/g_o}{f/f_o} \equiv g(v/v_{max})$$

is plotted in figure 3-14 and was obtained by dividing the ATP fluxes plotted in figure 3-13 by the force data represented in figure 3-12b. Substitution of this and 3-22 into 3-21, and noticing that v/v_{max} is the same for the overall muscle as for the sarcomere yields

$$\dot{G} = \beta F g(v/v_{max}) \qquad 2\text{-}23$$

where $$\beta \equiv \frac{\dot{g}_o}{f_o} \frac{\bar{\ell}}{\bar{\ell}_{sarcomere}}$$

Since all terms except $\bar{\ell}_{muscle}$ are intrinsic sarcomere properties, they can be assumed constant for all muscles, which makes β a function of the average muscle length only. This results in the final chemical power expression

$$\dot{G} = \beta(\bar{\ell}) F g(v/v_{max}) \qquad 3\text{-}24$$

where all variables are measured on the whole muscle.

The expression $g(v/v_{max})$ in 3-24 cannot be obtained in closed form from the AM model equations so a curve fit procedure was used to obtain a continuous function. The curve of figure 3-14 was fit by both a polynomial and an exponential function. The former gave a more accurate expression although it required six terms to do so, and reasonably accurate fits with the exponential were not possible unless the negative and positive velocities were con-

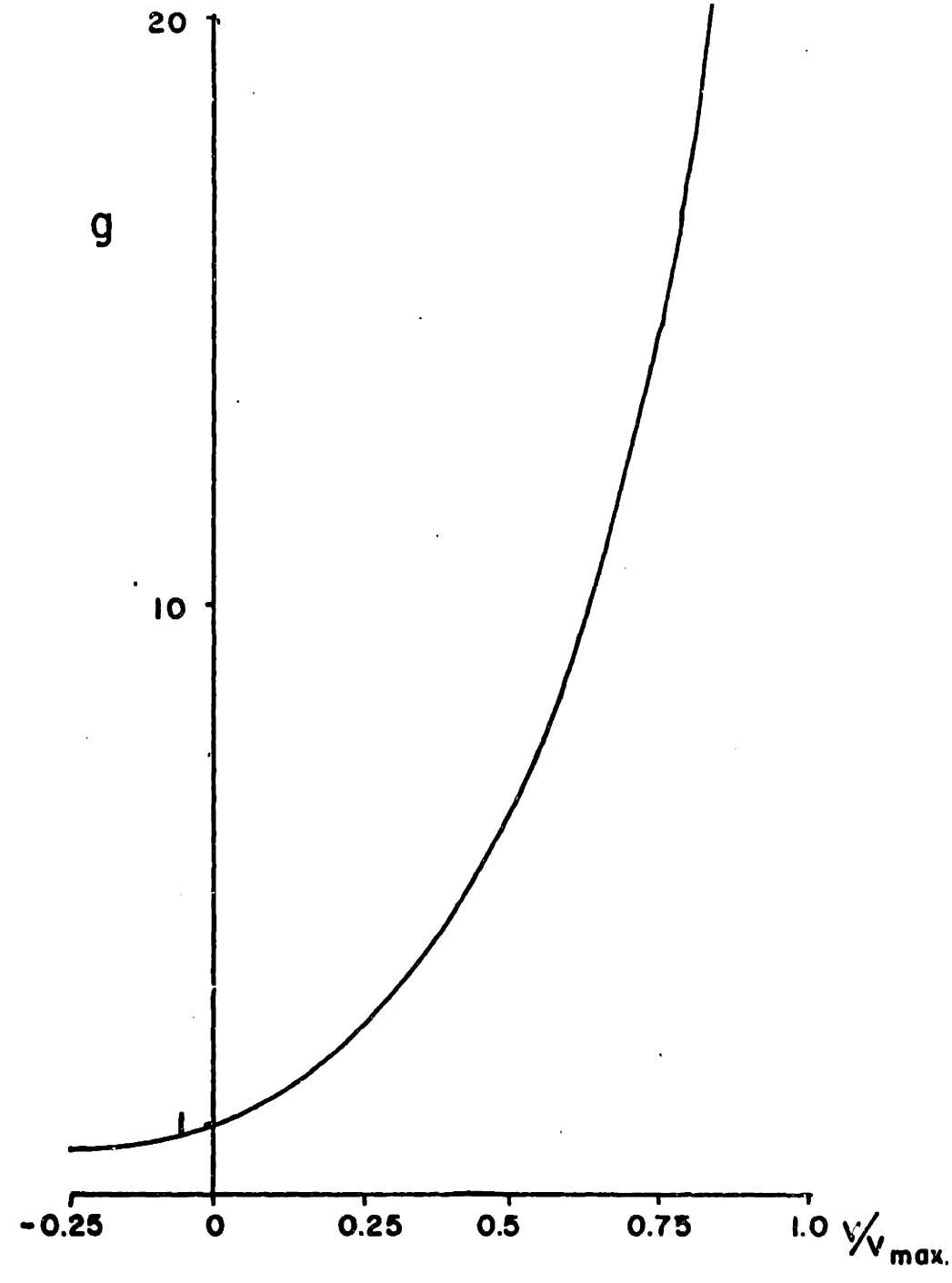

Fig. 3-14 The Ratio of the AM Chemical Power Input over the Force Output

This curve represents the cost coefficient for a particular muscle since multiplication of the instantaneous muscle force by this curve gives an estimated power consumption level.

sidered separately.

The exact expression used is

$$g(v/v_{max}) = 1.0 + 3.6\,v + 16.0\,v^2 + 25.5\,v^3 - 31.2\,v^4 - 155.0\,v^5 + 213.0\,v^6 \qquad 3\text{-}25$$

where $v \equiv v/v_{max_{muscle}}$

The disregard for absolute values in the above development is because the penalty function to which this model is to be applied requires only relative powers, thus any convenient normalization can be used. As a further consequence of this, the term β can be written simply as the muscle length, which leads to the final model expression for the relative intermuscular chemical power

$$\dot{G}_o = \bar{\ell} F g(v/v_{max}) \qquad 3\text{-}26$$

The requirements of relating chemical power to muscle force and end point velocity have been met. Notice that the normalization of the gross muscle force by the maximum isometric force is not a valid operation here since, for example, larger but chemically identical muscles would exhibit lower energy consumptions that smaller muscles producing identical power outputs, due to the relationship between maximum isometric force and muscle volume. The only differentiation in this model between muscle fiber types is in the assignment of v_{max} to a particular muscle. Maximum velocity is frequently taken as a measure of the intrinsic speed of the chemical reactions (Barany (1967)) and/or the dominant metabolic mechanism, (i.e. aerobic or

anaerobic), see Thorstensson et al. (1976).

Transmission of mechanical power to skeletal members

The previous section produced a model that predicts muscle chemical power requirements given the mechanical power pairs: force and velocity at the ends of the active muscle tissue. The question to be addressed here is whether the force - velocity trajectory at the skeletal attachment is identical to that of the muscle tissue or if the transmission tissues add to the dynamics of the system.

Muscle generally terminates in passive tissues known as tendons; those in turn insert into the bones. There are also passive tissues within and around the active fibers which must be considered. The compliance of the tendons, although low, can become significant especially when long or slender cases are considered such as the tendon of gastrocnemius, (Assmussen (1974), Bartell (1975)). In addition, other passive tissues can at times share some of the tension in muscle. Clearly these properties must be accounted for so that the muscle velocity can be accurately derived from external measurements of skeletal motion.

A useful mechanical analog of muscle is the "spring dashpot" model shown in figure 3-15, (from Jewell and Wilkie (1958)) along with its bond graph equivalent. The contractile element is a source of mechanical power, that can be represented by the active tissue that comprises bundles of fibers composed of the elements described previously. The parallel elastic element anatomically represents fascial sheathing and internal connective of the muscle, which can bear tension at certain extensions of the muscle, plus some internal tissues which delineate the sarcomeres and fibrils.

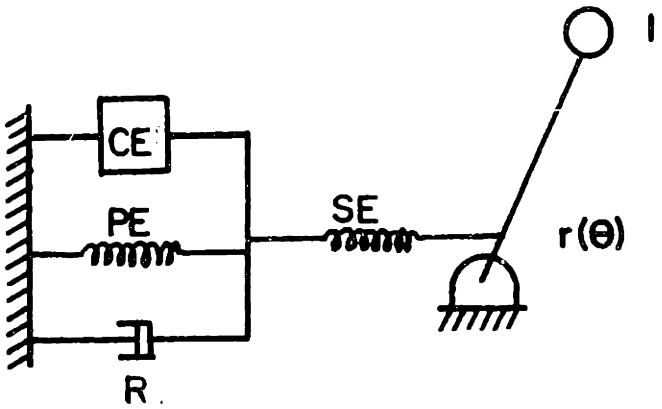

CE : Contractile Element
PE : Parallel Elastic Element
SE : Series Elastic Element
R : Internal Damping

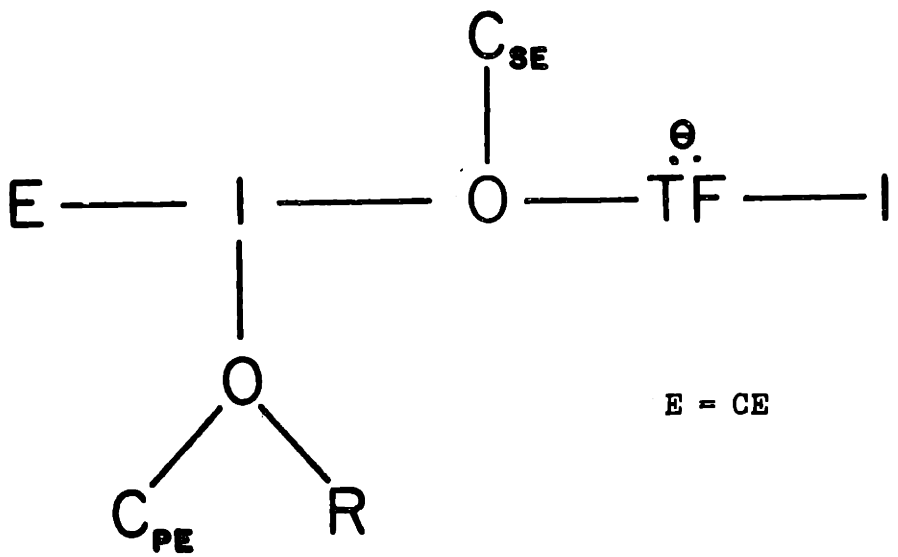

Fig. 3-15 Mechanical Model of Muscle from Jewell & Wilkie(1958) and its Bond Graph Equivalent

Finally the tendon is represented by a series elastic element (SE) between all the above elements and the load.

The contractile element (CE) as shown in figure 3-15 represents a series of sarcomeres each consisting of the actin and myosin proteins plus certain other connective tissues. It was shown earlier that a certain elasticity located somewhere in the myosin filament, (although not necessarily in the S1 unit of HMM), was an essential element in the sliding filament model. The strain dependent rate constants discussed in Appendix A effectively introduce damping into the CE, consequently the AM model has already accounted for both the sarcomere elasticity and damping, which are often represented separately in mechanical models and used as the basis for phenomenological analysis of muscle mechanics (e.g. Pasley et al. (1974) and Hatze (1975)).

The parallel elastic element (PE), representing fascial and intrafiber connective tissue load bearing, is often assumed to carry little load during normal muscle use. The characteristic length-tension curve of isometrically contracting muscle from Hill (1953), (figure 3-16), shows the contribution of the PE when lengths above the rest length are encountered. Tensile tests on cadaverous muscle fascia by Yamada (1970) exhibited a similar non-linearity in their elasticity (figure 3-17). Further confirmation of this result comes from the length tension studies of Gordon et al. (1966), on isolated muscle fibers. With all connective tissues removed, no passive force bearing was possible and the resulting length tension curve (figure 3-18) exhibits a clear drop off to zero force at extreme lengths.

For the purpose of this study, the contribution of the PE will be neglected, due in part to its small contribution to the tension at nominal muscle lengths (Jewell and Wilkie (1958)), and to the difficulty of obtaining

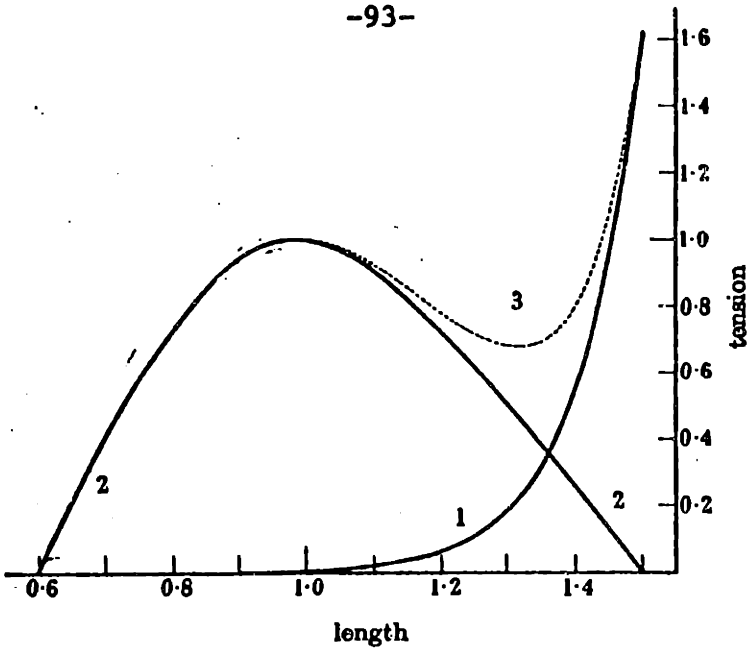

Fig. 3-16 Diagram of tension-length relations of sartorius muscle of frog or toad. (1) At rest passively stretched; (2) extra force developed during maximal tetanus; (3) dotted line, total force in maximal tetanus, sum of (1) and (2). The length is given as a fraction, or multiple, of the standard length in the body; the tension, of the maximum force developed.

(from Hill(1953))

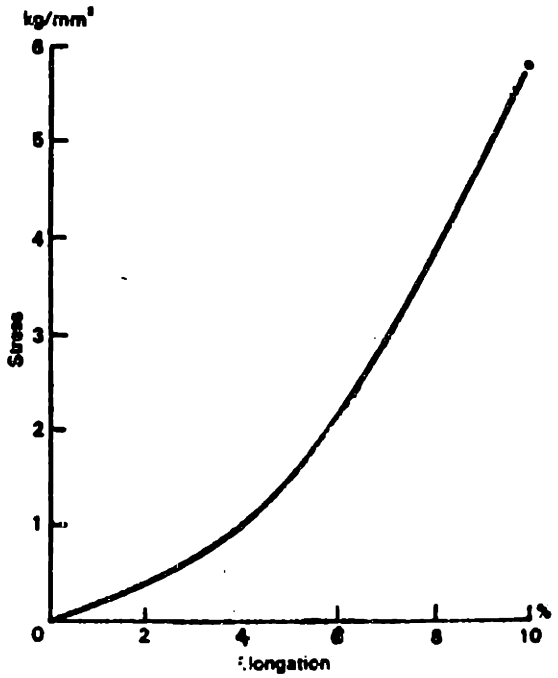

Fig. 3-17 Stress-strain curve in tension of calcaneal tendinous tissue of persons 20 to 29 years of age. (from Yamada(1968))

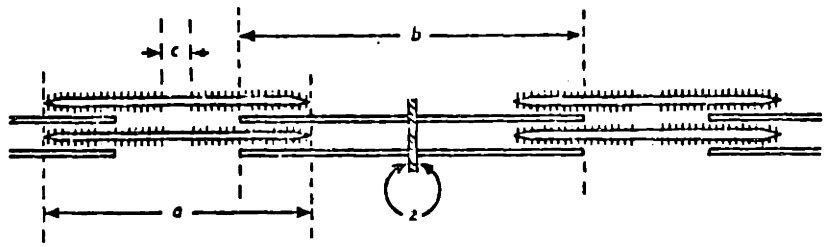

. Schomatic diagram of filaments, indicating nomonclature for the relevant dimensions.

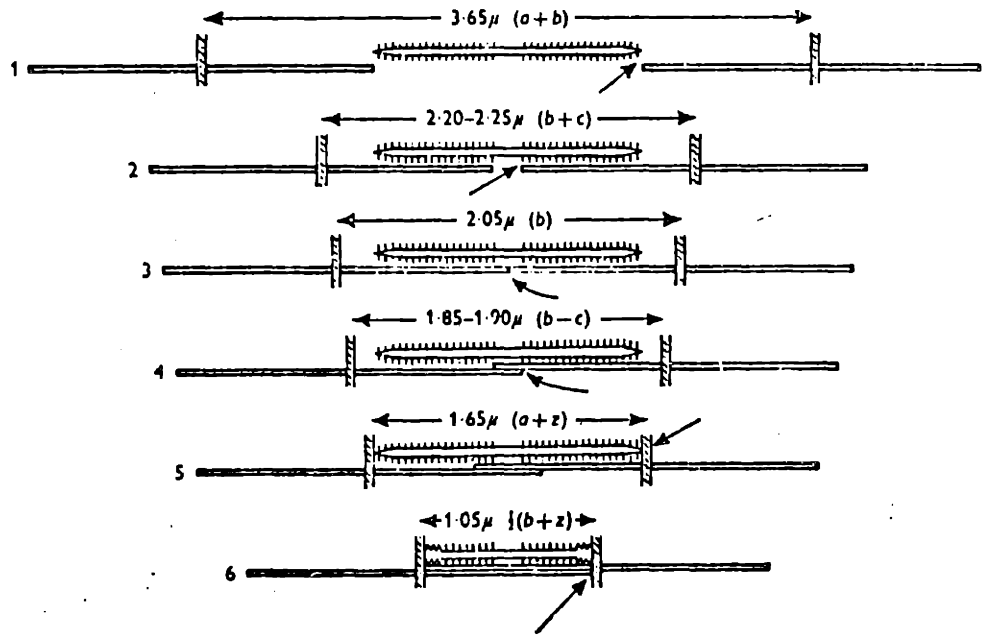

Critical stages in the increase of overlap between thick and thin filaments as a sarcomere shortens.

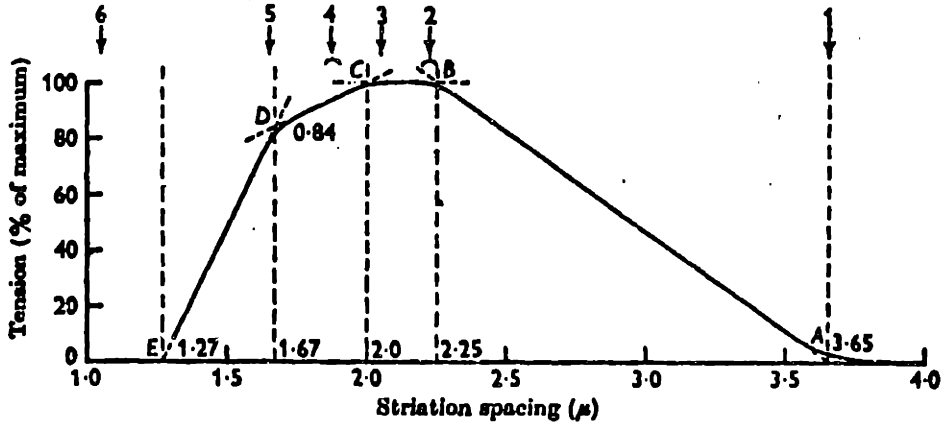

Schematic summary of results. The arrows along the top are placed opposite the striation spacings at which the critical stages of overlap of filaments occur, numbered as above

Fig. 3-18 Length - Tension Relationship for an Isolated Muscle Fiber (from Gordon et al. (1966))

exact data on its properties for individual muscles in the leg.

By far the potentially most significant element in a study of muscle energetics is the series elasticity. Although Yamada (1970) has shown that human calcaneal tendons are relatively stiff material ($E = 890 \frac{Mt}{mm^2}$) their in vivo cross-sectional areas and lengths can make their energy storage capacities considerable. Both Assmussen (1974) and Margaria (1976) report higher overall muscle efficiencies during movements which permit rapid use of any stored elastic energy than if the movement is designed to damp out this energy before it can be used. Under these conditions significant energy storage in the tendons is apparent, however, its contribution during normal walking is uncertain.

The effect of this spring-like connection between the muscle and bone is illustrated in the bond graph of figure 3-15. Essentially the relationship between the measured bone attachment velocity and the muscle velocity required in equation 3-26 becomes a dynamic or state dependent one. Although the spring transmits the force with full fidelity, the muscle velocity will now depend on both the bone attachment velocity and the rate of change of the force. This can be seen in the following development.

The elastic properties of tendon as reflected in the stress-strain data of Yamada (1970) and Bartel (1975) are essentially non-linear. As shown in figure 3-19 (plotted as stress vs. strain) the elasticity becomes linear beyond a certain strain (ε_1) with the corresponding stress (σ_1), and this line extends back to zero stress at ε_∞. A suitable expression for fitting this curve (see appendix A) is:

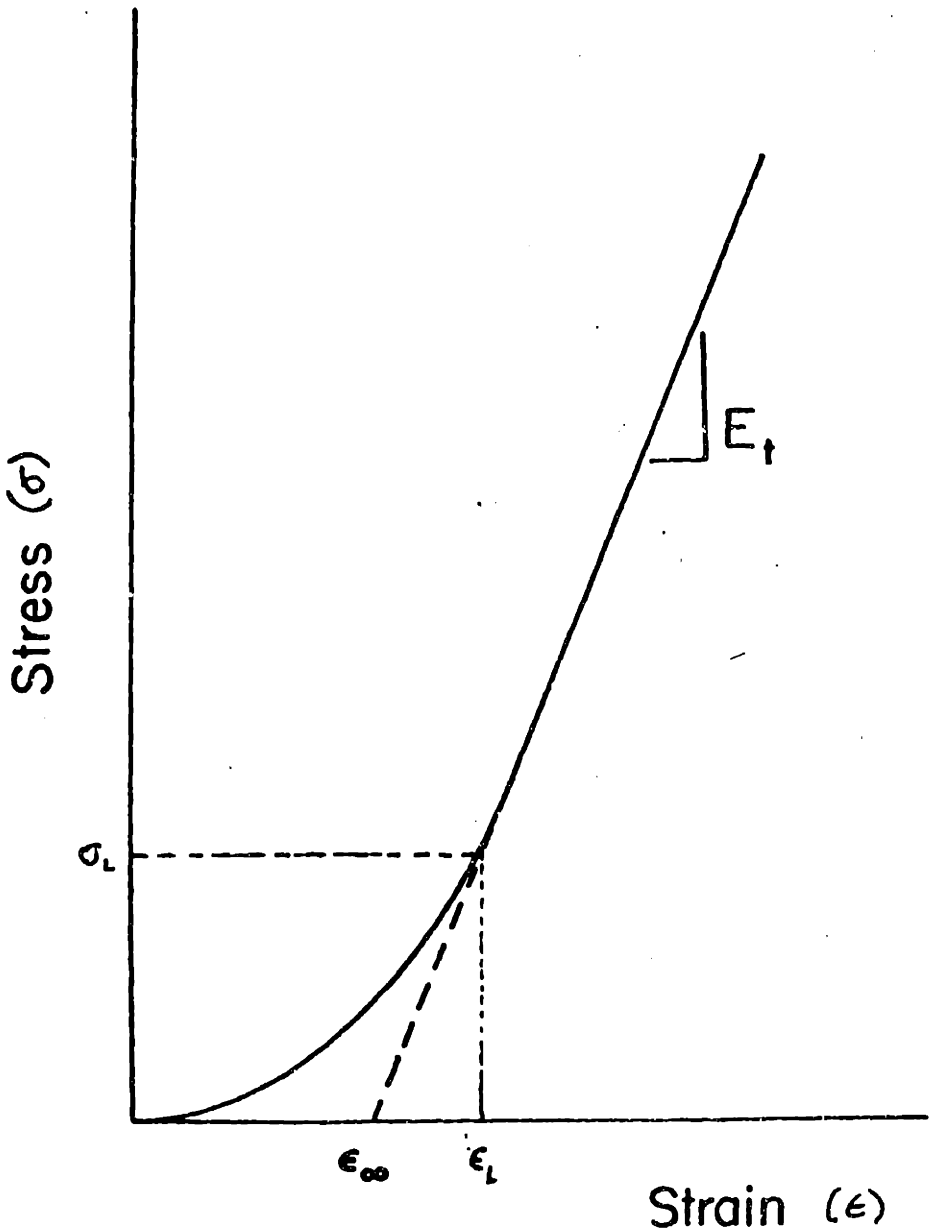

Fig. 3-19 General Description of Force-Deflection Curve for Tendon and Ligament Showing Tangent Modulus, E_t, and Strain Intercept, ϵ_∞. (from Bartel (1975))

$$\varepsilon = \frac{1}{E_\infty}\sigma + \varepsilon_\infty(1 - e^{\sigma/4\sigma_1}) \qquad 3\text{-}27$$

From the results of appendix A the parameters of this expression can be written in terms of the linear modulus of elasticity (E_∞), the equivalent strain at zero stress (ε_∞), and the stress at the beginning of the linear behavior (σ_2) as defined in figure 3-19. The final expression is:

$$\varepsilon = \frac{1}{E_\infty} + (1 - e^{-\sigma/4\sigma_1}) \qquad 3\text{-}28$$

Converting this to the measureable force ($F = \sigma/A$) and tendon elongation ($x = \ell\varepsilon$) requires data on the cross sectional area (A) and the length of the tendon (ℓ). The elongation of the tendon due to the applied force is now:

$$x = \frac{1}{E_\infty}\frac{F}{A} + \varepsilon_\infty (1 - \exp(-F/4\sigma_1 A))\ell \qquad 3\text{-}29$$

The desired velocity difference between the ends of the tendon is found from the time derivative of the elongation (equation (24)):

$$\dot{x} = \frac{dF}{dt}\left(\frac{\ell}{E_\infty A} + \frac{\varepsilon_\infty \ell}{4\sigma_2 A}\exp(-F/4\sigma_1 A)\right) \qquad 3\text{-}30$$

Finally, this velocity is defined from:

$$\dot{x} = \dot{x}_{skeletal} - \dot{x}_{muscle}$$

The muscle velocity, given only the force time history and the velocity of the skeletal attachments is:

$$\dot{x}_{muscle} = \dot{x}_{skeletal} - \frac{dF}{dt}\left(\frac{\ell}{E_\infty A} + \frac{\varepsilon_\infty \ell}{4\sigma_2 A}\exp(-F/4\sigma_1 A)\right) \qquad 3\text{-}31$$

The major problem remaining is the determination of the parameters muscle tendon length (ℓ), and cross sectional area (A). In a manner similar to Bartel (1975), these canbe obtained from cadaver measurements under appropriate assumptions of area uniformity and muscle - tendon tissue interface location.

However, the central question here is:how significant is the tendon compliance of the leg muscles to this analysis? As will be detailed in the next chapter, this finding will have considerable impact on the solution method used for the force optimization. Certainly the compliance of the long tendons of the horse or kangaroo is high enough to make them significant energy storage elements, but is the same true of human tendons?

Referring to the data of Yamada shown in figure 3-17, a worst case analysis can be performed using the least stiff portion of the curve. A linear fit to the lower end of the curve gives an elastic modulus $E = 2.0 \times 10^8$ N/m^2. With this lienar elasticity, a simple spring analogy can be developed. The velocity drop across a spring Δv, which here represents $v_{skeletal} - v_{muscle}$, can be expressed

$$\Delta v = F/k \qquad 3\text{-}32$$

which is the linearized form of equation 3-31, and the spring constant

$$k \equiv \frac{A}{\ell} E$$

$A \equiv$ area of the tendon

$\ell \equiv$ length of the tendon

An estimate for the upper bound of dF/dt can be made from the AM force simu-

lations. When scaled to typical muscle strengths and adjusted to body temperatures this bound is

$$dF/dt_{max} \cong 12{,}000 \text{ N/sec}$$

The calcaneal or achilles tendon provides a worst case example for the aspect ratio ℓ/A and can be estimated from cadavers or anatomy texts. Approximate figures yield $A = .25 \text{ cm}^2$ and $\ell = 10$ cm, or $k = 5 \times 10^4$ N/m. Substituting all of these into equation 3-32:

$$\Delta v_{max} = \frac{12000 \text{ N/sec}}{50000 \text{ N/m}} = 0.24 \text{ m/sec}$$

As will be shown later, maximum muscle velocities are in the range 2.5 to 6.0 muscle lengths/m, so for the assumed length of 0.3m for the gastrocnemius muscle,

$$0.13 \leq \Delta v_{max}/v_{max} \leq 0.31$$

These figures do appear to make tendon elasticity a possibly significant energy storage element, however, this is a worst case analysis and would apply to only a few of the muscles considered here. The majority of the leg muscles have much shorter or less slender tendons than the calcaneal, so this small subset of significant elastic elements does not warrant the difficulties of the requisite optimization procedure illustrated in the next chapter. However, a more detailed and exact analysis of muscle function would have to examine the tendon contribution more closely. For some human motions, particularly ballistic motions where the rate of change of force will be at its maximum, neglecting the tendon elasticity would be very haz-

ardous.

Results and verification

Using the model presented in this chapter, the static muscle efficiency data of Hill (1964) and Kushmerick (1969) has been shown to apply to limited dynamic ranges of operation, ($\leq$ 10 Hz.) and the curve has also been extended to cover the stretching (negative power) regime of operation. In the final expression for the chemical energy

$$\dot{G} = \bar{\ell}\, Fg(v/v_{max})$$

are contained three macroscopic quantities, the average length, the force and the normalized contraction velocity. The first is a constant for any given muscle and acts as a weighting coefficient for the rest of the expression. A possible physical interpretation of this term is that it is a reflection of the series arrangement of sarcomeres in a muscle. If two muscles of different length are undergoing isometric contractions at the same force level, the longer muscle will require more chemical energy simply because there are more active sarcomeres to supply with power. (This apparent disadvantage is of course balanced by the fact that longer muscles will have lower contraction velocities, so they are to be favored once muscle mechanical output begins).

The force and velocity term are more obvious in that they constitute the mechanical power pairs and should appear in a power expression. It is noteworthy, however, that the chemical power is a linear function of force but a highly non-linear function of velocity as shown in figure 3-14. In fact the sensitivity of the chemical power input requirements to velocity

changes drastically over the physiological range of velocity. At the high velocities the use of any muscle force is costly whereas at zero and negative velocities, the significance of the velocity vanishes over a considerable range. Indeed, for static muscle use such as postural control, defining minimum energy consumption is identical to minimizing force, except that the length of the muscles acts as a weighting coefficient. This observation lends a stronger physiological base to the minimum force optimizations performed for static postures by Arvikar (1975) and Penrod (1974).

The relationship of the force and velocity to the chemical power requirements of muscle can be useful in seeking indirect verification of the model result since, by definition of the problem, no data exists on efficiency of dynamically contracting muscles. If the velocity of the muscle or muscles is constant, the chemical power requirements should vary in proportion to the force; conversely, if the force is held constant, the chemical power should vary with velocity in a manner similar to the curve representing $g(v/v_{max})$. No such control experiments have been performed on isolated muscle, however, at least two studies of locomotion and concomitant energy consumption can be applied here, in an average sense, to help examine the model.

The experiments of McMahon et al. (1976), investigated the relationship of oxygen consumption, hence energy consumption, of walking and running animals (humans, dogs, and horses) to the load carried by the animal. The energy consumption was shown to vary linearly with the external load carried, and, by making an argument about muscle force - load proportionality, the linear relationship of energy consumption to muscle force was established. The additional observation that gait patterns remained fixed for the various

loads implies that the velocity trajectories of the muscle remained unchanged with load. Assuming that the force distribution did not change drastically with load, these experiments point to a linear energy consumption or average power - muscle force relationship when average velocities are held fixed. Although the instantaneous nature of the model has not been investigated, the ability to predict average powers in dynamic situations has.

Turning to the velocity term, the walking speed-energy expenditure experiments of Cotes (1960) are useful. In these experiments, now repeated often, the relationship of oxygen consumption to forward walking velocity was found to be approximately quadratic. Before jumping to comparisons of the curve of the function $g(v/v_{max})$ to a quadratic function, the constancy of the muscle forces in this case must be considered. Since the subjects were asked to walk at increasing speeds, the acceleration involved in this walking were quite clearly increased, with concomitant increase in muscle force required to produce these accelerations. However, assuming that this effect is small, these results do point to a nonlinear, monotonic relationship between muscle energy consumption and velocity, again determined on a time averaged but dynamic muscle use basis. The final test of the model must be deferred until chapter 6 where this velocity-energy consumption relationship can be checked based on the results of actual minimum muscle energy optimizations.

In the later use of this model for the minimum energy optmizations, a value for v_{max} must be estimated. Pedotti et al (1978) present 2.5 * rest length of the muscle. This is in accord with estimates from <u>in vivo</u> human tests adn the muscle velocity data presented in chapter 6 tends to confirm that estimate.

Chapter 4 Formulation of the Optimization Procedure

Introduction

In this section the method of solving the optimization problem posed in chapter 1 is addressed. The muscle energy model developed in chapter 3 will have the greatest influence on the form of the optimization and several cases (including static and dynamic optimizations) are examined, each of these related to the assumptions made in the muscle model. Finally, the specific optimization procedure to be used here is examined and its data requirements, to be addressed in chapter 5, are described.

The fundamental problem of muscle redundancy was posed in an optimization framework in chapter 1. The working hypothesis, restated here is: determine the muscle forces necessary for walking that minimize the energy consumption of the muscles over a given period of time. Writing the expressions which describe this process (equations 1-2 and 1-3) in matrix form:

$$\min_{\underline{f}} J \qquad 4\text{-}1$$

$$J = \int_T g \, dt \qquad 4\text{-}2$$

subject to (at least) the moment constraints:

$$R(t)\,\underline{f}(t) = \underline{m}(t) \qquad 4\text{-}3$$

$\underline{f}$ ≡ vector of muscle forces

$\underline{m}$ ≡ vector of joint moments

g ≡ expression relating chemical power to mechanical power in muscle

R ≡ matrix of position (or time) dependent muscle moment arms.

Additional constraints are also possible, especially limits on muscle force which can be expressed:

$$\underline{D}\underline{f} \leq \underline{d}$$

where D and d are the constraint matrix and vector respectively, and either or both can be functions of time.

This problem, as with most optimizations, can be viewed in at least two ways depending on the application: 1) solve an indeterminate set of equations (the constraints in this case, or a multi-input dynamic system in the case of optimal control) by optimizing a function of the variables in those equations or 2) optimize a cost function subject to certain constraints on the variables in that function. The latter view predominates in the mathematics of optimization, however the former view is more appropriate here since the major concern is satisfying the joint moment constraint equations, whereas the cost function serves primarily as the vehicle for this process.

Applying this perspective, the problem here is to solve a static (i.e. no time derivatives involved) time varying, non-square matrix equation (4-3) by minimizing an expression which reflects the energy consumption of the muscles (equation 4-2). It is the form of this "penalty function" that determines the mathematical formulation of the problem, and two extremes of penalty functions will be examined here: the static and the dynamic cases.

Dynamic optimizations

Starting with the more general case, the dynamic penalty function, it will be assumed that the general function g in equation 4-3 is a function of the force, its first time derivative, and time:

$$g = g(\underline{f}, \dot{\underline{f}}, t) \qquad 4\text{-}5$$

This expression could represent the muscle model of chapter 3 if tendon compliance was included. Since the penalty function (J) has time derivatives, it is state dependent, that is the evaluation of J requires knowledge of at least the previous force state over the period of interest (T). The problem is now referred to as a dynamic optimization. While many techniques exist for solution of dynamic optimization problems, the two methods examined here, because of their intrinsic differences, are variational calculus methods and dynamic programming.

The variational approach suggests itself since it deals with functionals, (for example, force trajectories) which can be characterized by an integral that represents the cost of each trajectory. The general form of the variational problem in matrix, integral form is:

$$\min_{\underline{u}} \int_{t_1}^{t_2} L(\underline{u}, \dot{\underline{u}}, t)dt \qquad 4\text{-}6$$

which has the solution

$$\frac{d}{dt}\frac{\partial L}{\partial \dot{\underline{u}}} - \frac{\partial L}{\partial \underline{u}} = 0 \qquad 4\text{-}7$$

known as the Euler equation, where $\underline{u}$ is the control variable associated with $\underline{f}$ in equation 4-5. The necessary constraints can be appended to the Lagrangian (L) by the use of a Lagrangian multiplier (Hildebrand (1962)) which results in the Hamiltonian:

$$H = L + \underline{\lambda}(D\underline{u} - \underline{d}) \qquad 4\text{-}8$$

where

$$D\underline{u} = \underline{d} \qquad 4\text{-}9$$

defines the equality constraints on $\underline{u}$. The solution of this system is simply the Euler equation in H:

$$\frac{d}{dt}\frac{\partial H}{\partial \underline{\dot{u}}} - \frac{\partial H}{\partial \underline{u}} = 0 \qquad 4\text{-}10$$

This equation can be expressed in an expanded form (assuming a completely general H):

$$\frac{\partial^2 H}{\partial \underline{\dot{u}}^2}\,\ddot{\underline{u}} + \frac{\partial^2 H}{\partial \underline{u}\partial \underline{\dot{u}}}\,\dot{\underline{u}} + \left(\frac{\partial^2 H}{\partial t \partial \underline{u}} - \frac{\partial H}{\partial \underline{u}}\right) = 0 \qquad 4\text{-}11$$

which illustrates that the Euler equation is actually a second order, non-linear, vector differential equation in $\underline{u}$. If $\underline{u}$ has the dimension n, 4-11 provides n independent equations, but the constraints introduce the vector $\underline{\lambda}$ of dimension m, therefore the unknowns total n+m. The additional m equations are provided by the constraint equation 4-9, and the problem is now that of solving 4-11 and 4-9 simultaneously for n+m variables.

Solution of this system of equations, however, requires an iterative approach since no apriori knowledge of $\underline{\lambda}(t)$ is available. Borrowing on the general gradient method for solution of the open loop optimal control problem (Bryson & Ho, 1969) the following algorithm is proposed.

1) Use a static optimization method (such as linear programming) to get the initial conditions $\underline{u}(0)$.

2) Guess trajectories for $\underline{\lambda}(t)$ (probably constants).

equations. With the local minimum and speed of convergence problems added to this, viewed against the questionable significance of the time derivative term $\dot{\underline{f}}$ (which reflects the tendon compliance, see chapter 3) such a complex solution procedure seems unnecessary. This approach does, however, appear preferable to that of dynamic programming if the dynamic penalty function must be considered. The reasons for this are considered next.

The basic concept of dynamic programming is that a global minimum or maximum can be found by concatenating a series of local minima or maxima, therefore the optimum trajectory is found by solving a series of local optimizations (Hadley (1964)). However, dynamic programming is, in general, applied to problems where the constraint equations are dynamic and the penalty function is static (and where the initial conditions are uncertain) as in the multi-input optimal control problem. This is of course just the opposite of the present problem, and the ramifications are significant.

The former application is well illustrated in Kirk (1969, Chap. 3). To illustrate the application of dynamic programming to equations 4-2 and 4-3 with g again a function of force and its time derivative, as in equation 4-5, consider the following formulation. The dynamic programming formalism can be expressed in discrete form most easily and, since numerical solution is required, this form is appropriate. At discrete time intervals, the elements of the control vector f are also discretized into possible values. Starting from a previously determined (in time) optimal value for the control vector, $\underline{f}(t_1)$, all possible paths to time t_2 are investigated until that vector $\underline{f}(t_2)$ is found that minimizes the penalty function. ($f(t_1)$ must be known so that $\dot{\underline{f}}(t_2)$ can be approximated). However, the presence of equality

constraints on $\underline{f}$, (equation 4-3), makes the choice of any $\underline{f}(t_2)$ difficult (if not impossible) since all chosen control vectors must satisfy 4-3. This means that a method of solving 4-3 for any (i.e. non-optimal) force vector is necessary, and by obvious circularity, the original problem of redundancy and indeterminancy returns. Clearly this cannot be done in a practical manner, which makes dynamic programming inappropriate for this problem.

The dynamic programming algorithm is illustrative, however, in pointing toward the proper formulation of this problem for the case where the dynamics of the penalty function vanish. Problems of this type are appropriately termed static optimizations.

Static optimization: linear programming

The muscle model presented in chapter 3, when tendon compliance is neglected, results in a static relationship between mechanical and chemical power. Thus the general penalty function:

$$J = {}_T\int g(\underline{u}, \dot{\underline{u}}, t)\, dt \qquad 4\text{-}13$$

reduces to:

$$J = {}_T\int g(u, t)dt \qquad 4\text{-}14$$

If the dynamic programming algorithm is followed now, it can be seen that the state dependence caused by the $\dot{\underline{u}}$ term has vanished and the problem is greatly simplified. In fact, the problem now reduces to one of a time series of apparently independent, static optimizations where at each time step the task is minimization of the penalty function subject to the constraints appropriate at that time. Unlike dynamic programming, where all such solu-

tions had to be enumerated (one for each possible future state), there is now only one solution at each time, and it does not depend on the previous or future solution. This time series of static optimizations can be expressed in discrete time form

$$\min_{\underline{u}} J: \quad J \equiv g(\underline{n}(nT), nT) \cdot T \qquad 4\text{-}15$$

subject to:

$$D\underline{u}(nT) = \underline{d}(nT) \qquad 4\text{-}16$$

$n \equiv$ time step

$T \equiv$ step interval

Thus the complete problem is expressed:

$$\min_{\underline{u}} \sum_{u=1}^{N} g(\underline{u}(nT), nT) \cdot T \qquad 4\text{-}17$$

subject to the constraint equation 4-16 for n=1...N.

This procedure can be tailored to the present problem: minimize muscle chemical energy input, g, as a function muscle force and time only ($f(\underline{f},t)$) over a cycle or cycles of walking (NT) subject to moment constraints appropriate to walking ($R\,\underline{f} = \underline{m}$). Noticing that muscle powers are additive, the penalty function becomes a simple sum over all the active muscles and the form of the optimization becomes:

$$\min_{\underline{f}} \sum_{n=1}^{N} \sum_{i=1}^{M} G_i(f_i(nT), nT) \cdot T \qquad 4\text{-}18$$

with

$$R(nT)\underline{f}(nT) = \underline{m}(nT) \qquad n = 1 \ldots N \qquad 4\text{-}19$$

and $G_i(f_i, nT)$, from chapter 3, is the chemical power expression

$$G_i(f_i, t) = f_i(t)g(v_i(t)) \qquad 4\text{-}20$$

(Notice that $v_i(t)$, the normalized muscle velocity, is expressed as a function of time only since it is determined by the limb kinematics which have fixed trajectories over the cycle).

With this information, a solution technique appropriate to this problem can be found. By writing 4-20 in the discrete time form, and clearly separating the function of velocity from the force:

$$G_i(nT) = f_i(nT) \cdot g_i(v(nT) \qquad 4\text{-}21$$

it is apparent that at a given time step n, this expression is linear with force and 4-18 is a linear combination of all the forces. Therefore, the actual optimization is one with a static, linear penalty function with static, linear constraints. These conditions define a linear program, which will be the method used in all optimization presented here. In addition to the equality constraints of equation 4-18, a linear program is capable of handling inequality constraints which can be useful, for example, in bounding the forces between physiological limits.

Linear programming

To best describe linear programming and its applications it is useful to return to the viewpoint described at the beginning of this chapter, that of solving a set of indeterminant equations (constraints) by optimizing a

function of those variables (the penalty function). Linear programming described in this way is a means of solving a set of simultaneous, non-square linear equations. The way in which an optimal solution is found and the general characteristics of that solution are best introduced by a simple example.

Consider the problem:

$$\min_{x,y} J; \quad J = 2x + y$$

$$\text{subject to:} \quad 2x - y = 4$$

$$x + 3y \leq 9$$

$$x \geq 0$$

$$y \geq 0$$

A graphical representation of this problem and its solution are shown in figure 4-1. The penalty function, described by the line $2x + y = \text{constant}$, as it decreases, moves into the constraint area. It continues to move intersecting the equality constraint line until $y = 0$. Any further movement of this line would violate the $y \geq 0$ constraint, therefore the minimum value of the penalty function has been found at $x = 2$, $y = 0$

From this example, an important general property of linear programming is evident: <u>all</u> solutions involving n variables and m <u>equality</u> constraints will have no more than m non-zero variables in the solution. In other words, linear programming takes a non-square set of linear equations and finds that square subset of variables that minimizes the penalty function. In the case where inequality constraints are present the same is true. These constraints have no effect until one of the variables saturates against one of them and

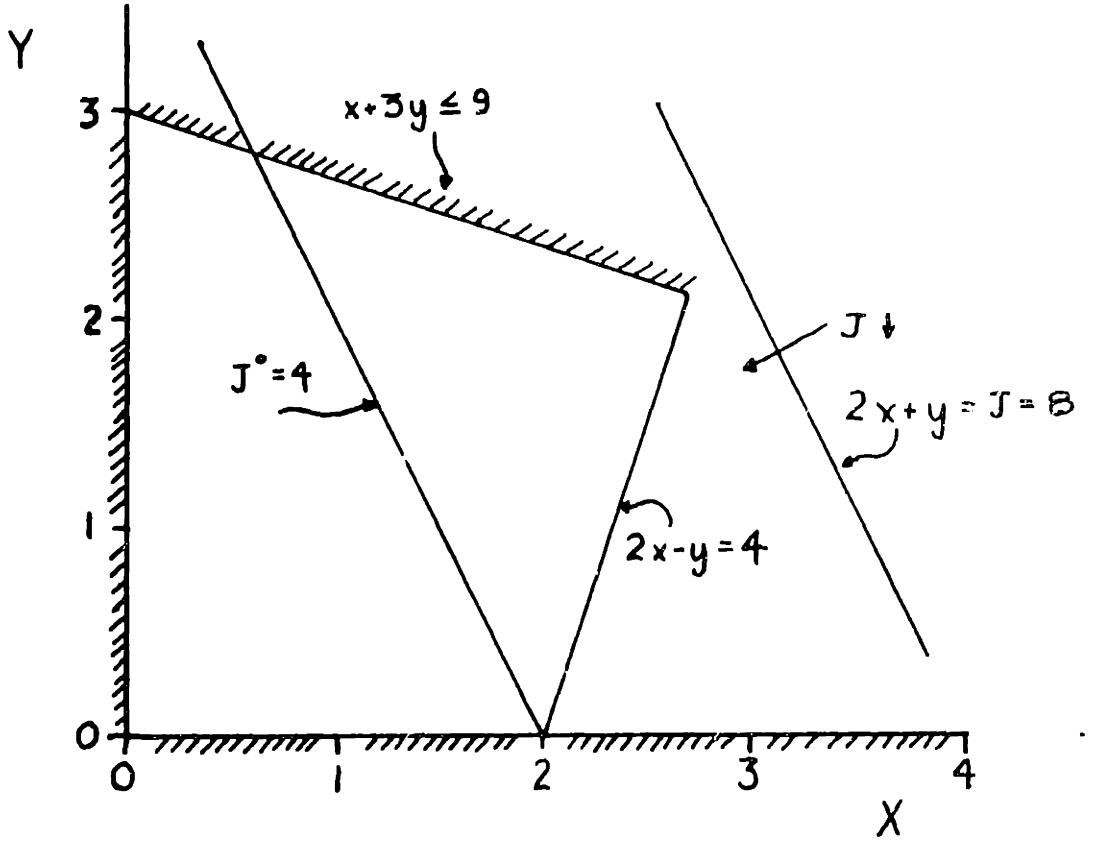

Fig. 4-1 Graphical Solution of the Linear Program:

$$\min J; \quad J = 2x + y$$

subject to:
$$2x - y = 4$$
$$x + 3y \leq 9$$
$$x \geq 0$$
$$y \geq 0$$

at that point the inequality constraint becomes an equality constraint thus increasing the possible non-zero solution space by one.

A potential solution algorithm, therefore, is one that first identifies all the possible combinations of square equation systems derived from the equality constraint matrix, the so-called basic solutions, and then picks the basic solution with the lowest (or highest) penalty function, updating the constraint matrix if any inequality constraints are reached. Such an algorithm would be correct but highly inefficient since linear programs tend to be large, and with n unknowns and m equality constraints there are $\binom{n}{m}$ possible combinations of variables to explore. A more efficient method is the revised simplex method which avoids this ennumeration by first finding any basic, feasible (i.e. within the constraints) solution, and then examining this solution against a set of "activity" variables (functions of the system variables, the constraints and the cost coefficients). The best direction to achieve the optimal solution can then be found and followed. In addition, the feasibility of arriving at <u>any</u> solution is quickly determined by this method. Specifics of the revised simplex method can be found in Hadley (1964).

Linear programming and muscle forces

The implication of the basic feasible solution as regards the muscle force problem are profound. Simply stated, without any constraints other than moments about the joints, the number of muscles active at any time will not exceed the degrees of freedom of the joints. A one degree of freedom muscle-joint system, under this formulation, needs only one muscle active at any time to be in equilibrium. For the problem of muscle forces in the leg with 31 muscles and 7 degrees of freedom, no more than 7 muscles will be

active at any instant, (unless an inequality constraint has been reached). It appears, therefore, that both the optimal criterion and additional constraints will have profound effects on the solution and these separate effects will be examined in chapter 6. For this problem, equality constraints, that is linear functions of muscle force, other than moment equations, do not exist. (Notice that if joint reactions are included as additional variables and the expressions for the muscle force contribution to these reactions are included in the constraint matrix, little has been gained, and some clarity has been lost. Since the number of variables has increased by the same amount as the number of constraint equations, and joint reactions will generally be non-zero, the number of possibly active muscles will not be increased by this procedure. It does, however, permit inclusion of the joint reactions in the penalty functions (as done by Seireg and Arvikar (1975)) more easily than if they are written into the penalty function only as implicit functions of force.

Proposed optimization and data requirements

The optimization to be used here is described by equations 4-18 and 4-19:

$$\min_{\underline{f}} \sum_{n=1}^{N} \sum_{i=1}^{M} G_i(f_i(nT), nT) \cdot T$$

with $$R(nT)\underline{f}(nT) = \underline{m}(nT)$$

Repeating the relationships of these variables to the physical problem: the function G_i represents the instantaneous chemical power requirements of muscle i, R(nT) is a matrix of three dimensional moment arms for all muscles

and will change with limb position and therefore with time, $\underline{f}(nT)$ are the muscle force magnitudes (R determines their directions), and $\underline{m}(nT)$ is a vector of moments about all three joints of the leg. Before executing this optimization process, data for muscle velocities (for $G_i(nT)$) muscle attachment points and their changes with time (for R(nT)) and joint moments (m(nT)) over a walking cycle must be obtained. The methods and experiments by which this is accomplished are described in the next chapter.

Chapter 5 Measurements and Experimentation

In this chapter experiments which involve the measurement of limb motion and myoelectric activity of leg muscles during walking are described. Also included are certain measurements of skeletal geometry required to locate the muscle moment arms about the joints. Finally, a method of calculating the joint moments given the limb motions will be described.

The objective of these experiments is to provide the data necessary for the optimization process set up in chapter 4 (anatomical information, limb kinematics, and joint moments) and to provide a measure of muscle activity for comparison with the predicted muscle forces through the use of myoelectric signals (MES). The experiments were performed on normal subjects under conditions as natural as the required instrumentation would permit. As stated in chapter 2 the nature of the problem formulation requires that solutions be found from data for individuals rather than from "typical" data, since the results are highly dependent on the individual subjects limb motions. Complete three-dimensional limb kinematic, joint moment, and simultaneously recorded MES data does not exist in the literature, thus a valid test of the minimum energy hypothesis and of the proposed optimization techniques demands experimentation.

Methods

Muscle geometry

An essential input to the muscle force optimization is the geometry of the muscles, specifically their attachment points relative to the joint centers of rotation. This information is represented by the matrix R in equation 4-19. The dearth of information about these attachments required direct measurements to be made. Although the muscles in the leg actually

appear much more like a distributed system with large areas of attachment and sometimes indistinct functional boundaries, reduction to point attachments and lumped function is adequate for the purpose of this investigation. (Carrying the distributed case to its extreme, one could imagine the muscles of the leg as continuously variable moment generators where appropriate regions of the muscle mass were activated to maintain the desired equilibrium, irrespective of anatomical boundaries. Studies on larger muscles (Hollinshead (1969)) have indicated that anatomical boundaries are not always consistent with functional boundaries especially when large attachment areas are encountered (for example, the gluteus maximus or adductor magnus muscles). A further assumption made here is that the muscles act along straight lines between the attachment points. Jensen (1975) has shown that this assumption is not always accurate, but he has also pointed out that it is the only practical representation. (Excentions to the straight line approximation are made here for the iliacus muscle which wraps around the head of the femur and the quadriceps group which acts on the patella and the patellar tendon).

With these qualifications, the following procedure was used to determine the muscle attachment points for the reduced set of muscle listed in table 5-1. Using several anatomy atlases, (Lopez (1971), Grant (1972), and Hollingshead (1964)), and observations on dissected human cadavers, the approximate centroid of attachment for each muscle was transferred to a human skeleton using boney landmarks for reference when possible. These skeletal members were then photographed in orthogonal planes (figures 5-1 to 5-3) and a location vector to each of these points from the appropriate joint center was measured from the photographs. The most difficult aspect

Fig. 5-1 Photo of Pelvis used to Determine Muscle Attachments

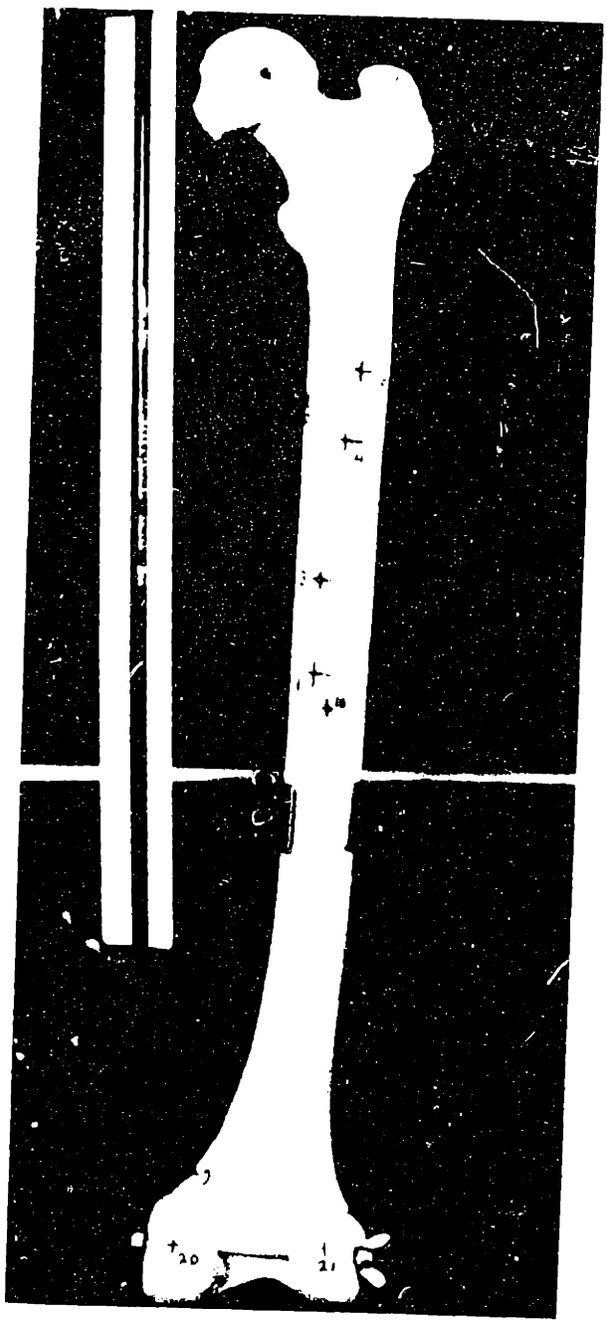

Fig. 5-2 Photo of Femur used to Determine Muscle Attachments

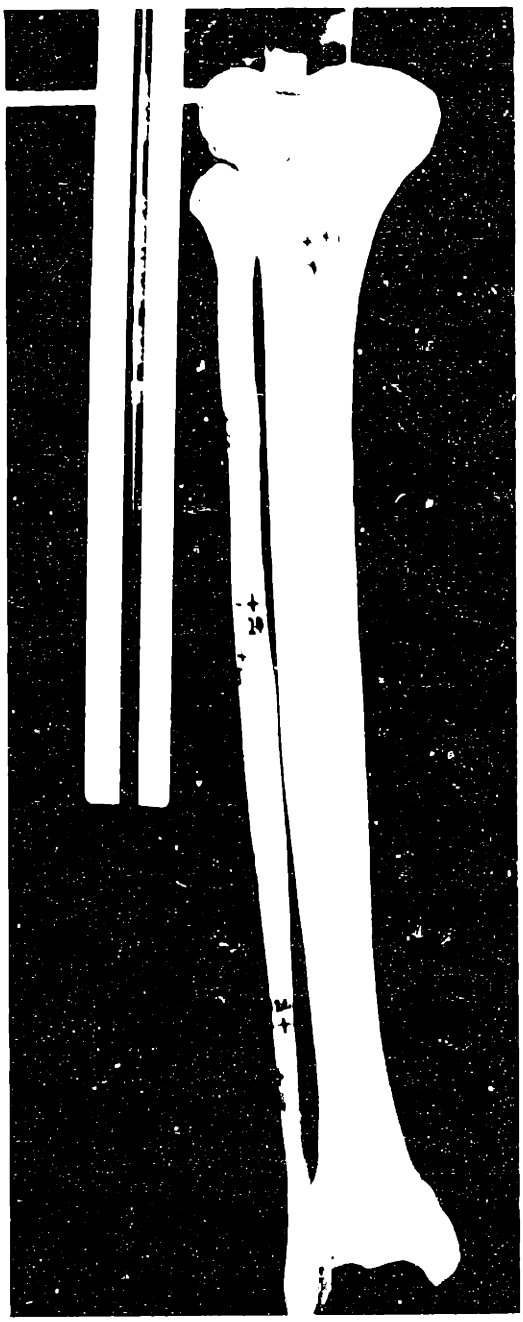

Fig. 5-3 Photo of Tibia used to Determine Muscle Attachments

of these measurements was approximation of the knee joint center since this is known to translate fore and aft during rotation of the knee (see Frankel et al. (1971)). For present purposes it was decided to measure from the rotation axis corresponding to the fully extended knee. This provides a well defined reference for later studies when dynamic tracking of the joint centers is anticipated.

The data for each skeletal segment was normalized to characteristic segment lengths chosen for their accessibility on the experimental subjects. These lengths were: pelvis: inter iliac crest distance, femur: greater trochanter to lateral femoral condyle of the knee, tibia: proximal to distal end of the fibula, and foot: foot length to big toe. This normalization procedure assumes that skeletal dimensions will dilate uniformly in all three dimensions, however, the validity of this one set of measurements for all subjects, even with the normalization, is not certain. An extensive study by Lew (1977) of various scaling methods, including uniform dilation, showed that increased accuracy could be obtained by using several characteristic dimensions for each limb, but the small increase in accuracy with this method would not be cost effective here considering its complexity. The muscle attachment data from these measurements is shown in Table 5-1.

Limb kinematics

Kinematic data for the limbs is required for two purposes: 1) the relative rotations of the limbs must be determined so that the muscle moment arms, muscle lengths and muscle velocities are known at all times, and 2) the joint moments will be calculated on the basis of displacement trajectories of the limbs. To collect this data, a unique measuring system was

	ORIGIN			INSERTION			SEGMENT #	
	X	Y	Z	X	Y	Z		
ADDUCTOR LONGUS	-0.29	-0.08	-0.04	0.06	-0.52	-0.02	1.	2.
ADD MAGNUS (EXT)	-0.16	-0.14	0.08	-0.04	-0.99	-0.03	1.	2.
ADD MAGNUS (ADD)	-0.16	-0.14	0.08	0.07	-0.44	-0.01	1.	2.
ADDUCTOR BREVIS	-0.25	-0.09	-0.02	0.08	-0.32	0.03	1.	2.
GLUTEUS MAXIMUS	-0.14	0.32	0.18	0.10	-0.25	0.04	1.	2.
GLUTEUS MEDIUS	-0.07	0.36	0.08	0.13	0.03	0.07	1.	2.
GLUTEUS MINIMUS	0.00	0.29	-0.01	0.15	0.01	0.04	1.	2.
ILIACUS	-0.02	0.28	0.01	0.02	-0.13	0.05	1.	2.
TENSOR FASCIA LATA	0.04	0.28	-0.13	0.13	-0.25	0.01	1.	2.
SEMITENDONOSUS	-0.08	-0.10	0.15	-0.02	-0.23	0.00	1.	3.
GRACILIS	-0.21	-0.12	0.01	0.00	-0.21	-0.05	1.	3.
SEMIMEMBRANOSUS	-0.06	-0.10	0.12	-0.06	-0.12	0.06	1.	3.
RECTUS FEMORIS	0.03	0.13	-0.11	0.03	-0.04	-0.09	1.	3.
SARTORIUS	0.08	0.21	-0.15	0.01	-0.22	-0.07	1.	3.
BICEPS (LONG)	-0.08	-0.06	0.15	0.10	-0.14	0.02	1.	3.
BICEPS (SHORT)	0.05	0.48	-0.03	0.10	-0.14	0.02	2.	3.
VASTUS LATERALIS	0.03	0.75	-0.02	0.03	-0.04	-0.09	2.	3.
VASTUS MEDIALIS	0.11	0.66	-0.07	0.03	-0.04	-0.09	2.	3.
VASTUS INTERMED.	0.16	1.05	-0.03	0.03	-0.04	-0.09	2.	3.
GASTROC (MEDIAL)	-0.08	-0.01	0.04	0.00	-0.15	0.19	2.	4.
GASTROC (LATERAL)	0.07	-0.01	0.04	0.00	-0.15	0.19	2.	4.
SOLEUS	0.07	0.78	0.02	0.00	-0.15	0.19	3.	4.
TIBIALIS ANTERIOR	0.07	0.73	-0.02	-0.04	0.03	-0.19	3.	4.
TIBIALIS POSTERIOR	0.07	0.57	0.03	-0.05	0.03	0.05	3.	4.
EXT. DIG. LONGUS	0.10	0.52	0.03	-0.05	0.01	0.06	3.	4.
EXT. HAL. LONGUS	0.06	0.22	0.03	-0.06	0.01	-0.17	3.	4.
FLEX. DIG. LONG.	0.01	0.42	-0.01	0.05	0.01	-0.18	3.	4.
FLEX. HAL. LONG.	0.07	0.38	0.03	-0.06	0.00	0.08	3.	4.
PERONEUS LONGUS	0.12	0.71	0.02	0.11	-0.05	0.04	3.	4.
PERONEUS BREVIS	0.09	0.36	0.04	0.11	-0.05	0.04	3.	4.
PERONEUS TERTIUS	0.07	0.18	0.03	0.14	-0.07	-0.12	3.	4.

Table 5-1 Normalized Muscle Attachment Points

The normalizing parameters are discussed in the text. Segment numbers: 1:pelvis, 2:femur 3:tibia, 4:foot.

used, called TRACK (The Real time ACquisition of Kinematic data) developed at M.I.T. by Conati (1977). The TRACK system permits tracking of multiple free bodies in three dimensional space and provides full three dimensional position and orientation data about each. This computer based system uses the SELSPOT (SELective SPOT identification) system, manufactured by SELCOM AB of Sweden, as the position measuring device and then converts this "raw" data into kinematic information. The SELSPOT system uses cameras that are sensitive to infrared light and have a detector plate that will generate currents proportional to the vertical and horizontal position of an IR point source focused on its surface. Using two obliquely positioned cameras, the three dimensional position of a given point can be calculated. By time multiplexing through up to 30 IR sources the SELSPOT system can track up to 30 points at a rate of 310 Hz. for each point. Infrared light emitting diodes (LEDS) are used as the light sources, and by attaching three or more LEDS on a given free body the orientation as well as the position of that body can be determined. If more than three LEDS per body are used, increased accuracy is achieved through the use of a least squares data fitting routine.

For this study six LEDS were attached to each segment, as shown in figure 5-4, and the motion of five segments: the trunk, and both of the thighs and shanks, was recorded. (Selection of these segments was necessitated by the limb dynamics model described later in this chapter). Attachment of the LED fixtures presented some significant problems. Ideally, the LEDS should not move relative to the skeletal members and should not be occluded from either camera's view. The latter was accomplished by having subjects walk toward the cameras (figure 5-5) and by displacing the fixtures

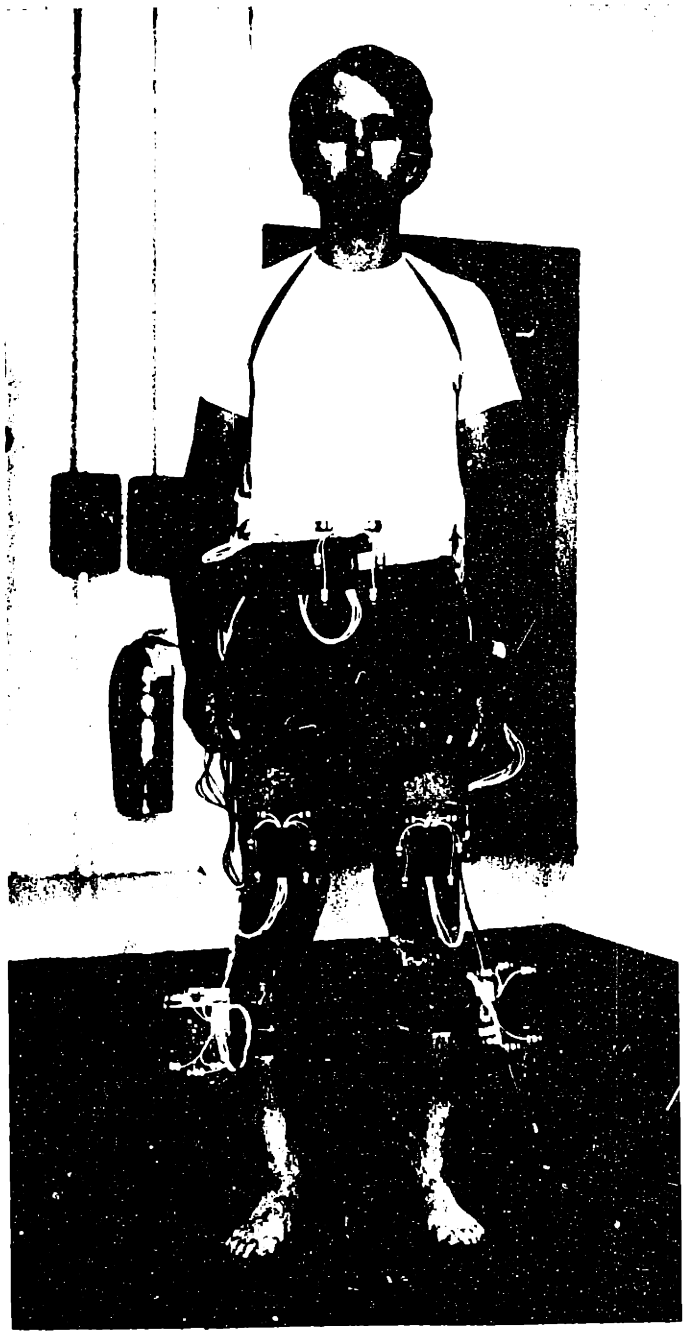

Fig. 5-4 Placement of LED Fixtures on the Skeletal Segments

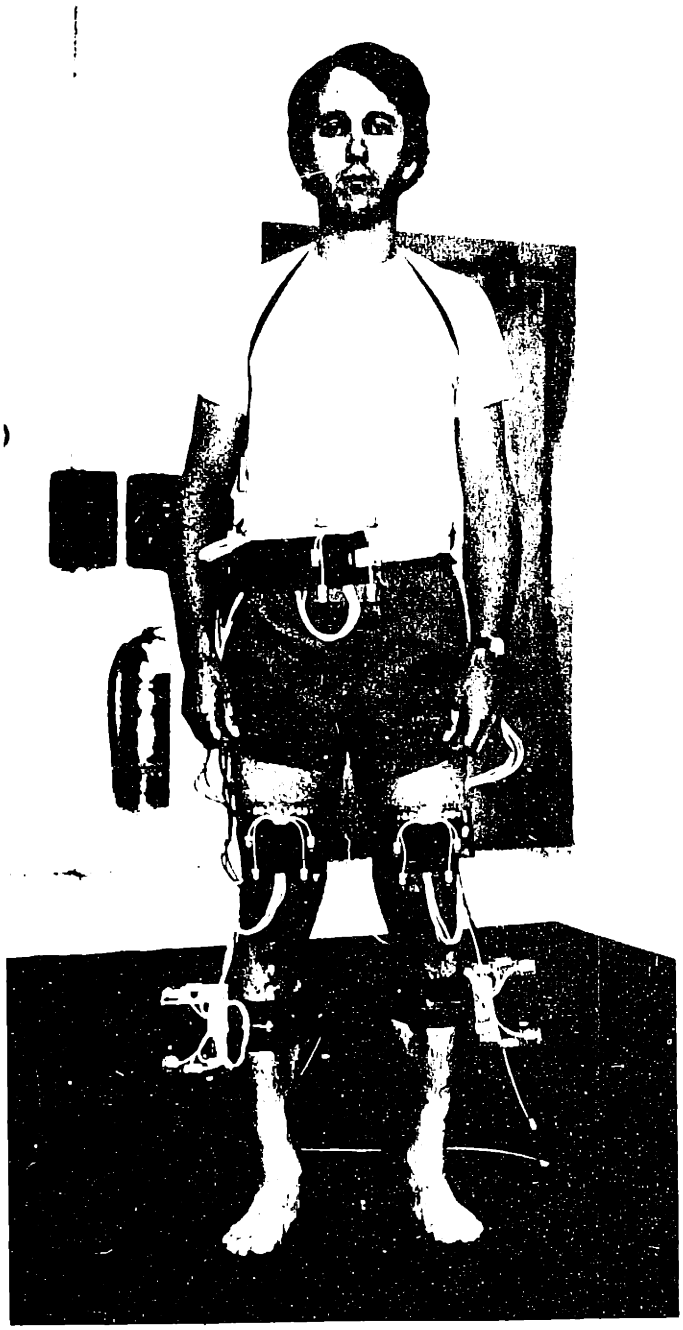

Fig. 5-4 Placement of LED Fixtures on the Skeletal Segments

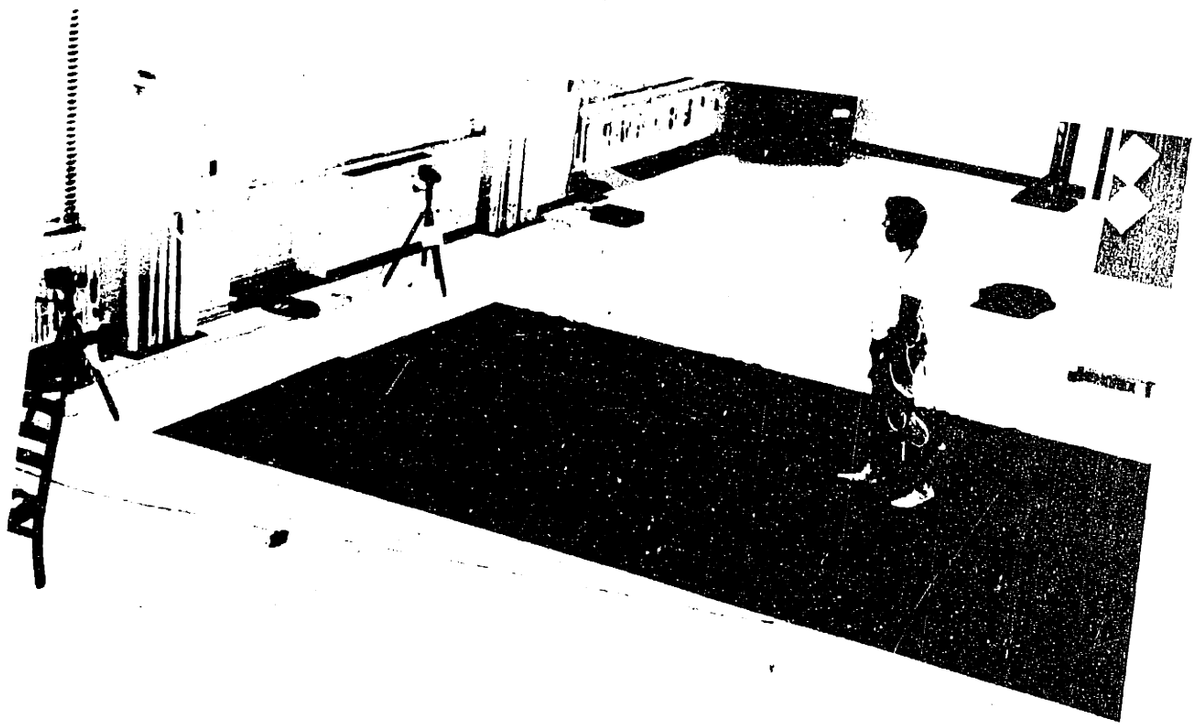

Fig. 5-5 Experimental Setup
The subjects walked on a thin carpet to reduce floor reflections. The TRACK cameras are at the left.

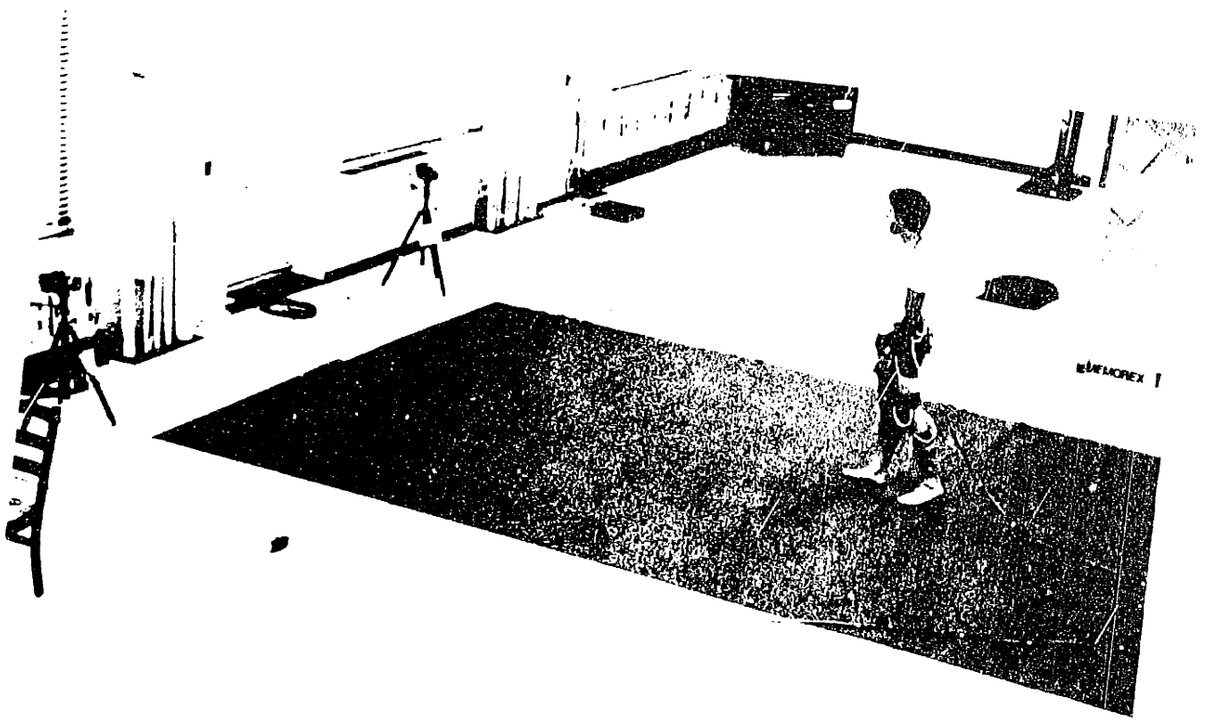

Fig. 5-5 Experimental Setup
The subjects walked on a thin carpet to reduce floor reflections. The THACK cameras are at the left.

for the shank laterally by 15 cm (figure 5-6). The problem of relative motion, however, caused the data to be corrupted with noise in the range of 8-10 Hz. (figure 5-7). While attachment to boney prominences would be ideal (see Levens et al. (1948)) willing subjects would be scarce, therefore, for comfort and simplicity the fixtures were simply strapped to the segments by wide elastic bands as shown in figure 5-4. The shank fixture, taking advantage of the accessible bone, was designed to lie against the lateral face of the tibia which does reduce relative motion. This gain was partially offset by the large rotational inertia of the extended tibia fixtures.

The most convenient data, from a dynamic modelling point of view, is the motion of the center of gravity of the members. Accordingly, the origin of each body fixed reference frame, represented by an LED fixture, was located at the approximate center of gravity of the appropriate segment using the data of Braune and Fischer (1889), and the position of each LED on each fixture was referred to these points. The TRACK system then used this information in all the position and orientation calculations.

The calculation of muscle length vectors (and their velocities), and the change of muscle moment arms with limb motion requires the relative rotation matrix between each of the skeletal segments. Since the TRACK system provides absolute rotation information (body rotations relative to a fixed reference frame) the relative rotation matrix must be calculated from the formula:

$$C_{12} = C_1^{-1} C_2 \qquad 5\text{-}1$$

C_1 = absolute rotation of body 1

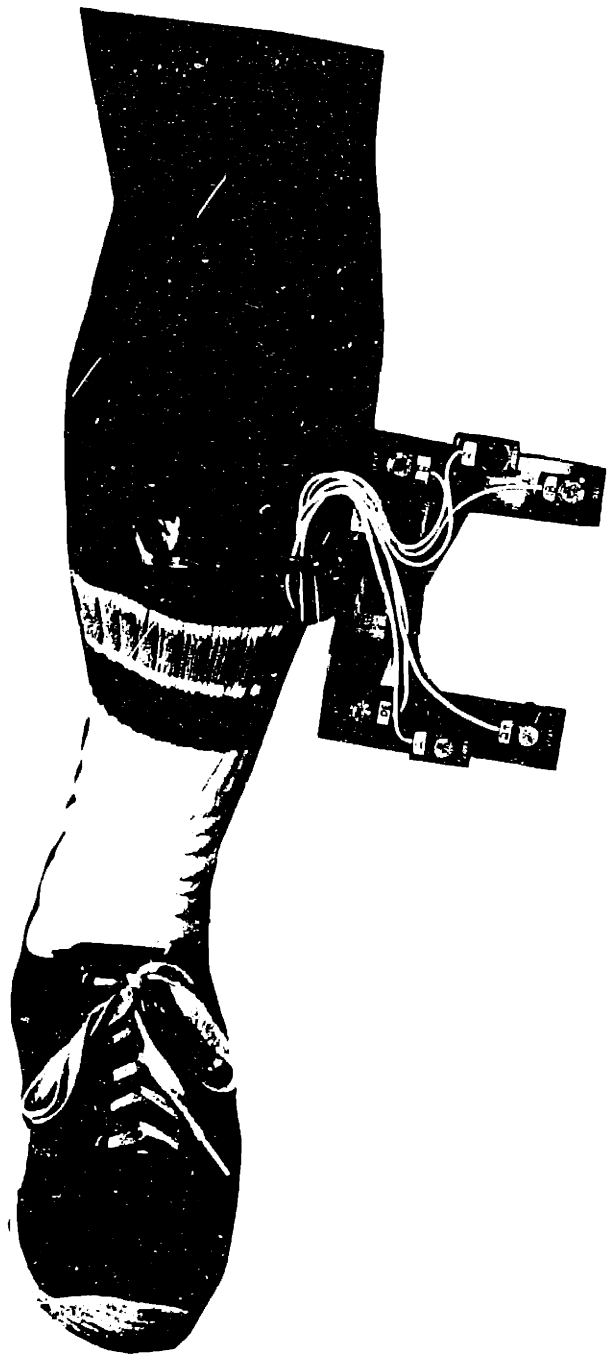

Fig. 5-6 Shank Fixtures

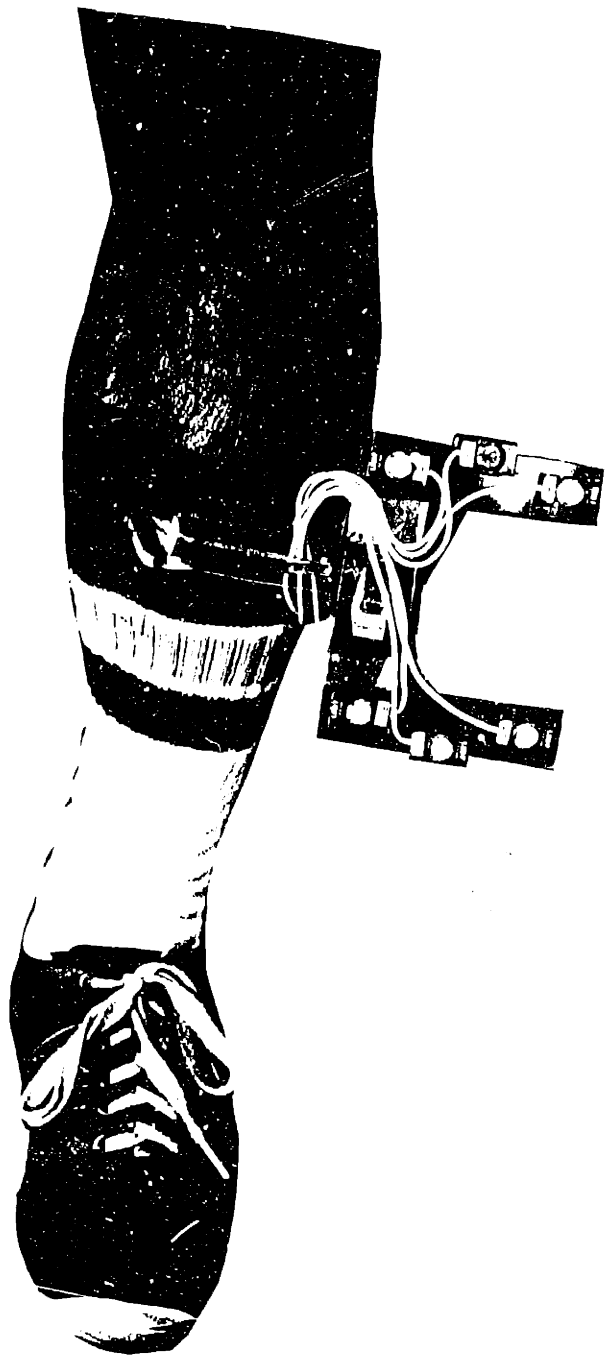

Fig. 5-6 Shank Fixtures

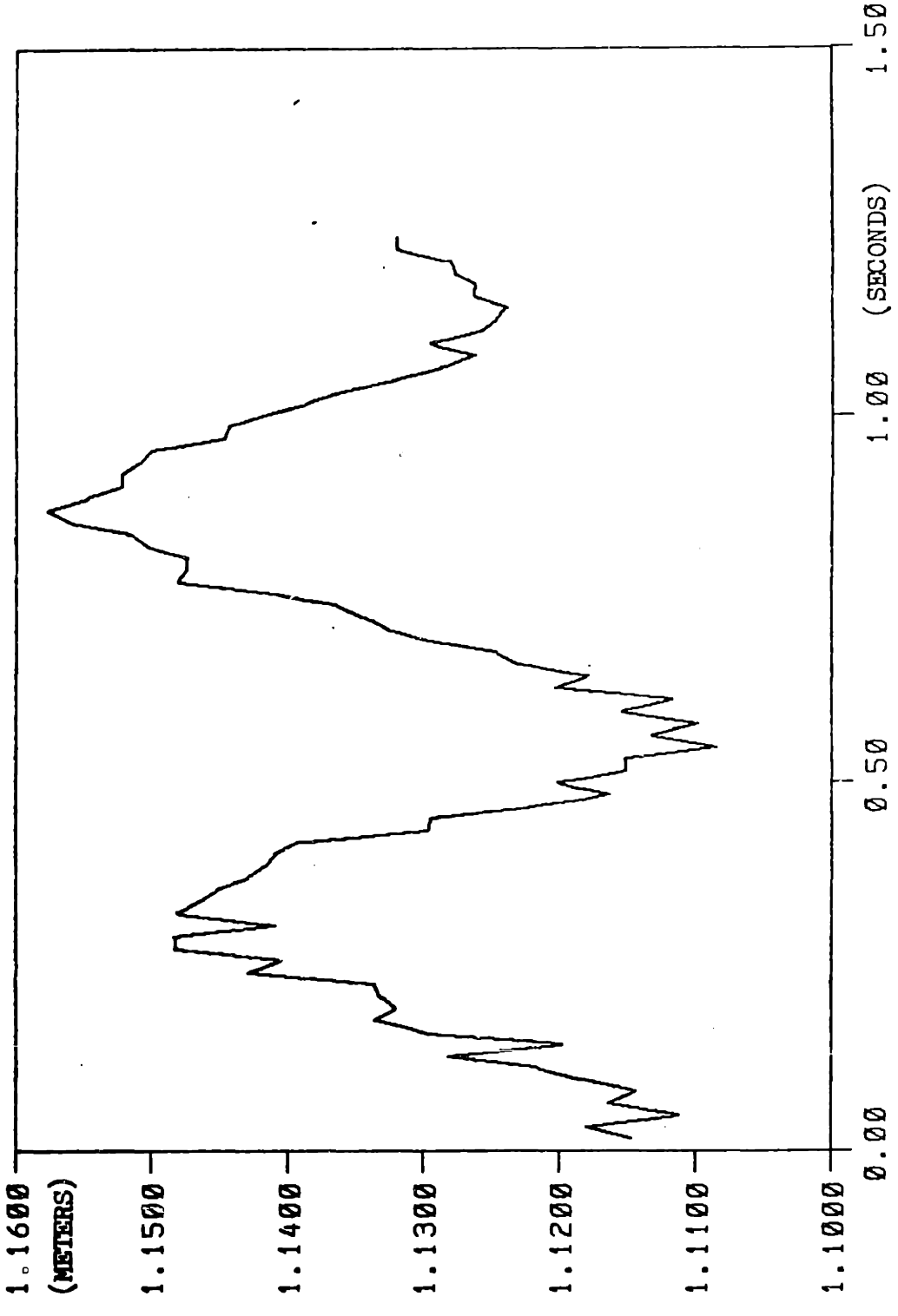

Fig. 5-7 Unfiltered TRACK Data for the Vertical Displacement of the Trunk

C_2 = absolute rotation of body 2

C_{12} = rotation of 2 wrt 1

To insure that the absolute rotation matrices are insensitive to the original placement of the LED fixtures on the segments, all orientation calculations were done with respect to a reference orientation for each body rather than to the fixed frame, otherwise constant rotation biases could be introduced which will affect the joint moment calculations. The reference rotation for each segment was determined by measuring the position and orientation of the fixtures (segments) with the subject stationary with the legs together. All subsequent rotation matrix calculations were made relative to these new reference frames using equation 5-1.

Details of the TRACK outputs and the post-processing used here are contained in appendix B.

Dynamic model of the lower limbs

The human body can be approximately modelled as a system of articulated, rigid, massy links, and given information about the motion of these links, the forces and moments acting on the system can be calculated. If each link is represented by a free body with a general set of forces and moments acting on its end points, as shown in figure 5-9, the equations of motion for each body can be written:

$$\Sigma\vec{F} = m\ddot{\vec{x}}_{c.g.} = \vec{F}_1 + \vec{F}_2 + m\vec{g} \qquad 5\text{-}2$$

$$\Sigma\vec{M}_{c.g.} = \frac{d}{dt}(I_{c.g.}\vec{\omega}) = \vec{M}_1 + \vec{M}_2 + \vec{r}_1 \times \vec{F}_1 + \vec{r}_2 \times \vec{F}_2 \qquad 5\text{-}3$$

$\vec{F}_1, \vec{F}_2 \equiv$ end forces applied at joint centers

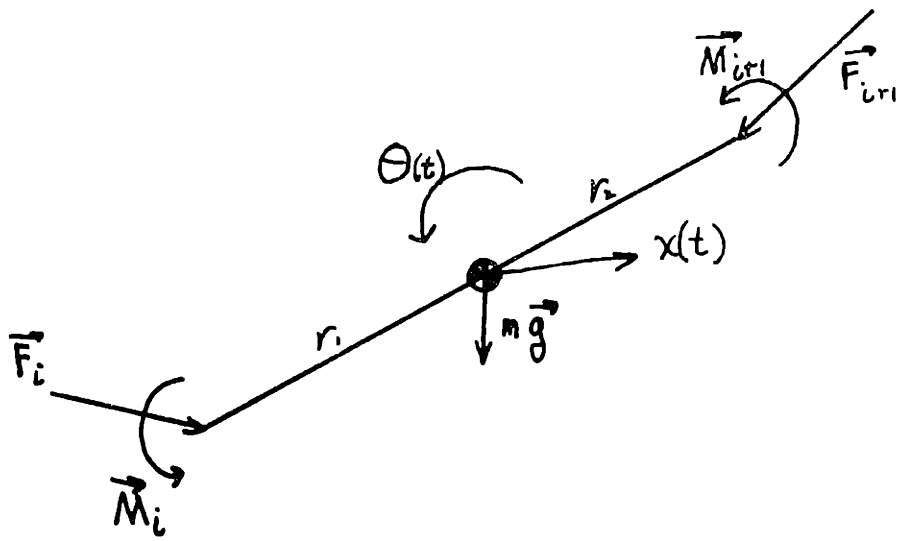

Fig. 5-9 Free Body Diagram of a Single Skeletal Link

$\vec{M}_1, \vec{M}_2$ ≡ joint moments

m ≡ mass

$I_{c.g.}$ ≡ moment of inertia about the center of gravity

$\vec{r}_1, \vec{r}_2$ ≡ moment arms of force vectors about the center of gravity

(Notice that the effect of muscle forces have been condensed into pure moment generators on the limb. This makes the problem solvable, but it also leaves the joint forces, F_1 and F_2 incomplete since the muscular component of this force must also be included).

From the kinematic information the accelerations $\ddot{\vec{x}} + \frac{d}{dt}\vec{\omega}$ can be derived. The methods used here are described in appendix B. The mass distribution information of Braune and Fischer (1889) was used to estimate m and I given characteristic lengths and diameters for each subject. With this information, equation 5-2 can be solved for the forces

$$\vec{F}_1 + \vec{F}_2 = m\ddot{\vec{x}}_{c.g.} - m\vec{g} \qquad 5\text{-}4$$

If a force plate is available to measure the foot - floor force, equation 5-4 can be solved completely for the foot segment with the foot forces as the input and the ankle force as the output. Since no force attenuation occurs across the joints, subsequent proximal segment equations can now be solved provided their motion is known. Similarly, knowing all forces and measuring the foot - floor moment, equation 5-3 can be used to solve for all the joint moments. This is essentially the method used by Bresler and Frankel (1950) as well as many other contemporary investigators.

If a force plate is not available, as was the case here, the most distal force (the foot force) cannot be measured and a slightly different approach must be taken. If the links are assembled into a complete lower limb system,such as shown in figure 5-10, there will be five force and five moment vector equations, one for each link. However, their are six unknown force and moment vectors. This indeterminateness can be resolved by considering the normal walking cycle. During most of the cycle one of the legs is swinging above the ground, thus the most distal force and moment on that leg is zero and the system of equations is solvable. However, a problem arises when both feet are on the ground, which occurs during double leg stance, the distinguishing characteristic of walking vs. running that occupies about 24% of the total cycle. During this time the distribution of forces and moments between the feet is unknown. McGhee (1976) approximated this force and moment transfer between the present stance foot and the present swing foot as a linear function of double leg stance time. To apply this to the present model shown in figure 5-10, consider the right leg in contact with the ground and the left leg was completing its swing phase. The dependence of the forces and moments would be expressed :

$$\vec{F}_0 = \vec{F}_1 + \vec{F}_6, \quad \vec{M}_0 = \vec{M}_1 + \vec{M}_6$$

$$\vec{F}_6 = \frac{t-t_1}{t_2-t_1} F_0 \qquad 5\text{-}5$$

$$M_6 = \frac{t_2-t}{t_2-t_1} \vec{M}_o \qquad 5\text{-}6$$

where t_1 = beginning of double leg stance

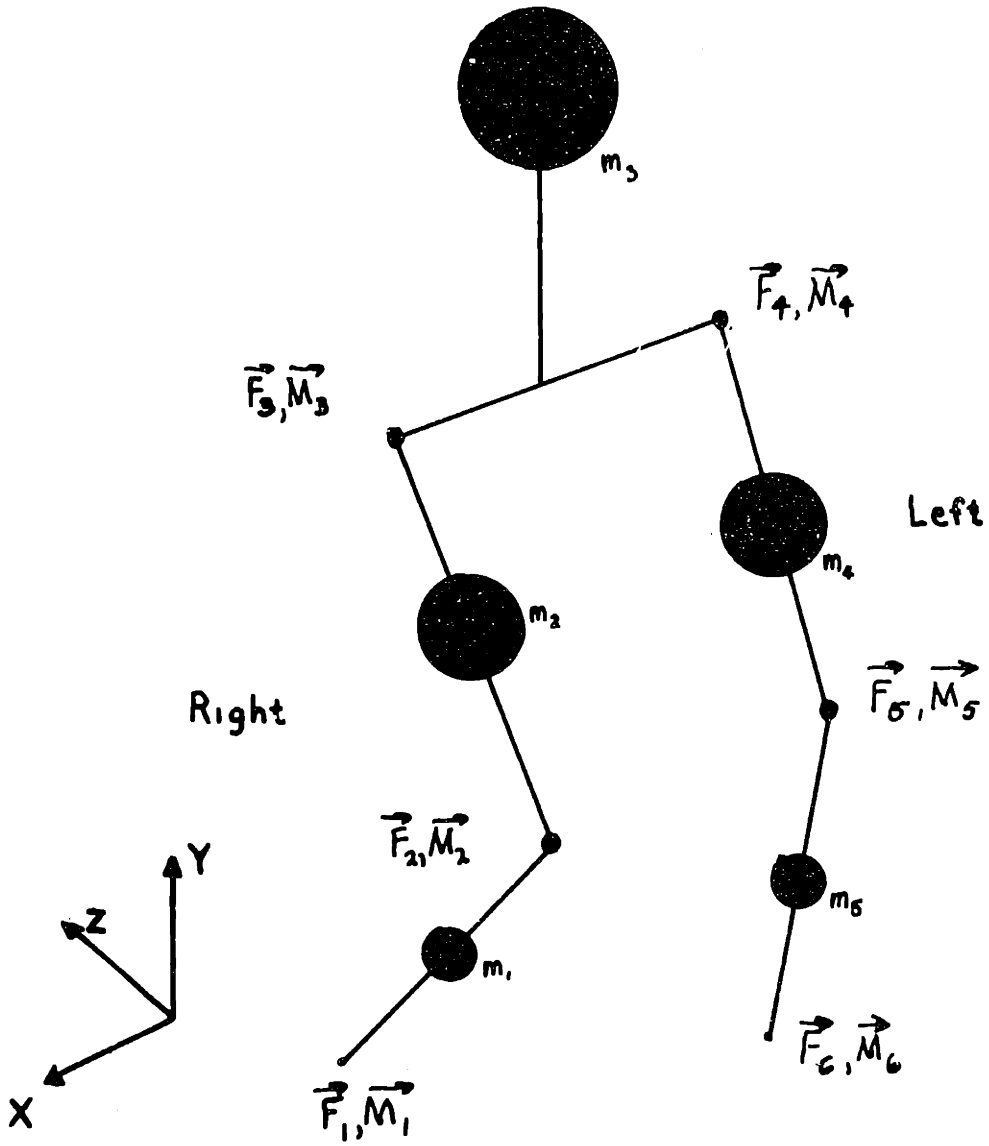

Fig. 5-10 Five Segment Dynamic Model

t_2 = end of double leg stance

F_1, M_1 = forces and moments on right ankle

F_6, M_6 = forces and moments on left ankle

This dependence between the force and moment vectors of the ankle again yields a solvable set of equations and all forces and moments for the model can be found for the entire walking cycle provided the timing of the double leg stance portion is measured. (The latter was accomplished by the use of foot switches on the heel and toe of the subejcts shoes).

This solution procedure was implemented in the following manner. Combining link equations 5-2 and 5-3 into a system describing the 5 link model of figure 5-10, the matrix equations

$$M\ddot{\underline{x}} = \Gamma \underline{f} + \underline{mg} \qquad 5\text{-}7$$

$$\frac{d}{dt}(I\underline{\omega}) = \Gamma \underline{m} + \underline{rxF} \qquad 5\text{-}8$$

can be written, where:

M = mass matrix (15 x 15 diagonal)

$\ddot{\underline{x}}$ = acceleration vector (15 element)

$\underline{mg}$ = gravity vector

$\underline{f}$ = force vector (15 elements)

I = inertia matrix (15x15)

$\underline{\omega}$ = angular velocity vector (15 elements)

$\underline{m}$ = moment vector (15 elements)

rxF = cross product vector

Γ = matrix of constants relating forces across the joints and the ankle dependence during double leg stance (15x15)

Solving these for the force and moment vectors yields:

$$\underline{f} = \Gamma^{-1} (M\ddot{\underline{x}} - \underline{mg}) \qquad 5\text{-}9$$

$$\underline{m} = \Gamma^{-1} \left(\frac{d}{dt} (I\underline{\omega}) - \underline{rxF} \right. \qquad 5\text{-}10$$

Implementation of the single leg stance - double leg stance algorithm is accomplished by using the appropriate set of force and moment vectors (i.e. for left leg stance, the right leg ankle forces are dropped from the vectors) and by using the proper Γ matrix for that set. There will be three Γ matrices, one for each single leg stance phase and one for the double leg stance phase. In single leg stance, the matrix reflects the coupling of equal and opposite forces across the joints, but for double leg stance the matrix incorporates equations 5-5 and 5-6 into the elements relating ankle forces and moments. The calculation routine must switch between these three matrices depending upon which phase of gait is occurring. During double leg stance the dependent ankle forces and moments must be calculated separately by application of equations 5-5 and 5-6 to the force set found above, which yields all six force and moment vectors.

A five segment human body model was used here because of the impracticality, at present, of instrumenting more than 5 segments. This reduction necessitates several assumptions. By not including the feet their inertial contribution to the ankle moments is neglected. This does not seem severe since the feet represent only 5.7% of the total leg weight (Drillis et al. (1964)). A greater loss is the lack of information about the foot position

and the ankle angle. As a result the assumption must be made that the ankle remains locked at zero degrees of flexion; consequently all muscle moment arms and lengths for ankle muscles will not change over the walking cycle.

By lumping the head, arms, trunk, and pelvis into one body (the HAT) the independent motion of these four elements is neglected. Probably the most significant of these motions is rotation of the trunk with respect to the pelvis and head about a vertical axis, which is normally accompanied by the characteristic swinging of the arms. The swing of the arms and rotation of the trunk tend to counterbalance an opposite rotation of the pelvis as the legs swing forward. By neglecting the arm swing, the calculated moments at the HAT - femur joints (the hips) will be higher than if arm swing were included. Although the HAT is rather massive, representing 63% of total body weight, this trunk rotation is of small magnitude and the concomitant error is not expected to be significant.

A final note on the actual calculations: the TRACK data is essentially position and orientation data referenced to the center of gravity of each segment in the absolute or fixed reference frame, therefore equation 5-9 can be solved by direct use of this data for the forces. The moment equation 5-10, on the other hand, is considerably more difficult to solve in the fixed reference frame because the inertia matrix as seen in this frame will change with time. However, if the equation is written instead in a body fixed reference frame, the inertia matrix will be constant, and if the body fixed frame is aligned with the principal axes of the segment the inertia matrix becomes diagonal. To properly evaluate the term

$$\frac{d}{dt}(I\underline{\omega})$$

with I expressed in a body fixed or relative frame, the angular momentum vector ($I\underline{\omega}$) is treated exactly like any other general vector, and the formula for the time rate of change of a vector in a rotating frame (Crandall et al. (1968)) is used:

$$\frac{d}{dt}(I\underline{\omega}) = I_{rel}\,\underline{\omega} + \underline{\omega} \times I_{rel}\,\underline{\omega}$$

This relationship is then applied to each segment in its respective body fixed frame. Before pre-multiplication by Γ^{-1}, as dictated by equation 5-10, each segment in the system must be referred to a common frame, the best choice being the fixed reference frame. With this modification, the moment equation of equation 5-10 becomes

$$\underline{m} = \Gamma^{-1}(C^{-1}(I\underline{\omega} + \underline{\omega}xI\underline{\omega} - rxF)_{rel})$$

where the elements of I and $\underline{rxF}$ are all referred to their respective body fixed frames and C^{-1} represents a 15 x 15 matrix that collects the individual segment rotation matrices along its diagonal. The resulting joint moments are thus referred to the fixed frame consistent with the joint force calculation.

The result of these calculations are moment - time histories for all of the leg joints and those components of the joint reaction forces due to inertial and gravitational influences only. (As stated earlier the total joint force will also have a large contribution due to the muscular forces that can only be determined after the joint moments are known).

Myoelectric measurements

A measure of muscle force is necessary for comparison with the forces calculated by the optimization procedure. Non-invasive methods are not available for this and the only measure of muscle activity suitable here is the myoelectric signal (MES), which reflects the electrical state of a contracting muscle and which can be roughly related to muscle force. For the purposes of these experiments a fourteen channel multiplexer was built to switch between fourteen electrode-preamplifier packages and to send the information out on a single line. (This design will make it possible, eventually, to transmit this data by FM radio telemetry eliminating the umbilical cord now required, however a high bandwidth receiver not presently available would be required). Details of the acquisition and recording system are contained in appendix C, but it is described briefly below.

On the skin above each muscle of interest, a preamplifier - electrode package (purchased from the University of Utah Projects and Design Laboratory) is taped securely in place. In areas where good contact could not be maintained in this way, the electrodes were separated from the preamplifier and taped to the skin. Short leads (~3 cm) were run to the preamp which was also taped to the skin. By keeping the preamp close to the electrodes the signal to noise ratio of the MES signal is kept high and the low impedance output of the preamps renders the cable length leading to the data acquisition system non-critical. As with most MES systems the electrodes are arranged in differential pairs to reject common signals, most importantly 60 Hz. noise, and a single remote ground electrode is provided.

The multiplexing system (worn on the subject's belt) is shown in figure 5-11. It provides power to the

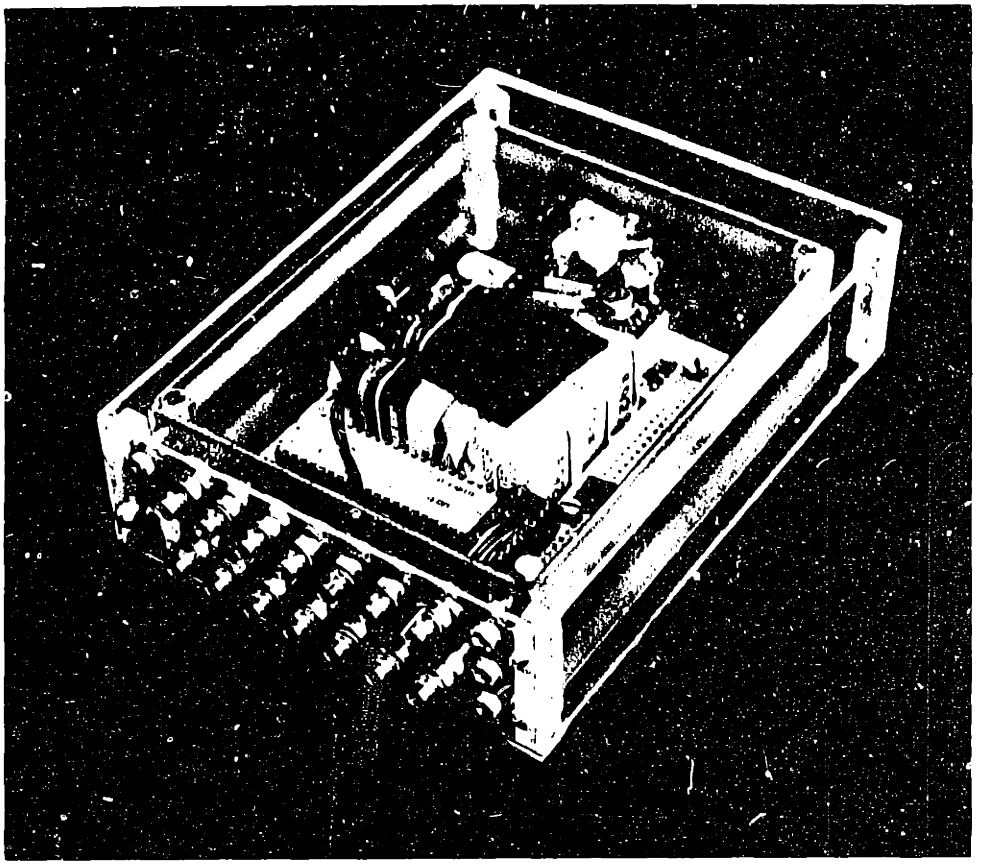

Fig. 5-11 The Fourteen Channel MES Multiplexer

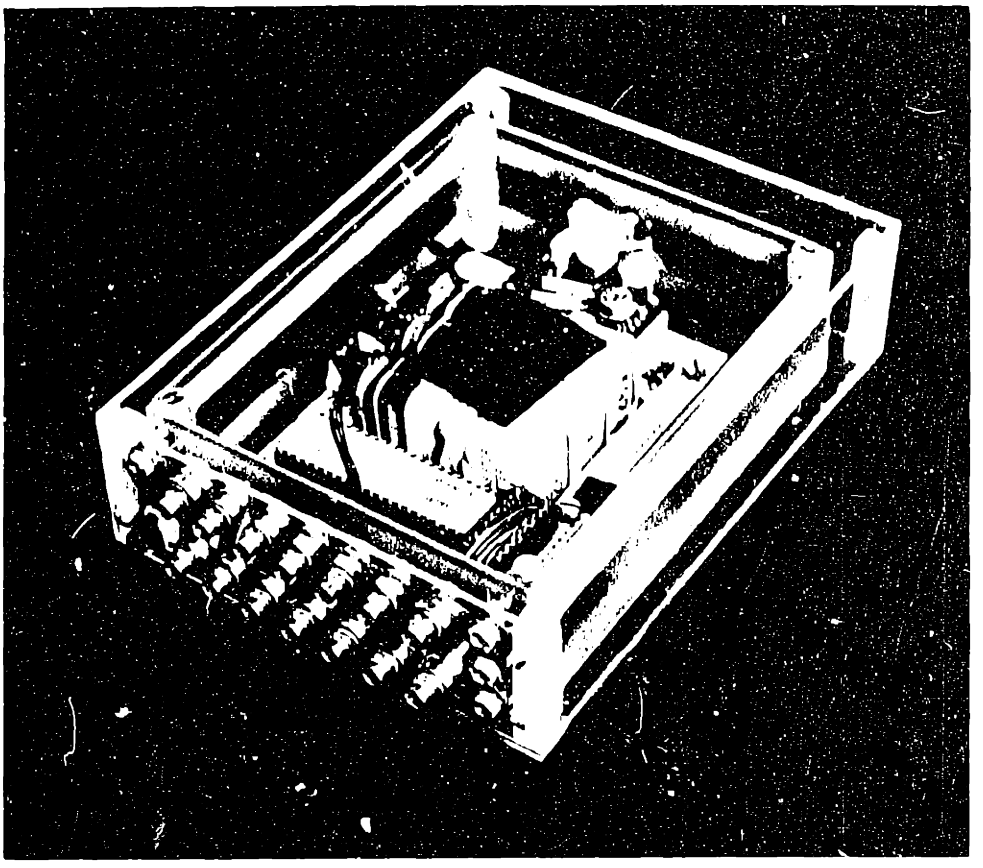

Fig. 5-11 The Fourteen Channel MES Multiplexer

preamps, switches between each separate preamp at a frequency of 1000 Hz., and provides a line driver for the umbilical cable to the recording system. In addition to fourteen myoelectric signals, a constant amplitude reference and synchronization pulse, and a ground level pulse are provided for a total of sixteen signals serially transmitted on the output line (see Appendix C) The 1000 Hz. switching rate between the electrode pairs (which means a 16 kHz. clock rate for the multiplexer) was chosen by assuming that the power spectrum of MES's is in a frequency band between 30 and 300 Hz. (Hogan (1977)); and, from Shannon's sampling theorem, the sampling rate should be at least two times faster than the high frequency roll off of the input signal. No local filtering of the signals was done prior to their transmission.

After sending the signals through an umbilical cord the multiplexed signal, which is essentially a 16 kHz. square wave of varying amplitude, is partially demultiplexed from a 16 on 1 channel to a 4 on 4 channel arrangement by a circuit specifically designed for this task (figure 5-13). This operation effectively lowers the square wave frequency on each of the resulting four channels to 4 kHz enabling them to be recorded on a multichannel FM tape recorder. The final demultiplexing of the "four on four" signals to sixteen separate signals is done off-line by computer. These individual signals are bandpassed between 30 and 300 Hz using a fourth order digital Butterworth filter, the absolute value taken, and can be low passed at 10 Hz using a second order digital Butterworth filter, according to classical MES processing as described by Hogan (1976). An example of one signal and the various stages of processing is shown in figure 5-14.

Electrode placement on the subject varied according to accessibility of the muscles and degree of surface body fat. On flat, nearly motionless

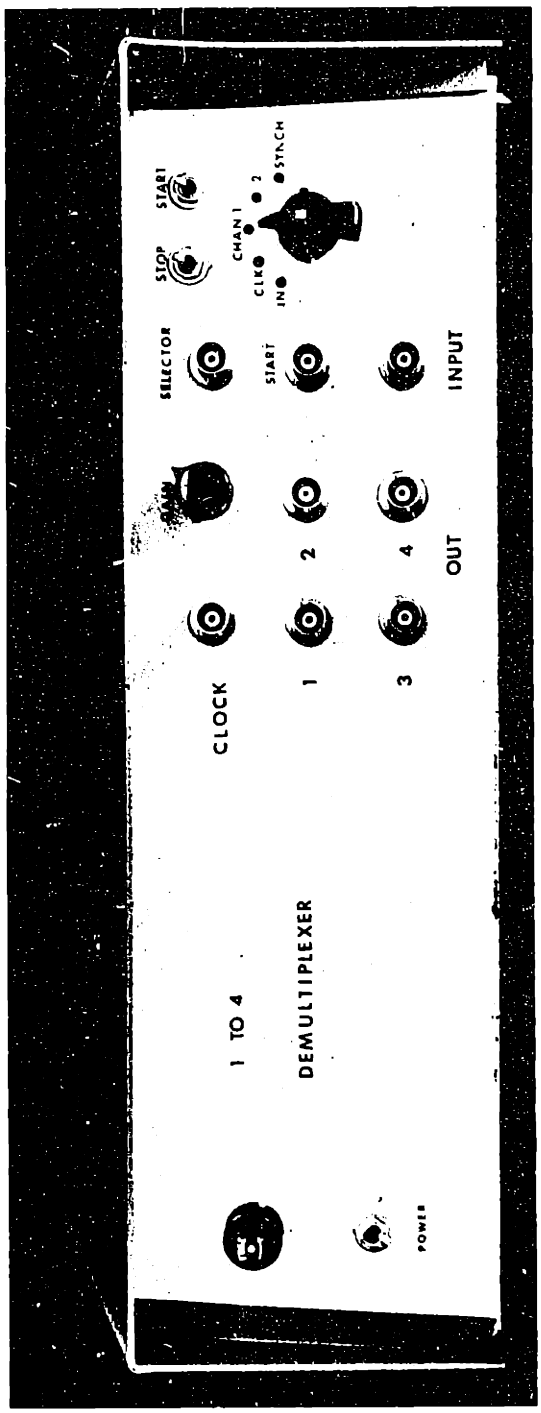

Fig. 5-13 16 on 1 to 4 on 4 Demultiplexer
(Circuit details are in Appendix C)

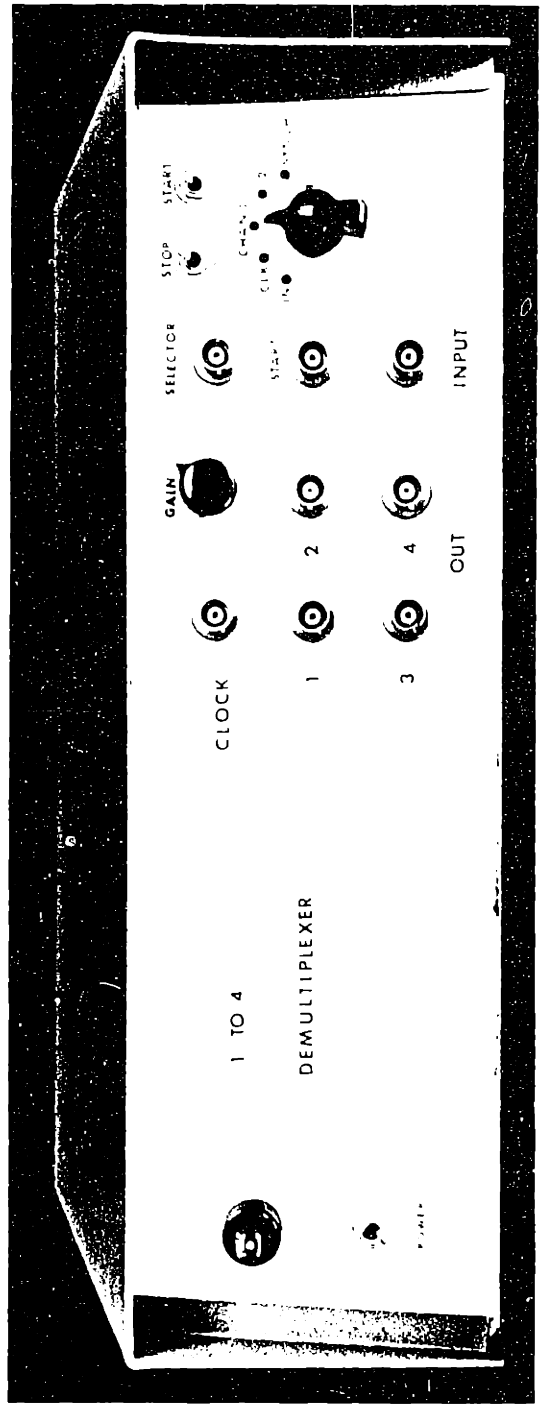

Fig. 5-13 16 on 1 to 4 on 4 Demultiplexer
(Circuit details are in Appendix C)

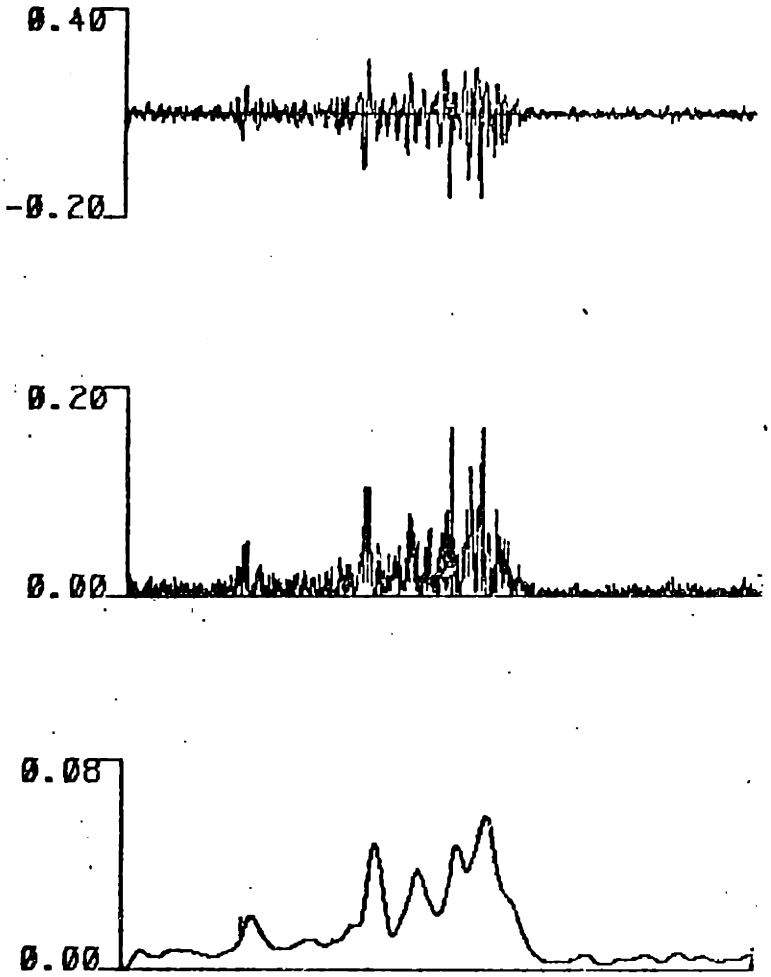

Fig. 5-14 Typical MES Data Obtained using the 14 Channel Multiplexed Acquisition System

This data is from the gastrocnemius muscle and is shown bandpassed (30,300 Hz.), rectified and low-pass filtered @ 20 Hz.

muscles such as gastrocnemius or tibialis anterior the separate electrodes were not needed, but on all others, particularly the hip muscles, remote electrodes were essential. These two arrangements are shown in Figure 5-15.

Signal strength varied according to electrode placement and no attempt was made to maximize output before taping the electrodes in place primarily because of TRACK LED placement considerations. Movement artifacts (large amplitude, low frequency signals $\leq$ 5 Hz) were a problem, but the bandpass filtering eliminated these effects provided the artifacts were not large enough to cause the recording system to lose synchronization or saturate momentarily.

Despite the availability of fourteen MES channels, only ten were used since only ten preamp packages were available at the time of the experiments.

Experimental protocol

Experiments designed to collect MES data from ten superficial muscles of the right leg and to record the position and orientation trajectories of the five segments used in the limb dynamics model were performed on two subjects. One trial consisted of recording data for one complete cycle of walking (both legs completing one cycle) and a window of data corresponding to right heel strike to right heel strike was taken from this cycle. This approach avoided filter transient problems associated with TRACK data processing. Kinematic and MES data were synchronized in time by recording a common start-stop signal. The precise timing of the various phases of the walking cycle, (swing and double leg stance in particular) was measured by foot switches attached to the heel

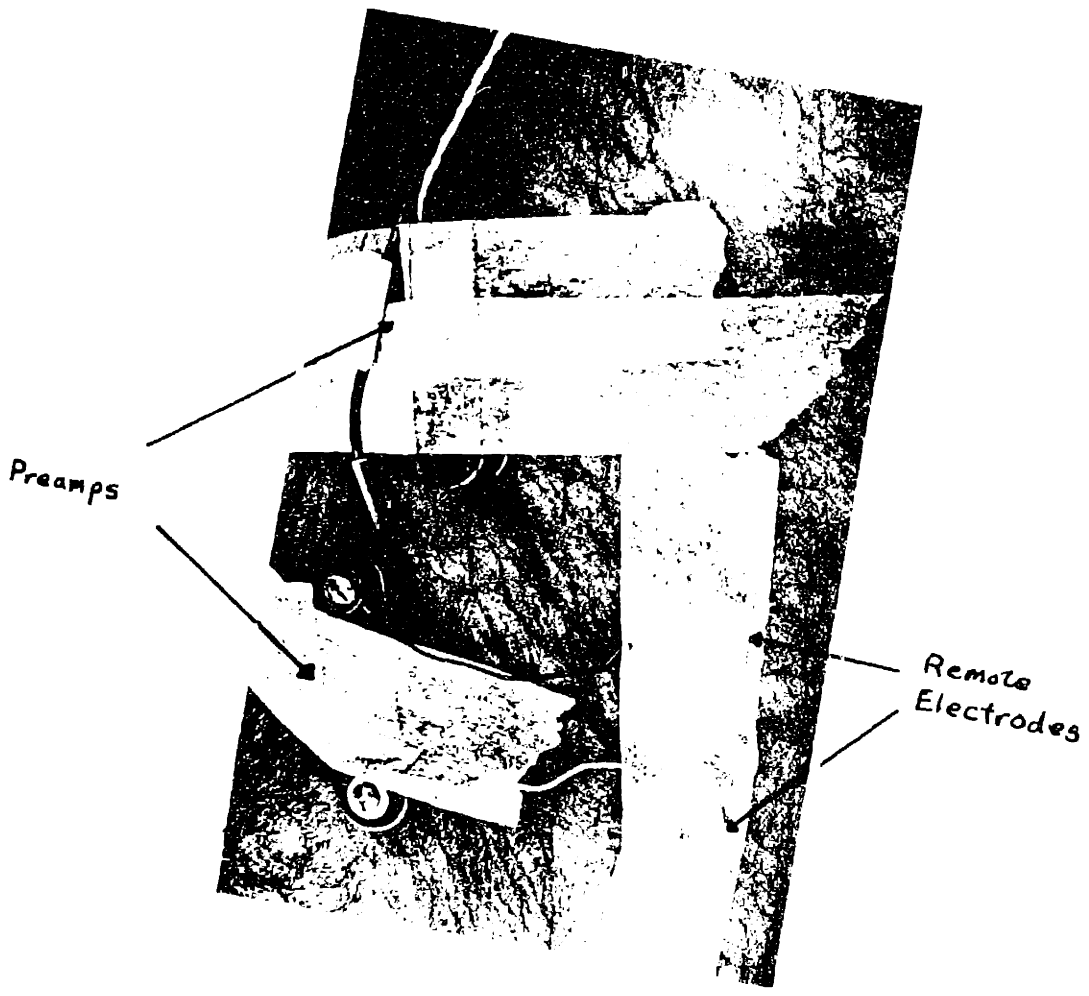

Fig. 5-15 MES Electrode Attachment Methods
Surgical tape is used to secure both the electrode and the preamp package.

and toe of the subjects' shoes.

Each subject was allowed several strides before the data was recorded and six to nine trials were performed on each subject. The subjects were asked to walk at various speeds, roughly classified as normal, fast, and slow, so that walking speed - energy consumption comparisons would be possible. Although heavily instrumented, as shown by figure 5-4, the apparent effect of this on the gait patterns was minimal after 15-20 minutes of wearing, according to the subjects.

Typical results

Complete presentation of the results will be deferred until the next chapter, however, the kinematic data along with the calculated moments for subject JRD are shown in figures 5-16 to 5-17. The effect of low-pass filtering of the TRACK data can be seen in the moment data of figure 5-17. The cutoff frequency used for this filtering, 5 Hz, was lower than desired. A discussion of the estimated frequency spectrum of joint angle movements is contained in Appendix D.

Noise problems and limited range of the TRACK cameras were the most critical problems in this study. The former is particularly a problem with the trunk where the small movements with nearly constant amplitude, additive measurement noise makes accurate position determination difficult. Also, owing to its large mass, these motion errors will be amplified during the moment calculations. The small range of the cameras, caused primarily by limited dynamic intensity range of the cameras, led to a signal to noise ratio for the TRACK data that varied inversely with the subjects distance from the cameras. The use of redundant LED's greatly diminished this problem.

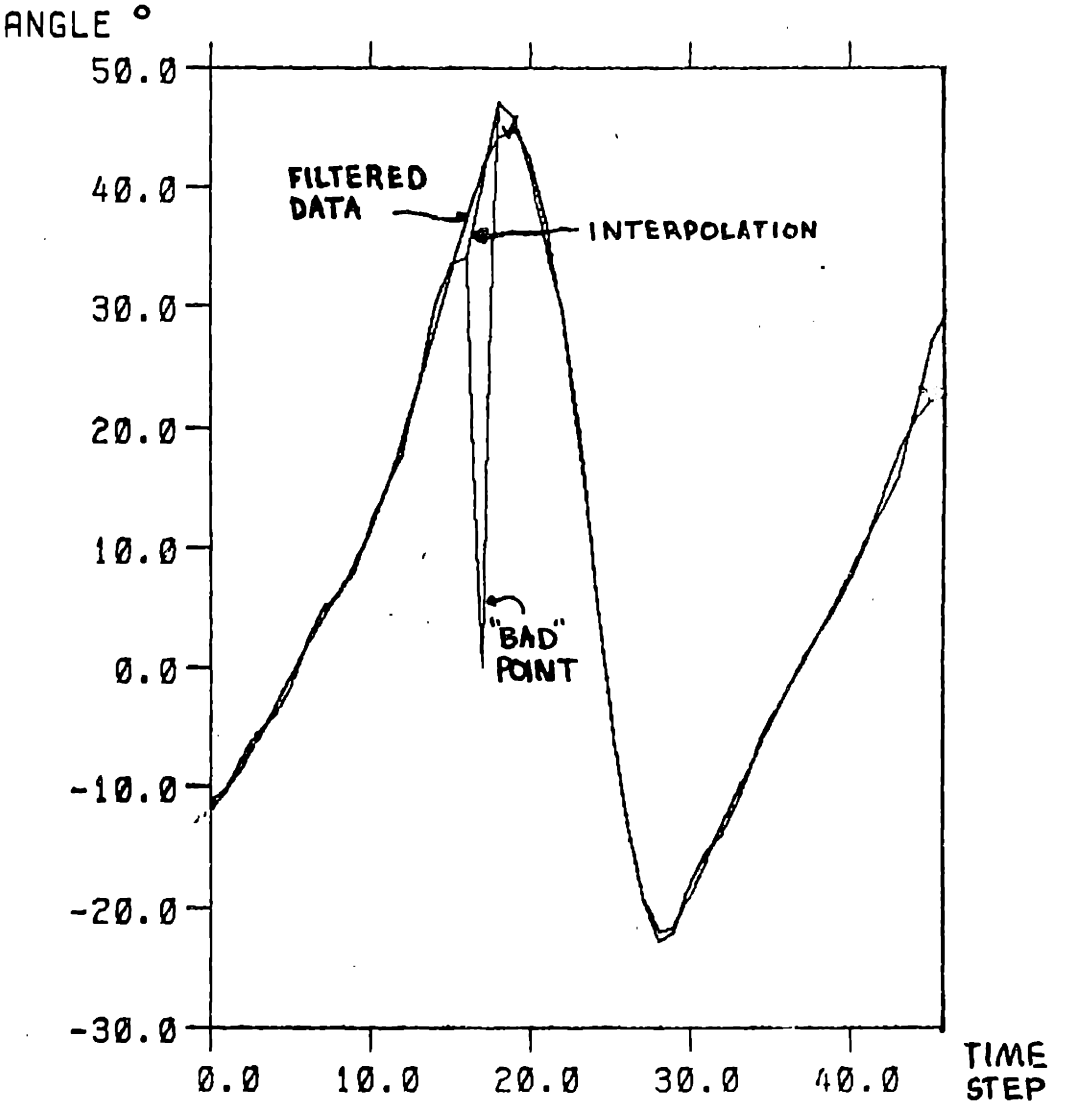

Fig 5-16 TRACK Angle Data for the Saggital Plane Rotation of the Shank
The effects of interploation across a "bad point" and subsequent low pass filtering are illustrated

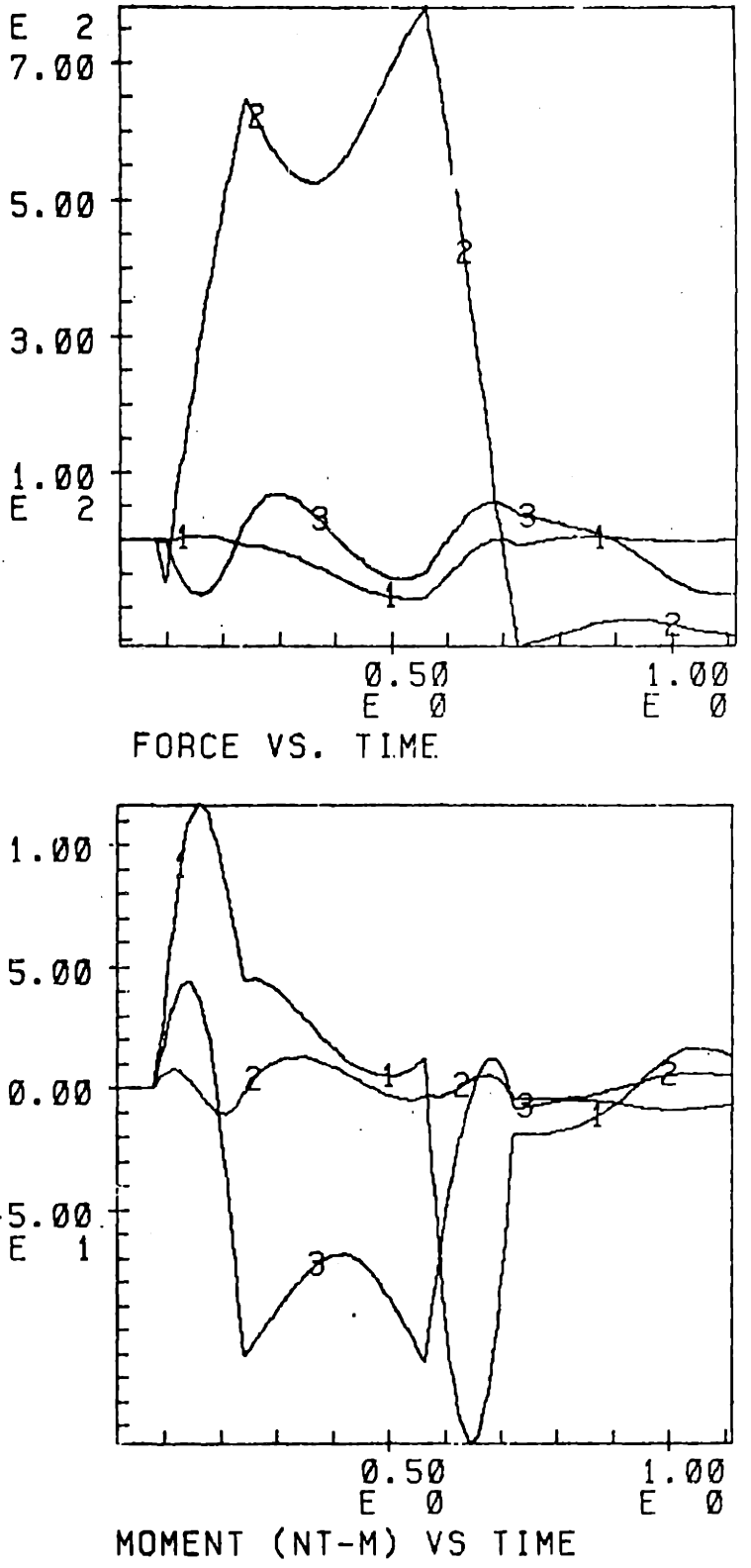

Fig. 5-17 Typical Force and Moment Data for the Hip from the Five Segment Dynamic Model

(1,2,3 correspond to x,y,z, in figure 5-10)

Chapter 6 Muscle Force Optimization Results and Observations

Using data from the experiments described in chapter 5, performed on two individuals, the resulting muscle force predictions based on the minimum energy criterion are presented. This prediction is compared to MES data for these two subjects. Initially, the optimization has no constraints other than the moment equilibrium condition in order to isolate the sensitivity of the solution to changes in the optimal criterion. Having explored this latter condition, the effect of adding inequality constraints based on maximum stress capabilities of the muscles is examined again using the quality of agreement with the MES's as a standard of judgment.

Finally, the change in average energy consumption rate with walking velocity is investigated for both minimum energy and minimum force case. This result is compared against the empirically determined oxygen consumption rate-walking velocity relationship.

Minimum energy results

In figure 6-1 the minimum energy muscle force solution for subject PDR is shown. The bandpassed MES data for this trial are shown in figure 6-2 and they are also indicated on the appropriate muscles on figure 6-1. The calculated joint moment data for this trial is shown in figure 6-3. For this small set of MES recordings the agreement with the force prediction is good. At the hip the gluteus maximus, medius and tensor fascia lata muscles all have MES activity envelopes that include the predicted force. The sartorius result is less good, but

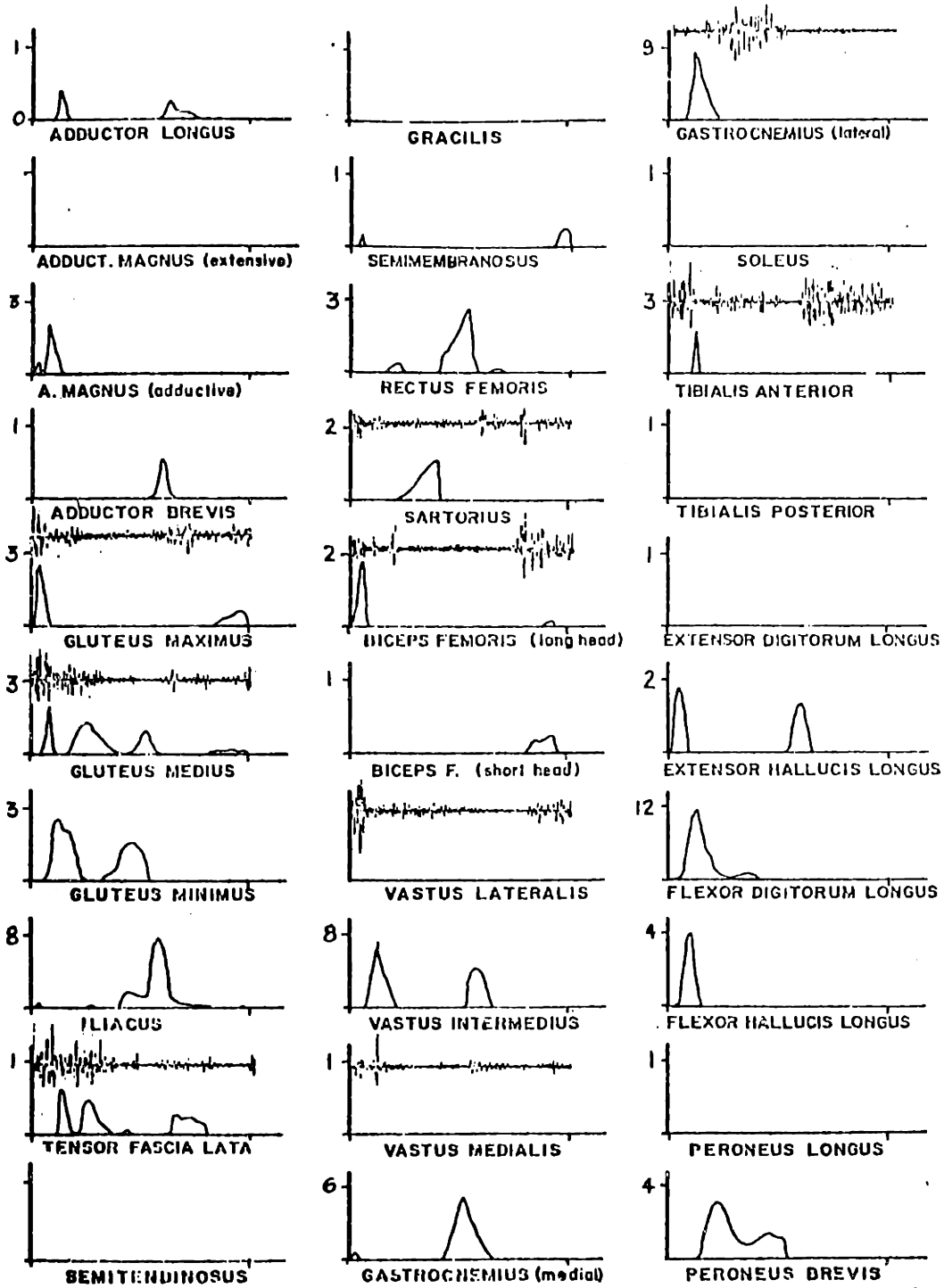

Fig. 6-1 Minimum Energy Optimization Results for Subject PRD Trial JE0101 with Selected MES Recordings
Scale is body weights versus one cycle of the right leg from right heel strike to right heel strike.

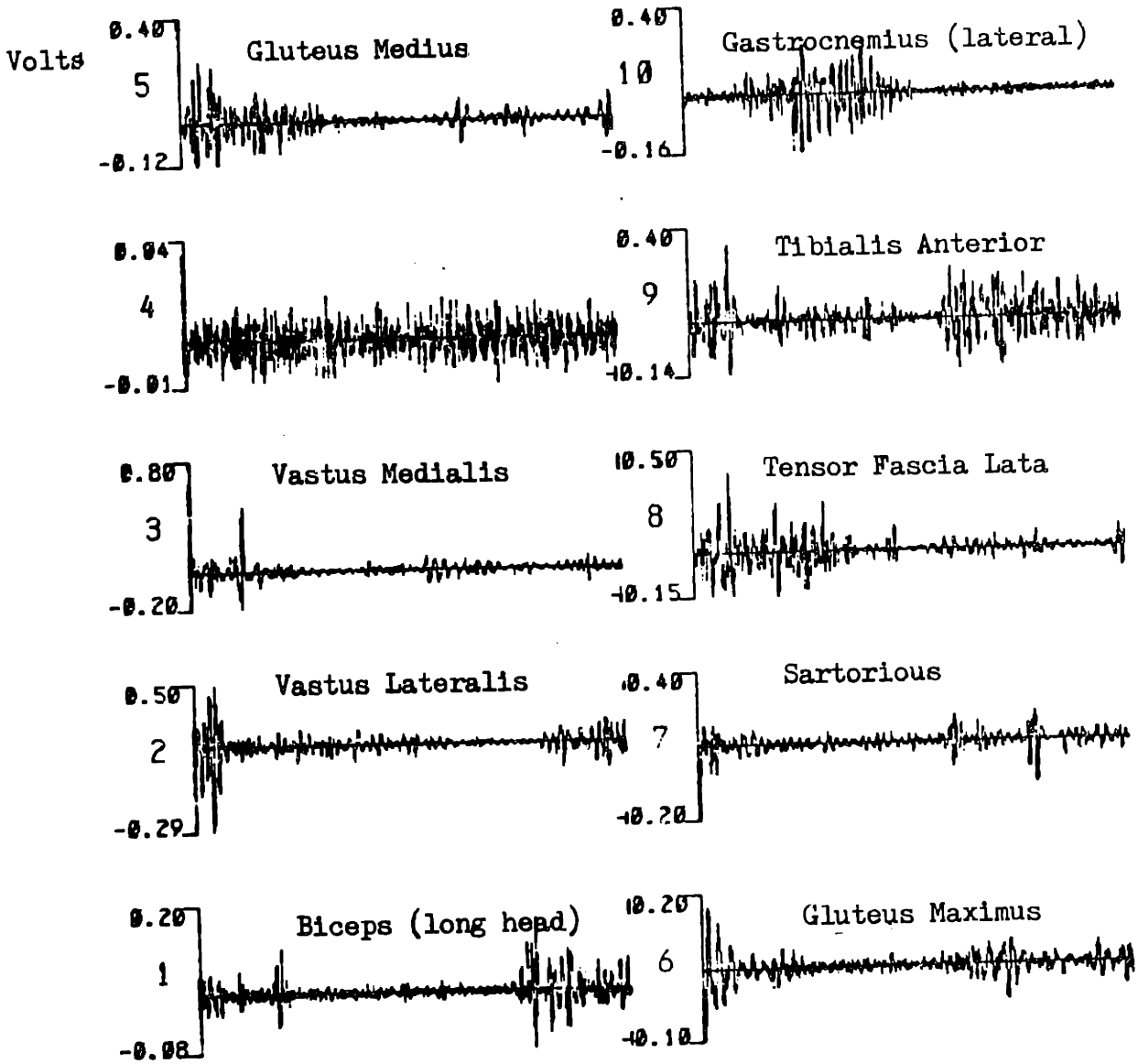

Fig. 6-2 Myoelectric Signals for Trial JE0101
Bandpassed between 30 & 300 Hz.

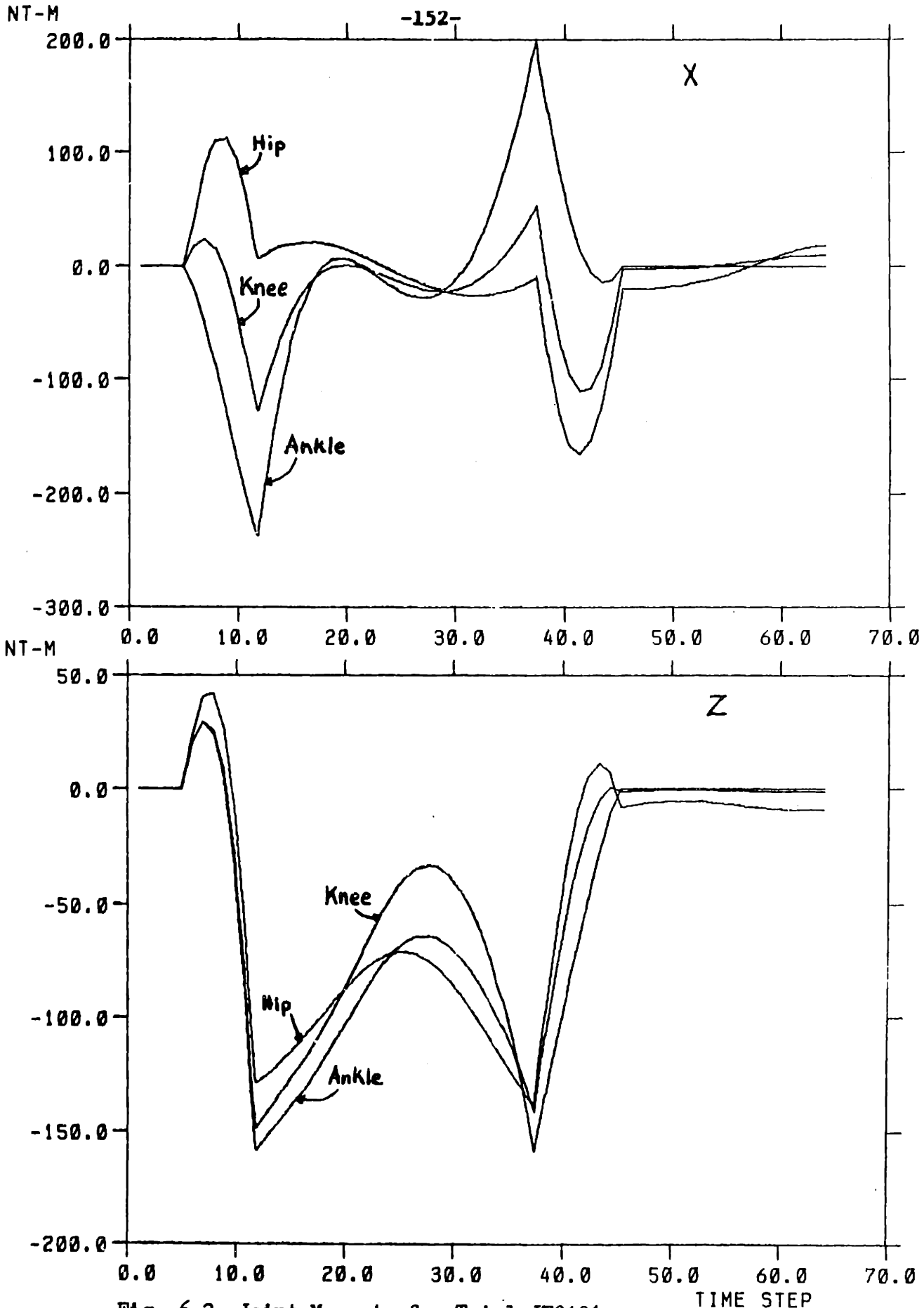

Fig. 6-3 Joint Moments for Trial JE0101

the MES here was not of high amplitude and thus not reliable. The vastus lateralis and medialis MES's agree well with the UCAL Berkely MES data (1953), but no force is predicted for these muscles by the optimization. The MES signal for the lateral head of the gastrocnemium muscle shows poor correspondence with the force prediction but would look better if compared to the medial gastroc. prediction. (The use of two separate heads of the gastroc. in the optimization may not be warranted for two reasons: 1) the major impact of this separation is at the knee, mostly on axial rotation which is specifically excluded by this model, and 2) previous experiments using only the MES recording equipment with electrodes on both heads of gastrocnemius always indicated similar activity in each, suggesting a lack of independence in their action, at least for level walking).

Finally, the predicted forces in the tibialis anterior muscle, the only exclusive ankle muscle from which MES's were recorded, are zero, while the MES shown strong activity. At this point it should be recalled that the ankle is assumed to be locked because no foot kinematics were recorded. This will influence not only the changes in the moment arms of the ankle muscles, but will also exclude the velocity term effect from the penalty function since all exclusive ankle muscles will have zero velocities. These effects plus certain muscle geometry assumptions at the ankle may account for the large forces seen in the flexor hallucis longus and flexor digitorum longus muscles. (These muscles are ankle flexors only secondarily since their primary function is at the toe joints).

In figures 6-4, 6-5 and 6-6 are shown the similar results for sub-

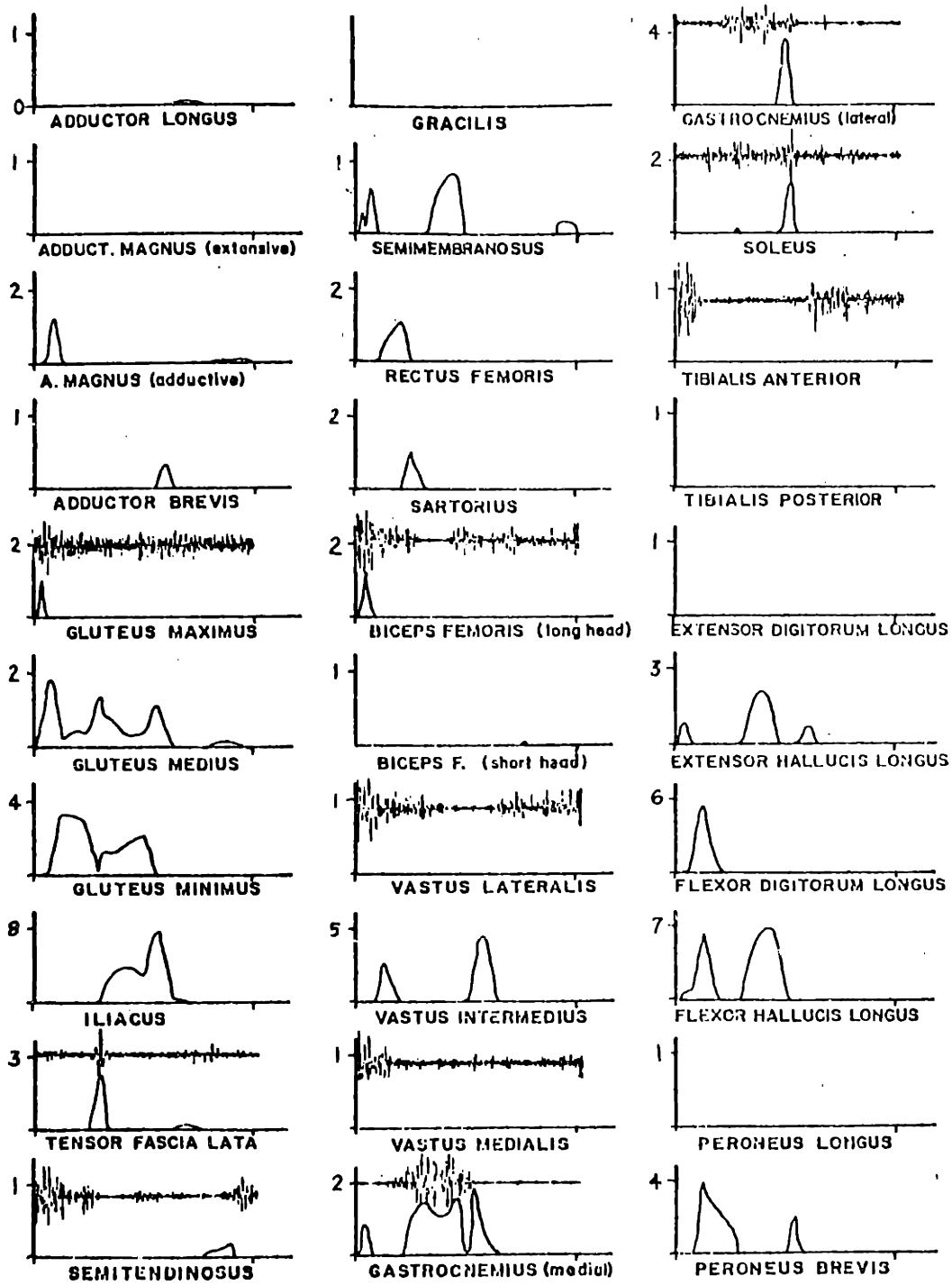

Fig. 6-4 Minimum Energy Result for Trial MY3007

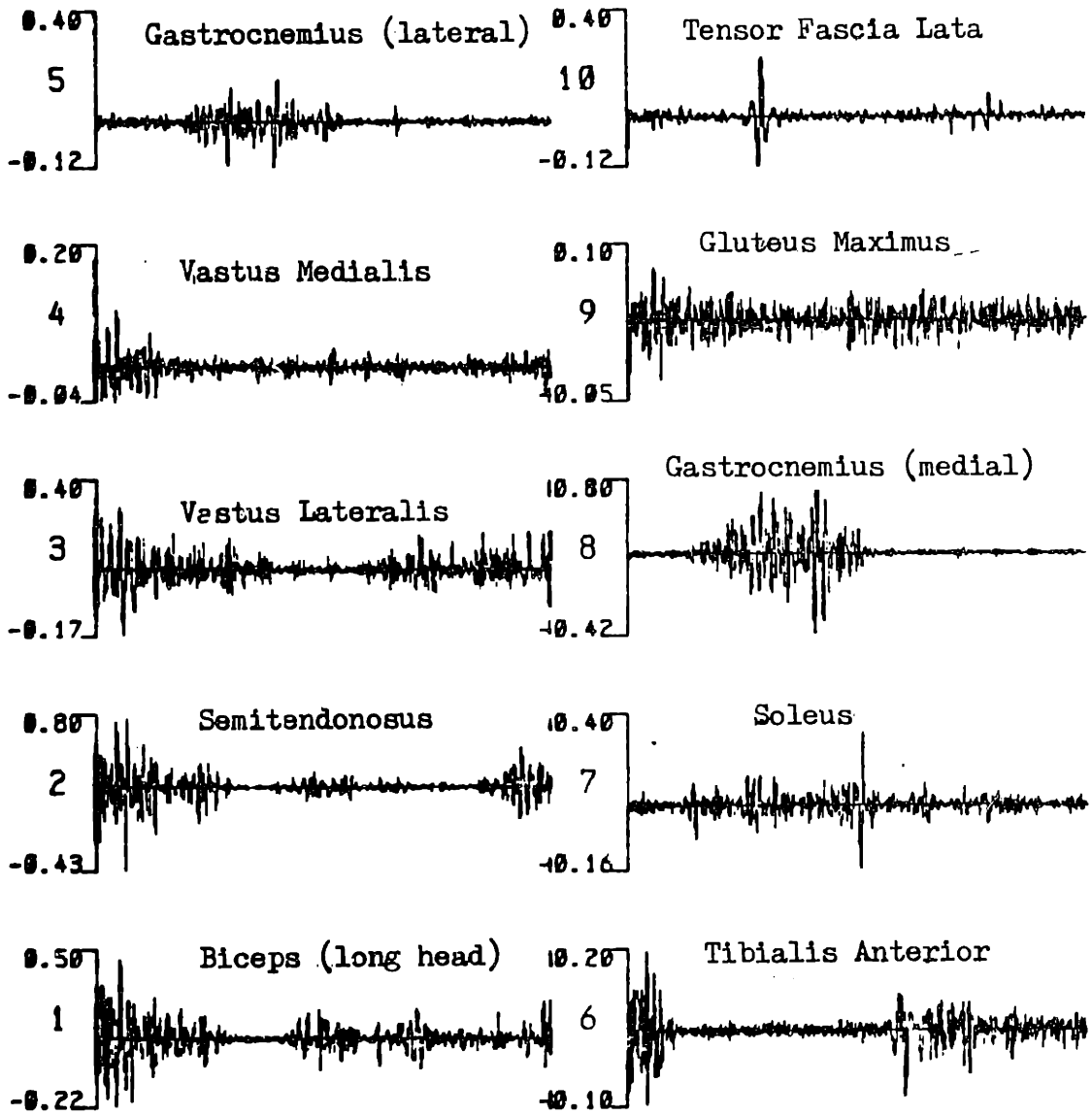

Fig. 6-5 MES Recordings for Trial MY3007
Bandpassed between 30 & 300 Hz.

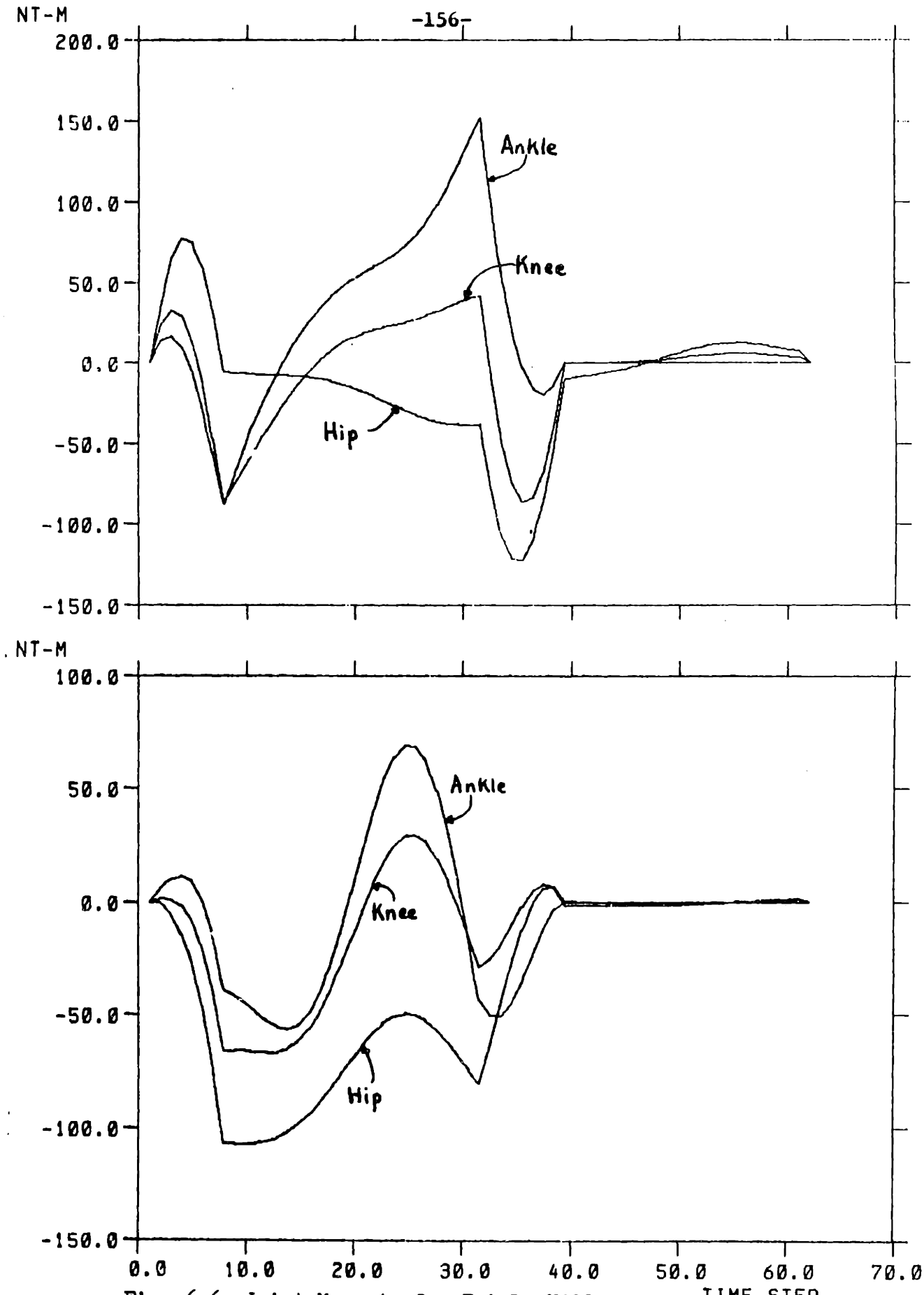

Fig. 6-6 Joint Moments for Trial MY3007

ject JRD walking at a "slow" pace. The MES signals recorded here were from a somewhat different set of muscles than with the previous test, but the combination serves to examine a larger total set of muscles. Looking only at the predicted forces, there is a clear similarity between these for JRD and PDR, one good indication being the lack of activity in the same muscles of each and similar force levels in the active muscles.

The MES agreement is about as good as before despite the fact that a different set of muscles is being compared. Starting from the top, the gluteus maximus muscle prediction shows good MES agreement, although the MES is not of high quality. The MES signal for the tensor fascia lata muscle corresponds closely to the predicted use both in magnitude as well as time. The semitendinosus muscle is used by the optimization only at the end of the walking cycle whereas MES activity appears at the beginning as well as at the end of the cycle. The extensive moment required at the hip (see figure 6-6) at the beginning of the walking cycle appears to be borne by the other hamstrings as evidenced by the predicted activity at the beginning of the cycle in the semimembranosus and biceps femoris muscles. The MES for the biceps also tends to confirm this function.

Neither the vastus lateralis or medialis muscles, members of the quadriceps group, are used by the optimization despite strong MES activity measured in them. Their function (extension of the knee) required at the early, middle and late portions of the walking cycle, as seen in the knee x axis moment curve in figure 6-6, can also be shared by the rectus femoris and vastus intermedius muscle, the other members of the

quadriceps group. The optimization appears to favor these latter two, noting of course that the rectus also exerts a flexive moment on the hip during the mid stance and toe off portion of the walking cycle cycle, (see hip x moment in figure 6-6).

An interesting observation can be made at this point. The MES signals for the semitendinosus and biceps, both biarticular muscles that tend to flex the knee as well as extend the hip, are activated simultaneously with the two vasti muscles, a clear indication of antagonistic muscle activity at the knee. The optimization, however, does not indicate this conflict. The reasons are two-fold. The optimization, by definition, will tend to exclude antagonistic activity since it must strive for equilibrium with a small set of muscles (owing to the basic solution restriction outlined in chapter 4) and the muscle force, as part of the penalty function, will tend to be minimized making antagonistic activity too costly. On the other hand, the measured antagonistic activity probably reflects stability considerations at the knee not included in the optimization model as well as the problem of equilibrium about axes other than the flexion-extension axis, which are also not included in the model.

The calf muscles in this trial were more completely instrumented for MES and their harmonious activity is well illustrated. The MES's for both heads of the gastrocnemius muscle and for the soleus muscle, all of which has the same function at the ankle, occur at similar times and with clearly identifiable intensity. It appears that future optimization attempts should lump the gastroc. heads together into a single functional unit. Note, however, that this optimization uses all three of

these muscles, but in a reciprocal rather than complementary fashion. The drop out of the force in the medial head of gastroc. is compensated for by the onset of activity predicted for the lateral gastroc. and for the soleus.

Again the agreement between MES and the optimization result from this point on down the leg deteriorates. This is shown by the tibialis anterior result and by the high forces again attributed to the ankle flexors. It is clear that accurate prediction of force levels in muscles acting on the ankle must await more detailed modelling of the foot, since many of these muscles have primary functions at other articulations of the foot. Until then, the use of decreasing detail as one moves down from the hip to the ankle, as done by Crowninshield (1978b), appears the most valid route, since crosstalk between the joints appears to be minimal.

Effect of the optimal criterion on the force solution

In this section the general effects on the force solution of changes in the penalty function are considered. For this purpose a third set of kinematic measurements, taken on subject JRD about one month after the previous experiment, will be used in the various optimizations. Although no MES data was taken for this run, the quality of the kinematic data was improved. Comparison of the force results for this trial using the same penalty function as previously (figure 6-7) with the results shown in figures 6-1 and 6-4 shows that they are quite similar, so the lack of MES data is not devastating. Since the present objective is to examine the minimum energy hypothesis as it

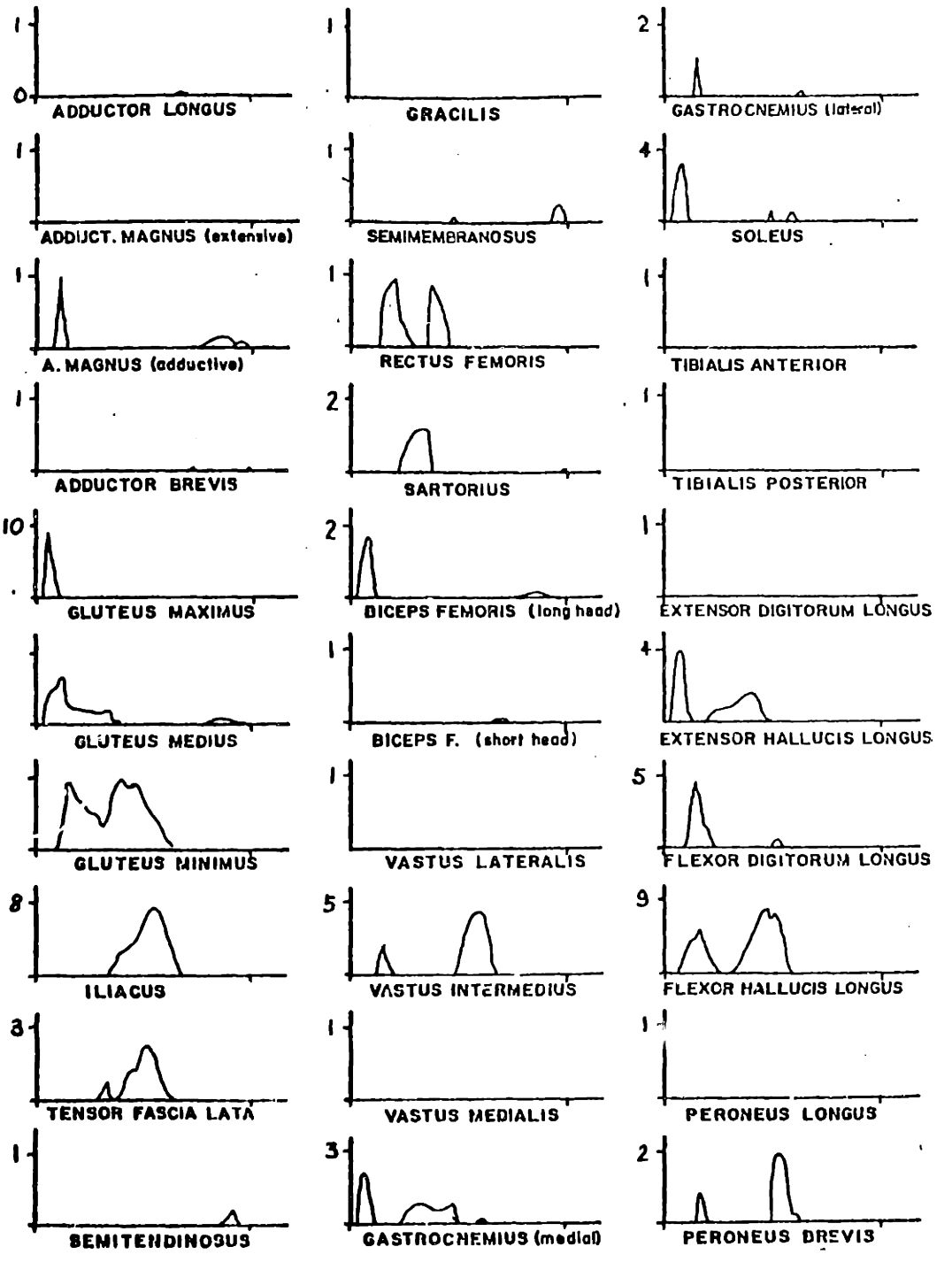

Fig. 6-7 Minimum Energy Result for Trial JE2301

affects the solution compared to other criteria, rather than the absolute fidelity of the solution, no MES comparisons will be attempted.

To examine the effect of the velocity term in the muscle energy model (equation 3-24), the maximum muscle velocity, used as a normalization constant, can be varied. Estimates of both 2.5 times the muscle length (used in the above optimizations) and 6.0 times the length were forwarded in chapter 3. The latter can be used to renormalize the muscle velocity data and the minimum muscle energy optimization performed on the same kinematic and moment data. This has the net effect of lowering the muscle velocities which will greatly decrease the effect of the velocity term in the muscle model because of its decreasing slope with velocity (see figure 3-14).

Comparing this result, shown in figure 6-8, with figure 6-7, it is apparent that only a minor change has occurred. The temporal characteristics of the two solutions are identical, however, the force levels are different in most cases. This is a result of a greater penalty being placed on certain higher velocity muscles in the former case, whereas this penalty is relaxed, and quite rapidly, in the lower velocity case. Since some muscles are penalized more for high velocities, their assigned forces will be lower to keep the overall penalty low, but this force "deficit" must be made up by other, mechanically less advantageous muscles, thus the overall level of force rises. If the value of the penalty functions for each of these runs is examined (see figure 6-9) it is also apparent that the higher velocity case has a slightly higher penalty associated with it. This of course translates

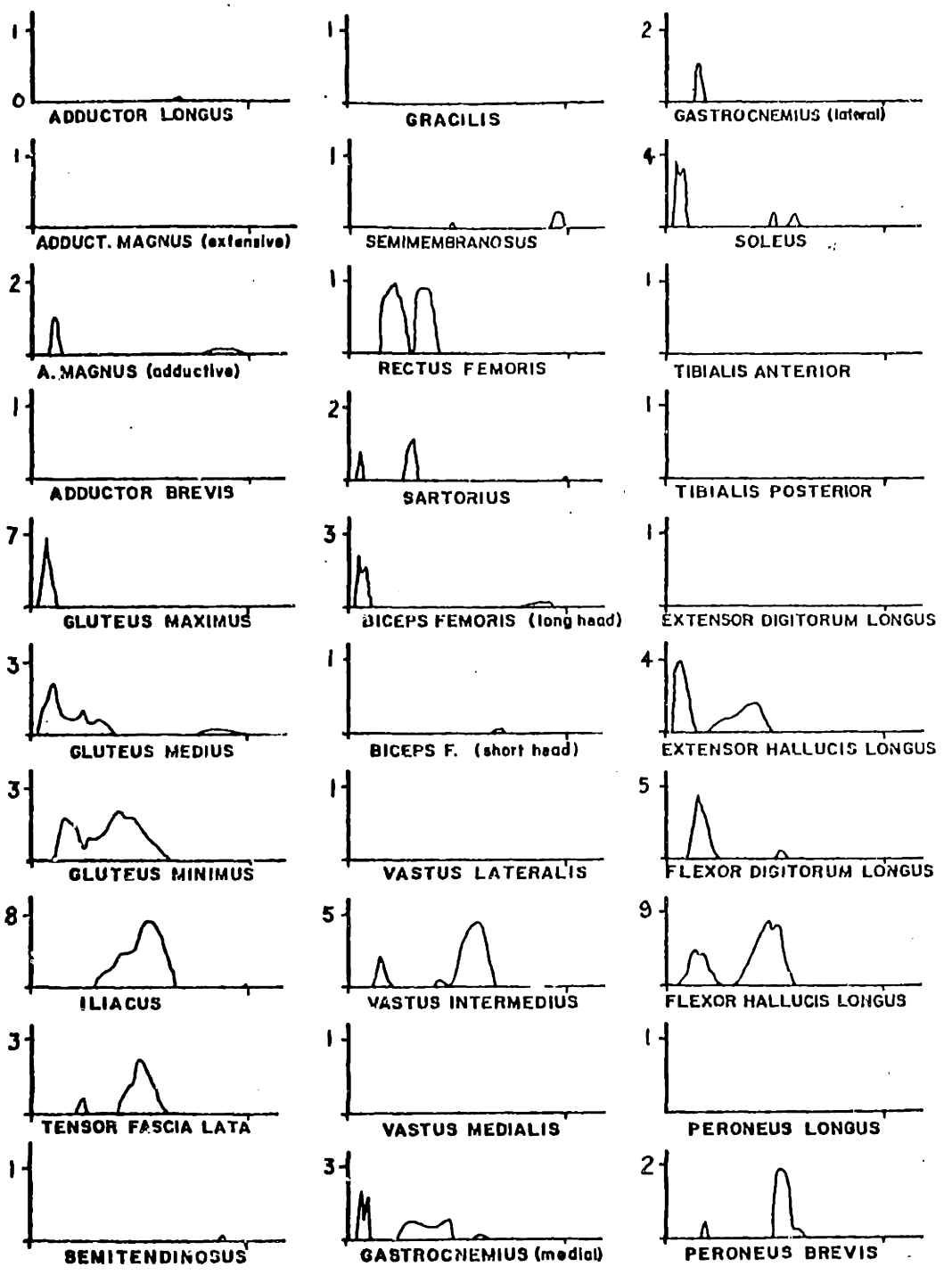

Fig. 6-8 Minimum Energy Result for Trial JE2301 with V_{max}=6.0 * 1

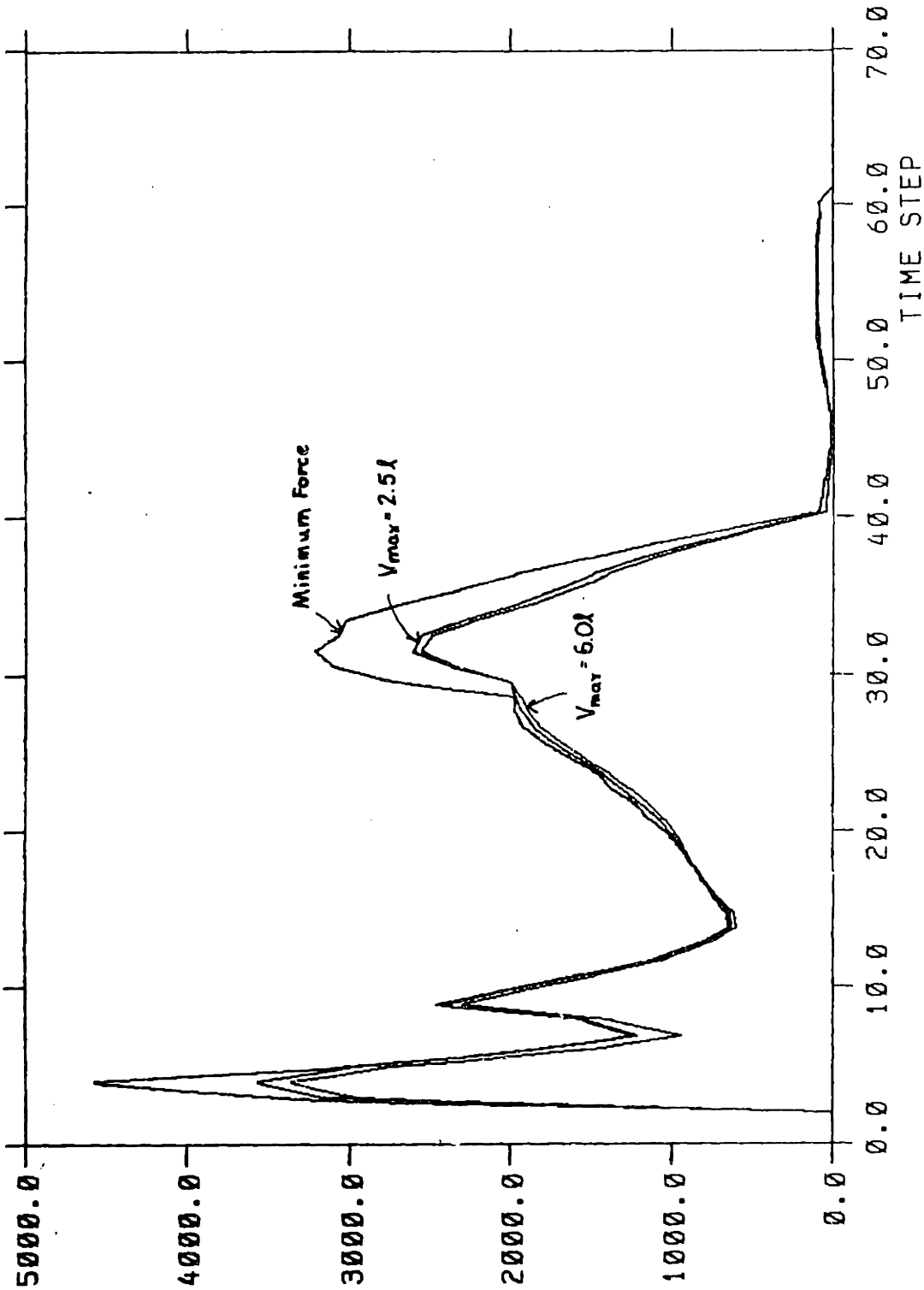

Fig. 6-9 Chemical Power for Trial JE2301 for Various Criteria
(The units for power are arbitrary)

to a higher overall energy consumption in the higher velocity case in accord with the muscle energy model. The difference in the penalty functions is surprisingly slight, however, which indicates that the muscle velocities play a much smaller role in determining the energy "penalty" of the muscles than do the forces.

The test of this apparently small effect of velocity on the energy penalty function is completed by the muscle force results shown in figure 6-10. Here the velocities of the muscles are assumed to be zero, which reduces the penalty function to a set of constant weighting coefficients based on the rest or average length of the muscles. The plot is quite similar, but not identical, to the previous two results (figures 6-7 and 6-9) which further demonstrates the weak role of the velocity term in determining the muscle force patterns under normal walking conditions.

The muscle velocities for the $v_{max} = 2.5\ \ell$ experimental trial are shown in figure 6-11. The majority of these velocity trajectories are bounded between $v/v_{max} \leq 0.25$, so these muscles will operate on the least steep portion of the $g(v/v_{max})$ function in the muscle energy expression, (see figure 3-14). This would explain the weak influence of the muscle velocity in determining the minimum energy solution, but as will be shown below, the velocity term cannot be entirely neglected.

A minimum force penalty function, one with all cost coefficients set to unity, was used for the optimization whose result is shown in figure 6-12. Here a dramatic difference is evident when compared with the results in figures 6-7, 8 or 10. The force levels are most clearly aligned with those of the zero velocity case (figure 6-10), but they are

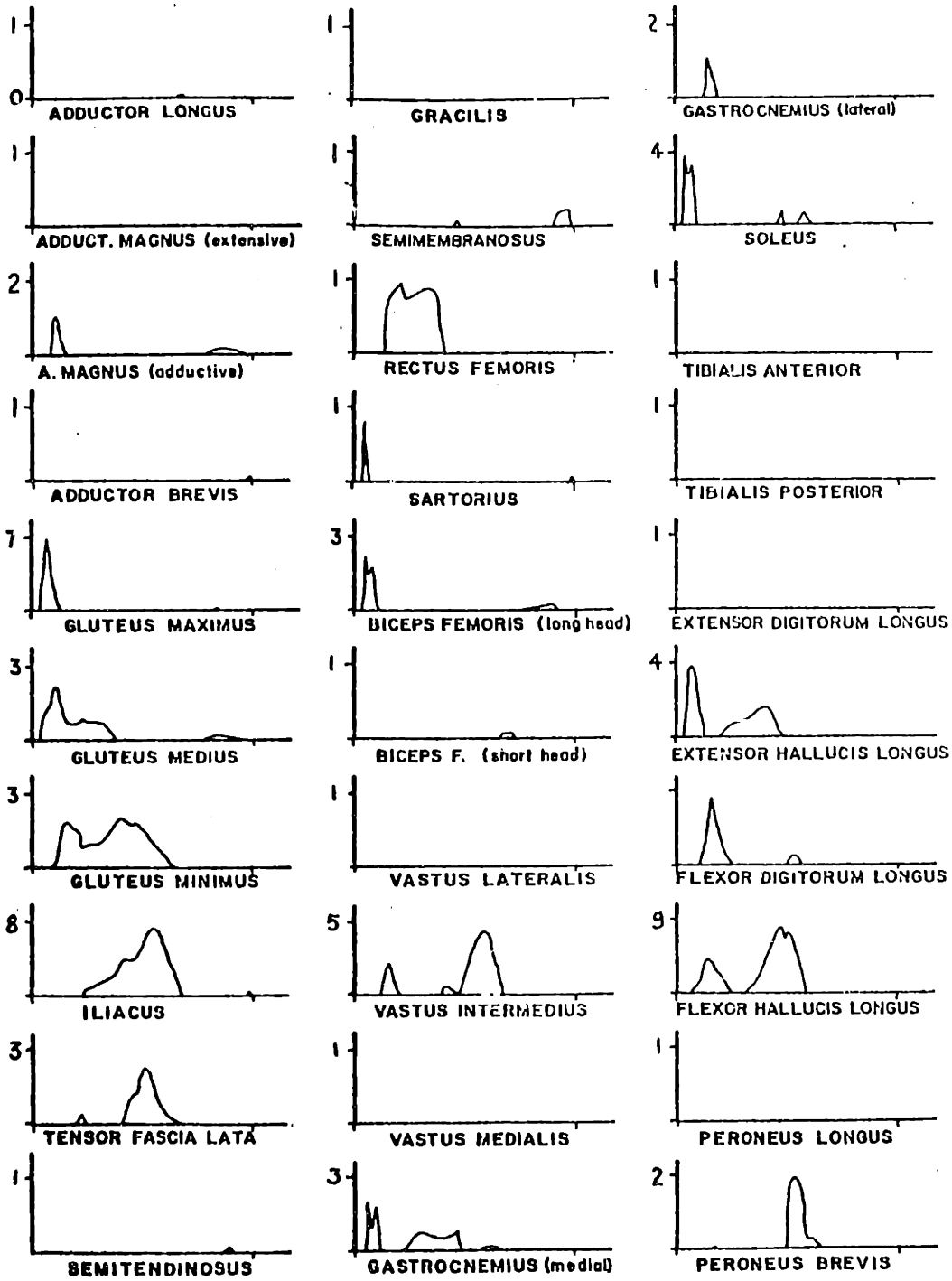

Fig. 6-10 Minimum Energy Result for Trial JE2301
$V_{max} = \infty$, therefore the muscle velocities are zero.

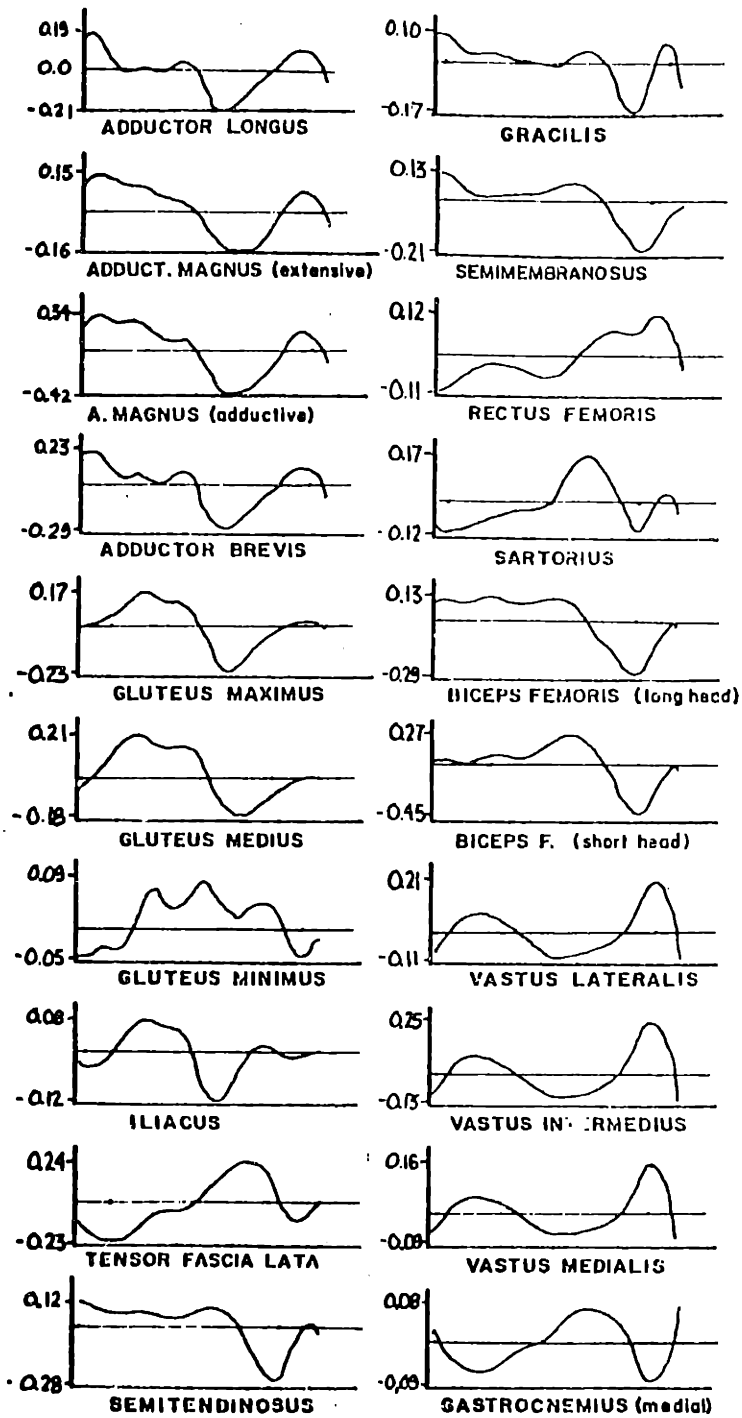

Fig. 6-11 Muscle Velocities for Trial JE2301; V_{max} = 2.5 * 1
The velocities are normalized by V_{max}

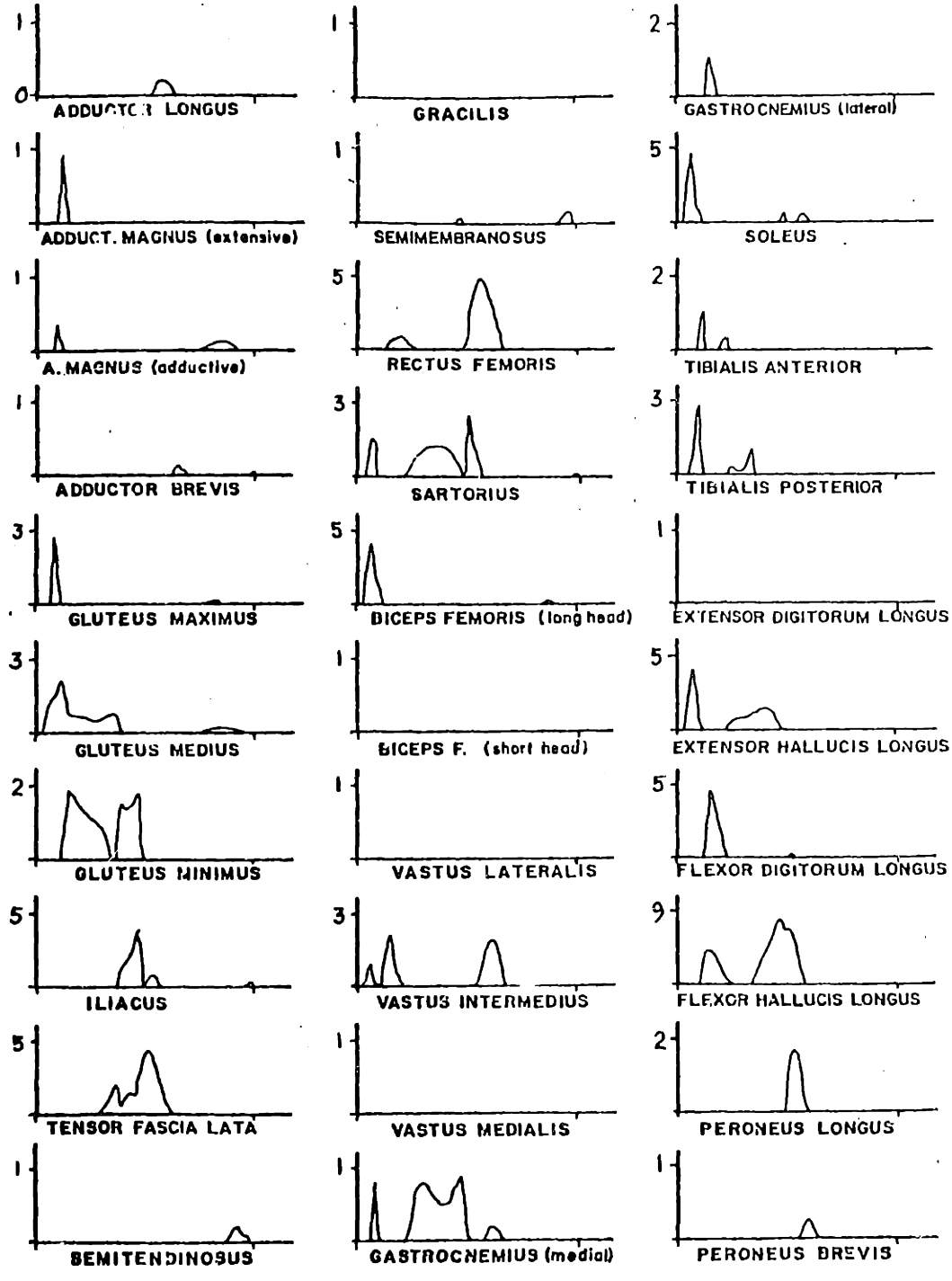

Fig. 6-12 Minimum Force Result for Trial JE2301

in general the lowest of all, as expected from the penalty function definition. Thus for the case of level walking, minimum force and minimum muscle energy, as defined here, constitute two quite different criteria. Just as apparent is the observation that minimizing energy is done at the expense of higher forces in the system, thus higher loads on the joints. The muscular component of the hip joint force for each of the above penalty functions is shown in figure 6-13. The difference between the minimum energy joint force and the minimum force case is about 15% at its maximum. (Notice that the joint force, while it appears to be an excellent check on the fidelity of the force solution, is actually just a reflection of the input moments. Since the moment arms of the various muscle around each joint do not change drastically during the walking cycle, the joint force due to muscular influences is actually the rectified, scaled joint moment curve for that particular joint. The resultant will thus only be as accurate as the calculated joint moments unless an accurate <u>in vivo</u> joint force measurement is available.

A higher energy consumption for the minimum force case is illustrated by the chemical power curves in figure 6-9, which are actually the penalty functions for the minimum energy optimizations, and an "external" application of the muscle energy model to the minimum force results. If the total energy for each of the three cases: minimum energy with v_{max} = 2.5 ℓ, with v_{max} = 6.0 ℓ, and minimum force, is calculated by summing all the instantaneous muscle power data for each of these runs, the result is

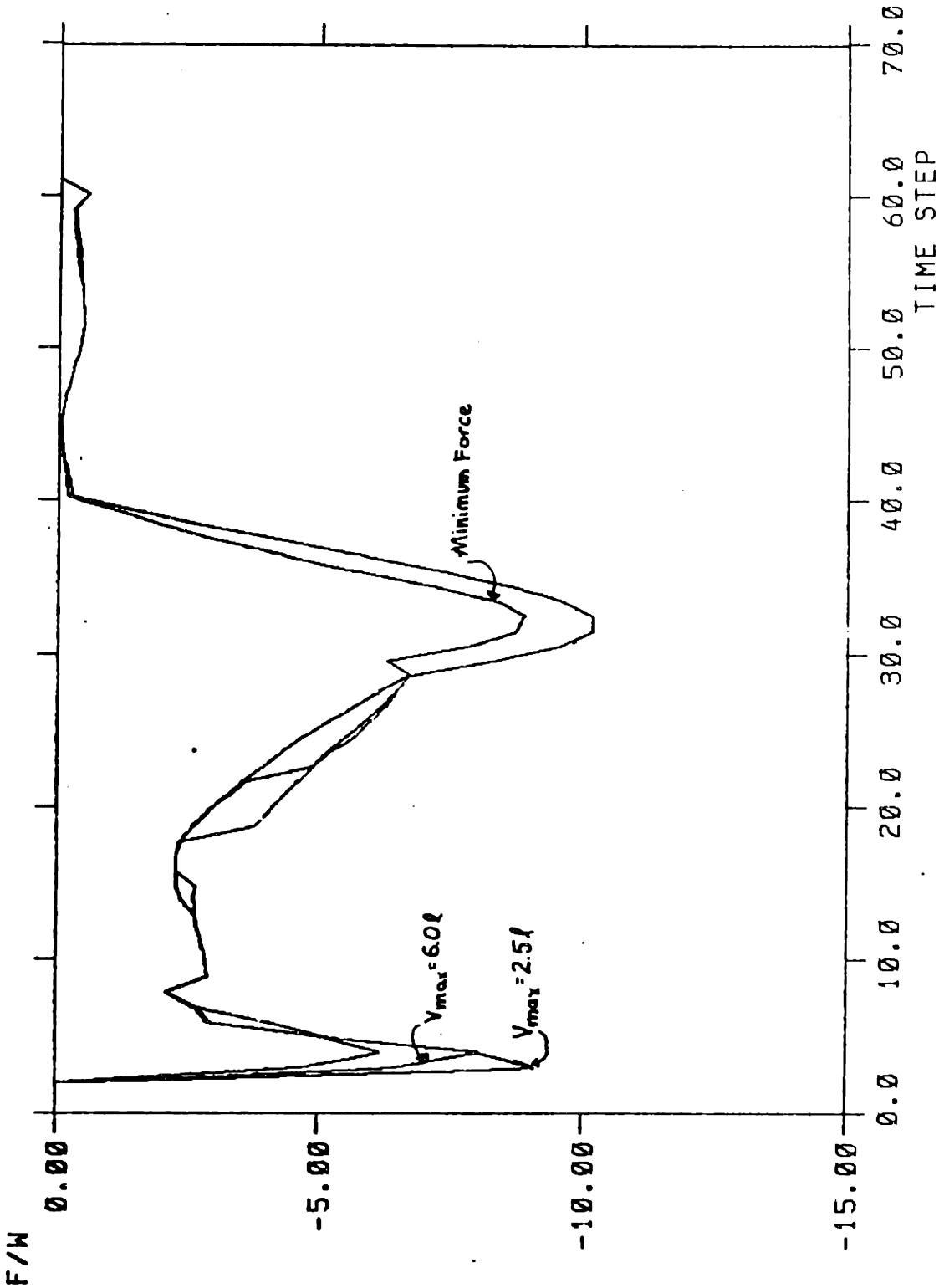

Fig. 6-13 Hip Joint Vertical Force (muscular component only) for Various Criteria
Trial JE2301

E_{cycle} = 60262 for v_{max} = 6.0 ℓ

61758 for = 2.5 ℓ

70478 for Minimum force

(where the energy units are arbitrary)

The minimum force solution requires about 15% more energy than the minimum energy case. There exists, therefore, a clear tradeoff between energy minimization and force minimization. Each individual muscle force plays a dominate role in all of the above optimizations, and it is possible that additional critical forces in the system, for example certain skeletal stresses, should be examined to help settle the dichotomy.

Each of the above optimizations point to the sensitivity of a general type of solution to variations in the cost coefficients of the penalty functions. The basic temporal character of the solution is determined almost entirely by the moment constraints, as illustrated by figure 6-14. The conclusion must be, at this point, that the greater controlling influence on the muscle force solution is the constraint system imposed on the optimization. This is, of course, entirely consistent with the philosophy of optimization forwarded in chapter 4, and will be explored further in the next section.

Effect of additional constraints

The moment equations, which are the origin of the muscle force problem addressed by this work, represent the major requirement placed on the musculoskeletal system. They will, as a consequence, have an

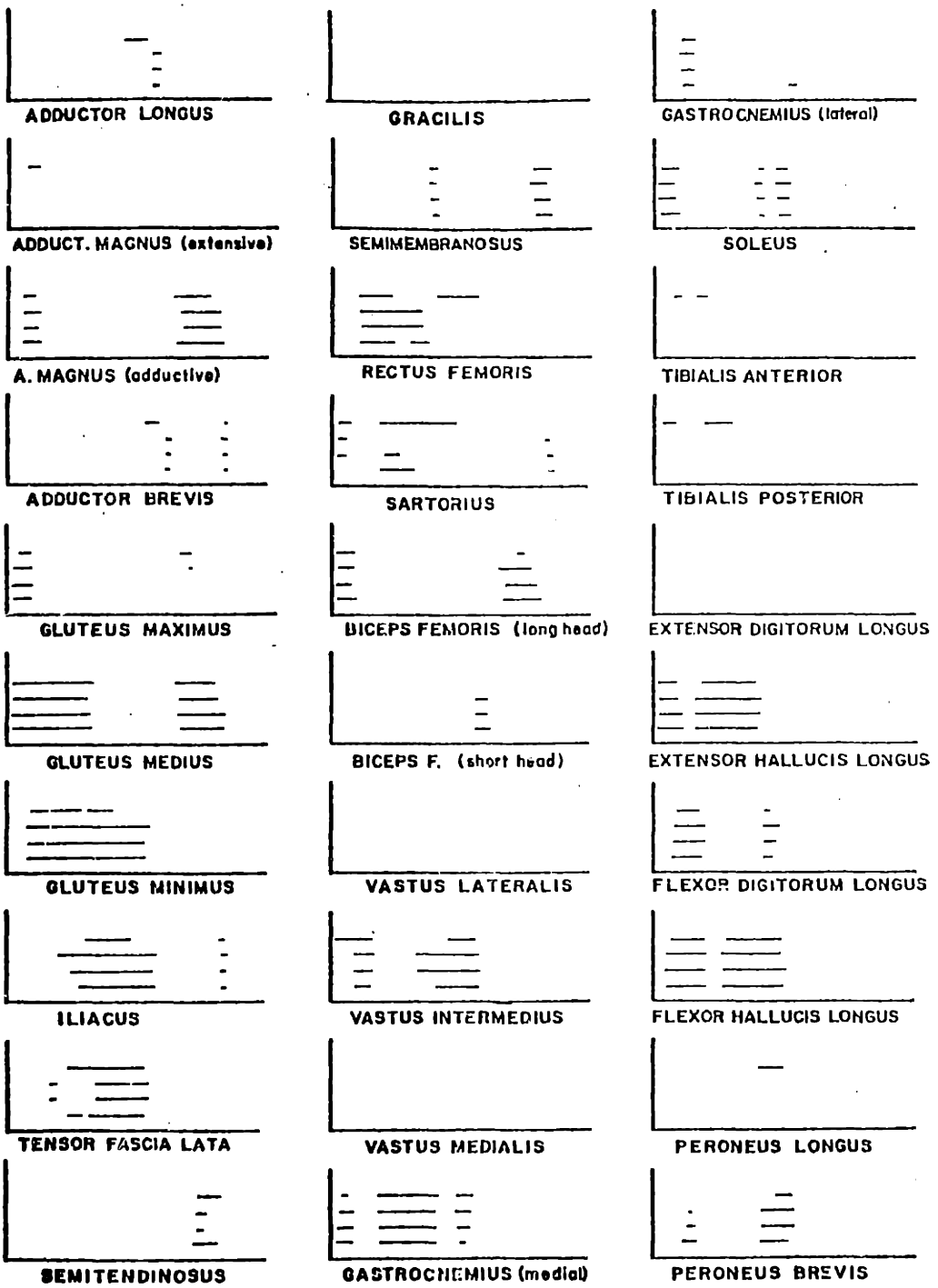

Fig. 6-14 Temporal Aspects of the Previous Optimal Criteria for Trial JE2301

The zero^{+} threshold is indicated ; from bottom to top: minimum energy criterion with V_{max} = 2.5,6.0 & ∞ * 1 and minimum force criterion.

obvious effect on the force optimization result. The general characteristics of the solution, as defined in the last section, should change in concert with the input moments or with structural modifications of the systems which directly affect the R matrix in the moment constraint equation.

Thus the question of incorporating additional constraints in the hope of better agreement with MES's should be addressed. Although not a focus of this work, this part of the muscle force optimization problem can be significant as shown by Chao et al. (1977) and Crowninshield (1978a). In keeping with the concept of using as much physiological information as possible in the optimization process, constraints which contain additional information about the muscles, other than that contained in the muscle energy model, should be considered first. One such addition will be illustrated here.

The maximum possible stress level in isometrically contracting muscle is nearly constant and can be approximated as 10 Kg/cm^2, (Chao and An (1977)). This information is not included in the muscle energy model but will have an impact on the solution. As noted by Pedotti et al. (1978) this stress level, according to the Hill force velocity relationship discussed in chapter 3, will be a function of contraction velocity, but the low velocities shown in figure 6-11 make a constant maximum stress approximation acceptable here.

Using the muscle cross sectional area data from Pedotti, and estimating the areas for muscles included here but not considered in their study, constant upper bounds on the individual muscle forces were placed on the hip and knee muscles. (The ankle muscles were not

bounded since no accurate data on cross sectional areas was available. Also, the inadequate functional constraints placed on the ankle and foot muscles as noted above would make the stress constraints somewhat irrelevant). The minimum energy optimization was then performed with these inequality constraints added and the resulting muscle forces are shown in figure 6-15.

Immediately obvious in the stress bounded solution is the increased distribution of activity over all of the muscles. This is quite predictable based on the comments in chapter 4 concerning the effect of inequality constraints in a linear program on the number of non-zero variables in the solution. Examining the force in the iliacus muscle, for example, it is apparent that the solution is not changed until the bound is reached, and only then are additional muscles brought into play. The inactivity in the vastus lateralis and medialis muscles has been changed, and the entire quadriceps group (rectus femoris and the three vasti muscles) now appears to share the knee extension load. This agrees much better with the MES recordings for the vasti group, and for these muscles at least the solution has been improved. In general, this indicates that the distinction between muscles should be made not only on the basis of geometric arrangement, which influences both moment arms and contraction velocities, but also on the basis of sharing functions where possible.

The result for the iliacus muscle illustrates the abrupt nature of the upper bounds, and use of muscle regularly at the upper bound of stress is not reasonable. In all probability a more practical constraint is one which limits the muscle activity to some fraction of the maximum

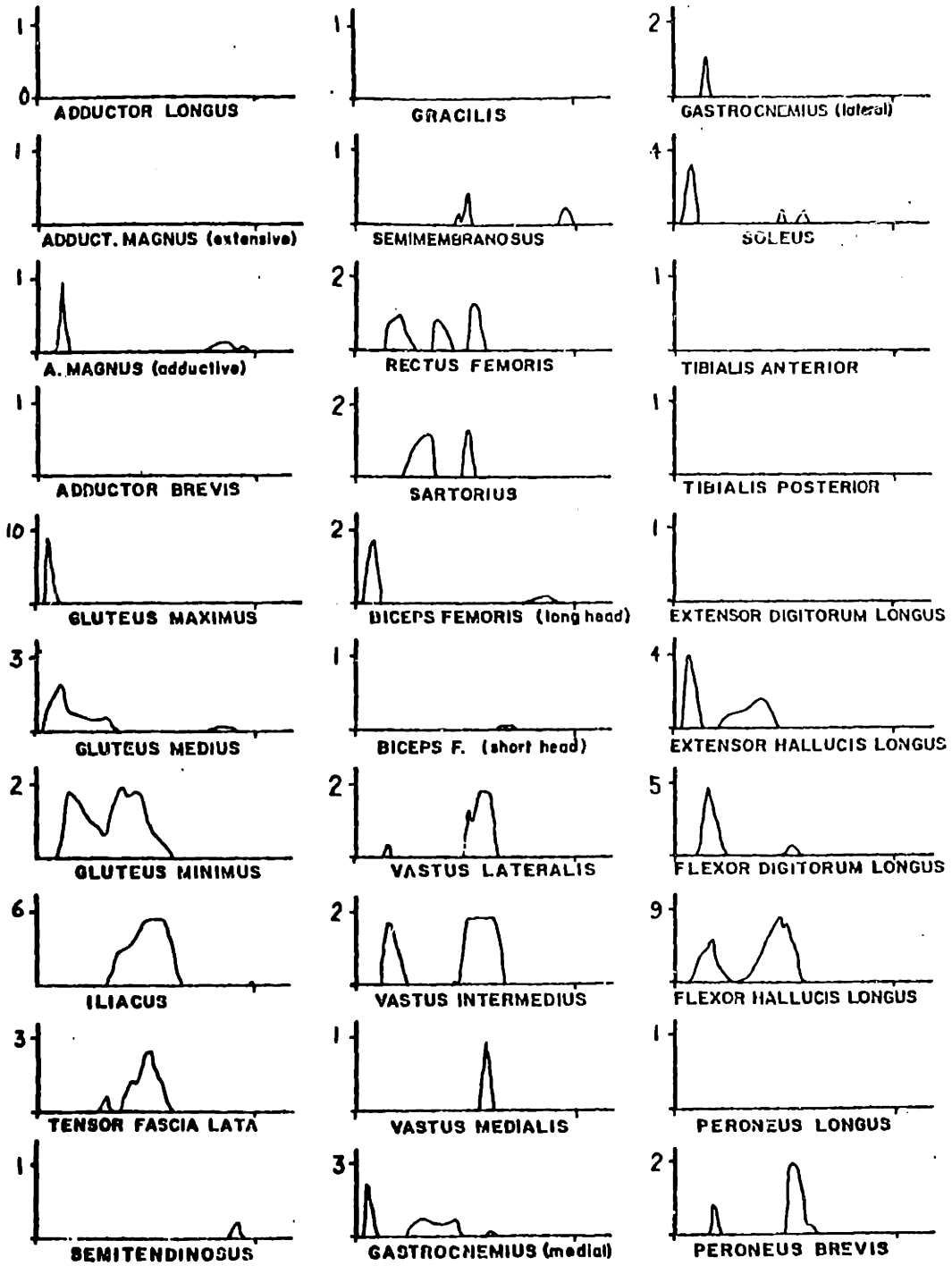

Fig. 6-15 Minimum Energy Result for Trial JE2301 with Maximum Stress Constraints Imposed

stress level, as investigated by Crowninshield (1978b). It is not clear, however, whether this causes an equal distribution of stress across the muscles since additional muscle will only be activated when others saturate.

Once again, the tradeoff in terms of energy consumption is shown by the chemical power curves for the stress limited case against the unlimited, (see figure 6-16). The constraints, while keeping the overall force levels lower, much as the minimum force solution did, add to the energy requirements of the muscles. The total cycle energy here is 64270 which represents an increase 10% over the unbounded minimum energy case. This is not unexpected since activating additional muscles should involve the use of energetically less advantageous muscles. Also, it should be expected that the use of additional anatomically distinct muscles would add to the energy burden, but this is not an explicit result of the present optimization.

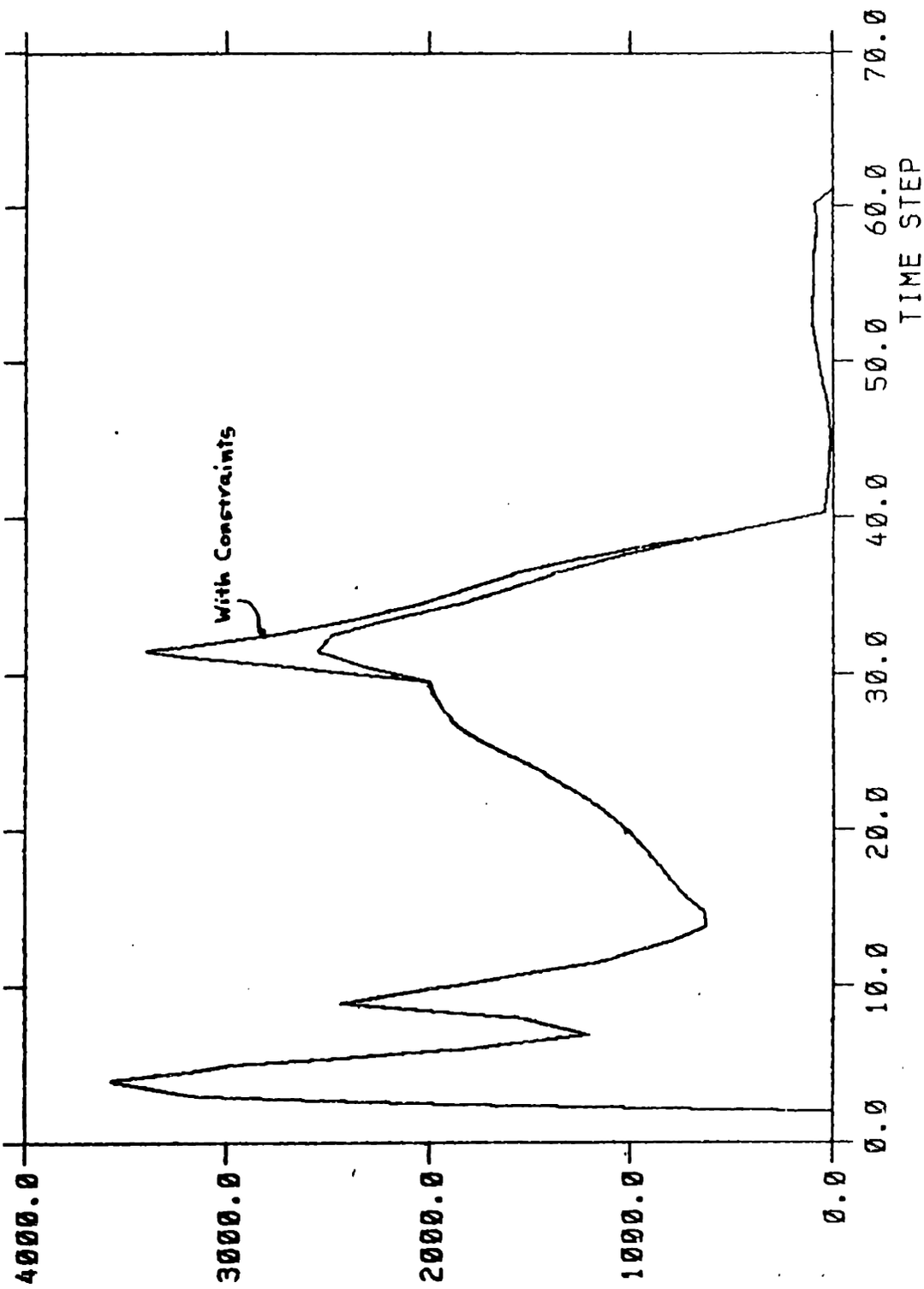

Fig. 6-16 Chemical Power for Trial JE2301, Minimum Energy, with and without Maximum Muscle Stress Constraints

Energy consumption versus walking speed

An additional experiment was performed to examine the predicted average power requirements for walking (defined as the total energy consumption of the muscles in one leg going through an entire cycle, divided by the cycle time) as a function of forward walking speed. Several researchers have made maesurements of this sort using average oxygen consumption rate as an indicator of energy expenditure (e.g. Cotes (1960) and Margaria (1976)), and their results can be compared with the energy rates predicted by the muscle force optimizations.

For these optimizations a series of six trials were run at various walking speeds. For each set of kinematic data (a single trial within the experiment) the average cycle energy rate or power was determined using both the minimum energy criterion and a minimum force criterion. (The latter was chosen because of the absence of any velocity dependence). The data from these trials appears in table 6-1 and is plotted in figure 6-17.

In figure 6-18 this same data has been plotted as the square of walking speed following the suggestion of Cotes, and regression lines for each criterion have been drawn. Note that the minimum force line is not only higher than the minimum energy case, as would be expected from the results in the earlier parts of this chapter, but it also has a greater slope. This can be traced to the "load shedding" from higher to lower velocity muscles that was illustrated earlier in the minimum energy case when only the velocity was increased. As walking speed increases both the joint moments and muscle velocities increase. Some muscles will become less advantageous energetically, owing to the

Table 6-1

Data from average power - walking speed experiments

trial #	speed (m/sec)	average power min. energy	average power min. force	cycle period (sec.)
3	0.70	415	472	1.35
9	0.89	435	487	1.29
1	1.23	545	649	1.14
6	1.73	1317	1461	0.95
2	1.83	1074	1317	0.98
5	1.93	1425	1578	0.95

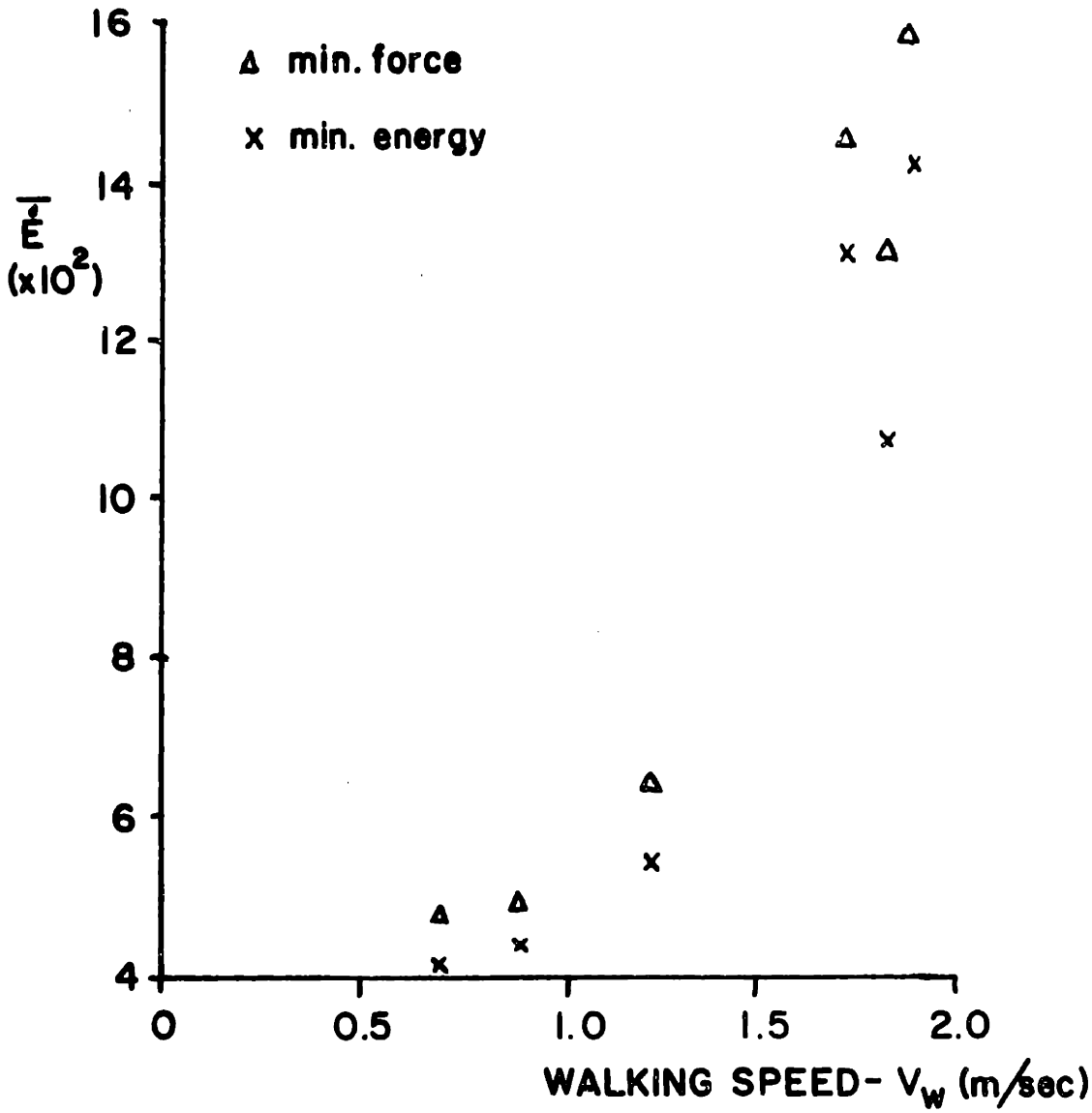

Fig. 6-17 Average Power Consumption as a Function of Walking Speed as Predicted by the Minimum Energy Optimization (Power Units are arbitrary)

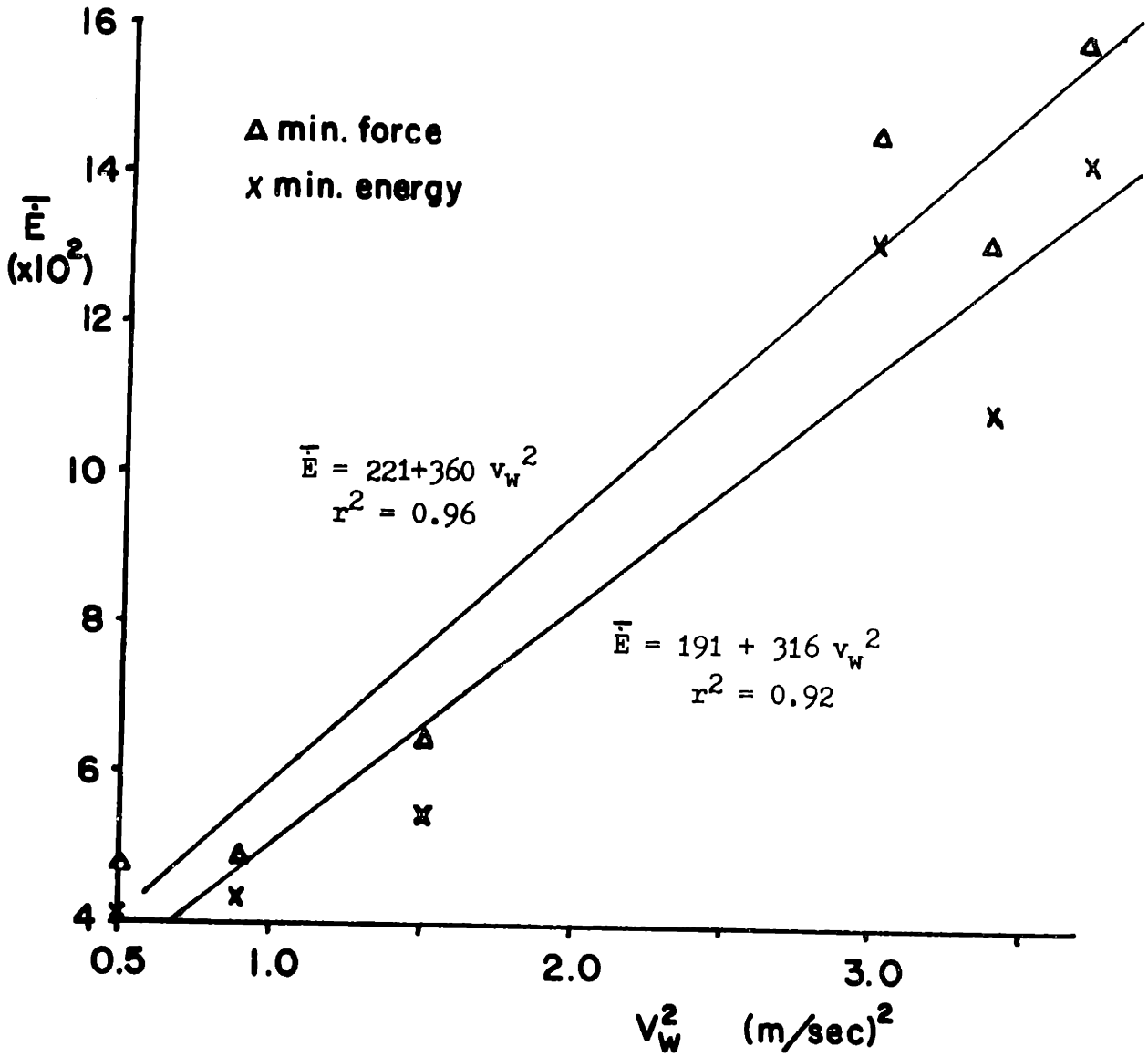

Fig. 6-18 Data from Fig. 6-17 Plotted against the Square of Walking Speed and with the Resulting Regression Lines

increased velocities, and their load will be reduced by transferring some of it to lower velocity muscles even though the latter will be mechanically less advantageous.

In the minimum force case no such direct velocity dependence appears in the optimization. As walking speed increases there will be concomitant muscle force increases from both increased stride length, which will increase the gravitational moments, and increased accelerations. The minimum force optimization will respond to these changes by increasing the force in the muscles already active with no regard for their energetic contributions. Thus the minimum energy criterion serves to mitigate the energy cost of muscle velocity increases while the minimum force criterion cannot. (Note that the transition from operating below the natural frequency of the swing leg to above it will not significantly affect these results since the high force levels during stance cause this phase of walking to be the major determinant of the cycle energy consumption. This is clearly illustrated by the cost function plots in figure 6-9).

For an absolute comparison, this data can be plotted against the oxygen consumption rate measurements of Cotes (1960) and Margaria (1976). Straight lines, representing the regression lines for the quadratic power-walking speed relationship, are plotted for both of these along with the minimum energy result in figure 6-19. Since the optimization average power data is in arbitrary units, each separate data set has been normalized by its value at $v = 1.0$ m/sec.

The slope, which is the crucial variable here, is considerably greater for the minimum energy case than for either the Cotes or Mar-

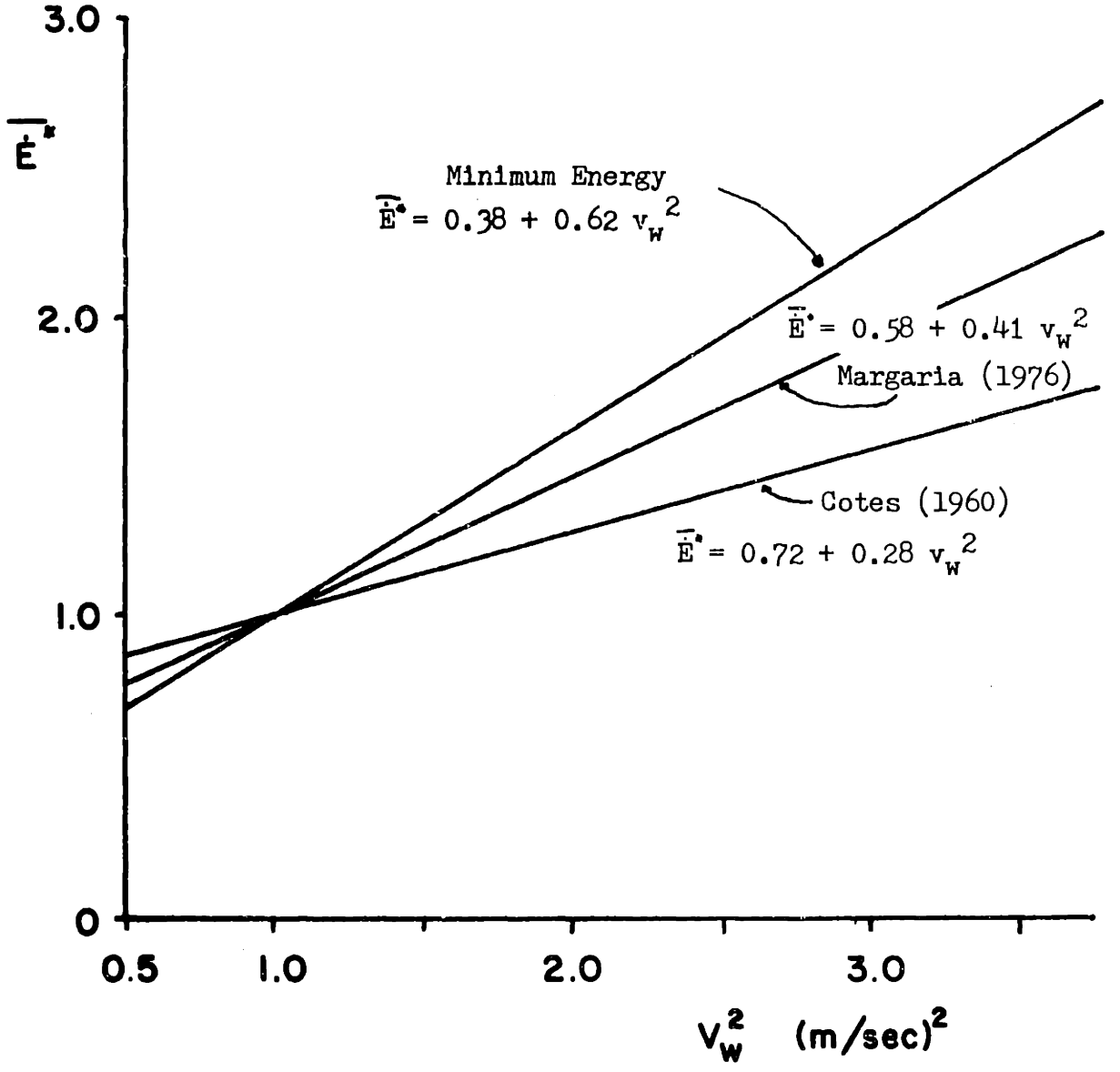

Fig. 6-19 Normalized Average Powers from the Minimum Energy Solution and from Cotes (1960) and Margaria(1976)

The latter two are the result of oxygen consumption measurements. All data has been normalized to the v = 1.0 value.

garia data. (The latter two are averages for many subjects, whereas the present trials were performed on a single individual). This observation does suggest, however, that the minimum energy criterion more closely matches the oxygen measurements than does the minimum force data. The limited data base here prevents any stronger inference, but the distinct difference between minimum energy and minimum force as criteria for muscle force distribution is illustrated.

Chapter 7 Conclusions and Recommendations

A minimum energy hypothesis was originally forwarded here as a means of solving for the muscle forces in the leg during walking given only that dynamic equilibrium at the joint was to be maintained. The implementation of this idea has not solved the problem, but it has demonstrated several important properties of muscle force optimizations.

It has been shown that the joint moment patterns (which are determined by the limb motions) establish the temporal characteristics of the force solution; and with a few important exceptions (inactive muscles, no antagonistic activity) these patterns correspond acceptably with MES recordings. This temporal pattern is hardly altered when different optimal criteria are used and it can only be strongly affected by additional constraints. Improvement in the solution defined only by the moments can be had by imposing upper bounds on the muscle forces. This activates more muscles and enhances the agreement with MES data.

The optimal criterion has its greatest impact on the relative load sharing among the muscles within the constraint-fixed temporal patterns. The use of a minimum muscle energy optimal criterion gives better agreement with total energy consumption measurements than do criteria that take no account of the energetics of the muscles; but without further experimentation it is not clear that the difference among all of the criteria examined here is significant. The tradeoff between predicted energy consumption and force, which is governed by the criterion choice, has been demonstrated and this suggests that critical stresses in the skeleton may also play an important role in the criterion definition. (However, Seireg and Arvikar (1975) have shown that including joint force

in the optimal criterion has minimal effect on the force solution). Additional data is necessary to completely evaluate these differences and among the most promising sources for this data is the in vivo measurement of hip joint forces using an instrumented femoral head prosthesis (see Carlson et al. (1974)). Only with this type of data can direct force magnitude comparisons be made for the different solutions.

Antagonistic muscle activity at the knee, present in the MES's but absent from the predicted result, is a clear result of insufficient information in the mechanical model. More detailed information concerning joint function is probably the more important omission here. It can be anticipated, however, that any optimization solution of this type will always show less activity than the real system since the latter must concern itself with disturbances that were "filtered out" of the problem formulation in chapter 1; and despite the almost involuntary nature of walking, the optimal muscle force patterns established through the learning process will not always be accomplished.

The muscle energy model presented in chapter 3 has herein been tested in the leg muscle force optimization. The results of the average power - walking velocity experiment demonstrate the separate effects of the linear force term and the non-linear velocity term in the muscle energy model. The increasing slope of the latter term with increasing velocity is responsible for the lower overall slope of the predicted average power-walking speed curve in the minimum energy case as opposed to the minimum force case, since this imposes a sharply increasing energy cost on higher velocity muscles.

Recommendations

The original intent of the minimum energy hypothesis was to have the thermodynamic model of muscle embody all relevant aspects of the tissue related to its use during walking. By the end of the muscle energetics modelling it was clear that certain essential properties had been excluded. The foremost among these are the velocity dependent maximum stress capabilities of muscle, and tendon compliance. The effect of the stress constraints has already been discussed, but the separate effect of the latter omission on the force solution should be investigated.

More accurate mechanical modeling of the musculo-skeletal system, especially the knee and foot, should be explored, both as separate, intensive investigations and as revisions of the present model. The overall philosophy of maximum incorporation of quantifiable physiological information relevant to this problem should act as a guide for future study.

At this point it would appear that efforts should be directed toward increasing the distribution of muscle force among the leg muscles rather than toward enhanced magnitude fidelity since the former has a comparative measure in MES's while the latter must await new measurement techniques. Optimization studies on less complex systems are possible, but human walking still provides the only example of a consistent and unique function, that of locomotion. Solutions developed on the upper limb, for example , must be sufficiently general to apply to the walking situation, and they then lose the advantage of a strong "natural" criterion such as minimum energy.

On a more practical level, the methods used here to determine joint moments should be improved, primarily by the use of a force plate, so that some closure on the calculations can be had. Incorporation of on-line joint rotation axis determinations and better methods of deriving (or avoiding the need to derive) limb accelerations should also increase the confidence in the calculated moments and through them the muscle force solution. The simplifications made in pursuing the muscle energy model must be further studied, most probably through a simplified dynamic model of the energy transfer processes, to more completely check the range of validity of the static muscle power model.

Individual muscle forces can be predicted using optimization techniques such as those demonstrated here. The optimization approach, in contrast with the use of greatly simplified, mechanical system models that permit easier solution, maintains the model correspondence with the real system with the virtue of steering future study in clearly identifiable directions. This study, combined with several others addressing the same problem (Seireg and Arvikar (1975)), Crowninshield (1978a,b), Pedotti et al. (1978), and Hardt (1978)) lays the analytical and experimental groundwork for more effective force optimization attempts that can rely on sound physiological bases for the system model and solution structure, while avoiding a completely iterative solution approach.

References

1. Antonsson, E.K., (1978), "The derivation and implementation of a dynamic three-dimensional linkage analysis technique," M.S. thesis Dept. of M.E. MIT.

2. Arvikar, J.A., (1974), " A comprehensive simulation of the human musculoskeletal system," Ph.D. thesis,University of Wisconsin.

3. Asmussen, E., (1974), "Apparent efficiency and storage of elastic energy in human muscle during exercise," Acta Physiol. Scand.,92, p.537-45.

4. Ayoub, M.A., Ayoub, M.M., and Walvekar, A.G., (1974), "Biomechanical model for the upper extremity using optimization techniques," Human Factors, 16, p.585-594.

5. Banks, H.H., and Green, W.T., (1960), " Adductor Myotomy and Obturator neurectomy for the correction of adduction contracture of the hip in cerebral palsy," JBJS, 42-A, p.111.

6. Barany, M., (1967), "ATPase activity of myosin correlated with speed of shortening," J. Gen. Physiol., 50, p.197.

7. Bartel, D.L., (1975), " A model of the digit of the horse for the study of locomotor disorders," in Proc. ofthe Int. Workshop on Voluntary Human Motion, Baykin: editor.

8. Bartholomew, S.H., (1952), " Determination of knee moments during swing phase of walking and physical constants of the human shank," Biomechanics Lab Report, UCAL Berkeley, series 11, issue 19.

9. Braune, W. and Fischer, O., (1889), " The center of gravity of the human body as related to the equipment of the German Infantry," translation and condensation of above in Human Mechanics, Tech. Rep. no.AMRL-TDR-63-123, AFSC, Wright-Patt. AFB, Ohio, 1964.

10. Bresler, B., and Frankel, J.P., (1950), " The forces and moments in the leg during level walking," Trans. ASME, 72.

11. Bryson, A.E., and Ho, Y.C., (1969), Applied Optimal Control, Ginn & Co., Waltham, p.130-147.

12. Cappozzo, A., Leo, T., Pedotti, A., (1975), " A general computing method for the analysis of human locomotion", J. Biomech., 8, pp.307-320.

13. Cappozzo, A., Figura, F., Marchetti, M., and Pedotti, A., (1976), " The interplay of muscular and external forces in human ambulation," J. Biomech., 9, pp.35-43.

14. Carlson, C., Mann, R.W., Harris, W.H., (1974), " A radio telemetry device for monitoring cartilage surface pressures in the human hip," IEEE Trans., BME-21, pp.257-264.

15. Carlson, F.D., and Wilkie, D.R., (1974), Muscle physiology, Prentice-Hall, Englewood Cliffs.

16. Carlson, F.D., and Sieger, A., (1969), " The creatine phosphotransferase reaction in idioacetate - poisoned muscle," J. General Physiol., 43, p.301-3.

17. Chao, E.Y., and Rim, K.,(1973), "Application of optimization principles in determining the applied moments in the human leg during walking," J. Biomech., 6, p.497-510.

18. Chao, E.Y., Opgrande, J.D., and Axmear, F.E., (1976), " Three dimensional force analysis of finger joints in selected isometric hand functios," J. Biomech., 9, pp.387-396.

19. Chao, E.Y., and An, K.N., (1977), " Graphical interpretation of the solution to the redundant problem in biomechanics," ASME paper 77-Bio-1.

20. Chow, C.K., and Jacobsen, D.H., (1971), " Studies of human locomotion via optimal programming," Math. Biosci., 10, pp. 239-306.

21. Clark, M.R., and Stark, L., (1975), " Time optimal behavior of huamn saccadic eye movement," IEEE Trans., AC-20, p.345-348.

22. Close, J.R., and Todd, F.N., (1959), " The phasic activity of muscles of the lower extremity and the effect of tendon transfer," JBJS, 41, p.189-208.

23. Cnockaert, J.C., Lensel, G., Pertuzon, E., (1975), " Relative contribution of individual muscles to the isometric contraction of a muscular group," J. Biomech., 8, p.191 - 98.

24. Conati, F.C., (1977), " Real-time measurement of three-dimensional multiple rigid body motion, " M.S. thesis, MIT Dept. of M.E..

25. Cotes, J.E., and Meade, F., (1960), " Energy Expenditure and energy demand in walking," Ergonomics, 3, p.97-119.

26. Contini, R., (1972), " Body segment parameters," Art. Limbs, 16, p.1-19.

27. Crowninshield, R.D., (1978a), " Use of optimization techniques to predict muscle forces, " J. of Biomechanical Engineering, 100, p.88-92.

28. Crowninshield, R.D., Johnston, R.C., Andrews, J.G., Brand, R.A., (1978b), " A biomechanical investigation of the human hip," J. Biomech., 11, p.75-85.

29. Cunningham, D.M., (1958), " Components of floor reaction during walking," Pros. Dev. Res. Proj. Report, UCAL Berkely, Series 11, Issue 14.

30. Curtin, N.A., Gilbert, C., Kretzschmar, K.M., and Wilkie, D.R., (1974), " The effect of the performance of work on the total energy output and metabolism during muscular contraction," J.Physiol, 238, p.455-72.

31. DeLuca, C.J., and Forrest, W.J., (1973), " Force analysis of individual muscles acting simultaneously on the shoulder joint during isometric abduction," J. Biomech., 6, p.385-393.

32. Dempster, W.T., (1955), " Space requirements of the seated operator," USAF WADC Tech. Report 55-159, Wright-Patt. AFB, Ohio.

33. Donath, M., (1978), " Human gait pattern recognition for evaluation, diagnosis, and control," Ph.D. thesis, MIT Dept. of M.E.

34. Drillis, R., and Contini, R., (1964), " Body segment parameters: a survey of measurement techniques," Art. Limbs, 8, p.44-66.

35. Dydynska, M, and Wilkie, D.R., (1966), " The chemical energetic properties of muscle poisoned with FDNB," J. Physiol, 184, p.751-69.

36. Eberhart, H.D., Inman, V.T., And Bresler, B., (1954), " The principal elements in locomotion," in Human Limbs and their Substitutes, Klopsteg : ed., Hofner, New York.

37. Ebhasi, S., and Endo, M., (1968), " Calcium ion and muscle contraction," Prog. Biophysics and Molec. Biol., 18, p.123-183.

38. Elftman, H., (1938), " Forces and energy changes in the leg during walking," Am. J. Physiol., 125, p.357-366.

39. Elftman, H., (1966), " Biomechanics of muscle with particular application to studies of gait," JBJS, 48A p. 315-329.

40. Evarts, E.V., (1972), " Feedback and corollary discharge: a merging of concepts, " Neurosciences Res. Symp. Summaries, 6, p.86-112.

41. Frankel, J., Burstein, A., and Brooks, D., (1971) JBJS, 53A, p.949.

42. Gergly, J., (1977), Comments presented at Cybernetic models of the human neuromuscular system, and Engineering Foundation Conference, Henniker N.H.

43. Gordon, A.M., Huxley, A.F., and Julian, F.J., (1966). " The variation in isometric tension with sarcomere length in vertebrate muscle fibers," J. Physiol., 184, p. 170-92.

44. Grant, J.C.B.,(1972), An Atlas of Anatomy, The Williams and Wilkins Co., Baltimore, 6th Edition.

45. Hadley, G. , (1964), Non-linear and dynamic programming, Addion-Wesley, Reading.

46. Harrington, W.F., (1971), " A mechanochemical mechanism for muscular contraction," Proc. Nat. Acad. Sci., 68, p.685-693.

47. Harris, W.H., (1969), " Role of intertrochanteric osteotomy in treatment of arthritis of the hip," Surg. Clin. of North America, 49.

48. Hatze, H., (1975), " A control model of skeletal muscle and its application to a time optimal biomotion," Ph.D. thesis, University of Stellenbosch.

49. Hatze, H., (1976), "A method for describing the motion of biological systems," J. Biomech., 9, p. 101-104.

50. Hildebrand, F.B., (1962), Advanced calculus for applications, Prentice Hall, Englewood Cliffs.

51. Hill, A.V., (1964), " The efficiency of mechanical power development during muscular shortening and its relation to load," Proc. Roy. Soc., 159B, p. 319-324.

52. Hill, A.V., (1960), " Production and absorbtion of work by muscle," Science, 131, p.897-903.

53. Hill, A.V., (1953), " The mechanics of active muscle," Proc. Roy. Soc. Lond., 141B, p.104-117.

54. Hill, D.K., (1940), " The time evolution of oxidative recovery heat of frog's muscle," J. Physiol., 98, p. 454-59.

55. Hill, T.L., (1974), " Theoretical formalism for the sliding filament model of contraction of striated muscle; part I, " Prog. Biophys. and Molecular Biol., 28.

56. Hogan, N.J., (1976a), " Review of the methods of processing EMG for use as a proportional control signal," Biomedical Engineering.

57. Hogan, N.J., (1976b), " Myoelectric prosthesis control: optimal estimation applied to EMG and the cybernetic consideration for its use in a man-machine interface," Ph.D. thesis, MIT Dept, of M.E.

58. Hollingshead, W.H., (1969), Anatomy for surgeons: the back and limbs, Hoeber, New York.

59. Homsher, E., Rall, J.A., Wallner, A., and Ricchiutti, N.V., (1975), " Energy liberation and chemical change in frog skeletal muscle during single isometric tetantic contraction," J. Gen. Physiol., 65, p. 1-21.

60. Huston, R.L., and Passerello, C.E., (1971), " On the dynamics of a human body model," J. Biomech., 4, p. 369-77.

61. Jensen, R.H., and Davy, D.T., (1975), " An investigation of the muscle lines of action about the hip: a centroid line approach vs. the straight line approach," J. Biomech., 8, p.103-110.

62. Jewell, B.R., and Wilkie, D.R., (1958), " An analysis of the mechanical components in frog's striated muscle," J. Physiol., 43, p.515-40.

63. Julian, F.J., Sollins, K.R., and Sollins, M.R., (1974), " A model for the transient and steady state mechanical behavior of contracting muscle," Biophys. J., 14, p.546-62.

64. Katchalsky, A., and Curran, P.F., (1965), Non-equilibrium thermodynamics in biophysics, Harvard U. Press, Cambridge.

65. Kirk, D.E., (1970), Optimal control theory: an introduction, Prentice Hall, Englewood Cliffs.

66. Kuby, S.A., Noda, L., and Lardy, H.A., (1954), " ATP - CR Transphosphorylase - III kinetic studies," J. Biol. Chem., 210, p.65.

67. Kushmerick, M.J., (1977), comments presented at " Cybernetic models of the human neuromuscular system," an Engineering Foundation Conference, Henniker, N.H.

68. Kushmerick, M.J., and Davies, R.E., (1969), " The chemical energetics of muscular contraction, II: the chemistry, efficiency and power of maximally working satorious muscles," Proc. Roy. Soc. Lond., 174B, p. 315-53.

69. Lehninger, A.L., (1970), Biochemistry, Worth Publishers, New York.

70. Levens, B., and Inman, V.T., (1948), " Transverse rotation of the segments of the lower extremity in locomotion," JBJS, p.859-72.

71. Lew, W.D., and Lewis, J.L., (1977), " An anthropomorphic scaling method with application to the knee joint," J. Biomech., 10, p.171-82.

72. Lopez - Antunez, L., (1970), Atlas of human anatomy, W.B. Saunders, Philadelphia.

73. Margaria, R., (1976), Biomechanics and energetics of muscular exercise," Clarendon Press, Oxford.

74. Margaria, R. (1972, " The sources of muscular energy," Sci. Amer., 226, p.84-91.

75. McClare, C.W.F., (1972), " A molecular energy muscle model," J. Theor. Biol., 35, p. 569-95.

76. McGhee, R.B., Koozekanni, S.H., Gupta, S.,and Cheng, T.S., (1976), " Automatic estimation of joint forces and moments in human locomotion from television data," Proc. of IV IFAC Symp. on Identification and Parameter Estimation, USSR.

77. McMahon, T., Looney, T.R., and Taylor, C.R., (1977), " Energetics of running with loads: linear relationship betwenn metabolic power and force," submitted to Nature.

78. Morris, J.R.W., (1973), " Accelerometry - a technique for the measurement of human body movements," J. Biomech., 6, p.729-736.

79. Morrison, J.B., (1970), " The mechanics of muscle function in locomotion," J. Biomechanics, 3, p.431-51.

80. Morrison, J.B., (1967), " The forces transmitted by the human knee joint during activity," Ph.D. thesis, University of Strathclyde.

81. Murray, M.P., (1967), " Gait as a total pattern of movement," Am. J. Phys. Med., 46, p.290-333

82. Muybridge, E., (1880), The human figure in motion, a collection of works from the period 1880-1910, Dover Publications.

83. Nubar, Y., and Contini, R. , " A minimum principle in biomechanics," Bull. Math. Biophys., 23, p.377-91.

84. Pasley, P.R., Clamann, H.P., Soechting, J.P., Stewart, P.A., Zahalak, G.I., and Duffy, J., (1974), " Quantitative models for partially activated skeletal muscle," ASME paper 74-WA/apm-17.

85. Paul, J.P., (1971a), " Load actions on the human femur in walking and some resultant stresses," Exp. Mech., 13, p.121-31.

86. Paul, J.P., (1971b), " Comparison of EMG signals from the leg muscles with the corresponding force action calculated from walkpath measurements," Conference on Human Locomotor Engineering, Inst. Mech. Engr.

87. Paul, J.P., (1965), " Bioengineering studies of the forces transmitted by joints (II), " in Biomechanics and Related Bioengineering Topics, Pergammon Press, R.M. Kenedi, ed.

88. Paynter, H.M, (1961), Analysis and design of engineering systems, MIT press, Cambridge.

89. Pedotti, A., Krishnan, V.V., Stark, L., (1978), " Optimization of muscle force sequencing in human locomtion," Math. Biosci,, 38, p.57-76.

90. Pedotti, A., (1977), " Study of motor coordination and neuromuscular activity in human locomotion, " to be published, Biol. Cybernetics.

91. Penrod, J., Day, D, and Singh, F., (1974), " An optimization approach to tendon force analysis," J. Biomech., 7, p.123-29.

92. Rydell, N.W., (1966), " Forces acting on the femoral head prosthesis," Acta Crtho. Scand., 37.

93. Saunders, J., Inman, V., Eberhart, H.,(1953), "The major determinants in normal and pathological gait," JBJS, 35A, p.543-58.

94. Schmerlick, M.I., and Cleland, W.W., (1973)," Inhibition of creatine kinase by chromium nucleotides," J. Biol. Chem., 248, p.8418.

95. Seireg, A., and Arvikar, R.J.,(1975)"The prediction of muscular load sharing and joint forces in the lower extremities during walking," J. Biomech., 8, p.89-109.

96. Seireg, A., and Arvikar, R.J., (1973), " A mathematical model for evaluation of forces in lower extremities of the musculo-skeletal system," J. Biomech., 6, p.313-26.

97. Stearns, S.D., (1975), Digital signal analysis, Hayden, Rochelle Park.

98. Steinder, A., (1953), " A historical review of studies and investigations made in relation to human gait," JBJS, 35A, p.540.

99. Thorstensson, A., Gimby, G., and Karlson, J., (1976), " Force-velocity relations and fiber compositions in human knee extensor muscles," J. Appl. Physiol., 40, p. 12-16.

100. UCAL Berekely, (1953), " The pattern of muscular activity in the lower extremity during walking," Prosthetics Research Report series 11, issue 25.

101. Winter, D.A.
" Kinematices of normal locomotion - a statistical study based on T.V. data," J. Biomech., 7, p.479-486.

102. Winter, D.A., Hobson, G.R., Granlow, R., (1972), " T.V. - computer analysis of kinematices of human gait," Comp. Biol. Res., 5, p. 498-504.

103. Woledge, R.C., (1971), " Heat production and chemical change in muscle," Prog. Biophys. Med. Biol., 22, p. 39-73.

104. Woledge, R.C., (1972), " In vitro calorimetric studies relating to the interpretation of muscle heat measurements," Cold Springs Harbor Symposium on Quantitative Biology, 37, p. 629-634.

105. Wood, J.E., (1977), comments presented at " Cybernetic models of the human neuromuscular system," an Engineering Foundation Conference, Henniker, N.H.

106. Wood, J.E., (1975), " Theoretical formalism for the kinesilogical trajectories of a computer simulated neuromusculoskeletal system," Ph.D. thesis, MIT dept. of M.E.

107. Yamada, H., (1970), Strength of biological materials, Williams and Williams, Baltimore.

Appendix A System Equations for the 3 state AM model

The biochemical state diagram of figure 3-7 (reproduced in figure A 1) is useful in deriving the dynamic system equations of the actin myosin system. Each circleof the diagram represents a potential or concentration (probability) of that state and the interconnecting lines represent paths for transition to a new state according to the associated rate constants. These rate constants are in fact the rates of the lumped chemical reactions which correspond to the various state interactions. Julian (1974) chose an Arrehnius activation energy form for these constants , which states that the rate constant is a function of the activation energy between the states:

$$k_{12} = C_{12}\, e^{-E_{12}/kT}$$

k_{12} = rate constant from 1 to 2

C_{12} = empirical constant

E_{12} = activation energy

k,T Boltzman's constant & Temperature

This activation energy as applied here is similar to the potential hill of autonomous chemical reactions(i.e. non- mechanochemical) but has the added parameter of the strain energy in the elastic element of the myosin (see figure A2). In general, therefore, the activation energy is a function of the strain, i.e. $E_{12} = E_{12}(x)$, where x is the strain in the myosin. Given that:

1) This spring is linear
2) The spring can carry compressive as well as tensile loads
3) The transition from state 2 to state 3 involves a fixed strain (designated h),

appropriate forms for the five constants can be written, (see Julian for details). The specific expressions used here were:

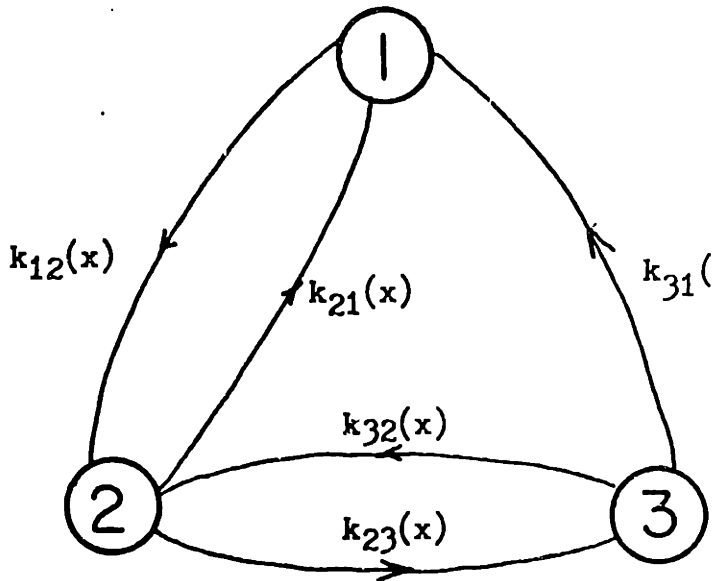

States

1-Detached

2-Attached, no strain

3-Attached, strained

1 - concentration or probability of state 1 $(p_1(t))$
2 concentration or probability of state 2 $(p_2(x,t)$
3 concentration or probability of state 3 $(p_3(x,t)$

k_{ij} - rate constant in direction i-j

x - relative displacement of AM when attached

Fig. A1 Biochemical State Diagram for the Three State AM Model

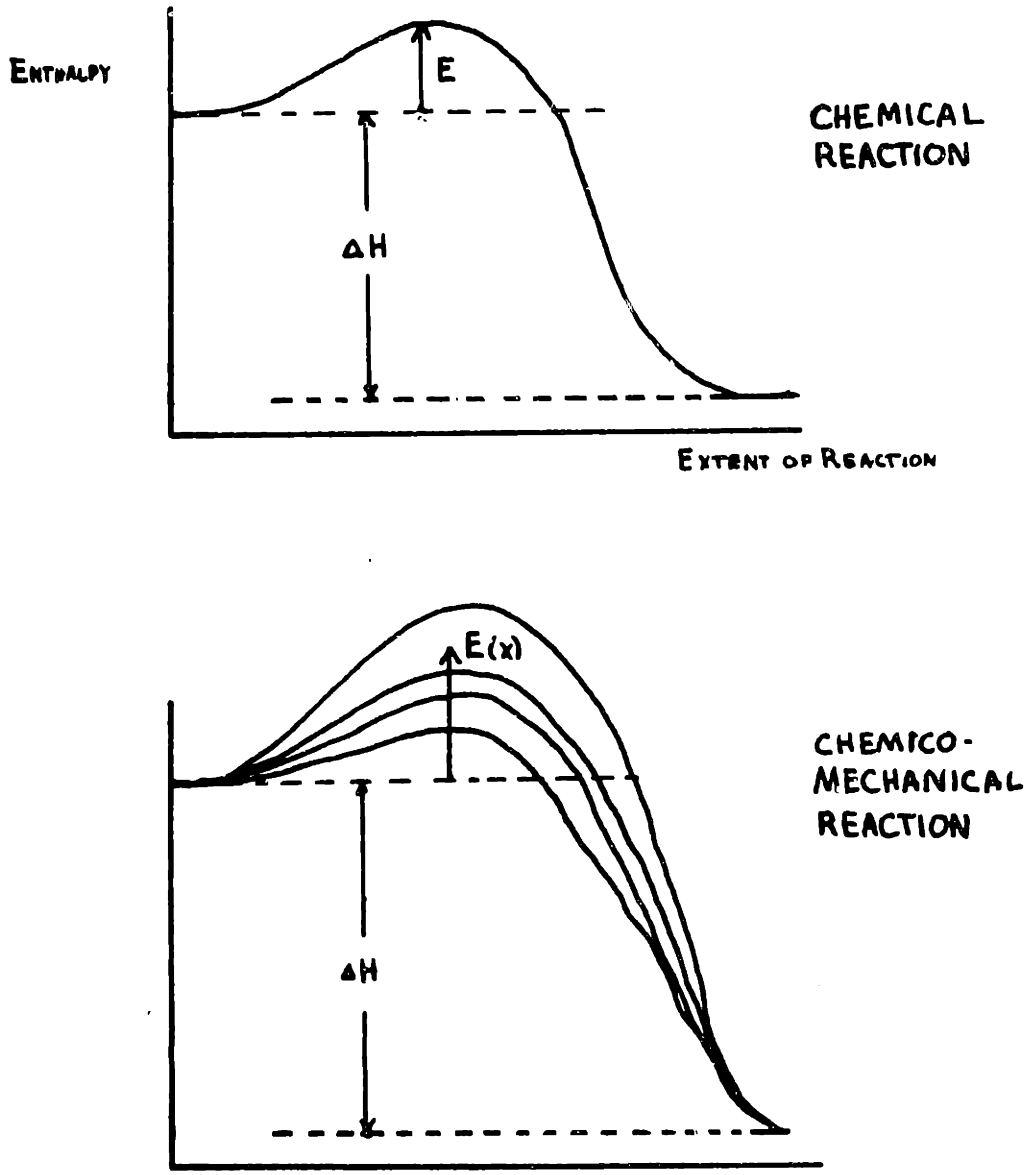

Fig. A2. Diagrams of Reaction Enthalpy Illustrating the Effect of the Elastic Element in the Mechanochemical Reaction

ΔH is the heat of reaction and E is the activation energy.

$$k_{12} = \begin{cases} 0 & 0 < x < 0 \\ 29\ 1/\text{sec} & x=0 \end{cases}$$

$$k_{21} = \begin{cases} 2.5 & x \leq 0 \\ 800(1-\exp(-K/2(2xh+h^2)/kT) & x > 0 \end{cases}$$

$$k_{23} = \begin{cases} 3633 & x \leq -h/2 \\ 3633(\exp(-K/2(2xh+h^2)/kT) & x > -h/2 \end{cases}$$

$$k_{32} = \begin{cases} 75 & x > -h/2 \\ 75\ \exp(-k/2(-2xh-h^2)) & x \leq -h/2 \end{cases}$$

where:

$$h = 10^{-8}\ m$$

$$K = 2.2 \times 10^{-4}\ N/m$$

These rate constants are plotted in figure A3.

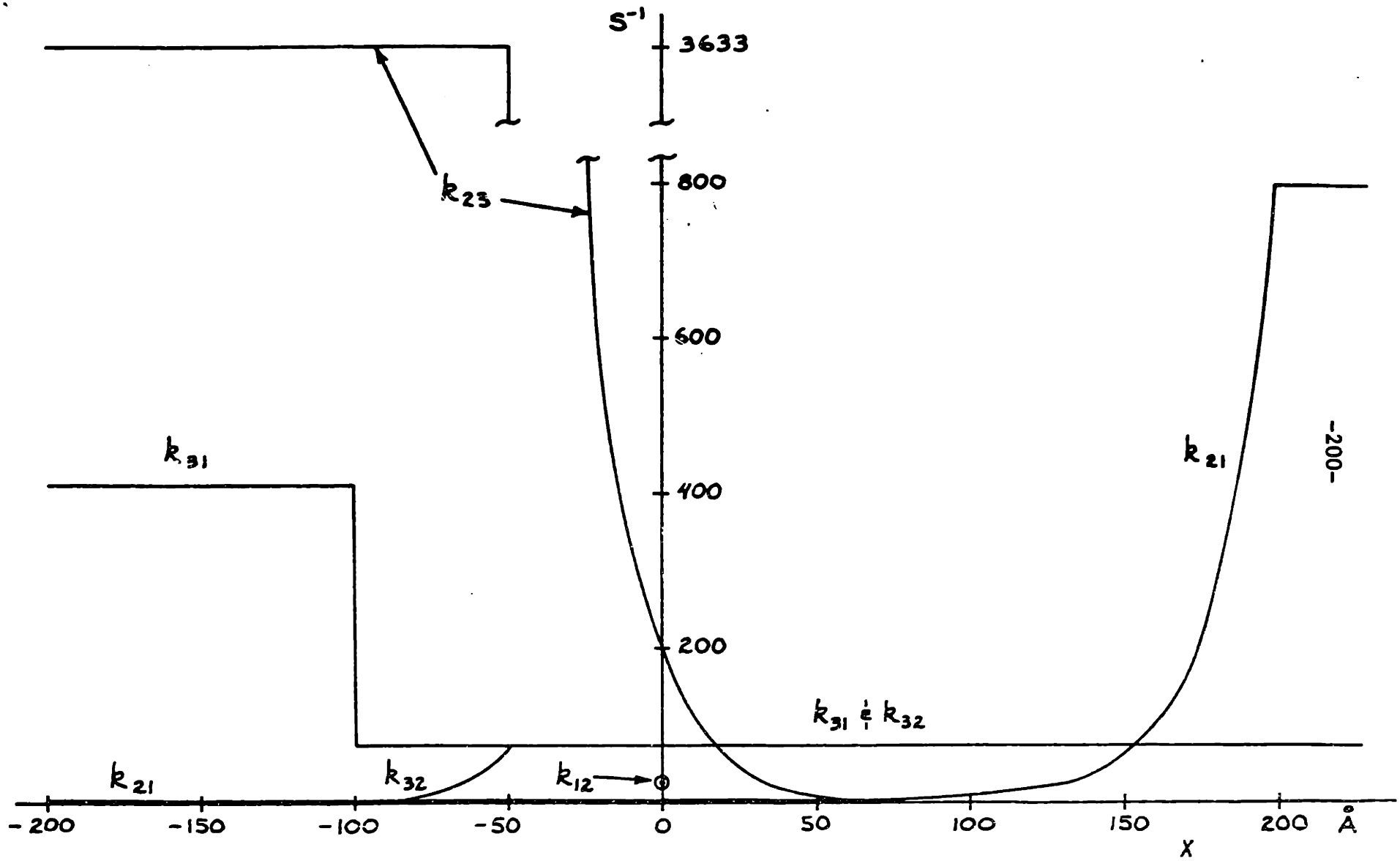

Fig. A3 Rate Constants for the AM Model (from Wood (1975))

The system equations can be written directly from the state diagram provided it is realized that the transition rates will be, in general, dependant upon the strain in the elastic element. Working directly from the state diagram the rate of change of the probaility distribution functions for each state are written as if these probabilities were driving potentials with the rate constants acting as the constitutive relationship for the respective transition. (The probability distribution functions can also be viewed as normalized concentrations of the various species, but these concentrations are two dimensional according to the dependance on strain.) This procedure yields:

$$\frac{\partial p_2(x,t)}{\partial t} + \frac{\partial p_2(x,t)}{\partial x}\frac{dx}{dt} = k_{12}\, p_1(t) + k_{32}\, p_2(x,t) - (k_{21}+k_{23})p_2(x,t)$$
$$p_2(x,t) \quad \text{(A1)}$$

$$\frac{\partial p_3(x,t)}{\partial t} + \frac{\partial p_3(x,t)}{\partial x}\frac{dx}{dt} = k_{23}\, p_2(x,t) - (k_{32}+k_{31})\, p_3(x,t) \quad \text{(A2)}$$

$$\frac{\partial p_1(t)}{\partial t} = \int_{-\infty}^{\infty} k_{21}\, p_2(x,t) + k_{31}\, p_3(x,t)\, dx - k_{12}\, p_1(t) \quad \text{(A3)}$$

note : all k_{ij} are functions of x

As they stand the equations are not soluble in closed form, the difficulty arising from both the partial differential form of the left hand side and the integral over space in equation A3. The following numerical method used by both Julian and Wood has been employed here. It is first assumed that $\frac{dp_1}{dt} = 0$, therefore $p_1(t)$=constant. Next the term $\frac{\partial p_i(x,t)}{\partial x}$ is assumed equal to zero corresponding to the isometric or zero sliding velocity case. The reduced equations then are coupled linear first order differential equations which have the solution:

$$p_2(x,t) = C_1(x)\, e^{-r_1 t} + C_2(x)\, e^{-r_2 t} + C_3(x) \qquad (A4)$$

$$p_3(x,t) = C_4(x)\, e^{-r_1 t} + C_5(x)\, e^{-r_2 t} + C_6(x) \qquad (A5)$$

$$p_1(t) = 1 - \int_{-\infty}^{\infty} p_2 + p_3 \, dx \qquad (A6)$$

where:

$$r_1(x), r_2(x) = -\tfrac{1}{2}(k_{21}+k_{23}+k_{31}+k_{32}) \pm \tfrac{1}{2}((k_{21}^2+k_{23}^2+k_{31}^2+k_{32}^2) + 2(k_{21}k_{23}+k_{23}k_{32}+k_{31}k_{32})-2(k_{21}k_{31}+k_{21}k_{32}+k_{23}k_{31}))^{\frac{1}{2}}$$

$$C_4(x) = p_3(x,0) - C_5(x) - C_6(x)$$

$$C_5(x) = (k_{23}p_2(x,0) - (r_1+k_{23}+k_{32})\, p_3(x,0)+r_1\, C_6(x))/ (r_1-r_2)$$

$$C_6(x) = k_{12}k_{23}p_1(0) / (k_{21}k_{31}+k_{21}k_{32}+k_{23}k_{31})$$

$$C_1(x) = (r_1+ k_{31}+k_{32})\, C_4(x)/ k_{23}$$

$$C_2(x) = (r_2+k_{31}+k_{32})\ C_5(x)/ k_{23}$$

$$C_3(x) = (k_{31}+k_{32})\, C_6(x) / k_{23}$$

Given the above assumptions, these equations are correct only when no filament sliding occurs and if $\frac{dp_1}{dt}$ = constant. However, they can be generalized by restricting their time range to times over which $\frac{dp_1}{dt}$ is small and by introducing non-zero velocitites by shifting the distribution $p_1(x,t)$ and $p_3(x,t)$ and amount Δx (from $\Delta x = v\Delta t$ where v is the sliding velocity and Δt is the time increment of the solution. The final method is to apply equation 4 - 6 over very short ime intervals, updating the initial conditions at each step, rather than having a continuous time soultion as with normal closed forms.

Appendix B TRACK Data Processing for Gait Analysis

The essential kinematic data from the TRACK system are the three dimensional position and orientation of each rigid body (skeletal segments) in the system. These data are presented as position coordinates of a reference point on the body and a Rodrigues vector (Conati (1977)). The latter represents, in a vector-like quantity, the rotation of a body relative to the fixed reference frame and has the form

$$\vec{\rho} = \tan(\theta/2)\hat{\rho}$$

where $\hat{\rho}$ specifies a unit vector and θ is the rotation about $\hat{\rho}$ from the reference position that will correctly orient the rigid body. By removing the $\tan(\theta/2)$ scaling, this "pseudo-vector" (so-called because it does not have the additive property of real vectors) can be differentiated to provide angular velocity and acceleration data. Actual rigid body orientation calculations are facilitated by the use of rotation matrices, which can be determined directly from the Rodrigues vector.

The two displacement vectors ($\underline{x}$ and $\underline{\theta}$) for all rigid bodies or segments in the system are first examined to find a complete data window (initial and final points can be lost) and "bad points" are located. The latter are TRACK samples that, owing to noise or optical distortion, cannot provide a satisfactory orientation calculation since the LED pattern on that body is not preserved. The resulting data gaps are filled by linear interpolation. The data is then low-pass filtered (usually at 5 Hz) with a 2nd order digital Butterworth filter (from Stearns (1975)) and the data is passed forward and backward through the filter three times to eliminate phase lag and to minimize filter trans-

ients. This filtered data is then twice differentiated using a five-point polynomial scheme (IBM SSP routine DET5). After each differentiation the data is again filtered to eliminate any higher harmonics introduced by the discrete filtering process. A rotation matrix is calculated from the filtered $\underline{\theta}$ data, and is at the same time re-referenced to a "zero" position of the particular experimental subject's limbs, rather than to the fixed TRACK reference frame.

In figure B-1 a typical "raw" displacement tracjectory is shown along with three stages of processing: interpolated and filtered, first time derivative (filtered) and second time derivative (filtered).

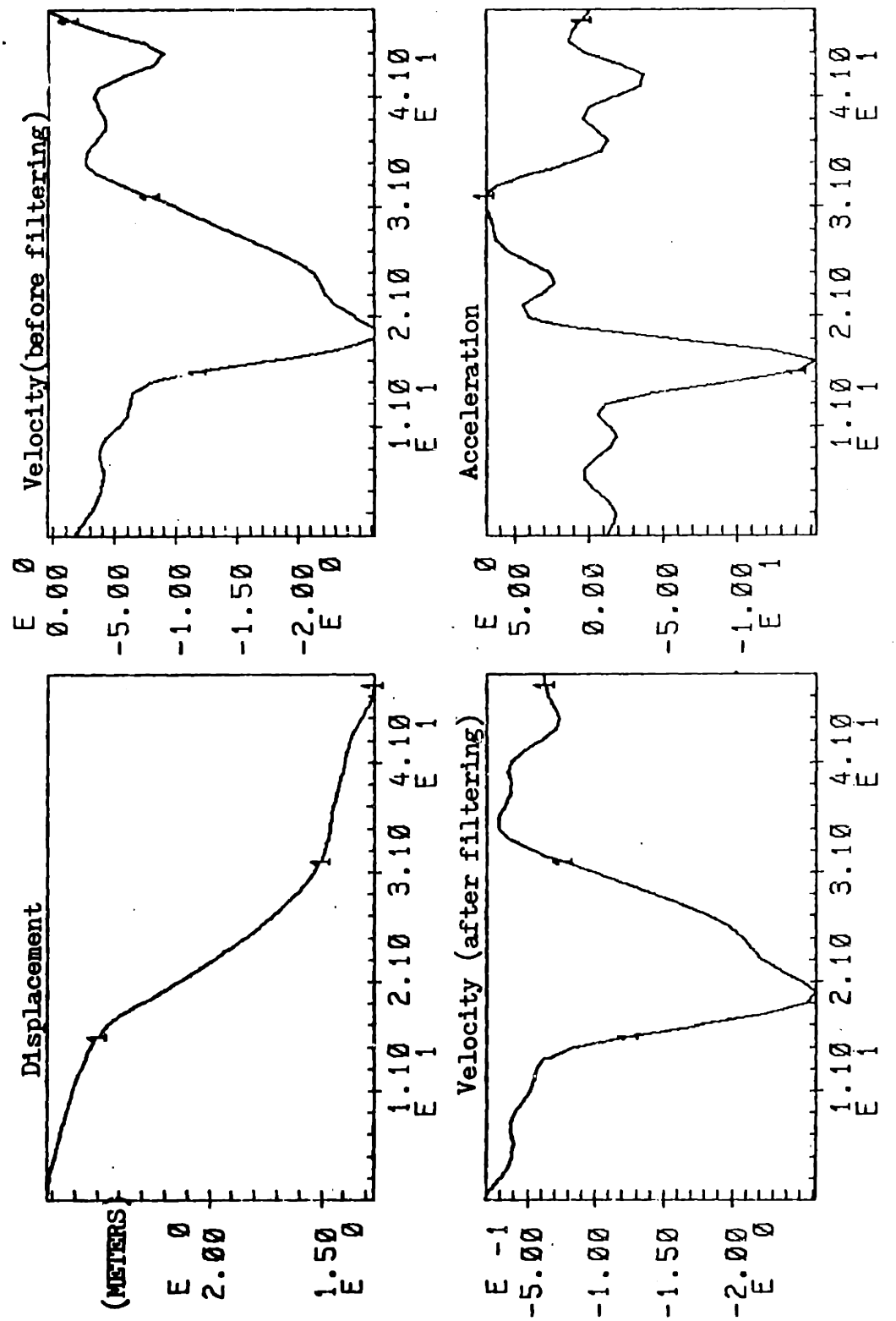

Fig B-1 Typical TRACK data for one Coordinate with Associated Processing

Appendix C Myoelectric Signal Acquisition Equipment

The myoelectric signal acquisition system used here consists of up to fourteen electrode preamplifier packages (obtained from Motion Control, Inc.), a sixteen channel multiplexer (designed by Ralph Burgess, staff engineer, and constructed by M.E. undergraduate Mark Stern), a 16 on 1 to 4 on 4 demultiplexer, and an Ampex FR1300 FM tape recorder with 7 FM channels and 1 AM channel.

The electrode - preamplifier packages consist of a differential pair of electrodes (1 cm metal disks) and a differential amplifier providing an input impedance of 10^{11} ohms, a gain of 300 in the frequency range 10 - 10,000 Hz, and a common mode rejection ratio of at least 90 dB.

The multiplexer serves to provide power for the preamplifiers (+5, -12v) and to switch serially among fourteen of these at a rate of 16 kHz. while adding a calibration pulse (2 v) and a ground reference pulse. (The circuit diagram for this device is shown in figure C-1). The result is a Pulse Amplitude Modulated (PAM) signal, where information about separate MES channels is contained in the amplitude of successive pulses as shown in figure C-2. With a switching or clock frequency of 16 kHz., each of the sixteen channels is effectively "sampled" at 1 kHz, which allows MES's approaching 500 Hz to be reconstructed.

The PAM signal appears just like a 16 kHz square wave and as such requires at least the 5th harmonic to be recorded for faithful reproduction, thus a recorder bandwidth of 90 kHz is necessary. Typical FM recorders operating at maximum tape speeds of 60 ips are usually limited

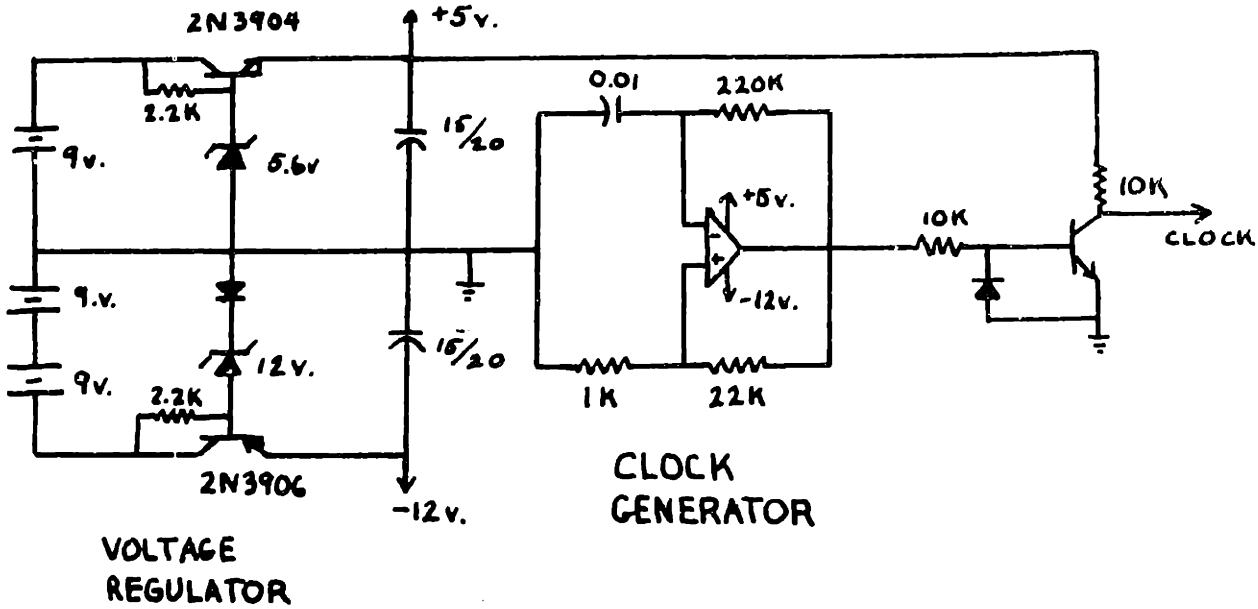

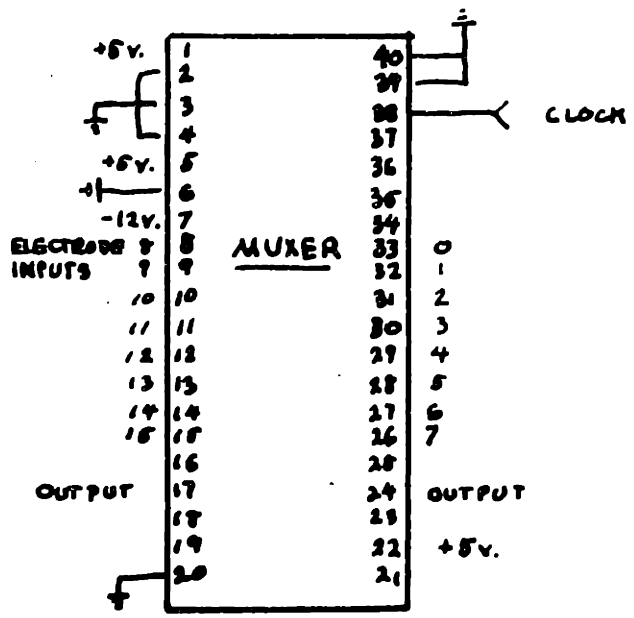

Fig. C-1 Circuit Diagram for MES Multiplexer

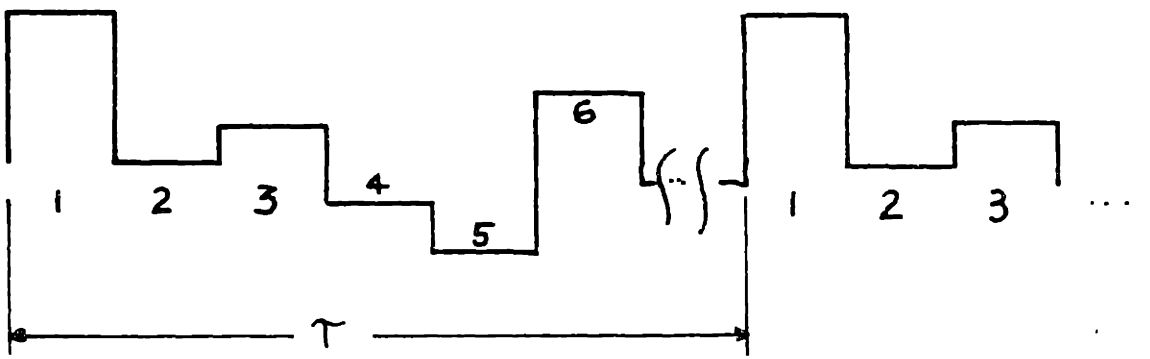

Fig. C-2 Pulse Amplitude Modulated Multiplexed Signal

Each "pulse" is a short sample of a separate data signal, and the cycle repeats in time τ, which is chosen short enough to prevent large changes in any of the signal between samples.

to a 20 kHz. bandwidth, so a method of lowering the bandwidth requirements must be used. This was accomplished here by partially de-multiplexing the 16 on 1 PAM signal to 4 separate PAM signals each with only 4 MES or reference signals on it. This lowers the individual PAM signal square wave frequency to 4 kHz and the 4 parallel PAMs can be recorded on 4 of the 7 FM recorder channels. A schematic diagram of the 4x4 de-multiplexer is shown in figure C-3 and the various stages of signal processing are shown in the timing diagram of figure C-4.

The basic operation of the device is as follows: the 16 x 1 PAM signal is received and the first pulse in the cycle, which is the 2 v calibration pulse, is separated out and used as a synchronizing signal. From this, the original 16 kHz clock signal is synthesized using a phase-locked loop frequency multiplier circuit. This clock signal is recorded on the AM recorder channel to facilitate the timing of the final demultiplexing done by computer.

This final separation of the MES's into 14 separate signals is accomplished with a PDP 11-40 with a Laboratory Peripheral System (LPS). The four data signals plus a fifth signal (which is the start-stop pulse from the TRACK system also recorded during an experiment) are connected to separate A/D channels of the LPS. The clock signal is sent to a Schmidt trigger that will initiate A/D samples. Also, the beginning of the entire 16 channel cycle must be detected so that the final channel assignments are correct, so the actual demultiplexing routine follows the sequence:

1) wait for the TRACK start signal on channel 0

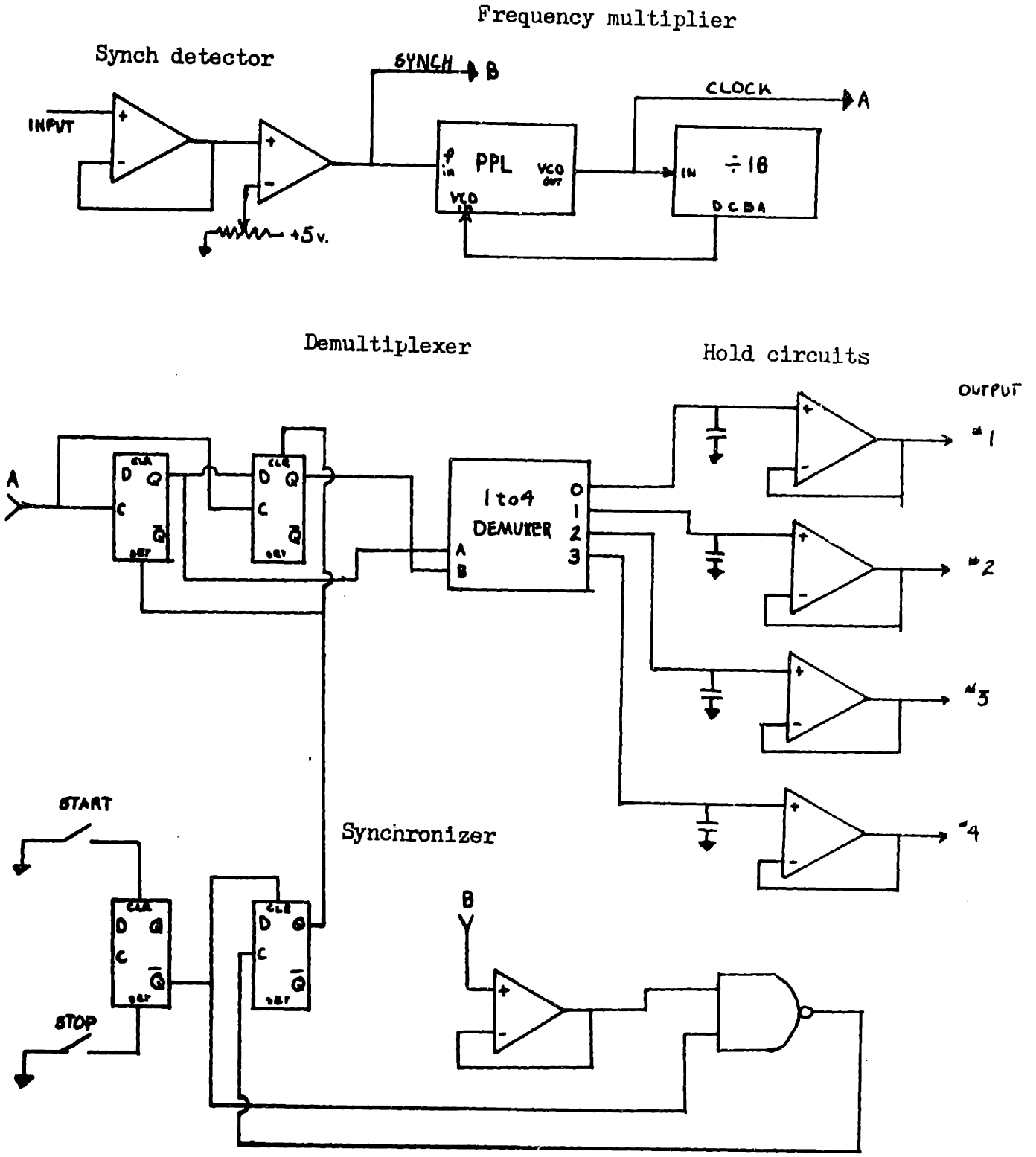

Figure C-3 Simplified Schematic Diagram of the De-multiplexer

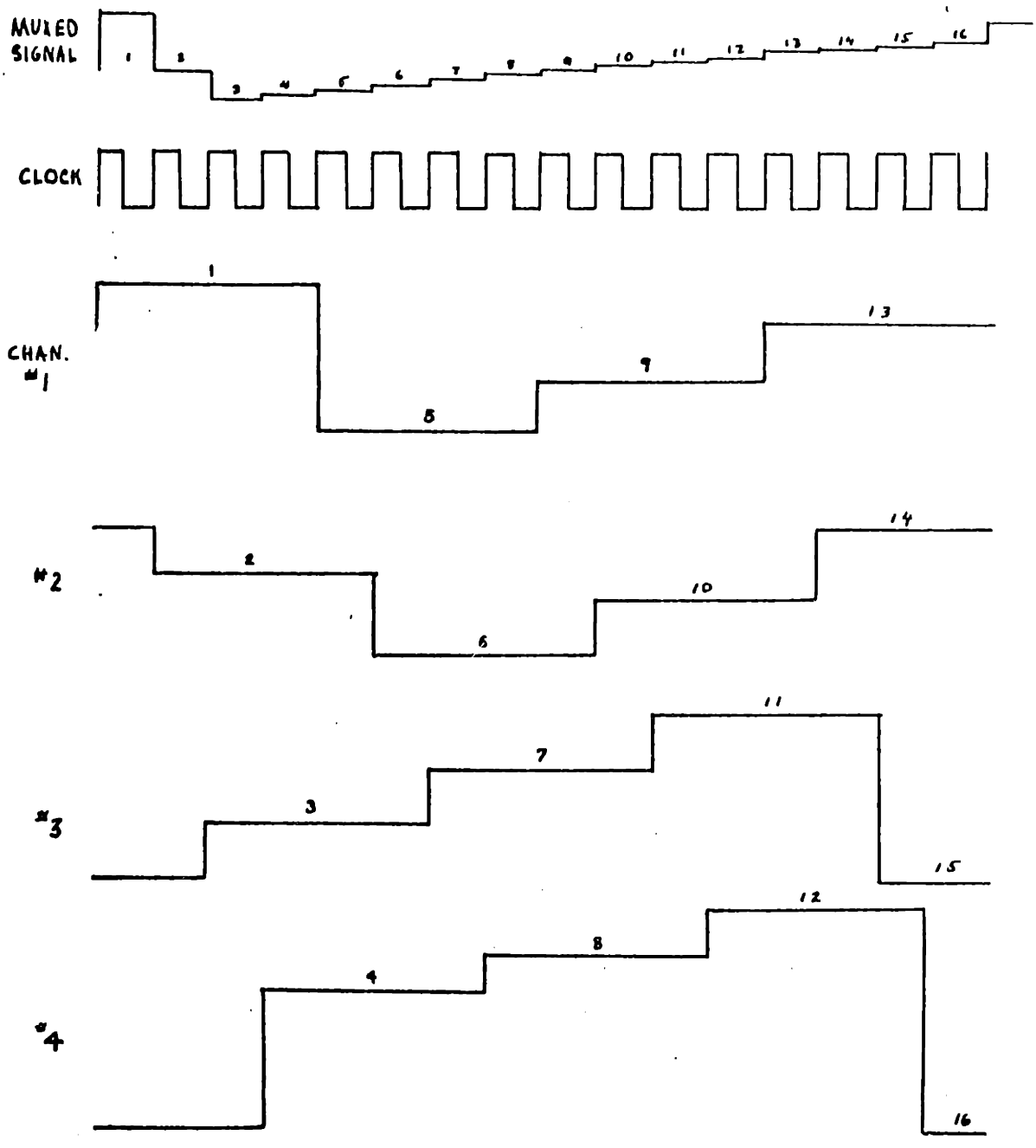

Fig. C-4 Timing Diagram for 4x4 De-multiplexer

2) wait for the 2 v. signal (synch.) on channel 1

3) wait for that signal to disappear

4) begin sampling and saving data on the 3rd input channel and continue sequencing through each of the four channels, triggered by the clock signal, until the data buffer is full.

Since the recorded signals have some transients in them (the reproduce amplifiers are underdamped) it is important that the individual data pulses were sampled after this "ringing" has died out. The actual timing of the sample point is set by changing the Schmidt trigger threshold. Owing to limited bandwidth of the LPS A/D's and programming considerations, the tape is played-back at 7 1/2 ips, which will reduce the clock rate (the frequency at which samples must be taken) to 2 kHz.

Once stored as a data matrix, the signals can be optionally band-pass filtered (zero phase lag 2nd order Butterworth filter), rectified, and low-pass filtered (zero phase lag 2nd order Butterworth). The separate signals can then be plotted on the Gould 5000 printer/plotter with up to 14 plots of 1000 points each on a single page.

Appendix D Frequncy Analysis of Limb Motion

Owing to measurement noise, the proper determination of joint angle trajectories must always involve low-pass filtering. This processing is particularly critical if numerical differnetiation of the data is anticipated. A method for estimating the frequency content of joint angle trajectories is presented below, and this can serve to guide the filter design and cut-off frequency selection.

Each segment of the lower limb can be approximated by a simple pendulum with moment generators at either the hip or knee, for this analysis all motion is two-dimensional, constrained to lie in the saggital plane. For a pendulum operating at small angles (+ 20^{o}) the natural frequency of oscilation is given by

$$\omega_{\circ} = \sqrt{g/\ell}$$

where g is the acceleration of gravity and ℓ is the distance from the center of rotation of the pendulum to its center of gravity. This linearized pendulum is equivalent to a second order, linear dynamic system. If a moment generator (M) is applied as an input and the resutling angle (θ) is taken as the output, the frequency response of the system will be such that the amplitude ratio θ/M, above $\omega_{\circ}$, will begin decreasing at a rate approaching $(\omega-\omega_{\circ})^2$. To maintain a constant output amplitude at frequencies above would require the moment to increase quadratically, and if the joint power ($M\omega$) is considered, the power requirements above $\omega_{\circ}$ will increase <u>cubically</u>. (For example, operation at ten times the natural frequency would require the moment to increase by a factor of 100 and the power by 1000 to maintain the output at a

constant level.

This indicates quite strongly that active use of the leg at frequencies much above the natural frequency is very costly energetically and therefore highly unlikely during walking. A good estimate of the frequency limit of leg joint angle trajectories should thus be somewhere just above the natural frequency.

Applying this model to the human shank-foot segment, articulated at the knee, the natural frequency of this system will set the lower bound for the cut-off frequency of a low-pass filter for processing measurements of joint angles. For an individual standing 1.8 m. tall, the center of gravity of the shank-foot segment will be 0.23 m. from the knee (Contini (1972)). This yields

$$\omega_{o\ \text{shank}} = \sqrt{\frac{9.8\ \text{m/sec}^2}{0.23\ \text{m}}} = 6.5\ \ 1/\text{sec} = 1.03\ \text{Hz}.$$

Thus, for walking, filter cut-off frequencies of a few hertz should be appropriate. However, the non-ideal nature of real filters, combined with this narrow frequency band of information, makes it crucial that either high order filters (ones with "sharp" cut-off characteristics) be used, and/or that the cut-off frequency be chosen with a safety margin above ω_o to avoid attenuation of any of the useful data. The best method would be to analyze the frequency content of the measure angle data, look for a separation between the angle data (which shoud be confined at or below the natural frequency) and the measurement noise, and design a filter to operate somewhere between these two ranges.